DRAFT International Standard

ISO/DIS 19901-1

ISO/TC **67**/SC **7**

Secretariat: **BSI**

Voting begins on:
2024-08-15

Voting terminates on:
2024-11-07

Oil and gas industries including lower carbon energy — Specific requirements for offshore structures —

Part 1:
Metocean design and operating considerations

ICS: 75.180.10

This document is circulated as received from the committee secretariat.

ISO/CEN PARALLEL PROCESSING

Reference number
ISO/DIS 19901-1:2024(en)

ISO copyright office
CP 401 • Ch. de Blandonnet 8
CH-1214 Vernier, Geneva
Phone: +41 22 749 01 11
Email: copyright@iso.org
Website: www.iso.org

Published in Switzerland

Contents

Page

Foreword

ISO (the International Organization for Standardization) is a worldwide federation of national standards bodies (ISO member bodies). The work of preparing International Standards is normally carried out through ISO technical committees. Each member body interested in a subject for which a technical committee has been established has the right to be represented on that committee. International organizations, governmental and non-governmental, in liaison with ISO, also take part in the work. ISO collaborates closely with the International Electrotechnical Commission (IEC) on all matters of electrotechnical standardization.

The procedures used to develop this document and those intended for its further maintenance are described in the ISO/IEC Directives, Part 1. In particular the different approval criteria needed for the different types of ISO documents should be noted. This document was drafted in accordance with the editorial rules of the ISO/IEC Directives, Part 2 (see www.iso.org/directives).

Attention is drawn to the possibility that some of the elements of this document may be the subject of patent rights. ISO shall not be held responsible for identifying any or all such patent rights. Details of any patent rights identified during the development of the document will be in the Introduction and/or on the ISO list of patent declarations received (see www.iso.org/patents).

Any trade name used in this document is information given for the convenience of users and does not constitute an endorsement.

For an explanation on the meaning of ISO specific terms and expressions related to conformity assessment, as well as information about ISO's adherence to the WTO principles in the Technical Barriers to Trade (TBT) see the following URL: Foreword - Supplementary information

This document was prepared by Technical Committee ISO/TC *67 Materials, equipment and offshore structures for petroleum, petrochemical and natural gas industries*, Subcommittee SC 7, *Offshore structures*

This third edition cancels and replaces the second edition (ISO 19901-1:2015), which has been technically revised.

The main changes compared to the previous edition are as follows:

— Clarification on the role of the metocean expert (Section 5.2 and Annex A.5.2)

— Additional information related to the determination of associated criteria (Section 5.3 and Annex A.5.3)

— Additional information related to the estimation of extreme/abnormal conditions (Section 5.7 and Annex A.5.7)

— Alignment of the wind normative and informative sections with API RP 2MET (Section 7 and Annex A.7)

— Additional information related to breaking/non-breaking wave kinematic estimation (Section 8.4.3 and Annex A.8.4.3)

— Expansion to section on additional environment factors to be considered (Section 10 and Annex A.10)

— Introduction of Normative and Informative text related to the verification of weather forecast information (Sections 12 and Annex A.12)

— Update to Offshore Canada Regional Annex (Annex D)

— Update to Sakhalin/Sea of Okhotsk Regional Annex (Annex E)

— Update to Caspian Sea Regional Annex (Annex F)

— Introduction of Mediterranean Sea Regional Annex (Annex H)

— Introduction of Brazil Regional Annex (Annex I)

— Re-introduction of US Gulf of Mexico Regional Annex (Annex J)

— Re-introduction of Coast of California Regional Annex (Annex K)

— Re-introduction of Overview of Regions Excluding Gulf of Mexico and California Regional Annex (Annex J)

A list of all parts in the ISO 19901-1 series can be found on the ISO website.

Any feedback or questions on this document should be directed to the user's national standards body. A complete listing of these bodies can be found at www.iso.org/members.html.

Introduction

The series of International Standards applicable to types of offshore structure, ISO 19900 to ISO 19906, constitutes a common basis covering those aspects that address design requirements and assessments of all offshore structures used by the petroleum and natural gas industries worldwide. Through their application the intention is to achieve reliability levels appropriate for manned and unmanned offshore structures, whatever the type of structure and the nature or combination of the materials used.

It is important to recognize that structural integrity is an overall concept comprising models for describing actions, structural analyses, design rules, safety elements, workmanship, quality control procedures and national requirements, all of which are mutually dependent. The modification of one aspect of design in isolation may disturb the balance of reliability inherent in the overall concept or structural system. The implications involved in modifications, therefore, need to be considered in relation to the overall reliability of all offshore structural systems.

The series of International Standards applicable to types of offshore structure is intended to provide a wide latitude in the choice of structural configurations, materials and techniques without hindering innovation. Sound engineering judgement is therefore necessary in the use of these International Standards.

The overall concept of structural integrity is described above. Some additional considerations apply for metocean design and operating conditions. The term “metocean” is short for “meteorological and oceanographic” and refers to the discipline concerned with the establishment of relevant environmental conditions for the design and operation of offshore structures. A major consideration in the design and operation of such a structure is the determination of actions on, and the behaviour of, the structure as a result of winds, waves and currents.

Environmental conditions vary widely around the world. For the majority of offshore locations there are little numerical data from historic conditions; comprehensive data often only start being collected when there is a specific need, for example, when exploration for hydrocarbons is being considered. Despite the usually short duration for which data are available, designers of offshore structures need estimates of extreme and abnormal environmental conditions (with an individual or joint probability of the order of 1×10^{-2}/year and 1×10^{-3} to 1×10^{-4}/year, respectively).

Even for areas like the Gulf of Mexico, offshore Indonesia and the North Sea, where there are over 30 years of fairly reliable measurements available, the data are insufficient for rigorous statistical determination of appropriate extreme and abnormal environmental conditions. The determination of relevant design parameters has therefore to rely on the interpretation of the available data by experts, together with an assessment of any other information, such as prevailing weather systems, ocean wave creation and regional and local bathymetry, coupled with consideration of data from comparable locations. In particular, due account needs to be taken of the uncertainties that arise from the analyses of limited datasets. It is hence important to employ experts from both the metocean and structural communities in the determination of design parameters for offshore structures, particularly since setting of appropriate environmental conditions depends on the chosen option for the offshore structure.

This part of ISO 19901 provides procedures and guidance for the determination of environmental conditions and their relevant parameters. Requirements for the determination of the actions on, and the behaviour of, a structure in these environmental conditions are given in ISO 19901-3, ISO 19901-6, ISO 19901-7, ISO 19902, ISO 19903, ISO 19904-1, ISO 19905-1 and ISO 19906.

Some background to, and guidance on, the use of this part of ISO 19901 is provided in informative Annex A. The clause numbering in Annex A is the same as in the main text to facilitate cross-referencing.

Regional information, where available, is provided in the Regional Annexes B to I. This information has been developed by experts from the region or country concerned to supplement the guidance provided in this part of ISO 19901. Each Regional Annex provides regional or national data on environmental conditions for the area concerned.

Oil and gas industries including lower carbon energy — Specific requirements for offshore structures —

Part 1: Metocean design and operating considerations

1 Scope

This part of ISO 19901 gives general requirements for the determination and use of meteorological and oceanographic (metocean) conditions for the design, construction and operation of offshore structures of all types used in the petroleum and natural gas industries.

The requirements are divided into two broad types:

— those that relate to the determination of environmental conditions in general, together with the metocean parameters that are required to adequately describe them;

— those that relate to the characterization and use of metocean parameters for the design, the construction activities or the operation of offshore structures.

The environmental conditions and metocean parameters discussed are:

— extreme and abnormal values of metocean parameters that recur with given return periods that are considerably longer than the design service life of the structure,

— long-term distributions of metocean parameters, in the form of cumulative, conditional, marginal or joint statistics of metocean parameters, and

— normal environmental conditions that are expected to occur frequently during the design service life of the structure.

Metocean parameters are applicable to:

— the determination of actions for the design of new structures,

— the determination of actions for the assessment of existing structures,

— the site-specific assessment of mobile offshore units,

— the determination of limiting environmental conditions, weather windows, actions and action effects for pre-service and post-service situations (i.e. fabrication, transportation and installation or decommissioning and removal of a structure), and

— the operation of the platform, where appropriate.

NOTE Specific metocean requirements for site-specific assessment of jack-ups are contained in ISO 19905-1, for arctic offshore structures in ISO 19906 and for topside structures in ISO 19901-3.

2 Normative references

The following documents, in whole or in part, are normatively referenced in this document and are indispensable for its application. For dated references, only the edition cited applies. For undated references, the latest edition of the referenced document (including any amendments) applies.

ISO 19900, *Petroleum and natural gas industries — General requirements for offshore structures*

ISO 19901 (all parts), *Oil and gas industries including lower carbon energy — Specific requirements for offshore structures*

ISO 19902, *Petroleum and natural gas industries — Fixed steel offshore structures*

ISO 19903, *Petroleum and natural gas industries — Concrete offshore structures*

ISO 19904-1, *Petroleum and natural gas industries — Floating offshore structures — Part 1: Ship-shaped, semi-submersible, spar and shallow-draught cylindrical structures*

ISO 19905-1, *Oil and gas industries including lower carbon energy — Site-specific assessment of mobile offshore units — Part 1: Jack-ups: elevated at a site*

ISO 19906, *Petroleum and natural gas industries — Arctic offshore structures*

WMO-No 306, *Manual on Codes*

3 Terms and definitions

For the purpose of this document, the terms and definitions given in ISO 19900 and the following apply.

3.1
abnormal value
design value of a parameter of abnormal severity used in accidental limit state checks in which a structure is intended not to suffer complete loss of integrity

Note 1 to entry: Abnormal events are typically accidental and environmental (including seismic) events having probabilities of exceedance of the order of 10^{-3} to 10^{-4} per annum.

3.2
chart datum
local datum used to fix water depths on a chart or tidal heights over an area

Note 1 to entry: Chart datum is usually an approximation to the level of the lowest astronomical tide.

Note 2 to entry: Chart datum may differ from one chart to another and care is required if cross referencing sites that are not on the same chart.

3.3
conditional probability
conditional distribution
statistical distribution (probability) of the occurrence of a variable A, given that other variables B, C, … have certain assigned values

Note 1 to entry: The conditional probability of A given that B, C, … occur is written as $P(A|B,C,...)$. The concept is applicable to metocean parameters, as well as to actions and action effects.

EXAMPLE When considering wave parameters, A may be the individual crest elevation, B the water depth and C the significant wave height, and so on.

3.4
design crest elevation
extreme crest elevation measured relative to still water level

Note 1 to entry: The design crest elevation is used in combination with information on astronomical tide, storm surge, platform settlement, reservoir subsidence and water depth uncertainty and is derived using extreme value analysis. Where simplified models are used to estimate the kinematics of the design wave, the design crest elevation may be different from (usually somewhat greater than) the crest elevation of the design wave used to calculate actions on the structure. In reality, the wave with the greatest trough-to-crest height and the wave with the highest crest will be different waves.

3.5
design wave
deterministic wave used for the design of an offshore structure

Note 1 to entry: The design wave is an engineering abstraction. Most often it is a periodic wave with suitable characteristics (e.g. height *H*, period *T*, steepness, crest elevation). The choice of a design wave depends on:

— the design purpose(s) considered,

— the wave environment,

— the geometry of the structure,

— the type of action(s) or action effect(s) pursued.

Note 2 to entry: Normally, a design wave is only compatible with design situations in which the action effect(s) are quasi-statically related to the associated wave actions on the structure.

3.6
expert
<metocean> individual who through training and experience is competent to provide metocean advice specific to the area or topic in question.

3.7
extreme water level
EWL
combination of design crest elevation, astronomical tide and storm surge referenced to either LAT or MSL

3.8
extreme value
representative value of a parameter used in ultimate limit state checks

Note 1 to entry: Extreme events have probabilities of the order of 10^{-2} per annum.

3.9
gravity wave
wave in a fluid or in the interface between two fluids for which the predominant restoring forces are gravity and buoyancy

Note 1 to entry: Wind-generated surface waves are an example of gravity waves.

3.10
gust
brief rise and fall in wind speed lasting less than 1 min

Note 1 to entry: In some countries, gusts are reported in meteorological observations if the maximum wind speed exceeds approximately 8 m/s.

3.11
gust wind speed
maximum value of the wind speed of a gust averaged over a short (3 s to 60 s) specified duration within a longer (1 min to 1 h) specified duration

Note 1 to entry: For design purposes, the specified duration depends on the dimensions and natural period of (part of) the structure being designed such that the structure is designed for the most onerous conditions; thus, a small part of a structure is designed for a shorter gust wind speed duration (and hence a higher gust wind speed) than a larger (part of a) structure.

Note 2 to entry: The elevation of the measured gust should also be specified.

3.12
highest astronomical tide
HAT
level of high tide when all harmonic components causing the tides are in phase

Note 1 to entry: The harmonic components are in phase approximately once every 19 years, but these conditions are approached several times each year.

3.13
hindcasting
method of simulating historical (metocean) data for a region through numerical modelling

3.14
infra-gravity wave
surface gravity wave with a period in the range of approximately 25 s to 500 s

Note 1 to entry: In principle an infra-gravity wave is generated by different physical processes but is most commonly associated with waves generated by nonlinear second-order difference frequency interactions between different swell wave components.

3.15
internal wave
gravity wave which propagates within a stratified water column

3.16
Joint North Sea Project Spectrum
JONSWAP
version of the Pierson-Moskowitz spectrum which accounts for the continued development of the spectrum through non-linear wave-wave interaction over time and space

3.17
long-term distribution
probability distribution of a variable over a long time scale

Note 1 to entry: The time scale exceeds the duration of a sea-state, in which the statistics are assumed constant (see 3.35 **short-term distribution**). The time scale is hence comparable to a season or to the design service life of a structure.

EXAMPLE Long-term distributions of:

— significant wave height (based on, for example, storm peaks or all sea-states),

— significant wave height in the months May to September,

— individual wave heights,

— current speeds (such as for use in assessing vortex-induced vibrations of drilling risers),

— scatter diagrams with the joint distribution of significant wave height and wave period (such as for use in a fatigue analysis),

— a particular action effect,

— sea ice types and thickness,

— iceberg mass and velocity,

— storm maximum significant wave height.

3.18
lowest astronomical tide
LAT
level of low tide when all harmonic components causing the tides are in phase

Note 1 to entry: The harmonic components are in phase approximately once every 19 years, but these conditions are approached several times each year.

3.19
marginal distribution
marginal probability
statistical distribution (probability) of the occurrence of a variable *A* independent of any other variable

Note 1 to entry: The marginal distribution is obtained by integrating the full distribution over all values of the other variables *B*, *C*, ... and is written as *P*(*A*). The concept is applicable to metocean parameters, as well as to actions and action effects.

EXAMPLE When considering wave conditions, *A* may be the individual crest elevation for all mean zero-crossing periods *B* and all significant wave heights *C*, occurring at a particular site.

3.20
marine growth
living organisms attached to an offshore structure

3.21
mean sea level
MSL
arithmetic mean of all sea levels measured over a long period

Note 1 to entry: Seasonal changes in mean level may be expected in some regions and over many years the mean sea level may change.

3.22
mean wind speed
time-averaged wind speed, averaged over a specified time interval and at a specified elevation

Note 1 to entry: The mean wind speed varies with elevation above mean sea level and the averaging time interval; a standard reference elevation is 10 m and with an averaging time of 10 min. See also **3.11 gust wind speed** and **3.46 sustained wind speed**.

3.23
mean zero-crossing period
average period between (up or down) zero-crossing waves in a sea-state

Note 1 to entry: In practice the mean zero-crossing period is often estimated from the zeroth and second moments of the wave spectrum as $T_z = T_2 = \sqrt{m_0(f)/m_2(f)} = 2\pi\sqrt{m_0(\omega)/m_2(\omega)}$.

3.24
monsoon
seasonally reversing wind pattern, with associated pattern of rainfall

Note 1 to entry: The term was first applied to the winds over the Arabian Sea which blow for six months from northeast and for six months from southwest, but it has been extended to similar winds in other parts of the world.

3.25
most probable maximum
value of the maximum of a variable with the highest probability of occurring

Note 1 to entry: The most probable maximum is the value for which the probability density function of the maxima of the variable has its peak. It is also called the mode or modus of the statistical distribution.

3.26
operating conditions
most severe combination of environmental conditions under which a given operation is permitted to proceed

Note 1 to entry: Operating conditions are determined for operations that exert a significant action on the structure. Operating conditions are usually a compromise: they are sufficiently severe that the operation may generally be performed without excessive downtime, but they are not so severe that they have an undue impact on design or safety.

3.27
polar low
depression that forms in polar air, often near a boundary between ice and sea

3.28
residual current
residual water level
part of the total current or water level that is not constituted from harmonic tidal components (i.e. the tidal stream or tidal height)

Note 1 to entry: Residual currents are caused by a variety of physical mechanisms and comprise a large range of natural frequencies and magnitudes in different parts of the world.

3.29
return period
average period between occurrences of an event or of a particular value being exceeded

Note 1 to entry: The offshore industry commonly uses a return period measured in years for environmental events. For a rare event, the return period in years is equal to the reciprocal of the annual probability of exceedance of the event.

3.30
scatter diagram
joint probability of two or more (metocean) parameters

Note 1 to entry: A scatter diagram is especially used with wave parameters in the metocean context (for example in fatigue assessments). The wave scatter diagram is commonly understood to be the probability of the joint occurrence of the significant wave height (H_s) and a representative period (T_z or T_p).

3.31
sea floor
interface between the sea and the seabed and referring to the upper surface of all unconsolidated material

3.32
sea-state
condition of the sea during a period in which its statistics remain approximately stationary

Note 1 to entry: In a statistical sense the sea-state does not change markedly within the period. The period during which this condition exists depends on the particular weather condition at any given time, however it is often assumed to be three hours in extra-tropical conditions, however it may be as short as 1 hour in tropical cyclonic conditions.

3.33
seabed
materials below the sea in which a structure is founded, whether of soils such as sand, silt or clay, cemented material or of rock

3.34
seiche
oscillation of a body of water at its natural period

3.35
short-term distribution
probability distribution of a variable within a short interval of time during which conditions are assumed to be statistically stationary

Note 1 to entry: The interval chosen is most often the duration of a sea-state.

3.36
significant wave height
statistical measure of the height of waves in a sea-state

Note 1 to entry: The significant wave height was originally defined as the mean height of the highest one-third of the zero up-crossing waves in a sea-state. In most offshore data acquisition systems the significant wave height is currently taken as $4\sqrt{m_0}$, (where m_0 is the zeroth spectral moment, see 3.38 spectral moment) or 4σ, where σ is the standard deviation of the time series of water surface elevation over the duration of the measurement, typically a period of approximately 30 min.

3.37
site-averaging
averaging extreme values from a number of individual sites

Note 1 to entry: used to take account of the localised extent of phenomena such as tropical cyclones or meso-scale eddies e.g. warm core rings in the Gulf of Mexico

3.38
site-pooling
concatenating datasets from several sites into a single dataset for extremal analysis, with the length of the dataset equating to the sum of the individual datasets

Note 1 to entry: used to take account of the localised extent of phenomena such as tropical cyclones or meso-scale eddies e.g. warm core rings in the Gulf of Mexico

3.39
soliton
solitary wave or wave packet travelling on an internal density discontinuity which, as a result of the cancellation of nonlinear and dispersive effects, maintains its shape and speed over extended distances

EXAMPLE Internal tides which form on the density gradient within the water column may interact with the continental slope and form internal solitary wave packets.

3.40
spectral moment
n^{th} spectral moment
integral over frequency of the spectral density function multiplied by the nth power of the frequency, either expressed in hertz (cycles per second) as $m_n(f) = \int_0^\infty f^n S(f)\,df$ or expressed in circular frequency (radians/second) as $m_n(\omega) = \int_0^\infty \omega^n S(\omega)\,d\omega$

Note 1 to entry: As $\omega = 2\,\pi\,f$, the relationship between the two moment expressions is: $m_n(\omega) = (2\pi)^n\, m_n(f)$.

Note 2 to entry: The integration extends over the entire frequency range from zero to infinity. In practice the integration is often truncated at a frequency beyond which the contribution to the integral is negligible and/or the sensor no longer responds accurately. Care should be taken when utilizing moments of order higher than 2, as for standard spectral models, the 4th moment will not converge; the value is in effect determined by the choice of truncation.

3.41
spectral peak period
period of the maximum (peak) energy density in the spectrum

Note 1 to entry: In practice there is often more than one peak in a spectrum.

3.42
spectral density function
energy density function
spectrum
measure of the variance associated with a time-varying variable per unit frequency band and per unit directional sector

Note 1 to entry: Spectrum is a shorter expression for the full and formal name of spectral density function or energy density function.

Note 2 to entry: Within this part of ISO 19901, the concept of a spectrum applies to waves, wind turbulence and action effects (responses) that are caused by waves or wind turbulence. For waves, the spectrum is a measure of the energy traversing a given space.

3.43
squall
strong wind event characterized by a sudden onset, a duration of the order of minutes and often, a sudden decrease in speed

Note 1 to entry: A squall is often accompanied by a change in wind direction, a drop in barometric pressure, a drop in air temperature and heavy precipitation.

Note 2 to entry: The WMO classification of a squall requires the wind speed to increase by at least 8 m/s and attain a top speed of at least 11 m/s, lasting at least one minute in duration.

3.44
still water level
abstract water level used in the calculation of elevations at which actions are applied.

Note 1 to entry: still water level is typically used for the calculation of:

— wave kinematics for global actions,

— wave crest elevation for minimum deck elevations,

— maximum elevation of ice actions.

Note 2 to entry: Still water level, also referred to as storm water level, is an engineering abstraction calculated by adding the effects of tides and storm surge to the water depth but excluding variations due to waves (see Figure 1). It may be above or below mean sea level.

3.45
storm surge
change in sea level (either positive or negative) that is due to meteorological (rather than tidal) forcing

3.46
sustained wind speed
time averaged wind speed with an averaging duration of 10 min or longer at a specified elevation

3.47
swell
wave that was wind-generated but has travelled out of its generation area and has no relationship with the local wind

3.48
track-shifting
method of perturbing the track (intensity, radius) of historical tropical cyclones to increase the duration of the record artificially

3.49
tropical cyclone
closed atmospheric circulation around a zone of low pressure that originates over the tropical oceans

Note 1 to entry: The circulation is counter-clockwise in the northern hemisphere and clockwise in the southern hemisphere.

Note 2 to entry: At maturity, the tropical cyclone may be one of the most intense storms in the world, with wind speeds exceeding 90 m/s and accompanied by torrential rain.

Note 3 to entry: In some areas, local terms for tropical cyclones are used. For example, tropical cyclones are typically referred to as hurricanes in the Gulf of Mexico and North Atlantic, while in the East Asian Sea and NW Pacific they are called typhoons. In the South Pacific and South Indian Ocean, however, they are commonly referred to as cyclones.

Note 4 to entry: The term cyclone is also used to refer to a tropical storm with sustained wind speeds in excess of 32 m/s (Beaufort Force 12).

Note 5 to entry: In the Australian region the term 'tropical cyclone' refers to a warm-cored, non-frontal low-pressure system of synoptic scale developing over warm waters, and having organised convection and a (10-minute mean) wind speed of at least 34 knots (17,4 m/s), extending more than half way around near the centre and persisting for at least six hours.

3.50
tsunami
long period surface waves caused by displacement of a large volume of a body of water, normally an ocean

Note 1 to entry: The vertical movement of the sea floor is often associated with fault rupture during earthquakes or with seabed mud slides.

3.51
units
SI units are used throughout this document

3.52
water depth
vertical distance between the sea floor and still water level

Note 1 to entry: As there are several options for the still water level, there may be several water depth values. Generally, design water depth is determined to LAT or to mean sea level.

Note 2 to entry: The water depth used for calculating wave kinematics varies between the maximum water depth of the highest astronomical tide plus a positive storm surge, and the minimum water depth of the lowest astronomical tide less a negative storm surge, where applicable. The same maximum and minimum water depths are applicable to bottom-founded and floating structures, although water depth is usually a much less important parameter for floating structures. Water depth is, however, important for the design and analysis of the mooring system and risers for floating structures.

3.53
wave spectrum
measure of the amount of energy associated with the fluctuation of the sea surface elevation per unit frequency band and per unit directional sector

Note 1 to entry: The wave frequency spectrum (integrated over all directions) is often described by use of some parametric form such as the Pierson-Moskowitz or JONSWAP wave spectrum.

Note 2 to entry: The area under the wave spectrum is the zeroth spectral moment m_0, which is a measure of the total energy in the sea-state; m_0 is used in contemporary definitions of the significant wave height.

3.54
wave steepness
characteristic of individual waves defined as wave height divided by wave length

Note 1 to entry: For periodic waves, the concept is straightforward as H / λ. For random waves, the definition is normally used with the significant wave height (H_s) and the wavelength that corresponds with the mean zero crossing period (T_z) of the wave spectrum in deep water. The significant wave steepness is then defined as $H_s / \lambda_z = H_s / [(g/2\pi)\ T_z^2]$.

3.55
wind spectrum
measure of the variance associated with the fluctuating wind speed per unit frequency band

Note 1 to entry: The wind spectrum is an expression of the dynamic properties of the wind (turbulence). It reflects the fluctuations about and in the same direction as a certain mean wind speed, usually the 1 h sustained wind speed. There is hence no direction variable associated with the wind spectrum within this part of ISO 19901.

Note 2 to entry: As the sustained wind speed varies with elevation, the wind spectrum is a function of elevation.

4 Symbols and abbreviated terms

4.1 Symbols

$D(\theta)$	wave directional spreading function
$D(f,\theta)$	general form of the wave directional spreading function
d	water depth
$F_{coh}(f;P_1,P_2)$	coherence function between turbulence fluctuations at $P_1(x_1, y_1, z_1)$ and at $P_2(x_2, y_2, z_2)$
f	frequency in cycles per second (Hertz)
f_1	mean wave frequency of the wave spectrum ($f_1 = 1/T_1 = \omega_1 / (2\pi)$)
f_a	apparent wave frequency ($f_a = 1/T_a = \omega_a / (2\pi)$)
f_e	encounter wave frequency ($f_e = 1/T_e = \omega_e/ (2\pi)$)
f_i	intrinsic wave frequency ($f_i = 1/T_i = \omega_i/ (2\pi)$)
f_p	peak or modal frequency at the peak of the spectrum ($f_p = 1/T_p = \omega_p/ (2\pi)$)
f_z	average zero-crossing frequency of the water surface elevation ($f_z = 1/T_z = \omega_z/ (2\pi)$)
g	acceleration due to gravity
H	height of an individual wave
H_b	breaking wave height
H_N	maximum height of an individual wave having a return period of N years. Both H_{max} and H_{mp} are also used in this context
H_s	significant wave height
$I_u(z)$	wind turbulence intensity at z m above mean sea level
k	wave number = $2\ \pi / \lambda$
m_n	n^{th} spectral moment (either in terms of f or ω). In particular, m_0 is the zeroth spectral moment and is equivalent to σ^2, the variance of the corresponding time series

S	spectral density function, energy density function
$S(f)$, $S(\omega)$	wave frequency spectrum
$S(f, \theta)$, $S(\omega, \theta)$	directional wave spectrum
S_{JS}	JONSWAP spectrum for a sea-state
S_{PM}	Pierson-Moskowitz spectrum for a sea-state
S_{OH}	Ochi-Hubble spectrum for a total sea-state consisting of a combination of two sea-states with a general formulation
T	wave period; also period in general
T_0	standard reference time-averaging interval for wind speed of 1 h = 3 600 s
T_a	apparent period of a periodic wave (to an observer in an earth-bound reference frame)
T_e	encounter period of a periodic wave (to an observer in a reference frame that moves with respect to earth as well as the wave; the frame is usually fixed to a moving vessel)
T_i	intrinsic period of a periodic wave (in a reference frame that is stationary with respect to the wave, i.e. with no current present)
T_p	modal or peak period of the spectrum
T_z	mean zero-crossing period of the water surface elevation in a sea-state
T_1	mean period of the water surface elevation in a sea-state, defined by the zero and first-order spectral moments
t	Time
U_c	free stream current velocity
U_{c0}	surface current speed at $z = 0$
U_{ref}	reference wind speed, U_{ref} = 10 m/s
$U_c(z)$	current speed at elevation z ($z < 0$)
$U_w(z,t)$	spatially and temporally varying wind speed at elevation z above mean sea level and at time instant t
$U_w(z)$	mean wind speed at elevation z above mean sea level averaged over a specified time interval
$U_{w,1\,h}(z)$	1 h sustained wind speed at elevation z above mean sea level
$U_{w,T}(z)$	sustained wind speed at elevation z above mean sea level, averaged over time interval $T < 1$ h
U_{w0}	1 h sustained wind speed at 10 m above mean sea level (the standard reference speed for sustained winds)
$u_w(z,t)$	fluctuating wind speed at elevation z around $U_w(z)$ and in the same direction as the mean wind
$V_{in\text{-}line}$	component of the current velocity in-line with the direction of wave propagation
x,y,z	coordinates of a right-handed orthogonal coordinate system with the xy-plane at the undisturbed still water level (for waves and currents) or mean sea level (for winds) and the $z$axis positive upwards

z	vertical coordinate [measured upwards from the still water level (for waves and currents) or mean sea level (for winds)]
z_r	reference elevation for winds above the mean sea level, z_r = 10 m
z_s	stretched vertical coordinate for waves and currents (measured upwards from the still water level)
γ	shape parameter of the peak enhancement factor in the JONSWAP spectrum
η	water surface elevation above still water level as a function of time and location
θ	wave direction angle
$\bar{\theta}$	mean wave direction
θ_c	direction of the current velocity relative to the wave direction
Λ	wavelength or Ochi-Hubble spectrum peak enhancement factor
σ	standard deviation of the water surface elevation in a sea-state
σ_a, σ_b	parameters in the peak enhancement factor of the JONSWAP spectrum
σ_{sw}	parameter defining the width of the symmetric swell spectrum (equals the standard deviation of the Gaussian function)
ϕ	directional spreading factor
ω	angular frequency (radians per second $\omega = 2\pi f$)

4.2 Abbreviated terms

HAT	highest astronomical tide
LAT	lowest astronomical tide
MSL	mean sea level
PSU	practical salinity unit
UI	uncertainty interval
VIV	vortex-induced vibration

5 Determining the relevant metocean parameters

5.1 General

The owner or operator of an offshore installation is responsible for the selection of the environmental conditions applicable to specific design situations or for particular operations.

The selection shall consider:

— the type of structure being designed or assessed,

— the nature of the operation to be undertaken (e.g. construction, transportation, installation, drilling, production, etc.),

— the limit state considered (e.g. ultimate, fatigue, accidental),

— any additional company or regulatory requirements.

NOTE In addition to accidental events, the accidental limit states relate to abnormal environmental events, including abnormal level earthquakes (ALE), see ISO 19900.

The type of metocean information that may be required includes:

a) extreme and abnormal metocean parameters, which are required to develop extreme and abnormal environmental actions and/or action effects. These parameters are used to define design situation(s) while the extreme and abnormal environmental actions and/or action effects are used to perform design checks for ultimate limit states and accidental limit states respectively.

b) long-term distributions of metocean parameters in the form of cumulative conditional or marginal statistics. These parameters are used:

   — to define design situation(s) and to perform design checks for the fatigue limit state, or

   — to make evaluations of downtime/workability/operability during a certain period of time, for the structure or for associated items of equipment.

c) long-term time series of metocean parameters for use in response-based analyses.

d) short-term environmental conditions, which are required:

   — for carrying out checks for serviceability limit states,

   — for developing actions and action effects to determine when particular operations may safely take place, and

   — for planning construction activities (fabrication, transportation or installation) or field operations (e.g. drilling, production, offloading, underwater activities).

Depending on the geographical region and the offshore operations involved, other environmental conditions may be required for specific design situations or for particular operations.

5.2 Expert development of metocean criteria

Reliable estimates of (very) low probability environmental events may be made using a number of different approaches, including analysis of all data values, annual or monthly maxima, or peak-over-threshold events. Implicit in the use of each approach are assumptions about the data used, the statistical procedures applied, and the interpretation of the results.

Metocean experts are specialists who have knowledge spanning the areas of meteorological and oceanographic processes, data gathering techniques, data interpretation, statistical methods and offshore design practices to enable them to develop reliable criteria appropriate for differing types of designs or operations. Development of environmental conditions and associated metocean parameters for designs where actions (action effects) with long return periods are required shall be developed by or in consultation with a metocean expert.

For regions subject to continuous, seasonal or periodic ice events such as sea ice and icebergs, metocean experts should be supplemented by experts in the relevant ice hazards.

5.3 Selecting appropriate parameters for determining design actions and action effects

Environmental actions and associated action effects used in the design and assessment of offshore structures are dominated by one or more metocean parameters depending on factors including:

— the structural form (e.g. fixed jacket, semisubmersible or monohull),

— the geographical location (e.g. regions where strong currents may be present),

— the exposure of individual structural elements to wind, wave, current or ice action,

— the limit state being addressed.

Information on the metocean parameters appropriate to each structural form is presented in the relevant structure-specific standards in the ISO 19900 series of publications. The final choice of metocean parameters to be used to determine design actions or action effects should be carried out in consultation with structural engineers.

Where wave actions dominate, the wave condition(s) to be considered for a particular design situation may be specified through:

a) long-term statistical distributions of the oceanographic parameters describing the wave climate at the location of interest over many years;

   Where adequate data are available, the statistical distributions may reflect the joint occurrences of oceanographic parameters. Alternatively, only marginal distributions are provided. From these long-term distributions, appropriate oceanographic design parameters should be derived that are compatible with the design situations involved.

b) short-term descriptions of one or more design sea-states, in conjunction with one or more design values of winds and currents;

   A design sea-state should be described by a wave spectrum in terms of a significant wave height, a representative frequency or period, and a mean wave direction. Where appropriate, the wave spectrum may be supplemented with a directional spreading function, see 8.3. A design current is specified by a surface velocity and its velocity profile over the water column, including its direction, see Clause 9.

c) one or more individual design waves, in conjunction with one or more design winds and currents.

   A design wave shall be specified by its height and period, together with an appropriate wave theory from which the wave kinematics may be derived, as well as (an) associated direction(s), see Clause 8. A design current is specified by a surface velocity and its velocity profile over the water column including its direction, see Clause 9.

The above descriptions shall be supplemented by associated meteorological conditions that are relevant for the particular design situation considered. For strongly correlated parameters, whilst simple linear or non-linear regression models may be used to identify a most-probable or median associated value of other parameters, more advanced method (see A.5.3) better reflect the extremal correlation structures between two or more parameters. This approach also allows estimation of the conditional distribution of the associated parameter given the occurrence of the return period (RP) event. For sensitivity analyses, this allows a percentile range of the conditional distribution of the associated parameter to be used e.g. 2,5 % to 97,5 %.

For weakly or un-correlated parameters, the chances of simultaneous occurrence of extreme events of both parameters are very small. In this case, the return period event together with exploration of the action effects of a percentile range of the unconditional distribution of an associated parameter, again such as 2,5 % to 97,5 % should be used.

The selection of the most appropriate specification a), b) or c) above depends on the data that are available for the location of interest, the type of structure concerned, the design situation involved and the limit state considered. It is entirely appropriate that a different selection is made to suit different structure types, different design situations and different limit states.

If the current is known to dominate design actions on the structure, the selection of associated wave heights and wind speeds for a given current velocity should be considered.

If ice in the form of sea ice, icebergs etc. could occur, relevant design situations shall be defined and environmental parameters shall be developed in accordance with ISO 19906. ISO 19906 also includes provisions for other environmental phenomena encountered in arctic and cold regions, such as snow and ice accretion, and ice encroachment.

Where environmental actions for structural design are not dominated by wave, current or ice conditions (but, for example, by wind or earthquakes), special consideration shall be given to the selection of the relevant metocean parameters in combination with those other events.

5.4 The metocean database

A site-specific metocean database shall be established containing information on:

— significant wave heights, periods, directions and spreading,

— current speeds and directions at a number of depths throughout the water column,

— wind speeds and directions,

— sea ice, icebergs, snow and ice accretion,

— water levels, and

— other relevant metocean parameters (air and water temperatures, water salinity, etc.).

The database may be established either by site-specific measurements over a period of years or by numerical modelling (hindcasts) of historical events. If numerical simulations are used, the simulated results shall be calibrated (or verified) against appropriate measurements.

Where possible, the database should be sufficiently long to encompass all the physical processes which may be encountered during the lifetime of the structure. Where this is not possible, the metocean criteria derived directly from the database should be modified appropriately.

5.5 Storm types in a region

General information on the various types of storms which may affect the structure shall be used to supplement available data.

When determining the appropriate environmental conditions, it is important to separate storms of different types, for example, monsoons and typhoons, before performing an extreme value analysis. Furthermore, it may be necessary to set operating limits for a particular structure for particular storm types and seasons.

5.6 Directionality

In some locations, representative storm tracks and topographic features may provide fetch limitations on wave heights from specific directions, or tidal or general circulation currents may be in a predominant direction. For design in such situations, different wave, wind and/or current magnitudes may be used for different approach directions, provided that sufficient reliable data are available to derive them. However, the owner of the structure shall ensure that the overall reliability of the structure is not compromised by the use of such lower directional environmental conditions.

If reliable directional information is not available, conservative assumptions shall be made with respect to relative directions of winds, waves and current.

5.7 Extrapolation to extreme and abnormal conditions

Designers require metocean parameters at (very) low probabilities or recurrence rates, e.g. with a return period of 100, 1 000 or 10 000 years. Where data covering such long periods are not available, an extrapolation of existing data is necessary. Many extrapolation methods are used and there is no universally accepted method; expert advice should be sought, and the following key elements of the extrapolation methodology are important to consider:

— Extrapolations based on continuous frequency distributions are strongly discouraged. Peaks-over-threshold (storm-based) or block maxima approaches support statistical independence for the data points in the extrapolated data set.

— For water levels and currents, extrapolation should be carried out on the nondeterministic (residual) component only. The deterministic (tidal) components should be added to the extrapolated residual component on the basis of joint-probability analyses if sufficient data exists. If insufficient data exists for

the tidal component, add the Mean High-Water Spring for diurnal and semi-diurnal tidal locations; or, for mixed tidal locations, add the Mean Higher High Water.

In general, the longer the data set the more accurate the extrapolation will be. However, even with long data sets, estimates of (very) low probability parameters can still depend to a considerable degree on the extrapolation method and sampling variability. Confidence intervals can be estimated to assess the uncertainty due to sampling variability.

For some phenomena for which the area of most extreme conditions in an event is quite limited compared to the overall area of the region in which they occur, such as tropical cyclones in the Gulf of Mexico and offshore Northwest Australia, or the Loop Current and warm core rings (eddies) in the Gulf of Mexico, site-averaging (calculating extremes at individual sites, and averaging the results together) or site-pooling (concatenating the hindcast data from several sites into one set, with length of the combined set equal to the length of the hindcast period multiplied by the number of sites) is recommended for the determination of extremes. These techniques serve to smooth out local variability in extremes determined at single locations resulting from the limited area of affect of these phenomena. An important consideration in applying site-averaging or site-pooling is to choose sites which are far enough apart such that they provide independent realizations of the local conditions, but not to choose sites which are so far apart that true spatial variations in extremes are smoothed over. For tropical cyclones, where site-averaging or site-pooling is not feasible due to proximity to irregular coastlines or the presence of islands, track-shifting may be applied, whereby the tracks of historical storms are randomly perturbed, assuming the population of storms repeats over time. Care should be taken in inferring great reductions in uncertainty when site-pooling (or tracking shifting), for while the effective length of the data set is multiples of the length of the hindcast record, a key assumption is made that the overall regional climate will repeat multiple times with little variation, i.e. no events more severe than those observed will occur, and those that do occur, will follow tracks or paths similar (but not completely identical) to those observed historically.

Monte Carlo methods can also be used to create synthetic databases of phenomena like tropical cyclones or warm-core rings associated with boundary current features, for the assessment of extreme (100 years) and abnormal (10,000 years) conditions. Care should be taken to ensure an adequate historical record of the parameters needed to characterize the phenomena is used in developing the synthetic model.

5.8 Metocean parameters for fatigue assessments

The fatigue limit state may govern the design of individual structural components in fixed and floating offshore structures in several parts of the world.

Fatigue is an accumulation of damage caused by the repeated application of time-varying stresses which may result from the environmental actions to which the structure is exposed.

Fatigue limit state assessment of a structure requires specification of all environmental conditions that are expected to occur during the entire period of the structure's exposure, i.e. its construction phase, including transportation, and its design service life. The specification of the environment is given by the long-term distribution(s) of one or more metocean parameters. The metocean parameters relevant for the fatigue assessment depend on the type of structure and the location under consideration. The distribution(s) of the relevant parameter(s) shall be determined from the metocean database, taking due account of the requirements for the structure being considered.

When computing the cumulative fatigue damage over the life of the structure using the distribution of relevant parameters, it should be kept in mind that this is an estimate of the expected long-term fatigue damage. In such assessments, by their very nature, rare events are weighted with a low probability of occurrence. In some cases, however, it should be considered how much damage a structure may accumulate during a rare event which imposes a relatively low number of very large amplitude stress cycles. Such “low-cycle fatigue assessments” ensure that the occurrence of a single extreme or abnormal event does not consume a significant proportion of the overall fatigue life of a structural system.

For some components and types of structures, cyclic stresses due to vortex-induced vibrations (VIV) in steady currents or winds should also be considered.

Structures in ice environments may experience dynamic ice actions and ice-induced vibrations that should be considered in accordance with ISO 19906.

Information on the metocean parameters appropriate to the fatigue assessment of different forms of offshore structure is presented in the relevant structure specific standard in the ISO 19900 series of publications.

5.9 Metocean parameters for short-term activities

Transportation, installation, maintenance and removal of a structure are scheduled activities that are weather-sensitive. Operation of a structure includes regular and routine activities that are also weather-sensitive. Some of these activities are sensitive to high winds, while others are sensitive to currents, swell, wave heights, wave periods, wave directions or combinations thereof.

Examples of weather-sensitive scheduled short-term activities are:

a) transportation of the structure over a relatively short distance,

b) installation of fixed steel offshore structures, including;

   1) lifting, launching, upending and placement on the seabed,

   2) the period following placement but prior to and during piling, and

   3) the period following piling but prior to and during pile grouting and until the grout sets,

c) installation of fixed concrete offshore structures, including;

   1) placement on the seabed, and

   2) the period following placement but prior to and during any grouting and until grout setting,

d) establishment/re-establishment of a floating structure at the operating location, including the setting of mooring systems,

e) installation and foundation pre-loading for jack-ups,

f) topsides installation,

g) underwater operations, including inspection and repair, and

h) removal for decommissioning or reuse.

As well as being critical and expensive, these activities usually require a weather window with low environmental conditions for significant durations, e.g. sufficient to allow for all piling and pile fixing. Consequently, the accuracy of short-term forecasting may be as important as the values of the metocean parameters.

Examples of routine activities that are weather-sensitive include:

— use of cranes for lifting to and from supply boats;

— use of cranes for moving items around decks;

— under-deck access;

— use of drilling derrick, particularly derrick movements;

— helicopter movements;

— personnel transfer operations by boat.

These activities generally have different weather sensitivities.

Limiting criteria shall be established for each activity. In many cases the limitations are established by considering the safety of personnel.

It is useful in the planning of a development or the planning of a specific activity to know that the probability of the metocean parameters exceeding the criteria for particular activities is sufficiently low for sufficient time to complete these activities. The probability of sufficiently calm conditions for a given location typically varies on a seasonal basis.

Predictions of the variation in the relevant metocean parameters should be made from the metocean database. Predictions should provide either the proportion of time and the durations for which metocean parameters are expected to remain within limiting criteria, or the probability of the values of certain metocean parameters being exceeded. Seasonal variations (by month or by quarter) should be reported if these are significant. In addition, it should be considered and made clear to users of such criteria that in addition to seasonal variations in operational conditions, there may be significant year-to-year variations.

In order to identify an appropriate weather window within which to perform the short-term activity, a weather forecast will be required. This shall be provided by a competent organisation. Section 12 provides details concerning the verification of forecast products.

5.10 Metocean parameters for medium-term activities

Medium-term activities such as tows and transportation of a structure or structural members, particularly when involving long exposed tows, are scheduled activities which are weather sensitive but which have durations significantly longer than the length of the available weather forecast; typically in excess of 72 hours. For such activities, certain design criteria may be required, such as sea-fastening load criteria.

For transportation, the design criteria should be defined, consisting of the design wave, design wind and, if relevant, design current. Where the transportation transits through different geographical areas, the maximum wave and maximum wind may not occur in the same area, in which case it is necessary to check the extremes in each area, to establish governing load cases.

To derive return period metocean extremes for ocean-going tows, an industry recognised methodology (e.g. SafeTrans) or other certified methods or standards should be used.

Weather forecasts play an important role in the planning and execution of medium-term activities. As such, a weather forecast shall be provided by a competent organisation.

6 Water depth, tides and storm surges

6.1 General

The water depth at the site, including variations in the water depth, shall be determined where significant for the type of structure being considered.

The range of water depths at a particular site is important for the design of structures as it affects several parameters, including:

— environmental actions on the structure,

— elevations of boat landings, fenders, and cellar deck on bottom-founded structures,

— riser length/stroke on floating structures, and

— mooring forces for taut or vertically moored floating structures.

For the purpose of design or assessment, the water depth may be considered to consist of a more or less stationary component, this being the water depth to a reference chart datum (e.g. LAT or MSL), and variations with time relative to this level (see Figure 1). The variations are due to the astronomical tide (see 6.2) and to the wind and atmospheric pressure, which may create storm surges (which may be positive or negative) (see 6.3). Other variations in water level may result from long-term climatic variations, sea floor subsidence or

episodic events such as tsunamis. Water level variations may have a relatively minor impact in deep water, but may be considerably more important in shallow water.

It is important for the design of all structures (and in particular bottom-founded structures in shallow water) to have a good knowledge of the joint distribution of the tide, the storm surge height and the crest and trough elevations of the waves.

6.2 Tides

Tidal variations are the result of the gravitational and rotational interaction between the sun, moon and earth and are regular and largely predictable; they are bounded by the highest astronomical tide (HAT) and the lowest astronomical tide (LAT) at the site.

The variations in elevation of the daily astronomical tides determine the elevations of boat landings, fenders, splash-zone treatment, conductors and risers, and the upper limits of marine growth for bottom-founded structures.

At latitudes where the inertial period is close to the diurnal and semi-diurnal periods, the inertial energy may cause inaccuracies in the tidal harmonic analysis. This may particularly affect the latitudes close to 30 degrees in both the northern and southern hemispheres.

Tidal levels shall be established from a minimum of 6 weeks, preferably 12 months of high quality, site specific, water level measurements. Harmonic analysis shall be undertaken to establish the HAT and LAT, using a prediction over a period of 18,6 years.

The residual water levels shall be determined as the deviation of the predicted water levels from the measured water levels.

6.3 Storm surges

Storm surges are meteorologically generated. Since the generation of surges is unrelated to tides, their occurrences are randomly superimposed on tidal variations. In deep and modest water depths, tidal and storm surge elevations may be arithmetically added to good approximation. In shallow water, tide and surge may interact due to nonlinear bottom friction effects. Since surges cause water level variations additional to tides, total still water levels above HAT and below LAT may occur.

6.4 Extreme water level

The extreme water level is derived through a combination of 'design crest elevation', astronomical tide and 'storm surge' referenced to either LAT or MSL.

The combination is best calculated by using the joint probability of occurrence of tide, surge and wave crest. However, if there are insufficient data to model this reliably, conservative assumptions may be used, e.g. summation of the ‘design crest elevation’ and the ‘still water level’ of the same return period. Note that the method described in ISO 19902 for determining the deck height in Section A.6.3.3.2 is indicative and should not be used for final design purposes.

The effects of climate change on mean sea level over the lifetime of a structure should be assessed, especially for projects with 30+ year life spans. The latest Intergovernmental Panel on Climate Change (IPCC) provides recommendations on sea level rise that may be adopted. Alternatively, site-specific data may be collected and analysed.

Extreme water level is a starting point for ascertaining the minimum height of the main deck of a bottom-founded structure. Allowance should also be made for platform settlement, reservoir subsidence and water depth uncertainty.

Structures with large diameter columns may modify the incident wave field, resulting in changes to the extreme water level (and other wave properties) estimated in the absence of wave/structure interactions. Such changes may need to be addressed as part of the design process.

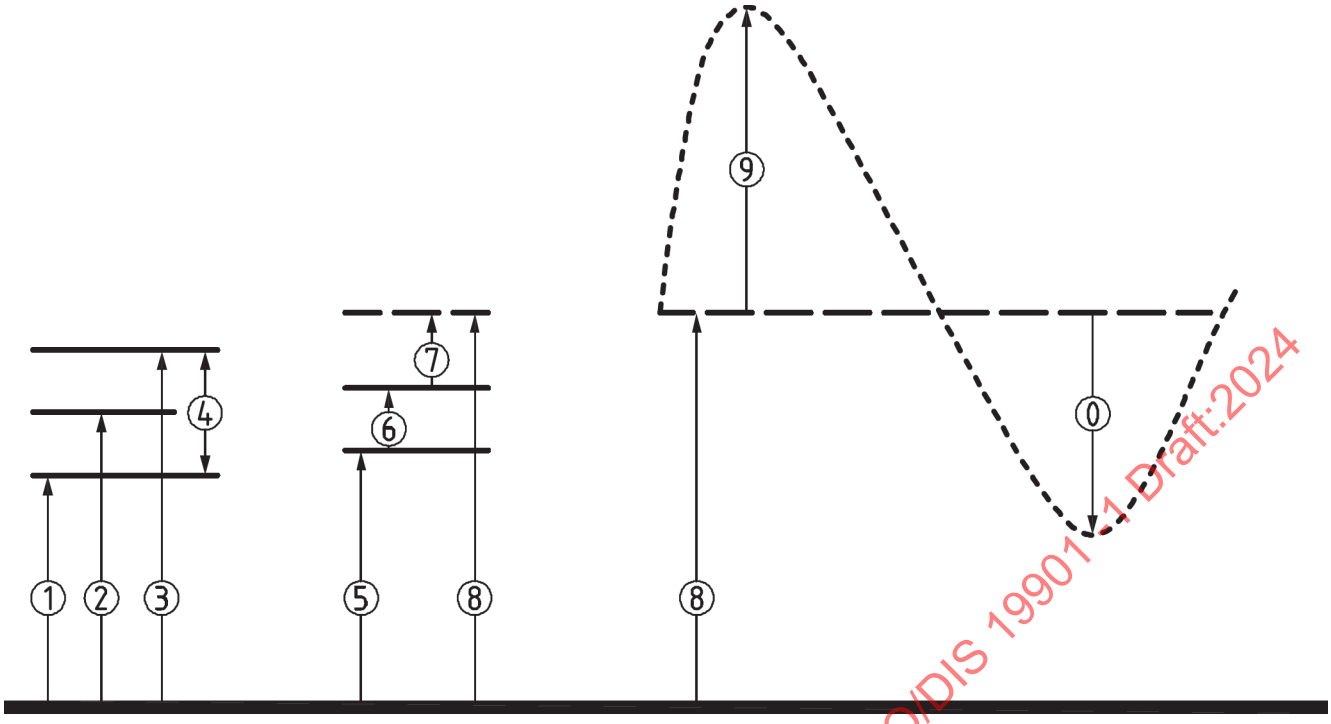

a) Tides **b) Tide + storm surge = still water level** **c) Wave profile superimposed on water level**

Key

Key to distance elevations

1	Lowest astronomical tide (LAT)	6	Tide associated with storm (shown positive but may be positive or negative)
2	Mean sea level (MSL)	7	Storm surge (shown positive but may be positive or negative)
3	Highest astronomical tide (HAT)	8	Still water (or 'storm water') level
4	Tidal range	9	Crest elevation
5	Tidal datum (commonly LAT or MSL but may be other)	0	Trough elevation

Key line types

▬▬▬	Seafloor
———	Tide levels
— — —	Surge or surge+tide levels
-------	Wave profile

Figure 1 — Water depth, tides and storm surges

7 Wind

7.1 General

Wind speed and direction vary in space and time. Normally, wind speed time-series data at a site are only available at a single elevation. It is unusual to have multiple measurements on the tens to hundreds of metres horizontal-length scales relevant to offshore structures. Furthermore, time series are often only available at time scales much longer (e.g. 10 min to 3 h) than the natural response periods of most structures. On length scales typical of even the largest offshore structures, the mean and standard deviation of the wind speed, averaged over durations of the order of an hour, do not vary horizontally, but they do change with elevation (wind profile). For averaging durations shorter than 1 h, there will be periods with higher mean speeds and increased spatial variation. As such, typical practice is to specify wind criteria at a clearly specified averaging interval and reference elevation. The most commonly used reference elevation is 10 m above mean sea level. Wind profile factors, gust factors, auto- or coherence spectra appropriate to the local wind

regime may then be applied in conjunction with the reference winds to appropriately account for fine-scale spatial and temporal effects.

Wind speeds are classified as either:

— sustained wind speeds, or

— gust wind speeds.

The elevation and averaging interval of any wind speed or gust should always be reported.

Extreme gusts occur due to a variety of phenomena. These include squalls, thunderstorms, downbursts, tornados, water spouts, all of which are relatively short-lived. The ratio of maximum gust wind speed to hourly mean wind speed at any one location in these examples may be large.

However, gusts also occur during periods of high hourly mean wind speed due simply to turbulence, but in this case the ratio of maximum gust wind speed to hourly mean wind speed over the sea is typically less than about 1,5.

Wind conditions shall be determined by proper analysis of wind data. Guidance on collecting wind data is given in A.7.1.

To determine appropriate design situations for offshore structures with regard to wind, the extreme, abnormal and operationally relevant wind conditions shall be specified in accordance with the type of structure and the nature of the structure's response. Wind turbulence in gusts has three-dimensional spatial scales related to their duration. For example, 3 s gusts are coherent over shorter distances and therefore affect smaller components of a structure than 15 s gusts. For structures (structural components) that are subject to appreciable dynamic response, it may be necessary to take the time variation of actions caused by wind into account.

Further guidance is provided below, while procedures for determining actions and action effects caused by wind for different types of structure shall be in accordance with the relevant structure-specific standard in the ISO 19900 series of publications.

7.2 Wind actions and action effects

Wind acts on the topsides and that portion of the structure that is above the water, as well as upon any equipment, deck houses, bridges, flare-booms and derricks that are located on the topsides. As the wind speed varies with elevation, the height of the component shall be taken into account. A vertical wind profile that may be used is discussed in 7.3 and provided in A.7.3.

For the design of offshore structures that respond globally in a nearly static fashion, global actions caused by wind are generally much less important than those caused by waves and currents. However, for the local response of certain parts or of individual components of these structures, the action effects caused by wind may be significant. Global actions on structures shall be determined using a time-averaged design speed in the form of a sustained wind speed. For the design of individual structural components, a time-averaged wind speed may also be adequate, but the averaging duration shall be reduced to allow for the smaller turbulence scale that may affect individual components. Local actions on individual components shall therefore be determined using a gust wind speed. Guidance on the selection of appropriate averaging times is given in A.7.2.

For the design of offshore structures (or structural components) that are subject to appreciable dynamic response, the time and spatial variation of the wind speed needs to be accounted for. A dynamic analysis of a structure (or structural components) is generally necessary when the wind field contains energy at frequencies near the natural frequencies of the structure (structural components). Such analyses require detailed knowledge of the wind turbulence intensity, the wind frequency spectrum and its spatial coherence (see 7.4).

A special case of dynamic response is the VIV of relatively slender structures subjected to steady winds in which alternate vortex shedding excites components. Components of fixed steel offshore structures may

be exposed to VIV during construction and transportation. Flare structures and telecommunication towers may also be susceptible to VIV throughout their lives.

Wind should be considered in detail for compliant bottom-founded structures and floating structures.

7.3 Wind profile and time-averaged wind speed

The vertical profile of the mean wind speed in storms is usually expressed by a logarithmic function. Adjustments to the wind profile at a particular location or under certain conditions may be made when appropriate measured data from an offshore location are available (i.e. measured data for the kind of event used in design).

7.4 Wind spectra

If a structure (or a structural component) exhibits appreciable dynamic response due to wind action, the temporal and spatial variations of the wind speed shall be considered. Turbulent wind may be viewed as an evolving field of vortices being swept past the structure. Additional turbulence is generated by the structure itself. The most accurate wind actions are derived from physical testing in a boundary-layer wind tunnel, or by using computational fluid dynamics. Useable results may be obtained from a time series of wind velocity generated by adding spectral frequency components (mathematically as described below for waves) to the mean wind speed. In the absence of three-dimensional wind modelling, only the speed fluctuations in the mean wind direction may be described. An appropriate form of the frequency spectrum for wind speeds in the mean direction is given in A.7.4. The spatial variation of the wind speed in the mean direction between two points in space is expressed by means of a coherence function (see A.7.4).

The concept of a wind spectrum is only applicable to stationary wind conditions. As squalls are transient (non-stationary), the temporal and spatial variations of the wind speed in a squall cannot be described by a wind spectrum. Analysis of actions and action effects caused by squalls requires the specification of a time series of wind velocity, which captures the transient squall peak.

8 Waves

8.1 General

Surface waves are generally very important for the design of offshore and coastal structures. Facility design requires the specification of the operational wave statistics and extreme and abnormal return-period wave conditions comprising spectral and/or deterministic wave height and period parameters, direction of wave propagation and the spread of the directions.

Ocean waves are irregular in shape, vary in height, length and speed of propagation, and travel in many directions. In general, small waves in deep water may be regarded as the linear superimposition of many small individual sinusoidal components, each of which is a periodic wave with its own amplitude, frequency and direction of propagation; with linear waves the components have random phase relationships with respect to each other. Linear superposition of waves may be described as a wave spectrum defining the amplitude of waves for frequencies and directions.

For larger waves, generally occurring at low probabilities (long return periods), waves are not linear. Interactions of wave components of differing frequencies and directions change the shape of the waves, an effect being that higher wave crests occur compared to those estimated using linear wave assumptions. In intermediate and shallow water depths, the nonlinearity of the waves increases and becomes very important.

Waves may be described as either:

— a sea-state, defined by either the frequency-direction wave spectrum or the frequency spectrum (see 8.3) or

— an individual wave, defined by wave height (or crest height), period and water depth (this wave is also called a deterministic or single wave) (see 8.4).

In a sea-state, the wave energy may be distinguished into two broad classes: wind-seas and swells. Wind-seas are generated by the local wind, while swells consist of wind-driven waves that have travelled out of the generation area, and have no relationship with the local wind.

The range of wave conditions that may occur at the site of the structure shall be specified. For operational conditions, details of the occurrence and joint occurrence of wave heights, periods, directions, spectral shape and spreading of waves shall be specified. For extreme or abnormal conditions, the return-period values of waves shall be specified. Associated values and ranges of wave periods and water depths shall also be specified.

It may be required to partition the wave energy spectrum into swell and wind sea components.

In determining the operational, extreme or abnormal wave conditions, the physical processes which lead to the wave forms at the site shall be considered. In this respect, nonlinear effects may be significant (e.g. breaking).

The response of a structure to waves depends on, among other things, its dynamic response characteristics. Structures with significant dynamic response (i.e natural periods around the wave frequencies or their second-order components) require wave energy spectra or time series of the surface elevation for their analysis. These may be specified in a number of ways; a common approach is to use a sea-state defined by a standard wave frequency spectrum, with a given significant wave height, a representative frequency/period, a mean wave direction and, sometimes, a directional spreading function. It is important to define the range of wave conditions which may be experienced at the facility site.

For structures that only respond in a quasi-static manner, it may be sufficient to use individual periodic waves. The most important wave parameters required to describe a single, periodic design wave are its height, crest elevation above still water level, period and direction of travel. The wave kinematics properties may then be estimated using the local still water depth. The distribution of individual waves in a given sea-state may be estimated from statistical wave parameters, such as the significant wave height and the mean zero-crossing period.

In some applications, periodic or regular waves may be used as an adequate abstraction of a real sea for design purposes. Periodic waves are also the building blocks for the linear random wave model. Where closer agreement to real waves is required, fully nonlinear wave models are available for use, but require careful calibration for application to design conditions to ensure consistent structural reliability levels are achieved.

It is often desirable to specify the duration associated with sea-states. Traditionally, 3 h durations are often specified. However, durations actually depend on the particular weather situation and how the criteria will be applied to design. In differing parts of the world, significant wave heights near the peak of a storm may be nearly constant over durations that could either be significantly shorter or significantly longer than 3 h. Furthermore, if the intention of specifying a duration is to design to a response at a given *N*-year target return period level, then the duration necessary to achieve this response shall be carefully considered. The *N*-year response is not necessarily achieved during the peak of the *N*-year sea-state. The most rigorous way to ensure that the *N*-year response is achieved is through a response-based design approach.

8.2 Wave actions and action effects

Wave conditions shall be specified in an appropriate way for the type of structure under consideration, for extreme, abnormal and normal (operating) conditions.

The linear spectral model for waves is presented in 8.3. Regular periodic wave models are presented in 8.4. The height of the highest wave crests in extreme and abnormal metocean conditions may be of special significance, see 8.7.

Procedures for determining actions and action effects caused by waves for different types of structure shall be in accordance with the relevant structure-specific standard in the ISO 19900 series of publications.

8.3 Sea-states — Spectral waves

8.3.1 Wave spectrum

The sea-state may be described in terms of the linear random wave model by specifying a wave spectrum, that defines the energy in different frequency and/or direction bands. In most cases, the wave spectrum is represented by empirical equations defining the distribution of energy over frequency and/or direction. Parameters typically required for defining a wave spectrum for design are the significant wave height and a representative frequency or period. For many applications, wave direction, wave spreading and peakedness of the wave spectrum are also required.

There are several standard wave-frequency spectra in use; the most appropriate spectral form depends on the geographical area, the severity of the sea-state and the application concerned.

Wave spectra may be determined from site-specific measurements and numerical wave modelling. Use of wave spectra from measurements generally provides the more accurate description of the spectral content of the sea-state, and should be used in preference to numerical models to define ambient spectral shapes and extreme spectral shapes. Spectral fitting to measured spectra is generally required for application to design, though in some cases this will not be adequate and measured spectra should be recommended for direct application to design (e.g. where the wave spectrum is used to drive response models within a response-based approach).

Spectral fitting should be used to define spectral shapes with parametric forms of wave spectrum, and the parameters of the selected spectral shape should be defined as part of the ambient and extreme design metocean conditions.

Further discussion and guidance on wave spectra and the most common parametric forms for the wave spectrum are given in A.8.3.1.

8.3.2 Directional spreading

As the water surface elevation in a sea-state is in reality three-dimensional (short-crested), the wave frequency spectrum may be supplemented by a directional spreading function. Parametric forms for the wave directional spreading function are given in A.8.3.2.

8.3.3 Wave periods

The spectral description of waves requires specification of a representative wave period, for example, the peak spectral wave period. Other wave periods (e.g. the average zero crossing period) or a range of periods may also be required to support specific forms of analyses.

8.3.4 Wave kinematics — Velocities and accelerations

Linear (or Airy) theory is a first-order approximation for real waves. It is based upon a linearization of the free-surface boundary conditions and as such is only valid for waves of low steepness.

Wave kinematics may be determined from a wave spectrum by linear superposition of the individual components of wave velocity and acceleration. However, extrapolation of the kinematics associated with the higher frequency components into the crest of a wave may lead to significant errors. This is often referred to as 'high frequency' contamination. Commonly applied engineering approximations avoid this by stretching the kinematics to the instantaneous free surface; for example, using linear stretching [also known as Wheeler stretching or Delta stretching (see A.8.4.2 and A.9.4.1)]. These approximations may be non-conservative and so should only be used where their application may be shown to be justified.

Better approximations are recommended and are provided by nonlinear wave models (see 8.6).

8.4 Regular (periodic) waves

8.4.1 General

A single regular (periodic) wave may be defined by characteristic parameters, for example, height and period. Water depth is also required. The characteristic parameters should be chosen to suit both the wave theory to be applied and the loading recipe. For example, when applying a 'Stokes 5th wave theory' approach within the context of the API RP 2A loading recipe (for fixed jacket platform design), the height and period should be the zero-downcrossing height and period.

For determination of actions by individual waves on structures, a nonlinear periodic wave theory may be used with a calibrated loading recipe. Calibrated loading recipes for drag-dominated structures are coded in typical loading software. Stokes 5th wave theory is commonly used for these types of structure. Other wave theories, such as Extended Velocity Potential and Chappelear theory, may also be used, if used with a loading recipe calibrated for these wave theories. An appropriate order of numerical solution shall be selected as appropriate to the water depth, wave height and wavelength.

As an alternative to periodic wave theories, representative waves from a random sea derived with wave theories such as New-wave theory may be used.

In addition, realistic representation of ocean waves is possible with fully nonlinear numerical wave models, but their use in the calculation of design actions shall be calibrated.

8.4.2 Wave period

The period of the regular (periodic) wave should be established to be consistent with the sea-state(s) in which the wave is likely to exist.

8.4.3 Wave kinematics — Velocities and accelerations

Wave particle velocities and accelerations for periodic waves may be calculated using an appropriately selected wave theory.

Discussion on the wave theories, range of convergence and references is given in A.8.4.

Most periodic wave theories do not account for wave directional spreading in their kinematics. Where appropriate, directional spreading may be approximately modelled in periodic waves by multiplying the horizontal velocities and accelerations by a wave directional spreading factor ϕ (see A.8.3.2.2).

The choice of whether to determine wave kinematics on the basis of non-breaking wave or breaking wave kinematics should normally be made on the basis of the wave being assessed. However, the extra effort required to calculate breaking wave kinematics may not be warranted if it may be demonstrated that the associated actions represent an insignificant contribution to overall actions being assessed.

8.4.3.1 Non-Breaking Waves

Away from a wave crest, or if the waves are not highly nonlinear or breaking, simpler models may be used which may be delineated by the effective water depth. This may be defined in terms of kp.d, where kp is the wave-number corresponding to the spectral peak, and d is the water depth. In the case of:

— Intermediate and deep water (kp.d ≥ 1,2), second-order irregular wave theory should be used.

— Intermediate to shallow water when the waves remain in the dispersive regime (0,6 ≥ kp.d ≥ 1,2), very few simple wave models are accurate, Molin Stretching should be used.

— Shallow water where the waves are non-dispersive (kp.d ≤ 0,6) a high order Stream function solution should be used.

Alternative solutions that neglect either the irregularity or nonlinearity of waves, and that do not consider wave breaking, may be used, including:

— Wheeler stretching, or

— Delta stretching, or

— Stokes V solutions.

Note All simpler models or alternative solutions may underestimate the velocities in the crest of a wave. However, they may be appropriate provided that the design recipe has been calibrated for the conditions to which these approximations are being applied.

8.4.3.2 Breaking Waves

Waves in the ocean are irregular, nonlinear, directionally spread and may break through spilling or plunging. The occurrence of wave breaking is not restricted to shallow water and may occur in any water depth.

Wave breaking may result in a large increase in water particle velocities at high elevations in the crest of a wave.

Note The inclusion of wave breaking is important for calculating wave-in-deck loads, local loading on elements high in the water column and wave slamming on columns.

In instances where wave-breaking provides the governing load case and is not already accounted for in the design recipe, breaking wave kinematics calculation may be based on one or more of the following methods:

— fully nonlinear wave models; and/or

— computational fluid dynamics (CFD); and/or

— laboratory testing; and/or

— full scale measurements.

Validation could be through comparisons with laboratory test results or by comparison with independent CFD models.

8.4.4 Intrinsic, apparent and encounter wave periods

Wave periods appear to differ depending on the relative velocities of wave propagation and the reference frame of an observer. This is due to the Doppler effect. For example, an observer moving against the direction of the waves encounters successive wave crests more quickly than an observer travelling in the same direction as the waves.

When waves are superimposed on a (uniform) current, the intrinsic reference frame for the waves travels at the speed and in the direction of the underlying current.

Three particular situations are as follows.

a) An observer travelling at the same speed and in the same direction as the current is stationary with respect to the intrinsic reference frame and will therefore measure the intrinsic wave period T_i.

b) An observer on a fixed structure is stationary relative to the seabed and measures the apparent wave period, T_a. If the waves are travelling in the same direction as the current, approaching wave crests pass the structure more quickly than if there was no current and consequently the apparent period is shorter than the intrinsic period. Similarly, if the waves are travelling against the current the apparent period is longer than the intrinsic period. If there is no current, the fixed structure is stationary with respect to the intrinsic reference frame and hence $T_a = T_i$.

c) An observer on a moving vessel (having a velocity relative to the seabed) measures the encounter wave period, T_e. The difference between T_e and T_i depends on the relative speeds and directions of the moving vessel and of the current. If the moving vessel is travelling at the same speed and in the same direction as the current, then $T_e = T_i$.

See A.8.4.4 for the relationship between T_i, T_a and T_e.

Wave kinematics for the calculation of actions caused by waves shall be derived from the intrinsic wave period (or the intrinsic wave frequency).

8.5 Maximum height of an individual wave for long return periods

If regular (periodic) waves are adequate for use as a design wave for an offshore structure, the height of an individual wave with a specified return period (e.g. H_{100}) shall be used.

The data derived from measurement programmes or provided directly from hindcasts are typically time series of significant wave height (Hs) and representative periods such as mean zero-crossing period (Tz) or spectral peak period (Tp). The required long-term individual wave height for a return period of N years, H_N, should be established by convolution of long-term distributions derived from these data with a short-term distribution of individual wave heights in a sea state. This can either be done using numerical integration or Monte Carlo approaches. Calculation of the wave in this manner differs from the calculation of the expected maximum wave in a sea state, which, if determined for the N year sea state, will be less than the true N year individual maximum wave height (or crest).

For deep and intermediate water depth locations, the Forristall distribution generally provides a good estimate of the wave heights in many sea states although some experimental results indicate that where non-linear effects are significant it may under-estimate the maxima. For shallow water, the Forristall distribution tends to be conservative for large sea states as it does not include the effects of wave breaking. For locations dominated by long-period swell, the Rayleigh distribution may provide the best characterization of the wave heights.

Further details are presented in A.8.5.

8.6 Linear and non linear wave models

Either linear spectral waves or periodic waves are commonly applied in the design of offshore and coastal facilities. However, these representations are an abstraction of real ocean waves. Linear spectral representations ignore the nonlinear interactions between waves of different frequencies and directions, whereas periodic waves ignore the irregular nature of waves. The linear random wave models and regular waves most often used for design and analysis are convenient approximations. However, they are not always very accurate in defining the position of the free surface, kinematics beneath the surface or, in consequence, local or global actions. Neither regular nor linear random wave theories give the correct elevation of the wave crest or kinematics over the water column.

Real ocean surface waves are random, broad-banded, directionally spread and nonlinear. Thus, for many purposes, a more accurate nonlinear carefully calibrated random wave model may be helpful, or even essential.

In practice, the extension of spectral representations to second order may provide an adequate approximation of the surface profile and kinematics of moderately steep waves when considering global loads on a bottom-founded structure. However, where waves become steep and/or break the kinematics in the vicinity of the crest of the wave will be significantly larger than those derived using standard linear or second order wave models. Therefore, in cases where these wave crests impact topside components or other structural elements (such as Emergency Shut-Down Valves or caissons), the loading will be much higher, and a fully nonlinear model shall be used to calculate the loading.

8.7 Wave crest elevation

Distributions of extreme and abnormal crest elevations which account for the nonlinear nature of large-amplitude waves are required for setting minimum deck heights on bottom-founded structures and for assessing the probability of green water intruding onto the topsides of all types of structures, decks and hulls which are intended to be kept above the waves.

For structures where there can be significant wave-structure interaction (e.g. for structures with a caisson or with very large diameter legs), the possible enhancement of the crest elevation due to the presence of

the structure shall be considered. This enhancement often does not lead to large increases in the global actions on the structure, but can impose significant local pressures on items located on the underside of the topsides. It can also impede operations (particularly under-deck) and local measures to reduce its effect can be necessary.

The statistics of the wave crest elevation component of the total water level (i.e. the combination of crest, tide and surge) should be determined both for a single point in space (i.e. point statistics) and also for an area equivalent to that covered by the lowest topsides structural element (i.e. area statistics). The latter approach accounts for short-crestedness of seas and reflects the increased chance of a crest impacting somewhere on the deck as its area increases.

For structures which are sensitive to exceedance of airgap, consideration should be given to the increased probability of exceedance associated with the effect of area statistics when assessing structural reliability against the target implied by the relevant code and the calculation of local loading on safety critical elements that sit below the design total water level.

In shallow water and for gently-sloping seabeds of gradients less than 1 in 100, the non-linear behaviour of waves should be considered.

9 Currents

9.1 General

Currents affect the design, construction and operation of offshore structures in various ways. In addition to their impact on the environmental actions and action effects on the structure, they affect the location and orientation of boat landings and fenders, may create sea floor scouring, and often have an adverse effect on operating practices. All of these factors may influence the structure's design.

The current velocity generally varies through the water column. Information on the vertical profile is given in 9.3. Where currents co-exist with waves, the current profile is stretched and compressed with the water surface elevation; guidance on current profile stretching is provided in 9.4. Currents may also be modified by partly transparent structures, see 9.5.

9.2 Current velocities

Like wind, current speeds vary in space and time but at much lower rates. Therefore, currents may generally be considered as a steady-flow field in which velocity is only a function of depth.

The total current velocity is composed of tidal currents, resulting from astronomical forcing, and residual currents. The components of the residual current may include circulation and storm-generated currents, as well as short- and long-period currents generated by various phenomena such as density gradients, wind stress and internal waves.

Depth-averaged tidal currents are regular and predictable. Circulation currents are relatively steady, large-scale features of the general oceanic circulation. Examples include the Gulf Stream in the Atlantic Ocean and the Loop Current in the Gulf of Mexico, where surface velocities may be in the range of approximately 1 m/s to 2 m/s. While relatively steady, these circulation features may meander and intermittently break off from the main circulation feature to become large-scale eddies or rings, which then drift at a speed of a few kilometres per day. Velocities in such eddies or rings may approach or exceed that of the main circulation feature. These circulation features and associated eddies occur in deep water beyond the shelf break, but in some areas of the world they may affect shallow water sites.

Storm-generated currents are caused by the wind stress and atmospheric pressure gradient throughout a storm. Storm current velocities are a complex function of the storm intensity and meteorological characteristics, bathymetry and shoreline configuration, and water density profile. In deep water along open coastlines, surface storm currents may be roughly estimated to have velocities up to 3 % of the 1 h-sustained wind speed during storms. As a storm approaches the coastline and shallower water, the storm surge and current may increase, and after a storm has passed inertial currents may persist for some time.

Currents may be intensified and directionality steered close to shore and in deepwater near steep bathymetry (e.g., Sigsbee Escapement). When using regional current measurements to develop criteria for a specific site, the bathymetry surrounding the measurement sites shall be compared to the bathymetry of the site for which criteria is being developed, and if there are significant differences the implications of the differences shall be established.

In the surf zone, breaking wave action sets up a longshore current. This effect shall be explicitly addressed for pipeline landfall criteria and other infrastructures in the surf zone.

Sources of information about the statistical distribution of currents and their variation with depth through the water column are generally scarce in most areas of the world. To avoid encountering problems during early phases such as exploration drilling, concerted measurement campaigns are required to acquire the data, particularly in remote, deep water areas near the edges of continental shelves. In deep water areas (water depths typically greater than 200 m) such as in the Gulf of Mexico, the West of Shetlands region and along the northern and eastern coasts of South America, currents are a major consideration in carrying out offshore operations and in the design of structures.

The variation of current velocity with depth shall be determined by an experienced metocean expert.

9.3 Current profile

The variation of current speeds and directions through the water column shall be determined for the specific location of the structure, taking into account all available information. In general, current profiles vary in strength and direction through the water column. Where the density does not vary significantly through the water column, the direction of the current velocities over the full water column is usually relatively uniform and simple profiles are appropriate; guidance is provided in A.9.3. Where the density varies through the water column, or different water masses flow into the region, more complex current profiles are common.

9.4 Current profile stretching

Current speeds and current profiles are determined for still water conditions, although in some situations they are applicable to storm conditions. The current profile is modified by the presence of waves, with a component of the current being present throughout the water column from sea floor to free water surface (between wave crest and wave trough).

Wave kinematics, adjusted for directional spreading where appropriate, shall be vectorially combined with the current velocities, and adjusted for blockage where appropriate (see 9.5). As the current profile used in design is specified only up to the storm still water level, the profile to the local instantaneous wave surface shall be modified by some means, see A.9.4.

9.5 Current blockage

The current velocity around and through a structure is modified by blockage. The presence of the structure causes the incident flow to diverge, with some of the flow going around the structure rather than through it. For structures that are more or less transparent, the current velocities within the structure are reduced from the free-stream values.

The degree of blockage depends on the type of structure. For dense, fixed-space frame structures it will be large, while for some types of transparent floaters it will be very small. More specific advice for the treatment of current blockage for different types of structure is given in the relevant structure-specific standard in the ISO 19900 series of publications.

9.6 Tidal Currents

Inertial currents at latitudes where the inertial period is close to the diurnal and semi-diurnal periods may cause inaccuracies in the harmonic analysis of measured current velocities in the same way as for water levels (Section 6.2). Internal tide effects may also cause problems as they may modify and smear the periods of the pure tidal fluctuations.

10 Other environmental factors

10.1 Marine growth

Marine growth on submerged structural components and other parts of a structure may have a significant influence on the hydrodynamic actions to which the structure is exposed.

The influence of marine growth on hydrodynamic actions is due to increased dimensions and increased drag coefficients due to roughness, as well as to the increased mass and its influence on dynamic response and the associated mass inertial forces. Where sufficient information is available, the loading coefficients may be selected based on the nature of the marine growth.

Structural components may be considered hydrodynamically smooth if they are either above HAT or sufficiently deep such that marine growth is sparse enough to allow its effect on roughness to be ignored. However, caution should be exercised, as a small increase in roughness may cause an increase in the drag coefficient to a level similar to that corresponding to a rough surface.

The type and thickness of marine growth varies with depth and depends on location, the age of the structure and the maintenance regime. Experience in one area of the world cannot necessarily be applied to another. Where necessary, site-specific studies shall be conducted to establish its likely type, thickness and depth dependence.

More specific advice for the different types of structure is given in the relevant structure-specific standard in the ISO 19900 series of publications.

10.2 Tsunamis

Tsunamis are water waves caused by impulsive disturbances that displace a large water mass in the sea. The main disturbances causing tsunamis are earthquakes, but they may also be generated by seabed subsidence, landslides, underwater volcanic eruptions, nuclear explosions, and even impacts from objects from outer space (meteorites, asteroids and comets). Their wavelength is several tens of kilometres and they have periods in the range of 5 min to 100 min. Their speed of propagation across the ocean is a function primarily of water depth; in the deepest oceans tsunami waves may travel at speeds of several hundred kilometres per hour.

In deep water, tsunamis have a low height and very long period and pose little hazard to floating or fixed offshore structures. Tsunamis contain more energy when they are generated in deeper water, and may be extremely destructive when they impact the coast. When they reach shallow water, the wave form pushes upward from the bottom to create a rise and fall of water that may break in shallow water and wash inland with great power.

The greatest hazard to offshore structures from tsunamis results from inflow and outflow of water in the form of waves and currents. These waves may be significant in shallow water, causing substantial actions on structures. Currents caused by the inflow and outflow of water may cause excessive scour problems.

Tsunamis travel great distances very quickly and may affect regions that are not normally associated with the disturbances that cause them. The likelihood of tsunamis affecting the location of the structure shall be considered.

10.3 Seiches

Coastal measurements of sea level in semi-enclosed bodies of water often show seiches with amplitudes of a few centimetres and periods of a few minutes due to oscillations of the local harbour, estuary or bay, superimposed on the normal tidal changes. Normally, variations are small enough offshore that they may be ignored, but if a structure is located in shallow partly enclosed seas, the effect of seiches should be considered.

10.4 Sea ice and icebergs

Sea ice and icebergs may affect the design and operation of structures. Before commencing design for, construction of, or operations on, structures in areas that are likely to be affected by sea ice and icebergs, adequate data shall be collected in accordance with ISO 19906, and may include:

— seasonal distribution of sea ice,

— distribution and probability of ice floes, pressure ridges and/or icebergs,

— effect of ice-gouges on the seabed from icebergs or ice ridges,

— type, thickness and representative features of sea ice,

— drift speed, direction, shape and mass of ice floes, pressure ridges and/or icebergs, and

— strength and other mechanical properties of the ice.

These data shall be used to determine design characteristics of the structure, as well as possible evacuation procedures.

For specific provisions for sea ice and icebergs, see ISO 19906.

10.5 Snow and ice accretion

Where relevant, snow accumulation and ice accretion shall be considered in the design of structures.

An estimate shall be made of the extent to which snow may accumulate on the structure and topsides, and of its possible effect on the structure.

Topsides icing may increase the diameter of structural components and may lead to a substantial increase in actions caused by wind and gravity, particularly for long, slender structures such as flares. Topsides snow and icing may also adversely affect the stability of floating structures and the operation of emergency equipment.

Icing from sea spray, freezing rain or drizzle, freezing fog, or cloud droplets shall be considered in the design.

For specific provisions for snow and ice accretion, see ISO 19906.

10.6 Thunderstorms and Lightning

Where required, thunderstorm and lightning occurrence should be based on meteorological observations, with observations that represent each day of the observation period uniformly. Care shall be taken to avoid biased databases which are observed only at particular times of the day.

Lightning occurrence shall be determined from lightning sensor measurements. Alternatively satellite and onshore measurements may be used.

Where required, monthly and seasonal occurrences of thunderstorms and lightning shall be provided.

10.7 Rainfall

Where required, total rainfall for each month of the year and/or season shall be given with daily average and daily maximum rainfall. The number of rain days each month shall be provided as well as the number of rain days which exceed prescribed levels of rainfall (e.g. number of days with rainfall exceeding 10 mm).

Rainfall intensity shall be prescribed on a return period basis.

10.8 Squalls and Downbursts

A squall is defined as a sudden increase of wind speed of at least eight metres per second (16 knots), the speed rising to 11 metres per second (22 knots) or more and lasting for at least one minute.

Where required, site specific quality controlled measured data shall be used to provide the occurrence rate and return period conditions of squall wind speeds.

Guidance on the vertical profile of squall winds is given in A.10.8.

Return period values of squall wind speeds shall normally be provided for 1, 10, 100 or 10,000 year return periods depending on the specific application. Return period analysis shall be undertaken in accordance with Section 5.7 of this document; and for squall winds return period values of the 3 s and 1-minute wind duration speeds are required. The 10-minute or 1-hour wind speeds for squalls shall not be quoted.

For specific applications, representative time histories may be required scaled to the appropriate return period, typically 100 or 10,000 years.

10.9 Internal Waves and Solitons

Internal waves/solitons are likely to occur, to some extent, whenever a thermocline is present. Where required, satellite data or historic measured data may be used to establish the likely presence, seasonal occurrence and inter-annual variability of internal waves. Satellite data may be used qualitatively and but should not be used to set design criteria.

Specialist modelling may be used to quantify likely current strengths in some types of internal waves.

Quantitative estimates of the presence or absence of internal waves and solitons, should be determined where possible through a minimum of 12 months of through water column current and temperature measurements (at approved spacing through the water column). A sampling interval of at least 1 min of the vector average current speed and direction, and temperature is recommended.

Total current should be decomposed into component vectors and tidal signal removed prior to extrapolating non-tidal current velocity to extreme values. Crest length should be determined.

For fatigue analysis, the occurrence and duration of solitons should be determined, for example from the half-life of the peak of the soliton current.

10.10 Shelf Waves and Eddies

If it is apparent from site-specific current measures and/or associated sea water temperatures that shelf-waves and/or ocean eddies are likely to be present, the phenomena may be characterised from examination of satellite observations.

The frequency of occurrence should be established in the region using the combination of measurements, satellite data and ocean circulation modelling.

The spatial scales (horizontal and through water column) of the features should be described.

Estimates of through water column current should be prepared for both shelf waves and eddies.

10.11 Infragravity Waves

For facilities in coastal waters which are sensitive to infra-gravity waves, site specific measurements of water surface elevation and current speed and direction should be undertaken for a minimum period of 12 months.

The measurements should be taken as continuous measurement of the average water level over a duration of a minimum of 5 seconds each 5 seconds.

Numerical modelling of infra-gravity waves should be undertaken to determine if facilities (ship motions at a wharf) will be subject to unacceptable effects from infra-gravity waves. Numerical models should be verified against measurements of infra-gravity wave events. Short stormy periods may be modelled for these numerical model assessments.

10.12 Seawater Temperature

Both through the water column and near the seabed water temperatures are required for facility and pipeline designs. Long term databases shall be accessed, if available, to provide long term statistics. Site specific measurements of sea water temperatures shall be undertaken for a minimum of 12 months to determine seasonal variation where this is not available through existing records.

10.13 Miscellaneous

Depending on circumstances, other environmental factors may affect operations and may consequently influence the design of structures. Appropriate data shall be compiled, including, where appropriate, records and/or predictions of:

— air temperature (maximum and minimum where appropriate),

— barometric pressure,

— cloudiness and cloud base levels,

— humidity,

— lightning,

— precipitation,

— salinity,

— seawater composition,

— solar radiation

— heat stress

— visibility,

— wind chill,

— phenomena specific to arctic and cold regions, see ISO 19906.

11 Collection of metocean data

11.1 General

Offshore metocean monitoring systems may vary from simple weather stations for aviation purposes, to complete data acquisition systems incorporating a wide range of sensors and sophisticated data processing, display, storage and transmission features. By providing real-time information for operational use and long-term records for engineering design purposes, offshore metocean monitoring systems play an important role in ensuring safe offshore operations.

This part of ISO 19901 is intended as an initial reference for offshore operators when planning metocean monitoring equipment on offshore installations. It provides guidance on both possible statutory requirements and the operator's own requirements, spanning applications such as weather forecasting, climate statistics, helicopter traffic, tanker loading, marine operations, etc.

The collection of metocean data is normally the result of requirements imposed by a regulator or other authority, and the operator's own needs. When specifying a metocean data collection system, the operator shall cater for the requirements of each of these organizations where they differ from those presented in this part of ISO 19901.

11.2 Common requirements

11.2.1 General

Procedures which ensure the proper functioning of the measuring and recording systems described in this part of ISO 19901, as well as instrument accuracy and calibration, shall be established and maintained.

Qualified personnel shall carry out observations, select, install, check and maintain the equipment and repair any faults or malfunctions. Service and calibration intervals on equipment shall be a maximum of one year. When new types of instruments are introduced, notification shall be given to all regular receivers of data.

Time references given in local or UTC (universal time coordinate) shall be recorded together with the measured data or derived parameters. The time reference should not be dependent on a manual resetting following a temporary cessation in operation of the system. Local user interfaces should clearly show both UTC and local time.

11.2.2 Instrumentation

The accuracy, range, type and location of the instruments should be determined with due regard to the purpose of the recordings.

11.3 Meteorology

11.3.1 General

Information concerning instrument accuracy and calibration requirements shall be established.

Data that cannot be measured by means of instruments shall be obtained by observation by qualified observers. Observers shall have completed relevant meteorological observer training. Consideration shall be given to suitable refresher training for observers to comply with local regulations.

11.3.2 Weather observation and reporting for helicopter operations

The specifications provided in this part of ISO 19901 address only metocean conditions, and do not constitute a complete system for offshore helicopter operations. The relevant local helicopter regulations shall be applied in order to ensure all necessary aspects are covered.

A complete aviation routine weather report is specified in WMO-No. 306, under code FM 15-XV Ext. METAR. The data are transmitted in a 'message' which consists of information derived from instrumental measurements and manual observations taken by a qualified observer.

The parameters included are:

— wind direction,

— wind speed,

— visibility [according to METAR specifications, and runway visual range (RVR) if available],

— weather,

— cloud,

— dew-point temperature,

— air temperature,

— air pressure (QNH – barometric pressure adjusted to sea-level),

— significant wave height, and

— sea surface temperature.

The wind measurements from the top of derrick are normally not representative for the wind field at the helicopter deck. A separate wind sensor shall be installed near the helideck to measure values representative for the wind field at the helicopter deck. This requirement may be waived if it may be clearly demonstrated that this is not necessary.

11.3.3 Weather observation and reporting for weather forecasting services

A complete weather observation report is specified in WMO-No. 306 under code FM 13-XIV Ext. SHIP. The message consists of information derived from instrumental measurements and manual observations taken by a qualified observer.

The parameters included are:

— wind direction,

— wind speed,

— air pressure,

— air temperature,

— sea surface temperature,

— humidity,

— wave height,

— wave period,

— clouds,

— visibility (MOR – meteorological optical range),

— weather, and

— icing.

Observations shall be made at standard synoptic hours, expressed in terms of UTC at which, by international agreement, meteorological observations are made simultaneously throughout the globe. Standard synoptic hours are 00, 03, ... 21 UTC. The observations shall be recorded in accordance with WMO-No. 306, under code FM 13-XIV Ext. SHIP (Section A, pp. 7-24).

11.3.4 Weather observation and reporting for climatological purposes

In addition to the data collected for the weather report (SHIP-format), the wave parameters of maximum wave height, peak period and wave direction shall be included if available. The normal recording interval shall be 1 h as a minimum, though more frequent recording is recommended, and the resolution of the data shall be in accordance with the instrument accuracy.

11.4 Oceanography

11.4.1 General

In the context of this part of ISO 19901, the term oceanography shall encompass

— ocean currents at specified depths,

— water level,

— sea temperature at specified depths,

— salt content (salinity) at specified depths,

— oxygen content at specified depths,

— icebergs, their size and drift,

— sea ice.

Ocean waves and sea surface temperature are defined as part of meteorology, and covered in 11.3.

Apart from ocean currents and water level, the measurements and observation of oceanographic parameters are not commonly included in platform metocean systems. The operator shall, however, consider his own need for collecting such data contingent upon the natural conditions at the location, the inadequacy of the database, the type of structure or installation, and the operational situation of the facility.

11.4.2 Measurements and observations

Ocean currents should be measured at fixed depths (or bins), and include at least three depths in shallow waters: near-surface, mid-depth and near-bottom. For measurements in deeper waters, more measurement depths are recommended to capture the spatial variability of currents with depth. The observation of sea ice and icebergs (size and drift), may be performed by combining e.g. manual observations, instrument recordings and remote sensing.

11.5 Data quality control

Procedures shall be established to ensure that collected data are processed and standard analyses carried out in such a way that the quality of the data may be verified. The analyses should be sufficiently extensive to allow all significant errors to be discovered. The data should be compared to other recorded data, to the extent this is practicable.

Local regulations may require the provision of metocean data and/or reports to a regulatory body or agency at regular intervals. Careful consideration shall be given to how these requirements will be met by the observation system and its operation.

12 Verification of Weather Forecast Information

12.1 General

In planning and undertaking operations which are sensitive to one or more metocean parameters, it is essential to understand the ability of the weather forecast organisation to provide a forecast that meets the clients' requirements.

Understanding forecast performance is important when planning and taking action based on forecast information, or when choosing a forecast provider. Forecast verification - comparison of the forecasts against observations - should be undertaken routinely in order to quantify the forecast performance. While the overall forecast performance is important and should be determined, special consideration should be given to those aspects of the forecast which are of most relevance, and forecast verification focus on these elements.

13 Information concerning the annexes

13.1 Information concerning Annex A

The clauses in Annex A provide additional information and guidance on clauses in the body of this part of ISO 19901. The same numbering system and heading titles have been used for ease in identifying the subclause in the body of this part of ISO 19901 to which it relates.

13.2 Information concerning the Regional Annexes

The annexes subsequent to Annex A present an overview of various regions of the world for which information has been developed by experts on each region, and is intended to supplement the provisions, information and guidance given in the main body and Annex A of this part of ISO 19901. They also provide some guidance relating to the particular region dealt with in each annex, as well as some indicative values for metocean parameters which may be suitable for conceptual studies. However, site- or project-specific metocean parameters shall be developed for structural design and/or assessment.

Annex A
(informative)

Additional information and guidance

A.1 General

Environmental conditions generally have a significant influence on the design and the construction of offshore structures of all types. In some areas of the world, the prevailing environmental conditions may also have an influence on the operational aspects of a structure, which in turn may affect the design of the structure.

The environmental conditions and metocean parameters discussed herein relate to the pre-service, the in-service and the removal phases of structures.

It is beyond the scope of this part of ISO 19901 to provide detailed instructions that may be followed to produce reliable estimates of extreme or abnormal conditions in all areas and in all cases.

Requirements for the calculation of environmental actions on offshore structures and the resulting action effects are given in ISO 19902 for fixed steel structures, ISO 19903 for fixed concrete structures, ISO 19904-1 for floating structures (monohulls, semi-submersibles and spars), ISO 19905-1 for site-specific assessments of jack-ups, ISO 19906 for arctic offshore structures and ISO 19901-3 for topsides structures.

A.2 Determining the relevant metocean parameters

A.2.1 General

The design parameters should be chosen after considering all of the relevant service and operating requirements for the particular type of structure.

Selection of environmental conditions and the values of the associated parameters should be made after consultation with both the structure designer and appropriate experts in oceanography, meteorology and related fields. The sources of all data should be noted. The methods used to develop available data into the desired metocean parameters and their values should be defined.

General information on the various types of environmental conditions that may affect the site of the structure should be used to supplement data developed for normal conditions. Statistics may be compiled giving the expected occurrence of metocean parameters by season, direction of approach, etc.

Of special interest for the planning of construction activities, platform operations and evacuation are the duration, the speed of development, the speed of movement and the extent of storm conditions. The ability to forecast storms in the vicinity of a structure is very important.

If the amount of metocean data available is very limited (particularly in the early phases of a project), the extreme and abnormal metocean conditions should be derived conservatively. If, in the judgement of the metocean expert, there is considerable uncertainty in the data, the extremes should be set too high rather than too low. A subsequent increase in extreme values later in a project may have both safety and economic consequences [1].

Figure A.1 presents an overview of the process involved in developing metocean parameters.

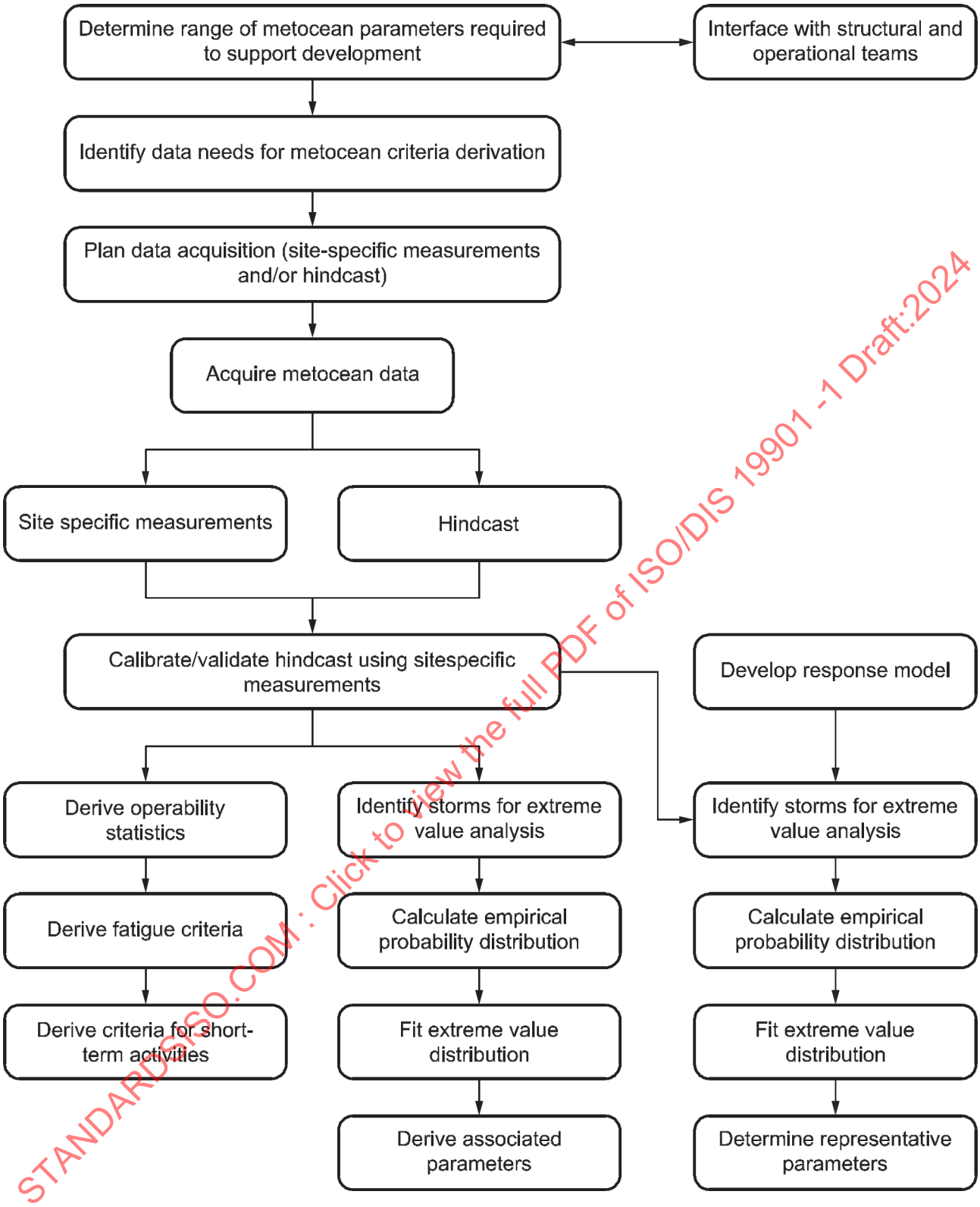

Figure A.1 — Overview of the process of producing metocean parameters

A.2.2 Expert development of metocean criteria

It is important to select a metocean expert(s) with experience in all facets of the process; this includes the hardware and software associated with data gathering (*in situ* or remote sensing), hindcasting procedures, data sampling and analysis procedures, and extreme statistical analysis techniques. Additionally, it is important that the metocean expert understands the purpose for which criteria are intended such that

appropriate criteria cases are provided and to highlight limitations to use or areas of particularly high uncertainty such that the criteria will be properly applied in design.

The approach used to determine metocean parameters is often dictated by the available data (measured, continuous, storm hindcasts, satellite, radar, etc.). Understanding of the methods used to record and analyse the data is critical; as is knowledge of how these methods and data may influence the selection of an analysis approach or possibly bias the result. A sound understanding of the data techniques is necessary in order to be able to account for them during interpretation of the datasets and to apply any corrections that could be necessary to the final estimates.

Given a suitable database of measured and/or hindcast data, it is important to investigate the sensitivity of estimates to the use of different datasets (measured or hindcast) and statistical analysis

procedures. It is important that the design engineer who will use the metocean parameters is aware of the uncertainty (preferably by a quantitative assessment) in the parameters provided. Relatively small changes in design estimates may significantly affect the reliability of offshore structures. Engagements between the metocean expert and the design team throughout the design process may help ensure proper application of criteria and that proper account has been taken of uncertainties associated with the development of metocean criteria.

A.5.3 to A.5.10 provide brief general descriptions of the principal considerations for deriving safe, reliable metocean parameters to support the design and operation of different types of offshore structures.

A.2.3 Selecting appropriate parameters for determining design actions or action effects

The design or site assessment of structures is often governed by extreme actions or extreme action effects caused by the local environment conditions. The conditions appropriate to design or site assessment are usually quantified in terms of the metocean parameters (e.g. a combination of extreme wave height, current and wind velocity) or the action effect (e.g. global bending moment on a hull).

The traditional approach to offshore structural design and assessment required the use of a predetermined set of metocean parameters (e.g. 100-year wave plus associated current). This type of approach is still widely used, its advantage being that the metocean parameters are well defined and understood, they may be determined prior to the detailed structural model being finalized, and the design process is simplified (in particular, the metocean parameters do not normally need to be revisited during detailed design). The disadvantages are that it does not tend to provide an optimized structure, nor does it facilitate the use of reliability- or risk-based approaches.

The shift in emphasis towards reliability-based approaches has led to the increased use of response-based methods. These require the determination of the *N*-year response or action effect (e.g. the 100-year overturning moment of a jacket structure or the bending moment of a drilling riser). An appropriate set of metocean conditions that result in the 100-year response may then be determined.

Reliability-based approaches provide a more rational basis on which to design or assess any structural form, in particular those that respond to complex combinations of metocean actions. However, they usually require a closer interaction between the metocean and structural models and experts, and if used to their full potential, the development of detailed structural response models. In addition, it is essential that appropriate account is taken of both aleatory and epistemic sources of uncertainty both in respect of the metocean and loading aspects of the analyses.

The term “100-year storm” has no meaning except as an informal description of a set of conditions that introduce the parameter or action effect.

The return period in years, for larger values of return period, may be taken as the inverse of the annual probability of exceedance of a parameter (e.g. a wave height or wind speed).

Parameters appropriate to the design or assessment of different forms of offshore structure are provided in the relevant ISO publication:

— ISO 19901-3 for topside structure;

— ISO 19902 for fixed steel offshore structures;

— ISO 19903 for fixed concrete offshore structures;

— ISO 19904-1 for floating offshore structures;

— ISO 19905-1 for site-specific assessment of mobile offshore units;

— ISO 19906 for arctic offshore structures.

Four methods are discussed below for defining an environment that generates the extreme direct action and, generally, also the extreme action effect, caused by the combined extreme wind, wave and current conditions. The methodologies may be applied for a case in which any return-period parameter dominates the action effect, but the examples given below are for the wave-dominated loading cases. Other methods are possible.

a) Specified return-period wave height (significant or individual) with "associated" wave period, wind and current velocities. A similar methodology may be applied where a parameter other than wave height dominates the action effect.

   This has been the established practice for deriving wind and current extremes occurring simultaneously with the wave height in some areas (e.g. USA). The specified return period is usually 100 years. It has also been used for deriving secondary parameters (such as wave periods) in the North Sea. The "associated" wave period, current, or wind is the value estimated to co-exist with the specified return-period wave height. The method is applicable if:

   — there is a statistically significant correlation between the associated value and the specified return-period wave height, and

   — the extreme global environmental action on the structure is dominated by waves.

   Where there is a correlation between the parameter and wave height simple regression models have historically been used to determine an absolute or in-line component of associated parameters. Whilst these linear or non-linear regression models may be applied, when extrapolation is being carried out to long return periods, there are better statistical methods available. These methods explicitly model the extremal correlation structure between parameters.

   One method, described in Heffernan & Tawn,[2] allows for associated values of one or more conditional parameters (e.g. Tp or wind speed) to be described for large values of a main conditioning parameter (e.g. Hs). As for the GPD for a single parameter, the approach outlined in reference [2] produces a description of the conditional parameters' probability distributions which is asymptotically correct for large values of the conditioning variable. The approach depends on first applying an Extreme Value Analysis to the marginal distributions of parameters and then fitting the asymptotic model to estimate the correlation structure. The fit that is produced is similar to a simple regression model but is more flexible and accounts for the simultaneous correlation structure between extremes of the main parameter and all of the associated parameters being considered. The approach also allows the estimation of environmental contours or 95 % ranges for associated parameters.

   If there is not a strong correlation between parameters or if the global environmental action is not dominated by a single parameter, then there is no explicit confirmation in any of these methods that the combination of the primary metocean parameter (e.g. wave height) and its associated parameters (e.g., current and wind velocities) will approximate to the return-period event for any global environmental action on a structure. In these circumstances, and if a response-based approach is not feasible, the most appropriate approach is to explore a selected percentile range of the distribution of associated parameters (typically, 2,5 % to 97,5 %) since no particular values of the associated parameter are more likely than others to occur at the time of large values of other parameters.

   Where tidal effects are relevant, it should also be recognised that although there may be a reasonable degree of correlation between Hs and surge, the correlation between Hs and total current/water level may be much weaker. In these circumstances, the best option may be to derive surge using a correlation method and then add on a tidal component separately taking into account the length of time for which the surge events persist.

When the present method is used for structures that are sensitive to wave period, the most onerous combination of wave height and period may be at a different period from that associated with the maximum specified return period wave height. Consequently, a reasonable range of variations in both period and wave height should be investigated to determine the most onerous combination of wave height and period with the same, or higher probability of occurrence than the specified return period.

b) Specified return-period wave height combined with the wind speed and the current velocity with the same specified return period, all determined by extrapolation of the individual parameters considered independently.

This method has been used in the North Sea and many other areas of the world, normally with a return period of 50 years or 100 years. A modified version, using the 100-year wave height and the 100-year wind speed combined with the 10-year current velocity, has been used in Norway.

The method is simple, independent of the structure, and may be determined from separate (marginal) statistics of waves, currents and wind. It always yields results that are conservative compared to either of the two other methods for the same specified return period when used to determine design actions for fixed structures, but is not appropriate for floating and other types of structure with significant dynamic response. By contrast, method c) below, when correctly applied, will always provide a good estimate of the specified return-period global environmental action.

c) 'Response-based analysis' which requires any “reasonable” combination of wave height and period, wind speed and current velocity that results in:

— the global extreme environmental action on the structure with the specified return period, or

— a relevant action effect (global response) of the structure (base shear, overturning moment, floater displacement, etc.) with the specified return period.

This method typically involves calculating one or more combinations of wave height (as the dominant parameter) and associated current and wind speed, which deliver one or several critical structural response functions (action effects), such as base shear or overturning moment on a fixed structure or horizontal displacement of a floating structure.[3],[4],[5] Directional effects of wind, wave and current, and water-depth fluctuation due to tide and surge, are fully accounted for. Storms are treated as independent events and short-term variability is taken into account. The long-term distribution of the structural response is then determined and from this its extreme and abnormal values. The same structural response function may be used to determine combinations of metocean parameters leading to the desired return-period extreme and abnormal responses. It should be noted that a set of parameters is not unique: several other related sets will produce the same result. In addition, the statistics may be used in the development of partial factors for environmental actions (action effects) as described below. Reference [3] describes the procedure in some detail.

Although this method may involve time and cost in developing software, it may provide a realistic set of design parameters — even if there is little correlation between waves, winds and currents. Thus, defining the specified return-period action or action effect has a significant advantage over defining the specified return-period wave height, either with associated or with specified return-period values of wind and current. The definition of the action or action effect should not use an arbitrary set of related wave, wind and current values that satisfies the specified return-period global environmental action or action effect, but should make a “reasonable” (expected) choice so as to correctly model the probable spatial distribution of global hydrodynamic actions over the structure. Reasonably accurate combinations of metocean parameters may be deduced from observing the combinations that cause the greatest responses in the storms used in developing response statistics.

Care should be taken in the application of a response-based approach where the final concept remains to be fully defined. As noted above, it is essential that appropriate account is taken of both aleatory and epistemic sources of uncertainty both in respect of the metocean and loading aspects of the analyses.

d) Environmental contours. Although a long-term response-based analysis is preferable, it is not always possible to derive the response reliably for a large number of combinations of input parameters. Where the dominant structural responses and their main contributing parameters are all known, and the effect of short-term variability is relatively small, the “environmental contour” approach may be used

instead to determine the response from a greatly reduced set of combined parameters all of which have the same probability of occurrence or exceedance.

The iFORM approach developed by Winterstein et al [5] is an approach often used in the industry although the probabilistic form of the conditional parameter will be different for every pair of parameters and typically the chosen distribution may fit well to the body of the data but may not be well suited to extrapolation into the tails. The Heffernan and Tawn[2] approach may also be used to develop these contours in a more generic sense [Jonathan et al 2010[232]].

There are many ways of deriving environmental contours [see Ross et al 2020[234] and Jonathan et al 2014[233]] all of which will produce slightly different contours, and which have pros and cons of which the user should be aware.

Additional consideration should be given to obtaining extreme direct actions (action effects) for locations where there are strong currents that are not driven by local storms. Such currents may be driven by tides or deep-water currents, such as the Loop Current in the Gulf of Mexico or the Gulf Stream. In this case, method a) may be acceptable if the storm-generated conditions are the predominant contributors to the extreme global environmental action (action effect) and if the appropriate "associated" value of tidal and circulation currents may be determined. However, method c) is conceptually more straightforward and preferable. Method b) is the simplest method and ensures an adequate design environmental action (action effect); however, this may be very conservative compared to the true global environmental action (action effect) of the required return period.

For many areas, substantial databases are becoming available with which it is possible to establish statistics of joint occurrence of wind, wave and current magnitudes and directions. However, with currents in particular, the models are often not of a good enough quality to enable detailed statistical analysis to be carried out on a time-step basis. In cases where this may be an issue, conservative assumptions (such as those implicit in approach b) should be made.

When data are of sufficient quality and length however, method c) above provides the most rigorous basis for estimating extreme action effects. The corresponding partial factors to be used in conjunction with the global environmental action (action effect) should be determined using reliability analysis principles, in order to ensure that an appropriate safety level is achieved. This approach provides more consistent reliability (safety) for different geographic areas than has been achieved by the practice of using separate (marginal) statistics of winds, currents and waves.

A.2.3.1 Additional Considerations

Extreme N-year criteria should be presented in tabular format for the three fundamental cases, as follows:

— Peak wind.

— Peak wave.

— Peak surface current.

On a regional basis, these load cases usually align with specific metocean phenomena, such as hurricanes, squalls, or the Loop Current. However, it is sometimes necessary to specify multiple sets of N-year criteria for winds, waves, or current when it is not clear which phenomena would lead to a higher load (this is particularly true in the case of currents). Extreme criteria tables must show the dominant parameter plus all associated parameters for each return period for both omnidirectional and directional cases.

The combinations of winds, waves and current that should be checked:

— Independent wind and associated currents and waves (sea and swell),

— Independent wave and associated currents, swell and winds, and

— Independent currents and associated winds and waves (sea and swell).

For selecting joint return period criteria for compliant structures, the directional differences between the wind and wave, wave and current, and wind and current as functions of wind speed, wave height and current

speed should be considered through the use of multivariate analysis or contours of the probability density function from an approved industry method to generate environmental contours between the conditioning variate and dependent variate. The contours may be scaled to the independent return period estimates.

Alternatively “force” or “response-based” analysis may be used.

For fixed platforms, joint criteria may be found using contours of the probability density function from an approved industry method to generate environmental contours between the conditioning variate and dependent variate. More detailed analysis may be undertaken using “forced-based” or “response-based” methods.

For strongly correlated parameters, whilst simple linear or non-linear regression models may be used to identify a most-probable or median associated value of other parameters, more advanced methods are available[2] which better reflect the extremal correlation structures between two or more parameters. Such approaches may also allow estimation of the conditional distribution of the associated parameter given the occurrence of the return period event. For sensitivity analyses, this allows a percentile range of the conditional distribution of the associated parameter to be used (e.g. 2,5 % to 97,5 %).

N-year associated parameters must be verified to be equal to or lower than the N-year independent values of the same parameter. If this is not the case, the independent fit of the parameter may need to be revisited or the associated value may need to be limited to the independent value.

For weakly or un-correlated parameters, the chances of simultaneous occurrence of extreme events of both parameters are very small. In this case, the return period event together with consideration of the action effects of a percentile range of the unconditional distribution of an associated parameter, again such as 2,5 % to 97,5 %. should be used.

A.2.4 The metocean database

There are various circumstances in which site-specific data from measurements or hindcasts should be analysed in order to produce metocean parameters, including the following:

— where regulatory requirements insist on the use of site-specific data;

— where the operator has field data in addition to the data used in producing the environmental conditions presented in standard guidance documents;

— where environmental conditions are not provided in standard guidance documents or are otherwise deemed by an operator to be inappropriate;

— where an operator wishes to produce metocean parameters for return periods other than those available in standard guidance documents; and

— where the structure’s response is such that available metocean data do not provide the basis for deriving appropriate metocean parameters (e.g. data to be used in the response-based analysis of a floating system).

A well-controlled series of measurements at the location of an offshore structure is a valuable reference source for establishing design situations as well as operating conditions and associated criteria. Because measurements taken over a short duration may give misleading estimates of long-term extremes, measurements are more often used to validate a hindcast over a longer period. However, care should be taken in comparing measured and hindcast data, in particular to address differences in:

— temporal averaging (e.g. 3 h hindcast H_s versus a H_s derived from a 20 min measurement),

— spatial averaging (e.g. hindcast may deliver a H_s over a 10 km × 10 km grid *versus* a measured ‘spot’ value).

The hindcast should be for as long a period as possible in order to capture the effects of climate variability; typically 20 years, ideally longer.

Producing long-period hindcast datasets of current may be difficult due to a lack of measured data, a lack of reliable data to drive the current models or the inability of models to faithfully reproduce important dynamic

processes in a region. In such cases, alternative means of addressing the impact of longer term climatic variations should be considered. From a practical standpoint, this may require multi-year measurement campaigns to capture a sufficient number of severe current event episodes necessary for developing estimates of extremes.

Extremes derived from short-term site-specific measurements should be used in preference to any indicative values presented in standard guidance documents only if care is taken to adjust the records to reflect long-term variability.

Climatic variations during the design service life of structures may result in changes in:

— water level (mean, tide, and/or surge),

— frequency of severe storms,

— intensity of severe storms, and

— associated changes in the magnitude and frequency of extreme winds, waves and currents.

Wave height depends on wind speed, direction, fetch and duration, all of which are potentially affected by changes in intensity, frequency and track of weather systems. The analysis of meteorological observations is affected by homogeneity problems in historical weather maps and data.

The various application(s) for the database should be considered when determining the type(s) of wave hindcast model calibrations which are most appropriate. For example, if a primary concern is to derive downtime estimates for tanker-offloading operations in a mild climate (e.g. through the use of persistence analyses), it is important to verify the accuracy of the database for low sea-states with a broad range of wave periods and directions. If the database is also used for deriving fatigue estimates on deep-water fixed or on bottom-founded compliant structures, the database should be verified for the full dynamic range of significant wave heights (H_s) and wave periods (T_p or T_z) in order to derive representative directional wave scatter diagrams — perhaps together with estimates of directional associated current profiles.

If the database is used for establishing extreme design parameters, it is important to establish that the database is as long and as accurate as possible. A judgement should be made on the suitability of the design parameters that have been developed, e.g. with respect to how climatologically representative the available database is. Factors that should be considered include the time over which the data have been collected, and whether this time was climatologically normal in terms of the frequency and strength of storms.

When extrapolating metocean databases to low probabilities of exceedance, it is assumed that the database is representative of long-term conditions. This hypothesis should continue to be tested and, if necessary, suitable allowances should be made to incorporate any residual uncertainty.

Reference [6] contains guidelines for safe practice for undertaking metocean and arctic surveys.

A.2.5 Storm types in a region

The definition of environmental conditions and the associated metocean parameters that may occur in different storm types is an important part of understanding the workability of various offshore operations, as well as determining the processes that will be needed to define the extreme and abnormal metocean parameters. For some areas, the definition of storm types is problematic, in particular in regions where tropical cyclones lose their identity and metamorphose into extra-tropical storms. Such storms may become very severe and their characteristics during the transition are not yet well understood[7]; the derivation of extreme and abnormal metocean parameters in such areas requires additional care.

A.2.6 Directionality

In locations where storm tracks, storm types, bathymetry or surrounding coastal morphology lead to significant variations in the strength of winds, waves and currents as a function of direction, it is often desirable to provide criteria by directional sectors. This may allow designers to optimize structures to local conditions. This may occur as structures are designed for strength but may also be important

when specifying operational criteria so that flare tower and boat landings may be placed to optimize safe operation.

One common approach to providing directional criteria is to specify conditions in 45° sectors. Alternatively, sectors may be "naturally" defined based on the directionality inherent in measured or hindcast data. When this is done, criteria may be specified in as few as four or five sectors. The sectors do not need to be of uniform size, and in general none should be smaller than 45° to avoid "over-optimization".

When directional criteria are specified, it is important to ensure that the overall reliability of the structure is not compromised by the use of such criteria. The metocean specialist may aid in this effort by discussing the assumptions, limitations and appropriate use of directional criteria with the structural design team. See references [8] and [9] for discussion on the use of directional criteria.

A.2.7 Extrapolation to extreme or abnormal conditions

The problem of determining low probability values of metocean parameters has become even more important because of the recent trend to use very rare events to directly calculate the failure probability of a structure. It is becoming increasingly common for owners and regulators to require consideration of the 1 000-year to 10 000-year events, i.e. the 10^{-3} and 10^{-4} annual probability of exceedance, respectively. Great caution should be used in extrapolating data to such extremely low probabilities.

There are two basic methods for calculating low probability values: the historical method and the deductive method. Both have their strengths and weaknesses.

The historical method takes data, either from measurements or model hindcasts, and fits the tail (low probability region) of the probability distribution with appropriate extreme value distributions. This method is well documented in reference [10].

When extrapolating datasets using the historical method:

— Probability distributions such as the Weibull or Gumbel distributions are commonly used in fitting metocean data, with a peaks-over-threshold (POT) approach used to select the data to be fit. A key assumption in using these distributions is that the metocean extremes at very rare return periods beyond the length of the data set will continue to follow the presumed distribution shape that was selected through comparisons with the (usually limited) underlying data set. Uncertainty intervals (UI) estimated using these distributions will likewise reflect the assumption that the data will always fit the selected distribution shape.

— The Generalised Pareto distribution (GPD) offers an alternative to assuming a presumed distribution shape such as Weibull or Gumbel, as it can be fit to any POT data irrespective of the probability distribution of the underlying dataset itself.[2] The only proviso is that the dataset is of sufficient length to allow for the asymptotic properties of the GPD to be effective, i.e. there are enough peaks to reach into the stable tail of the distribution. In order to determine whether there are enough events in the dataset, diagnostic approaches should be used, such as mean residual life plots, assessment of variation in fit parameters with threshold, assessment of changing return value with threshold. Due to the variable nature of the GPD tail, UI estimated using the GPD will often be much larger than those derived from the use of an assumed shape such as Weibull or Gumbel, and in some instances will yield UI that contain unphysical values of the phenomenon being modelled. In these instances, care must be taken to avoid the inclusion of unphysical results in the final derived extremes.

— For very short data sets, the GPD typically cannot be used due to tail instability, so distribution shapes such as the Weibull and Gumbel are often applied, with the understanding that a distribution shape is being assumed as noted above. For design purposes, the best solution in these circumstances is to endeavour to collect more data before carrying out the extrapolation. If this is not possible then an assessment of the uncertainty should be made such that this uncertainty is taken into account in the selection of the final design value; a common approach for doing so is to evaluate the UI, and select design values at a high confidence interval, such as the 90 % or 95 %.

— Confidence in estimates of rare events can often be improved by pooling data from nearby sites, especially in places where storms are sparse. Pooling is straightforward if the data source is a gridded hindcast model. There are other methods of reducing statistical uncertainty, such as averaging extreme estimates

from adjacent sites, but these can introduce bias and are inferior to pooling. Regardless of the method used, one should take great care to exclude sites that can be expected to be different from the site of interest because of a differing physical environment. For example, wave data from shallow-water sites should not be pooled with wave data from a substantially different water depth. The other concern with pooling is that if sites too close to one another are used, they will not provide independent realizations of the environment. Use of highly correlated nearby sites cannot only give a false sense of confidence in extreme values, but use of correlated points can lead to a low bias in the tail of the distribution. The optimal pooling distance depends on the storm type, storm length scale and local physical constraints (e.g. fetch limits in the case of waves, proximity to slope for deepwater currents), so that optimal separation distances for site pooling need to be carefully considered on a case-by-case basis.

Other potential pitfalls associated with pooling are:

1. Sampling the same storm multiple times leading to correlated storm peak data being included in an extrapolation. This may occur both in grid point pooling and track shifting and may be mitigated (somewhat) by ensuring a minimum spatial separation of grid points (or shift of the storm track).

2. Use of non-peak storm data in directional extreme value analysis. This is a symptom of the general sparsity of historical storm peak data in some directional sectors.

Both these pitfalls will lead to (in most cases) a negative bias in values of extreme hurricane parameters.

Care should be taken in inferring great reductions in uncertainty when site pooling (or track-shifting). These methods assume the length of the dataset has been extended to a multiple of the original hindcast dataset length through use of multiple grid points or multiple realisations of historical tracks. In reality, this is not the case because the variability in the data remains equivalent to that of the original dataset (not a multiple of it).

More details on these topics may be found in reference [237].

— The statistical uncertainty in estimated extreme parameters increases as the extrapolation extends beyond the length of the dataset. Metocean parameters with return periods up to a factor of three beyond the length of a statistically stationary dataset may be estimated with some confidence. Where more extreme extrapolation is required, care should be taken to account for the increased level of uncertainty, by, for example, providing a range of possible values and an indication of the size of the UI.

— The use of long-term numerical simulations of present-day climate to establish databases of hundreds or thousands of years of regional metocean conditions is being actively explored. Users of such are cautioned that implied reductions in UI from the use of these simulations in deriving metocean extremes must be weighed against the fact that the simulations can only be benchmarked against the past 50-100 years of historical data; there may be physical processes poorly understood / not represented in the simulations that correspond to higher UI than indicated by taking the simulations as truth.

The deductive method begins by breaking the regional event type into parameters whose probability may be determined from historical data, e.g. in the case of tropical cyclones this could be the peak wind speed, radius to maximum wind, central pressure and forward speed. Synthetic events are generated by combining the parameters accounting for their joint probability of occurrence. In the simplest case, where the parameters are statistically independent, the probability of a synthetic event simply becomes the product of the probabilities of each of the storm's parameters. In this way, very rare synthetic events may be constructed using parameters with relatively high and statistically confident probabilities. Parameters that are statistically correlated complicate the analysis, but may be handled provided that the joint probability distributions can be deduced from the historical data. The main disadvantage of the deductive method is that it is time-consuming to apply and in regions where events are physically complicated, it may be impossible to derive parameters that adequately describe the events. The deductive method is applicable only if the extreme event is due to a rare combination of parameters which occur reasonably frequently within their individual distributions.

Whichever method is adopted, the following recommendations and considerations are relevant:

— When fitting data, care should be taken not to mix data from one type of storm event (e.g. winter storms) with data from another type of storm event (e.g. hurricanes). The probability distributions of

the two types of extreme event are often a strong function of the storm physics (storm type), and mixing storm types may lead to non-conservative estimates of the extremes; each storm type should be fitted separately and then the combined statistics computed.

— Fitting should include as many events as possible to maximise statistical confidence in the fit.

— Bias should be removed from the data, whether the data are from measurements or from hindcast modelling. Biased data may lead to substantial offsets in the estimates of rare events which may be non-conservative because of the extrapolation process. Scatter (noise) makes the UI larger and any bias tends to increase as one extrapolates further beyond the data.

— Generally, it is preferable to extrapolate a noisy dataset of longer duration rather than a shorter-duration cleaner dataset. For example, a 50-year model hindcast dataset to estimate the 100-year storm is preferred to a few years of measurements, even though the hindcast results may have more scatter than the measurements. This assumes that bias has been removed from both data sources. It is emphasized that any model used to extrapolate data should be carefully validated against available measurements.

— Estimates of rare events should be checked to make sure they do not exceed some limiting state imposed by physical constraints, e.g. the wave-breaking limit in shallow water.

The best way to estimate the UI is to use a bootstrapping method and to fit a distribution to each bootstrap. There are many types of uncertainty that are present when extrapolating to long return periods and these include uncertainty in the underlying data model or measurement technique (epistemic uncertainty) as well as the basic random sampling uncertainty (aleatory uncertainty). In normal practice, parametric bootstrapping will only estimate the latter but suitable consideration should also be given to the potential errors and uncertainties that may exist in the underlying dataset as these will also increase the uncertainty in the accuracy of the final answer.

It should be noted that the inclusion of uncertainty in the determination of return values may result in higher values, particularly if using the GPD with bootstrapping, and determining the final return values not from the mean value associated with a given return period, but from the values associated with the mean of the probabilities corresponding to the desired return period. It is important to understand whether an assumption of uncertainty in the metocean return values is already included in loading recipes for fixed and floating structures. If not, then the uncertainty should be included in the underlying derivation of the metocean return values. Discussion with the structural engineer is recommended.

Where omni directional or seasonal criteria are relevant to the specific design or assessment case, appropriate consideration should be given. Relevant cases may include the design of mooring systems or the seasonal site assessment of jack-up units.

When extrapolating a directional parameter such as significant wave height or wind speed, one method used is that each direction sector is extrapolated separately, based on just the storm peaks that fall within that sector; and, the omni-directional extreme is derived by pooling all storm peaks into a single set. Alternatively, extrapolation can be based on the selection of the storm peaks in each sector associated with each storm (hence one storm could potentially result in storm peaks in various sectors).

To more rigorously take account of the complexity of environmental phenomena as they vary by season and direction, the following approach may be used[9]:

— Fit an EVA model to the underlying data which takes account of variation by season and direction. The model should include the distribution's parameters and the rate of occurrence of storm events within each season/direction bin.

— Simulate storm peak events from all seasons and directions then assign a storm shape to each storm peak as it decays in magnitude and changes direction.

— For extremes in each directional sector, apply the EVA to the largest in-sector value from each storm rather than only extrapolating the storm peaks themselves. Using storm peaks alone will under-estimate sectors in which the more severe sea-states/wind speeds etc. tend to occur during events where the peak occurs in adjacent sectors.

— Derive the omni-directional extreme by aggregating the probability distributions from each direction sector since this allows for the varying characteristics of phenomena to be properly captured and ensures statistical consistency between directional and omni-directional return values.

It is true that with any of these approaches there is some correlation between events in adjacent sectors, but this is typically small[9] and leads to a small amount of conservatism in the extremes from some directions (but not the omni-directional), but the alternative of ignoring large occurrences in some direction sectors will underestimate the extreme values.

A.2.8 Metocean parameters for fatigue assessments

A.2.8.1 General

Time-varying stresses in an offshore structure are due to time-varying actions caused by waves (with or without currents), gust winds and combinations thereof. Time-varying stresses for a fatigue assessment are characterized by the number of occurrences of various magnitudes of stress range (maximum stress minus preceding or following minimum stress), in some cases supplemented by the mean value of the stress range. Determination of the relevant metocean parameters should take due account of the required characterization for each case.

A.2.8.2 Fixed structures

Variable stresses during the in-place situation of fixed structures (either steel or concrete) are due to gust winds and waves, with or without the simultaneous presence of a current. The variable stresses caused by gust winds are normally small and, except for the design of some topsides components, may be neglected.

The effect of current is normally not taken into account, for the following reasons:

— current velocities co-existing with waves in other than extreme or abnormal environmental conditions are usually small and not in the same direction as the waves;

— the influence of current on stress ranges is generally much smaller than the influence on the maximum stress experienced.

The minimum requirement for the fatigue assessment of a fixed structure during the in-place situation is therefore an appropriate description of the site-specific wave environment during its design service life. This is ideally provided by the long-term joint distribution of the significant wave height (H_s), a representative wave period (T_z or T_p), the mean wave direction ($\bar{\theta}$) and the directional spreading around the mean wave direction. Wave-directional spreading is usually neglected or accounted for by a standard spreading function independent of the other three parameters (see A.8.3.2).

The long-term distribution should cover either the full duration of the design service life or the duration of a typical year. If annual distributions are used, it is assumed that the conditions during the typical year repeat themselves each year during the design service life. Seasonal distributions are not appropriate for fatigue assessments.

Where a deterministic fatigue assessment can be used for quasi-statically responding structures, the site-specific wave environment during the structure's design service life may be specified by the long-term marginal distribution of individual wave heights. This distribution can be derived from the wave scatter diagram.

Where vortex-induced vibrations (VIV) due to currents in the in-place situation are important, the long-term marginal distribution of site-specific current speeds should also be determined.

For VIV due to wind action in the pre-service condition, the long-term marginal distribution of sustained wind speeds during the construction period should be made available.

Where variable stresses due to gust winds cannot be disregarded (e.g. for separate support structures for vent stacks or flare towers), the two- or three-parameter wave scatter diagram should be replaced by a three- or four-parameter scatter diagram of the joint occurrence of waves and winds. In such special cases

the waves are as usual specified by H_s and T_z or T_p, supplemented if possible by $\bar{\theta}$, while the wind is normally specified by the sustained wind speed U_{w0} as being the parameter representative of gust winds (see A.7.4).

For slender structural components above water (e.g. drilling derricks, flare towers), the long-term marginal distribution of sustained wind speeds should suffice for a fatigue assessment due to excitation by both gust winds and vortex induced vibrations.

Requirements and guidance for the fatigue assessment of fixed steel and fixed concrete structures are given in ISO 19902 and ISO 19903 respectively.

A.2.8.3 Floating structures

In principle, the specification of all environmental conditions that are expected to occur during the floating structure's period of exposure is along similar lines as that for fixed structures. However, the behaviour of a floating structure under environmental actions is normally more complex than that of a fixed structure. Therefore, the long-term joint distribution of relevant metocean parameters should comprise more parameters than for fixed structures.

Floating structures experience oscillatory motions in six degrees-of-freedom due to wave action. Additionally, floating structures are subjected to slow variations in their position and their orientation, as a result of the simultaneous effects of wind, current and waves. The relevant metocean parameters and the way in which these are specified should suit the procedure being used. For requirements and guidance for the fatigue assessment of floating structures, see ISO 19904-1 for monohulls, semi-submersibles and spars.

A.2.8.4 Jack-ups

For requirements and guidance for the fatigue assessment of a jack-up during a site-specific application, see ISO 19905-1.

A.2.9 Metocean parameters for short-term activities

A.2.9.1 General

Almost all short-term offshore operations, and some offshore-related aviation operations, are sensitive to the accuracy, reliability and timeliness of weather forecasts. Planning prior to the operation is essential to enable safety plans to be properly completed, cost estimates to be accurately determined and any capacity limits on accommodation or transport to be defined.

The most common technique used in such planning exercises is the so-called “persistence” or “weather-window” analysis. This analysis is typically applied to a long-time series (e.g. with a duration of 10 years) of a metocean variable such as significant wave height, mean wind speed or current speed. More sophisticated analyses of multiple parameters (including wave period) may be necessary, in particular for operations involving floating systems.

EXAMPLE In order to plan a required operation at an installation safely, the average number of occasions in the months June to August when the significant wave height at a specific location may be expected to be below 1,5 m for a period of 36 h or more, when at the same time the wind speed should be less than 10 m/s, and the spectral peak wave period is less than 9 s, may be evaluated. It may be necessary to modify an operation to allow the limiting criteria to be relaxed.

In all cases, weather forecasts are likely to be needed both before and during the operations, and it is often worthwhile to collect real-time data on critical metocean parameters (such as wind speed and wave height/period) during the operation in order to assist with the accuracy and timing of the forecasts.

To estimate the duration of individual spells of either severe or calm weather, continuous data shall be used. The analysis shall be performed using either:

— Continuous measured data.

— Measured data in which any breaks have been infilled, using either alternative measured dataset or hindcast data.

— Hindcast data that is verified against an appropriate nearby measured dataset.

References [1] and [11] provide examples of applications of operations requiring metocean data, and reference [12] describes the types of metocean analyses which are often needed in studies to support the planning of floating systems operations.

A.2.10 Metocean parameters for medium-term activities

For medium-term activities such as transportation, the risk of encounter of extreme conditions is dependent on the length of time that the transport spends in those route sectors where extreme conditions are possible. If the length of time is reduced, then the probability of encountering extreme conditions is similarly reduced.

It is generally accepted that for a prolonged ocean transport the wind and wave design criteria should be those with a probability of exceedance per voyage in the range of 0,01 to 0,1. The exceedance level provided by the metocean expert should be matched to the design procedure being used and the requirements of the marine warranty surveyor to ensure an overall target reliability is achieved. The exceedance per voyage refers to the probability of a parameter (e.g. significant wave height) being exceeded over the course of a voyage. This should not be confused with percent exceedance values computed on the basis of exposure during a voyage, which refer to the percentage of time which a parameter will exceed given levels (and which may be of interest in estimating fatigue damage). In areas affected by tropical cyclones, slow tows which cannot avoid cyclones may need to meet an additional requirement of satisfying a seasonal cyclone condition (e.g. 10-year monthly extreme). In addition, for short tows where the exceedance per voyage values may be low, it may be appropriate to design to the 1-year monthly extremes if they are higher.

Where seasonal extremes are required, they must be reconciled with annual extremes. The worst seasonal extreme must be adjusted to match the annual extreme:

— If the worst seasonal extreme is lower than the annual extreme all seasons may be scaled up until the worst season is reconciled.

— If the worst seasonal extreme is higher than the annual extreme, either the fit of the annual extreme should be revisited or the worst seasonal extreme should be truncated at the annual extreme value

— Other company based approaches may be adopted provided the overall operational and/or safety goal is maintained.

A.3 Water depth, tides and storm surges

A.3.1 General

Changes in relative still-water level comprise several components, including atmospheric tides, storm surge effects, changes in mean sea level, vertical movement of the earth's crust, settlement and subsidence. Records in areas such as northern Europe over the past 100 years show a downward trend in relative still-water level, because the crust in this area is lifting at a faster rate than the rise in actual sea level. Apart from sudden tectonic movements, such as earthquakes, changes in relative sea level from tectonics and isostasy are unlikely to be significant during the design service life of a structure. However, there may be significant local crustal movements over periods of decades or so caused by local effects, such as sediment compaction and subsidence, including the effects of reservoir compaction.

Global sea level, and hence still-water level, has been rising and is expected to continue to rise with climate change through the 21st century and beyond; the magnitude of the increase is not expected to be uniform over the globe. See reference [13].

Changes in water depth due to changes in still-water level cause little change in tide and surge elevations unless depths are modified by many metres.

A.3.2 Tides

The best estimates of the water depth and of the fluctuations in water level (HAT, LAT, extreme surge elevation, and extreme total still water level) are derived from site-specific measurements with an offshore

tide gauge measuring pressure from the sea floor. If the tidal signal is dominant, adequate estimates of the tidal range at a given site may be obtained from one month of measured data. However, accurate estimates of extreme tides, including HAT and LAT, require at least one complete year of high-quality data from one location.

A method of analysing water level data requires:

— conversion of pressure measurements to equivalent depths, using density, temperature and atmospheric pressure corrections,

— harmonic tidal analysis, giving values of all significant tidal constituents and the mean water level,

— prediction of tides over 19 years (to account for the 18,6 year precession of the lunar nodes) and extraction of HAT and LAT,

— subtraction of predicted tides from measured levels, giving time series of storm surge elevations,

— separate statistical analyses of the tidal and storm surge elevations, and

— combination of the frequency distribution of tidal and surge elevations to give the required probabilities of total still water level.

When tide gauge measurements have not been made and water depth has been determined by local soundings, corrections should be made for the state of the tide by reference to published tide tables, co-tidal charts or the nearest available tide gauge.

A.3.3 Storm surge

Accurate estimates of the storm surge require a long dataset (at least 10 years), either measured or from a suitable hindcast. An approach based on estimating the extreme skew surge (the difference between the maximum observed sea level and the maximum predicted tidal level in a given tidal cycle), as opposed to the extreme non-tidal residual is described in reference [14].

A.3.4 Extreme water level

The return values of extreme water level are based on the largest combinations of tide, surge and wave crest. The largest of these values has even more potential than the crest alone of occurring in a seastate that is not at the largest Hs within the storm because of the contribution of the still water level to the overall sum. This is particularly true in shallower water locations where the wave heights are usually smaller and the tides and surges often larger than in deeper locations. For this reason, the variation of both the storm seastate and storm surge severity throughout a storm are important as it will affect their joint contribution to the overall extreme water level. Consideration should be given as to how to best represent this relationship given that it will vary throughout a storm history and will also typically vary by direction.

In order to also capture tidal effects, the use of hourly (rather than 3-hourly) datasets is recommended to ensure that the peaks of the tidal cycles are captured.

A.4 Wind

A.4.1 General

When making wind measurements, it is recommended that:

— the height of the wind measurement above mean sea level be known and be sufficiently high to be clear of disturbances to the airflow from the wave surface or from the structure,

— the averaging time of the wind speed measurement be known,

— the air and sea temperatures be measured to enable an evaluation of the atmospheric stability which may affect the wind profile and the wind spectrum (see A.7.3 and A.7.4) in low wind conditions,

— the anemometer not be aerodynamically shielded.

Reference [15] contains guidance on suitable measuring instruments and their use.

Measurements at a location away from the site of interest may be misleading, e.g. because of a sharp gradient in wind speed near a coastline. If it is decided to use such measurements because site-specific measurements are not available, allowance should be made (e.g. by the use of numerical models) for such effects. Wind measurements made over land should be corrected to reflect over-water conditions.

Wind data should be adjusted to a standard elevation of 10 m above mean sea level (the reference elevation z_r) with a specified averaging time such as 1 h. Wind data may be adjusted to any specified elevation different from the base value by using the wind profile given in A.7.3.

A.4.2 Wind actions and action effects

When determining appropriate design wind speeds for extreme and abnormal conditions, the projected extreme wind speeds in specified directions and with specified reference elevations and averaging times should be developed as a function of their recurrence interval.

For most offshore locations, long enough records of *in situ* wind data will not be available to establish reliable estimates of extreme and abnormal wind speeds. In such cases hindcast data are extremely useful. Even when hindcast data are available, calibration of the hindcast against measurements should be carried out if possible.

Important aspects of measurements to note (whether for direct use or as calibration data) are:

— the measurement site, date of occurrence, magnitude of measured sustained wind speeds, wind directions and gust wind speeds for the recorded data that were used during the development of extreme and abnormal winds, and

— the type of storm causing high winds, which is significant when more than one type of storm may be present in the region.

When determining appropriate design wind speeds for normal and short-term conditions, criteria of the following types may be desired:

— the frequency of occurrence of specified sustained wind speeds from various directions for each month or season;

— the persistence of sustained wind speeds above specified thresholds for each month or season; and

— the probable gust wind speed associated with sustained wind speeds.

In some instances the spectrum of wind speed fluctuations about the mean should be specified. For example, floating and other compliant structures in deep water can have natural sway periods in the range of a minute or more, a period at which there is significant energy in the wind speed fluctuations. Data on wind spectra are given in A.7.4.

For most purposes a relatively simple wind model, consisting of the scalar Formula (A.1) in the mean wind direction θ_w suffices:

$$U_w(z,t) = U_w(z) + u_w(z,t) \quad \text{(A.1)}$$

where

$U_w(z,t)$ is the spatially and temporally varying wind speed at elevation z above mean sea level and at time instant t;

$U_w(z)$ is the mean wind speed at elevation z above mean sea level, averaged over a specified time interval;

$u_w(z,t)$ is the fluctuating wind speed at elevation z around $U_w(z)$ and in the same direction as the mean wind.

The wind speed in a 3 s gust is appropriate for determining the maximum quasi-static local actions caused by wind on individual components of the structure, whereas 5 s gusts are appropriate for maximum quasi-static local or global actions on structures whose maximum horizontal dimension is less than 50 m, and 15 s gusts are appropriate for the maximum quasi-static global actions on larger structures.

When design actions due to wind need to be combined with actions due to waves and current, the following are appropriate:

— for structures with negligible dynamic response, the 1 h mean wind may be used to determine quasi-static global actions caused by wind in conjunction with extreme or abnormal quasi-static actions due to waves and currents;

— for structures that are moderately dynamically sensitive, but do not require a full dynamic analysis, the 1 min mean wind may be used to determine quasi-static global actions caused by wind, again for wind in conjunction with extreme or abnormal quasi-static actions due to waves and currents;

— for structures with significant dynamic response to excitation with periods longer than 20 s, a full dynamic response analysis to fluctuating winds should be considered.

A.4.3 Wind profile and time-averaged wind speed

A.4.3.1 Relationships for Different Storm Types

The most general formulations for wind profile and gust factors take into account atmospheric stability. The fairly simple relations presented here have implicitly taken stability into account by fitting to data in specific storm types. The relations are appropriate for engineering purposes in relevant storm types. For “extratropical storms,” it is recommended to use the profile and gust factors based on the Frøya measurements made offshore Norway.[16] It is presently recommended to apply these relations in A.7.3.2 to all storm types except tropical cyclones and convective storms (such as squalls). For tropical cyclones, the set of profiles and gust factors in A.7.3.3, based on the Engineering Sciences Data Unit (ESDU) relations, are recommended.[17,18] Analysis of measurements made in squalls offshore the Congo has found that profile and gust factors (A.7.3.4) seem to show a somewhat different nature than these other storm types[19].

A.4.3.2 Extratropical Storm Wind Profile and Time-averaged Wind Speed

Measurements of representative offshore conditions, in strong, nearly neutrally stable atmospheric wind conditions, suggest that the mean wind speed profile $U_w(z)$ in storm conditions can be more accurately described by a logarithmic profile as given in Formula (A.2) than by the power law profile traditionally used:

$$U_{w,1\,h}(z) = U_{w0}\,[1 + C\ln(z/z_r)] \qquad \text{(A.2)}$$

where

$U_{w,1\,h}(z)$ is the 1 h sustained wind speed at a height z above mean sea level;

U_{w0} is the 1 h sustained wind speed at the reference elevation z_r and is the standard reference speed for sustained winds;

C is a dimensionally dependent coefficient, the value of which is dependent on the reference elevation and the wind speed, U_{w0}. For z_r = 10 m, C = (0,057 3) (1 + 0,15 U_{w0})$^{1/2}$ where U_{w0} is expressed in metres per second (m/s);

z is the height above mean sea level;

z_r is the reference elevation above mean sea level (z_r = 10 m).

For the same storm conditions, the mean wind speed for averaging times shorter than 1 h may be expressed by Formula (A.3) using the 1 h sustained wind speed $U_{w,1\,h}(z)$ of Formula (A.2):

$$U_{w,T}(z) = U_{w,1\,h}(z)\,[1\text{-}0{,}41\,I_u(z)\,\ln(T/T_0)] \qquad \text{(A.3)}$$

where additionally

$U_{w,T}(z)$ is the sustained wind speed at height z above mean sea level, averaged over a time interval T < 3 600 s;

$U_{w,1\,h}(z)$ is the 1 h sustained wind speed at height z above mean sea level, see Formula (A.2);

T is the time-averaging interval with $T < T_0$;

T_0 is the standard reference time averaging interval for wind speed of 1 h = 3 600 s;

$I_u(z)$ is the dimensionally dependent wind turbulence intensity at a height z above mean sea level, given by Formula (A.4), where U_{w0} is expressed in metres per second (m/s):

$$I_u(z) = (0{,}06)[1 + 0{,}043\,U_{w0}]\left(\frac{z}{z_r}\right)^{-0{,}22} \qquad \text{(A.4)}$$

The equations in this subclause are typical engineering equations derived from curve-fitting through available data[16] and contain numerical constants that are valid only in the SI units of metres and seconds.

NOTE 1 Approximations to Formulae (A.2) and (A.3) using a power law may be adequate.

NOTE 2 For tropical cyclone winds, equations in A.7.3.3 are recommended, and for squalls, equations in A.7.3.4 are recommended.

NOTE 3 The above equations are not valid for the description of squall winds, since the duration of the squall is often less than 1 h.

A.4.3.3 Tropical Cyclone Storm Wind profile and Time-averaged Wind Speed

Within 100 m elevation of the sea surface, boundary layer corrections are insignificant and an ESDU based mean profile for tropical cyclone conditions may be simplified to a basic log-law profile. For tropical cyclone conditions the 1 h sustained wind speed at a height z above MSL is:

$$U_{w,1\,h}(z) = \frac{u_*}{0{,}4}\ln\left(\frac{z}{z_0}\right) \qquad \text{for } z \le 100 \text{ m} \qquad \text{(A.5)}$$

where u_x is the friction velocity and z_0 is the boundary-layer scaling parameter given by:

$$u_* = \sqrt{D_{d_{10}}}\,U_{w0} \qquad \text{(A6)}$$

$$z_0 = 10exp\left[-0,4/\sqrt{C_{d_{10}}}\right] \quad \text{(A7)}$$

For tropical storms, the drag coefficient C_{d10} is capped at higher wind speeds:

$$C_{d_{10}} = \begin{cases} (0,49+0,065U_{w0})10^{-3}, \text{ for } U_{w0} < 27,85\,m/s \\ 0,0023, \text{ for } U_{w0} \geq 27,85\,m/s \end{cases} \quad \text{(A8)}$$

The *T*-second gust at any elevation *z* is found by applying the peak gust factor $g_T(z)$ and turbulence intensity $I_U(z)$ to the 1 h wind at the given elevation as:

$$U_{w,T}(z) = U_{w,1h}(z)[1+g_T(z)I_U(z)] \quad \text{(A9)}$$

The gust factor and turbulence intensity are given by:

$$g_T(z) = \left[\sqrt{2\ln(T_0\nu)} + \frac{0,577}{\sqrt{2\ln(T_0\nu)}}\right]\left[1-0,193\left(\frac{T_u}{T}+0,1\right)^{-0,68}\right], \text{ for T} \leq 600 \text{ s} \quad \text{(A10)}$$

$$I_u(z) = \frac{u_* 7,5\eta\left[0,538+0,09\ln\left(\frac{z}{z_0}\right)\right]^{\eta^{16}}}{1+0,156ln\left(\frac{u_*}{f_C z_0}\right)} \cdot \frac{1}{U_{w,1h}(z)} \quad \text{(A11)}$$

The gust factor depends on the standard reference time T_0 = 3 600 s, the zero-upcrossing frequency ν, the integral time scale T_U and the scaling parameter η, which are described by:

$$\nu = \frac{0,007+0,213\left[\frac{T_u}{T}\right]^{-0,654}}{T_u} \quad \text{(A12)}$$

$$T_u = 3,12z^{0,2}$$

$$\eta = 1-6f_c z/u_*$$

The scaling parameter η and the turbulence intensity have an additional dependence on site latitude ψ (in decimal degrees) through the absolute value of the Coriolis parameter f_C:

$$f_c = 2\Omega sin|\psi| = 2\left(7,29\times10^{-5}\right)sin|\psi| \quad \text{(A13)}$$

where Ω is the rotation of the earth in radians per second.

The equations in this subclause are typical engineering equations derived from curve-fitting through available data and contain numerical constants that are valid only in the SI units of meters and seconds.

NOTE 1 The equations in this subclause are intended specifically for tropical cyclones. For other storm types, the equations in subclause A.7.3.2 or A.7.3.4 are recommended.

NOTE 2 In the original References [17, 18], Equation (A.5) contains a boundary layer correction term, which is insignificant over the lower 100 m of the atmosphere.

NOTE 3 In the limit, the gust factor in Equation (A.10) does not reduce to 1,0 for T = 3 600 s. For T = 3 600 s, Equation (A.5) may be used directly.

A.4.3.4 Squall Wind Profile and Time-averaged Wind Speed

Because squalls are transient wind events in which peak winds may be sustained for durations of less than 10 min, the reference wind speed for squall events is defined as the peak 1 min average wind speed at 10 m elevation. The peak 1 min wind speed at elevations other than 10 m may be estimated using a log-layer profile in the form:

$$U_{w,1\,min}(z) = \frac{\ln\left(\frac{z}{z_0}\right)}{\ln\left(\frac{10\,m}{z_0}\right)} U_{w,1\,min}(10\,m) \tag{A.14}$$

where

$$z_0 = 7{,}0\times10^{-10}\,m \tag{A.15}$$

The peak 3 s gust at a given elevation may be estimated from the peak 1 min wind at the same elevation by applying a gust factor:

$$U_{w,3\,sec}(z) = g_{3\,sec}(z)\,U_{w,1\,min}(z) \tag{A.16}$$

where

$$g_{3\,sec}(z) = 1{,}06 + 0{,}049\,1\exp\{-0{,}051\,4(z-10)\} \tag{A.17}$$

The equations in this subclause are typical engineering equations derived from curve-fitting through available data and contain numerical constants that are valid only in the SI units of meters and seconds.

NOTE 1 The equations in this subclause are intended specifically for squall events. For other storm types, the equations in subclause A.7.3.2 or A.7.3.3 are recommended.

NOTE 2 The basis [19] for the squall elevation and gust factors presented here are measurements made offshore the Congo at elevations between 10 m and 37,5 m above sea level.

A.4.4 Wind spectra

A.4.4.1 Spectra for Different Storm Types

Separate spectral forms are recommended for extratropical storms (see A.7.4.2) and tropical cyclones (see A.7.4.3). Squalls are inherently transient phenomena and therefore dynamic responses to squall events would most appropriately be analyzed in the time domain using realistic event histories.

Figure A.2 shows wind spectra using both the recommended forms for extratropical storms and tropical cyclones for 1 h sustained wind speeds of 20 m/s, and 40 m/s at elevations of z = 10 m and z = 50 m.

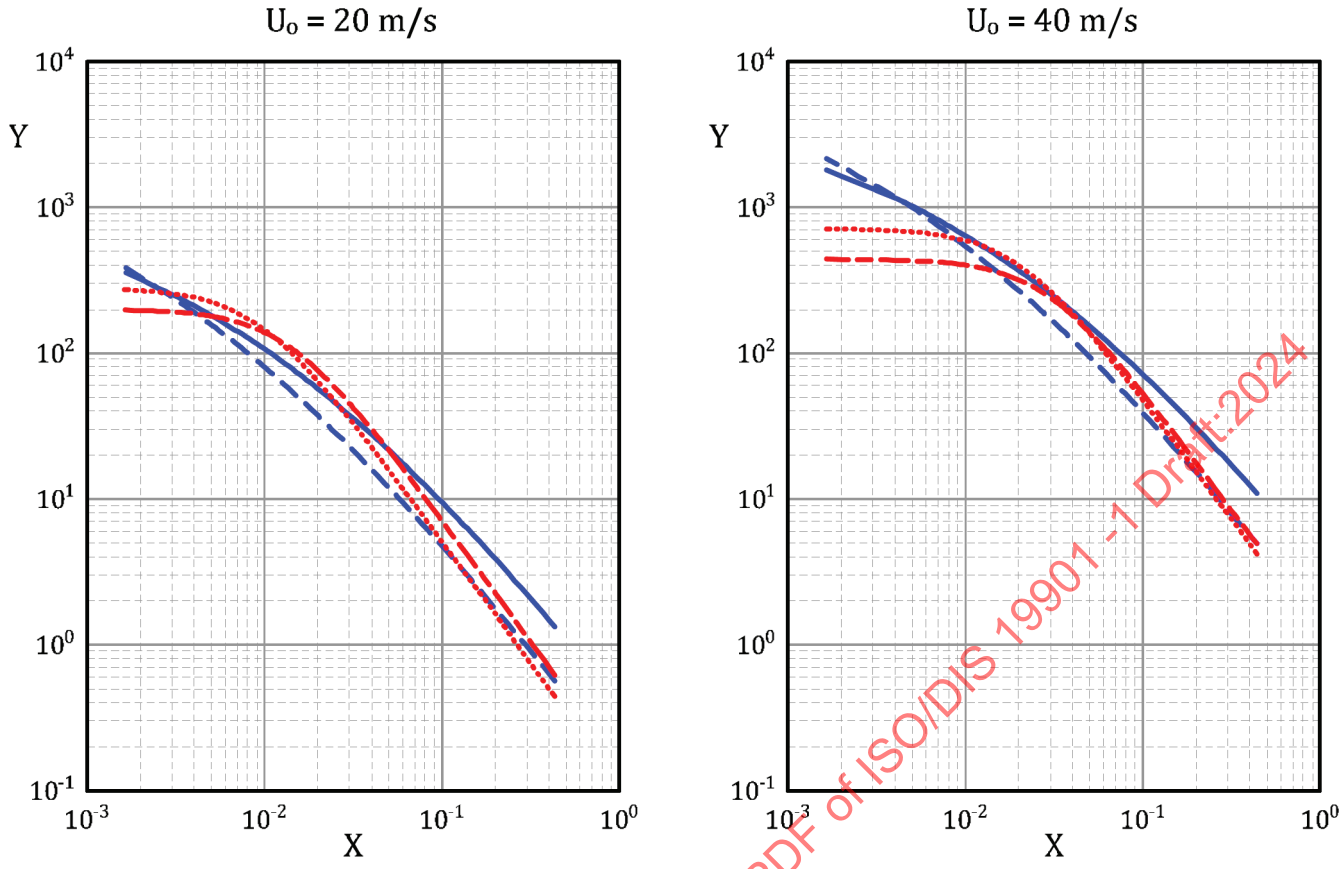

Key

X	frequency (HZ)		z=10 m tropical cyclone
Y	S(m^2/s)		z=50 m extratropical
	z=10 m extratropical		z=50 m tropical cyclone

Figure A.2 — Examples of wind spectra

A.4.4.2 Extratropical Storm Wind Spectra

Wind turbulence, i.e. the dynamic properties of the wind, depends on the stability of the atmospheric boundary layer. Stability, in turn, depends on the temperature difference between air and sea and on the mean wind speed. The equations in this subclause for the dynamic wind properties are appropriate for nearly neutral (slightly unstable) atmospheric stability in storm conditions.[16] For general atmospheric conditions where (in)stability is important, and for weaker wind conditions, a more complex formulation that allows deviations from neutral stability is more appropriate.

The fluctuating wind speed $u_w(z,t)$ (turbulence) may be described in the frequency domain by a wind spectrum, analogous to the way in which the wave spectrum describes the water surface elevation (see A.8.3). The spectral density function of the longitudinal wind-speed fluctuations at a particular point in space may be described by the one-point turbulence spectrum of Formula (A.17):

$$S(f,z) = \frac{\left(320\,m^2/\mathrm{s}\right)\cdot\left(\frac{U_{w0}}{U_{\mathrm{ref}}}\right)^2\cdot\left(\frac{z}{z_r}\right)^{0,45}}{\left(1+\tilde{f}^n\right)^{5/(3n)}} \tag{A.18}$$

Where:

$S(f,z)$ is the wind spectrum (spectral or energy density function) at frequency f and elevation z;

U_{w0} is the 1 h sustained wind speed at the reference elevation z_r (the standard reference speed for sustained winds);

U_{ref} is the reference wind speed, U_{ref} = 10 m/s;

f is the frequency in cycles per second (hertz) over the range 0,001 67 Hz < f < 0,5 Hz;

z is the height above mean sea level;

z_r is the reference elevation above mean sea level (z_r = 10 m);

$\tilde{f}$ is a non-dimensional frequency defined by Formula (A.18) where the numerical factor 172 has the dimension of seconds (s):

$$\tilde{f} = (172\,s)\, f \left(\frac{z}{z_r}\right)^{2/3} \left(\frac{U_{w0}}{U_{ref}}\right)^{-0,75} \quad \text{(A.19)}$$

n is a coefficient equal to 0,468.

The variance (i.e. the square of the standard deviation) of the wind speed fluctuations about the mean wind speed is by definition equal to the integral of the spectral density function over the entire frequency range from f = 0 to f = ∞. However, the data from reference [16], from which the spectral formulation in Formulae (A.18) and (A.19) has been derived, extend from f = 1/600 = 0,001 67 Hz to f = 0,43 Hz ≈ 0,50 Hz. The integral of the spectrum over frequency may thus only reflect wind speed fluctuations within this frequency range. Therefore, the integral of the spectrum will only correspond with a part of the total variance of the wind speed, and so caution should be exercised when relating the integral to available measurements to ensure that comparable frequency ranges are compared. It should further be noted that $S(f, z)$ from Formula (A.18) does not go to zero below the lowest frequency of f = 1/600 Hz considered in the measurements.

For practical applications, the wind spectrum at a point should be supplemented by a description of the spatial coherence of the fluctuating longitudinal wind speeds over the exposed surface of the structure or the structural component. In frequency domain analyses, it may be conservatively assumed that all scales of turbulence are fully coherent over the entire topsides. However, for some structures, it may be advantageous to account in the dynamic analysis for the less-than-full coherence at higher frequencies. The correlation between the spectral energy densities of the longitudinal wind speed fluctuations at frequency f between two points in space may be described in terms of the two-point coherence function. The recommended coherence function between two points $P_1(x_1, y_1, z_1)$ and $P_2(x_2, y_2, z_2)$, with along-wind positions x_1 and x_2, across-wind positions y_1 and y_2, and elevations z_1 and z_2, is given by Formula (A.20):

$$F_{Coh}(f, P_1, P_2) = \exp\left\{-\frac{1}{U_{w0}}\left[\sum_{i=1}^{3}(A_i)^2\right]^{1/2}\right\} \quad \text{(A.20)}$$

where

$F_{Coh}(f,P_1,P_2)$ is the coherence function between turbulence fluctuations at $P_1(x_1,y_1,z_1)$ and at $P_2(x_2,y_2,z_2)$;

U_{w0} is the 1 h sustained wind speed at 10 m above mean sea level, in metres per second (m/s);

A_i is a function of frequency and the position of the two points P_1 and P_2.

A_i is calculated from Formula (A.20):

$$A_i = \alpha_i f^{r_i} (D_i)^{q_i} \left(\frac{z_g}{z_r}\right)^{-p_i} \text{ in metres per second (m/s)} \quad \text{(A.21)}$$

where

f is the frequency, in hertz (Hz);

D_i is the distance, expressed in metres (m), between points P_1 and P_2 in the x, y and z directions for i = 1, 2 and 3 respectively, see Table A.1;

z_g is the geometrical mean height of the two points, $z_g = (z_1 \cdot z_2)^{1/2}$;

z_r is the reference elevation above mean sea level, z_r = 10 m;

α_i, p_i, q_i and r_i are coefficients given in Table A.1.

Table A.1 — Coefficients in Formula (A.20) for points P_1 and P_2

i	D_i	α_i	p_i	q_i	r_i
1	$\|x_1 - x_2\|$	2,9	0,4	1,00	0,92
2	$\|y_1 - y_2\|$	45,0	0,4	1,00	0,92
3	$\|z_1 - z_2\|$	13,0	0,5	1,25	0,85

A.4.4.3 Tropical Cyclone Wind Spectra

For tropical storms the representation of velocity spectrum at a given elevation z is as follows:

$$S(f,z) = \frac{4 I_u^2 U_{w,1\,h}(z) L_{u,x}(z)}{\left[1 + 70{,}8\left(\frac{f L_{u,x}(z)}{U_{w,1\,h}(z)}\right)^2\right]^{5/6}} \quad \text{(A.22)}$$

where f is the frequency in hertz and $L_{U,X}$ is the integral length scale and is a measure of the effective size of the turbulent eddies within the atmospheric boundary layer. It is a function of z and z_0 in the form:

$$L_{u,x}(z) = \frac{50 z^{0,35}}{z_0^{0,063}} \quad \text{(A.23)}$$

where z_0 is the boundary-layer scaling parameter for tropical cyclone winds defined by Equation (A.7).

Corresponding coherence functions have not been derived for the tropical cyclone spectrum.

A.5 Waves

A.5.1 General

The main factors to be considered when assessing the properties of waves at a particular site and their influence on the design, construction and operation of structures are described below.

— **Fetch limitations**

Wave growth is restricted by fetch length and width if the waves are generated by local winds. Reference [20] provides simple parametric expressions quantifying these effects, while more complete numerical models referenced below include these processes for much more general geometries.

— **Nonlinear wave effects**

In extreme storms, even in deep water, individual waves exhibit nonlinear behaviour. In shallow water, even under normal conditions, waves also exhibit nonlinear behaviour, as they are affected by the sea floor. In deep water, for waves that are not too high or too steep, linear wave theory (Airy) is adequate for describing the kinematics of the waves, but for higher or steeper waves in deep water and in shallow

water, higher-order theories are more appropriate to describe wave properties, such as the crest elevation and kinematics. Water is taken as shallow when the water depth/deep water wavelength of the spectral peak frequency is less than approximately 0,13[10].

— **Refraction**

As waves propagate into shallow water, their speed (which depends on their period and the local water depth) is reduced and they are refracted. For simple bathymetry and single wave periods, refraction may be estimated using Snell's Law or by ray plotting techniques as described in reference [20]. For more complex bathymetry and short-crested waves, a numerical method is more appropriate. Refraction can result in both increases and decreases in wave energy/heights as well as in changes in direction between adjacent sites within a shallow water area, depending on the bathymetric configuration. Currents can also cause refraction and should be considered, particularly where tides or rivers create strong currents.

— **Diffraction and reflection**

These processes may be important when waves encounter a protruding object, such as a breakwater or an island. The potential for focal points of wave energy occurring behind nearby islands or sea-mounts should be considered.

— **Shoaling and wave breaking**

As a periodic wave propagates into shallower water, its length is reduced but its period remains the same. For random waves it may be assumed that the spectral peak period remains the same. This process is known as shoaling. As the wave continues to propagate into shallow water, the wave steepens until the particle velocity at the crest exceeds the speed of the wave and breaking results. In shallow water with a flat seabed, the empirical limit of the wave height is approximately 0,78 times the local water depth for waves that are long-crested. The wave height of short-crested waves can approach 0,9 times the local water depth. The breaker height also depends on beach slope. In deep water, waves can break with a theoretical limiting steepness of 1/7. In addition, nonlinearity in the sea-state can increase the wave height due to nonlinear shoaling.

— **Crest elevations**

An accurate description of the distribution of extreme crest elevations at the site is needed to establish the minimum deck elevation of bottom-founded structures and to establish the likelihood of wave impact on the underside or deck of semi-submersibles. Wave-structure interactions can affect crest elevations, in particular where structures have large diameter columns. Shoaling and nonlinear processes affect crest elevations as waves move into shallow water. The proportion of the wave height above nominal still water increases as the water becomes shallower.

— **Bottom dissipation**

As waves move into shallow water, the horizontal oscillatory velocities at the bottom become large and turbulent dissipation results. This process may be captured in hindcast models, as shown in reference [21].

— **Wave-wave interaction**

Detailed directional wave spectra at several sites were examined in reference [22]. It was found that the evolution of the wave spectrum could be parameterized as a function of local water depth. It was proposed that this was due to the nonlinear wave-wave interactions between different wave frequency components.

— **Infra-gravity waves**

These are surface gravity waves with periods in the range of roughly 25 s to 300 s. In principle they can be generated by different physical processes, but are most commonly associated with waves generated by nonlinear second-order difference frequency interactions between different swell wave components. As swells propagate over shallow water, forced infra-gravity wave energy associated with swell wave interactions can be released and propagate freely. Forced and free infra-gravity wave energy can be

reflected from shore and can become trapped in shallow water due to refraction (edge-waves) or can propagate back out into deep water (leaky waves). Except in the surf zone, amplitudes are normally on the order of tens of centimetres. They are of particular importance when their periods match those of shallow-water moored vessels with lightly-damped surge responses, and dynamic responses result.

In view of the complexity of shallow-water processes, the best method of calculating wave height is usually through a comprehensive numerical wave model that includes the relevant processes outlined above. Reference [23] provides information on the accuracy of early wave models.

Estimates from many locations around the world indicate that the following accuracies may be achieved with hindcast models in either deep or shallow water:

— mean error (bias) in H_s of 0,1 m;

— coefficient of variation of 10 % to 15 % for storm peak H_s;

— coefficient of variation of approximately 20 % for all H_s over long continuous periods (e.g. 10-year hindcasts).

No wave sensor or wave model is ideal in its ability to accurately measure waves or reproduce still water level as a reference base. For example, operating constraints on bottom-founded offshore structures frequently mean that platform-mounted sensors do not measure the undisturbed sea surface. Similarly, wave buoys do not respond ideally in high sea-states, in particular they underestimate large crest heights. Wave models are only as good as the physics that are incorporated in them and the description of the input wind fields used to drive them. The strengths and weaknesses of any particular dataset should be recognized throughout the process of its analysis and interpretation.

When using hindcast data, care should be taken to ensure that hindcast waves are consistent with site-specific and reliable measured data recorded over the same period. In particular, the spatially and temporally averaged nature of hindcast data and the sampling noise inherent in many measurement datasets should be taken into account, and one or both datasets should be factored if necessary.

Reference [24] provides a description of a recording philosophy for waves. A description of methods for analysing wave data and calculating extremes may be found in references [10] and [3].

Experts, knowledgeable in the fields of meteorology, oceanography and hydrodynamics, should be consulted when developing wave-dependent environmental conditions and associated metocean parameters. In developing sea-state data, either in the form of statistical parameters characterizing the sea-state or in the form of representative individual waves occurring within the sea-state, consideration should be given to the following.

a) For normal conditions and short-term activities (for both seas and swells):

   1) the probability of occurrence and the average persistence of various sea-states for each month and/or season (e.g. environmental conditions with waves higher than 3 m from specified directions in terms of general sea-state parameters, such as the significant wave height and the mean zero-crossing wave period);

   2) the wind speeds, tides and currents occurring simultaneously with the above sea-states;

   3) the percentage of significant or individual wave heights, directions and periods within specified ranges (e.g. 3 m to 4 m high waves from the SE quadrant during each month and/or season).

b) For extreme and abnormal conditions:

   Estimated extreme and abnormal wave heights from specified directions should be developed and presented as a function of their return periods. Other data that should be developed include:

   1) the probable range and distribution of wave periods associated with extreme and abnormal wave heights, for the specification of individual design waves,

   2) the distribution of maximum crest elevations, and the wave energy spectrum in the sea-state producing extreme and abnormal wave heights,

3) the tides, currents, winds and marine growth likely to occur simultaneously with the sea-state producing the extreme and abnormal waves.

A.5.2 Wave actions and action effects

When considering extreme and abnormal conditions for design situations, the following points should be considered:

— The maximum height of an individual wave with a given return period is, in general, higher than the most probable maximum wave height of a 1 h or 3 h sea-state with the same return period.

— The highest action on, or the largest action effect in, a structure is not necessarily induced by the highest sea-state or the highest wave in a sea-state. This is due to the sensitivity of structures to the frequency content of waves in a sea-state, and the geometric particulars of the structure concerned.

— Waves and currents can create seabed scour around objects on or near the sea floor that obstruct free flow conditions. Examples where scour can occur are around the legs of structures and jack-ups, around subsea templates and underneath pipelines.

— Loads on submarine pipelines are complicated, because drag and lift loads are functions of the ratio of steady current to wave orbital velocity and the Keulegen-Carpenter number.

A.5.3 Sea-states — Spectral waves

A.5.3.1 Wave spectrum

A.5.3.1.1 General

The shape of wave spectra varies widely. The two broad classifications of sea-state are:

— Wind seas: Generated by the local wind; the corresponding shape of the wave spectrum will thus depend on the wind speed, the fetch length of the wind over open water and the duration during which the wind has been blowing. Within wind seas there is a further distinction between wave conditions that are fully developed and wave conditions that are still developing. In the first case, the sea is in a state of equilibrium: the energy input by the wind and the energy dissipation in the wave processes are in balance. In the second case, there is net energy input and the waves are consequently still growing.

— Swells: These are wind-generated waves that have travelled far from the generation region. Swell waves have no relationship with the local wind regime.

Spectral fitting is used to determine the parameters of parametric wave spectral shapes. In addition, for design it is sometimes required to separate the swell components of the wave spectrum from the wind sea components of the wave spectrum. To achieve this, spectral splitting and fitting is required. There are various methods of spectral splitting, from simple frequency division at a nominated frequency (such as 0,1 Hz/10 s) to complex wave-train tracking algorithms. Spectral splitting is used to provide a swell and/or wind sea spectral description which may be associated with prevailing conditions (as required for fatigue and operability assessments) and for extreme design conditions.

Some of the parametric formulations of the wave frequency spectrum $S(f)$ most frequently used in the offshore industry are presented below.

A.5.3.1.2 The JONSWAP spectrum and Pierson-Moskowitz spectrum

The JONSWAP (Joint North Sea wave project) wave frequency spectrum is a modification of the Pierson-Moskowitz spectrum. The JONSWAP wave spectrum was originally formulated in terms of wind speed and non-dimensional fetch. A form such as the one proposed by Goda,[25] which is expressed in terms of

significant wave height, peak spectral period and peak enhancement factor γ, is much more convenient for engineering purposes:

$$S(f)=\alpha H_S^2 T_p^{-4} f^{-5}\exp\left\{-1{,}25(T_p f)^{-4}\right\}\gamma^{\beta} \tag{A.24}$$

where

$$\alpha \approx \frac{0{,}062\,4}{0{,}230+0{,}033\,6\gamma-0{,}185(1{,}9+\gamma)^{-1}} \tag{A.25}$$

$$\beta = exp\left\{-\frac{\left(T_p f-1\right)^2}{2\sigma^2}\right\} \tag{A.26}$$

$$\sigma=\begin{cases}\sigma_a & \text{when} \quad f \le f_p \\ \sigma_b & \text{when} \quad f \ge f_p\end{cases} \quad \text{and} \quad \begin{matrix}\sigma_a=0{,}07 \\ \sigma_b=0{,}09\end{matrix} \tag{A.27}$$

In the above expressions

γ is a non-dimensional peakedness parameter (when γ = 1, the JONSWAP spectrum reverts to the Pierson-Moskowitz spectrum);

f_p is the peak frequency;

σ is the spectral width either side of the spectral peak.

The values of σ above and below the peak frequency of 0,07 and 0,09 used in the Goda formulation correspond to the mean values measured in the original JONSWAP formulation. It is common to use these values in the absence of other derived values. However, the values for σ and γ can vary widely between different times during the development of the sea-state and between different sites around the world. Therefore, when fitting measured spectra, the values of α, σ and γ may be varied to optimize the fit.

A.5.3.1.3 Swell Gaussian spectra

Wave frequency spectra for swells are generally much narrower in frequency content than spectra for wind seas. Long-period swells from distant storms are more or less symmetrical in shape around the swell peak frequency. Even so, the swell spectrum is frequently described using a JONSWAP function with a large peak enhancement factor. Use of the JONSWAP function has the advantage that the spectral shape of shorter-period swells, which tend to have broader spectra particularly above the peak frequency, may be described well. In addition, the JONSWAP spectrum does not leak energy below zero frequency. Nevertheless, the symmetric normal or Gaussian function is generally considered to be a better descriptor of swell, particularly long-period swell.

A symmetric swell spectrum may be defined in complete analogy with the normal or Gaussian probability density function as:

$$S(f)=\frac{H_s^2}{16}\frac{1}{\sigma_g\sqrt{2\pi}}\exp\left(-\frac{1}{2}\left[\frac{f-f_p}{\sigma_g}\right]^2\right) \tag{A.28}$$

where

f_p is the peak frequency;

σ_g is the parameter defining the width of the symmetric swell spectrum (equals the standard deviation of the Gaussian function).

Typical values of σ^g vary from 0,05 to 0,015. In application, spectral fitting should generally be undertaken to determine the range of values of the standard deviation.

In applying a Gaussian spectrum to design, care should be taken with the low frequency side of the spectrum, since values of the standard deviation (higher than ~0,01) may introduce energy at very low frequencies, including the zero frequency. For dynamically sensitive facilities, this may cause excessive and unrealistic responses.

A.5.3.1.4 The Ochi-Hubble form for bimodal seastates

The Ochi-Hubble spectral form[26] was developed for the purpose of describing dual-peaked (bimodal) wave spectra. The full bimodal spectrum is formed by combining two sea-state partitions as:

$$S_{\text{total}}(f) = S_1(f) + S_2(f) \tag{A.29}$$

Typically, one of these partitions describes a longer period swell component and the other partition describes shorter period seas. Each partition of the spectrum is defined as:

$$S_i(f) = \frac{\pi}{2}\left[\frac{\left\{4(4\lambda_i+1)\pi^4 f_{p,i}^4\right\}^{\lambda_i}}{\Gamma(\lambda_i)} \cdot \frac{H_{s,i}^2}{(2\pi f)^{4\lambda_i+1}} . exp\left\{-\left(\frac{4\lambda_i+1}{4}\right)\left(\frac{f_{p,i}}{f}\right)^4\right\}\right] \tag{A.30}$$

where

$H_{s,i}$ is the significant wave height of the i^{th} partition of the spectrum;

$f_{p,i}$ (= $1/T_{p,i}$) is the peak spectral frequency of the i^{th} partition;

λ_i is the spectral peak enhancement factor of the i^{th} partition;

Γ is the mathematical gamma function.

Note that since spectral energy is proportional to wave height-squared, the significant wave heights of the two spectral partitions do not add linearly. Rather the overall significant wave height in a bimodal Ochi-Hubble spectrum is given by:

$$H_{s,\text{total}} = \sqrt{{H_{s,1}}^2 + {H_{s,2}}^2} \tag{A.31}$$

A.5.3.1.5 General multi-modal spectra

The Ochi-Hubble spectrum is just one multi-modal spectral form. In general, multi-peaked spectra may be formed simply by adding spectral partitions as:

$$S_{\text{total}}(f) = \sum_{i=1}^{n} S_i(f) \tag{A.32}$$

If multi-peaked spectra are specified, the overall significant wave height is:

$$H_{s,\text{total}} = \sqrt{\sum_{i=1}^{n} H_{s,i}^2} \tag{A.33}$$

Torsethaugen [27] developed sets of bimodal spectra typical of the northern North Sea by combining pairs of JONSWAP spectra. In regions where the Gaussian spectrum is used to describe long-period swells (e.g. Nigeria) the Gaussian swells might be combined with a JONSWAP partition to describe local seas. In swell-dominated regions, it may also be advantageous to specify multiple-swell partitions as well as a sea. In such cases, *n* is three or higher. In principle *n* may be arbitrarily high, but in practice if *n* is higher than three it may be more straightforward to use a discrete numerical description of the spectrum rather than using a parameterized form.

A.5.3.1.6 Applications

The most appropriate form of the wave frequency spectrum for an offshore structure depends on the geographical area, the severity of the sea-state, whether the sea-state is fully developed or is still growing, and the application concerned. For example, for a short-term North Sea design storm condition, a unidirectional JONSWAP spectrum may be most appropriate, whereas for the modelling of a series of sea-states for a long-term fatigue analysis directionally spread, Pierson-Moskowitz spectra are often more appropriate. Similarly, for vessel downtime studies offshore West Africa, the use of a bimodal spectrum composed of a low-frequency swell spectrum from one direction and a high-frequency wind sea spectrum from a different direction could be appropriate.

Wave spectral shapes in shallow water do not generally conform to either the Pierson-Moskowitz or the JONSWAP forms, although a modified version of the JONSWAP spectrum is sometimes used (see reference [22]).

A.5.3.1.7 Definition of frequency

The wave frequency may either be expressed in terms of ω in radians per second (rad/s) or in terms of f in cycles per second or hertz (Hz). The relationship between these two frequencies is:

$$\omega = 2\pi f = \frac{2\pi}{T} \tag{A.34}$$

Since the energy per frequency band remains the same, i.e.

$$S(\omega)d\omega = S(f)df$$

the relationship between the two alternative expressions of the wave frequency spectrum is given by:

$$S(f) = 2\pi \cdot S(\omega) \tag{A.35}$$

A.5.3.2 Directional spreading

A.5.3.2.1 General

The directional characteristics of wave spectra are often assumed to be independent of frequency, allowing a separation of variables so that the directional wave spectrum may be expressed as the product of a wave directional spreading function $D(\theta)$ (see A.8.3.2.2), independent of frequency, and a wave frequency spectrum $S(f)$, which is independent of direction. The general relationship in Formula (A.35):

$$S(f,\theta) = D(f,\theta) \cdot S(f) \tag{A.36}$$

is then replaced by:

$$S(f,\theta) = D(\theta) \cdot S(f) \tag{A.37}$$

where the directional spreading function by definition satisfies the relationship:

$$\int_{-\pi}^{\pi} D(\theta)d\theta = 1 \tag{A.38}$$

Standard formulations for the directional spreading function may be found in the literature, for example in reference [10]. However, detailed directional wave information is not always available. In practical applications, unidirectional sea-states are often taken as a modelling assumption. However, if the influence of directional wave spreading is expected to be significant, sensitivity analyses should be performed to investigate the effect. In such cases, one of the distributions shown in Formula (A.39) may be used.

The directional spreading function $D(\theta)$ is a symmetric function around the mean direction $\bar{\theta}$. In the absence of information to the contrary, the mean wave direction may be assumed to coincide with the mean wind direction. There are three expressions for $D(\theta)$ in common use:

$$
\begin{aligned}
D_1(\theta) &= C_1(n)\cdot\left(\cos(\theta-\bar{\theta})\right)^n && \text{for } -\tfrac{1}{2}\pi \le (\theta-\bar{\theta}) \le +\tfrac{1}{2}\pi \\
D_2(\theta) &= C_2(s)\cdot\left[\cos\left(\frac{\theta-\bar{\theta}}{2}\right)\right]^{2s} && \text{for } -\pi \le (\theta-\bar{\theta}) \le +\pi \\
D_3(\theta) &= C_3(\sigma)\cdot\frac{1}{\sigma\sqrt{2\pi}}\cdot\exp\left[-\frac{(\theta-\bar{\theta})^2}{2\sigma^2}\right] && \text{for } -\tfrac{1}{2}\pi \le (\theta-\bar{\theta}) \le +\tfrac{1}{2}\pi \\
D_1(\theta) &= D_2(\theta) = D_3(\theta) = 0 && \text{for all other } (\theta-\bar{\theta})
\end{aligned}
\qquad \text{(A.39)}
$$

where

$$C_1(n) = \frac{\Gamma(n/2+1)}{\sqrt{\pi}\,\Gamma(n/2+1/2)}$$

$$C_2(s) = \frac{\Gamma(s+1)}{2\sqrt{\pi}\,\Gamma(s+1/2)}$$

$$C_3(\sigma) = 1$$

The functions all have a peak at $\theta = \bar{\theta}$, the sharpness of which depends on the exponent n in $D_1(\theta)$ or s in $D_2(\theta)$, or the standard deviation σ of the normal distribution $D_3(\theta)$. The coefficients C are normalizing factors dependent on n, s or σ, which are determined such that the integral of $D(\theta)$ over all θ is equal to 1,0. For appropriately chosen values of the parameters, the functions $D_1(\theta)$ and $D_2(\theta)$ are virtually indistinguishable.

In engineering applications, $D_1(\theta)$ is often used with n = 2 to n = 4 for wind seas; for n = 2, the corresponding factor $C_1(2) = 2/\pi$. For swells, the value n = 6 or higher is more appropriate.

If $D_2(\theta)$ is used, typical values of s are s = 6 to 15 for wind seas and s = 15 to 75 for swells.

A.5.3.2.2 Directional spreading factor

For engineering applications, the sea-state is often represented by a long-crested wave, assuming the wave energy only propagates in a single direction. This is an abstraction of a real sea. The directional spreading factor ϕ is used to reduce the kinematics (velocities and accelerations) of unidirectional wave theories to account for directionality.

Design wave procedures typically apply unidirectional waves. This is especially common practice for the static design of fixed steel structures of space-frame configuration. In a real sea, the directional spreading of the wave energy tends to result in peak global actions that are somewhat smaller than those predicted for unidirectional seas. As such, design recipes often allow a reduction in the horizontal velocity and acceleration obtained from unidirectional wave theories by the spreading factor.

Only the wave energy that travels in the principal wave direction contributes to the wave kinematics in that direction. The ratio of the in-line energy to the total wave energy is the “in-line variance ratio”. Since the kinematics are proportional to the square root of the wave energy, the directional spreading reduces the in-line kinematics under the highest point of the crest by a spreading factor that is equal to the square root of the in-line variance ratio. All of the energy in the wave spectrum contributes to the kinematics, so that the spreading factor is calculated by integrating the entire wave spectrum over frequency and direction.

The directional spreading factor ϕ is dependent on the type of storm in the area concerned and the distance of the site of interest from the storm centre. Though reference may be made to site-specific directional spreading data where these are available, caution should be exercised since such data are difficult to interpret. In addition, it should be noted that spreading data derived from hindcasts often lead to an

underestimate of ϕ. In general, the values in Table A.2 from reference [28] are appropriate for open water, where refraction and diffraction effects do not modify spreading.

Table A.2 — Directional spreading factors for open water conditions

Type of storm or region	Directional spreading factor ϕ
Low-latitude monsoons typically $\|\psi\| < 15°$	0,88
Tropical cyclones below approximately 40°	0,87
Extra-tropical storms for the range of latitudes $36° < \|\psi\| < 72°$	$1{,}019\,3 - 0{,}002\,08\|\psi\|$
NOTE 1 ψ is the geographical latitude in degrees. Additional information on directional spreading factors for other storm types and locations may be provided in the relevant regional annex. NOTE 2 In reference [28], it is noted that in extra-tropical storms there may be a trend of decreasing spreading with increasing storm severity. In extreme or abnormal extra-tropical storm events it may be advisable to consider specifying a lower degree of spreading (where this would be conservative).	

The wave directional spreading factor may be applied to kinematics which neglect the directionality of the sea-state.

The relationship between the spreading factor ϕ and the exponents n and s in the two formulations $D_1(\theta)$ and $D_2(\theta)$ in Formula (A.39) is given in Table A.3.

Table A.3 — Relationship between spreading factor ϕ and exponents n and s for directional spreading functions $D_1(\theta)$ and $D_2(\theta)$

Variable	$D_1(\theta)$	$D_2(\theta)$
Directional spreading factor ϕ in terms of n or s	$\phi^2 = \left[\frac{(n+1)}{(n+2)}\right]$	$\phi^2 = 0{,}5\left[1 + \frac{s\,(s-1)}{(s+1)\,(s+2)}\right]$
Exponent n or s in terms of directional spreading factor ϕ	$n = \frac{2\phi^2 - 1}{1 - \phi^2}$	$s = \frac{\left[3\phi^2 - 1 + \sqrt{\left(\phi^4 + 6\phi^2 - 3\right)}\right]}{\left(2 - 2\phi^2\right)}$

The spreading factor for low-latitude monsoons of ϕ = 0,88 in Table A.2 corresponds with n = 2,43 and s = 6,25. The factor given in Table A.2 for tropical cyclones of ϕ = 0,87 similarly corresponds with n = 2,11 and s = 5,60. For extra-tropical storms at a latitude $|\psi|$ = 60°, Table A.2 provides a spreading factor of ϕ = 0,895 which corresponds with n = 3,00 and s = 7,41.

A.5.3.3 Wave periods

In order to fully define a wave spectrum, a peak spectral wave period (T_p) or range of representative wave periods should be given (note that in some formulations T_z may be needed instead). Values of peak spectral periods associated with given H_s values are often determined through a regression analysis. Regression analyses may be performed on storm peak data or on all available data. The form of the regression may be linear, or sometimes nonlinear forms such as $T_p = aH_s^b$ allow a better fit to the underlying data. Since use of spectral data implies analysis of a structure with a dynamic response, strong consideration should be given to specifying a range of periods about the best fit values determined by regression. Alternatively, contours of H_s and T_p may be provided. Contours are usually used to capture the fact that, for a given value of significant wave height, wave periods much shorter or longer than the best fit value can occur, although they represent less likely H_s and T_p combinations.

In wave spectra formulations, the frequency parameter is the intrinsic frequency. However, a stationary structure (fixed or floating) in a wave field with current responds to the apparent frequency f_a. To be able to perform the response calculations, the wave frequency spectrum formulation should therefore be transformed into the apparent frequency. As the wave energy per frequency band is independent of the reference frame, $S(f_i)\mathrm{d}f_i = S(f_a)\mathrm{d}f_a$ and hence the wave spectrum in the apparent frequency becomes $S(f_a) = S(f_i)\mathrm{d}f_i/\mathrm{d}f_a$

The coordinate transformations are carried out using Formula (A.48), taking due account of the fact that the wave number k is a function of the intrinsic wave frequency f_i through Formula (A.49). However the wave actions on a spatially distributed structure cannot be determined accurately using this spectrum as both the wavelength and the kinematics are a function of the intrinsic period and not the apparent period.

Prior to undertaking any spectral conversion, it is important to establish the extent to which the wave spectra derived directly from either measured or hindcast data are likely to be representative of the apparent or intrinsic frequency spectra (or something in between).

The correct treatment of intrinsic and apparent wave periods is of particular relevance for structures whose design and/or assessment are sensitive to dynamic effects or the phasing of the wave loads as the wave progresses through the structure (e.g. certain jack-up units). In such circumstances an alternative approach may be more appropriate (e.g. one based on the modification of the wave particle kinematics to account directly for the current velocity). For further details see A.8.4.4.

A.5.4 Regular (periodic) waves

A.5.4.1 General

No guidance offered.

A.5.4.2 Wave period

The wave period T_{Hmax} associated with the maximum wave height may be estimated based on wave measurements or simulations of waves in extreme sea-states. Time series measurements of individual waves in extreme sea-states are rare and therefore site-specific measurement-based estimates are often not possible. The ratio of T_{Hmax}/Tp in large sea-states typically varies between 0,8 and 1,0. Reference [30] presents ratios of T_{Hmax}/Tp based on measurements made in different areas of the world which agree with this range, and further suggest that the ratio varies with spectral bandwidth. Simulation of extreme JONSWAP spectra with varying peak enhancement factors confirms this basic trend. For a JONSWAP spectrum with $\gamma = 1$ the expected ratio of T_{Hmax}/Tp is 0,9; as γ increases beyond a value of 5, the expected ratio approaches unity. Simulation of extreme sea-states using a spectral model (first- or second-order) may lead to refined estimates of T_{Hmax} and insight into the range of values which can be associated with large individual waves. Whether measured or simulated data are considered, it is sometimes insightful to consider looking at wave heights versus some measure of steepness rather than only considering H versus T.

As a practical matter, for shallow-water jacket structures where the response is not overly dynamic, approximate ratios of the period of maximum wave to the peak spectral period associated with the same return period significant wave height are often used. For tropical cyclones, a ratio of 0,90 to 0,92 is commonly assumed. In North Sea storm conditions, ratios from 0,88 to 0,96 are commonly used. For dynamic structures (fixed or floating), specifying a wide range or performing simulations in order to determine a range is prudent. Of course if a structure has a significant dynamic response, the use of a design wave approach using H_{max} and T_{Hmax} might itself be questioned. In such cases designers may need to consider a spectral approach in order to capture dynamic effects.

A.5.4.3 Wave kinematics — Velocities and accelerations

Several periodic wave theories may be used to predict the kinematics of two-dimensional regular waves. The different theories all provide approximate solutions to the same differential equations with appropriate boundary conditions. All compute a waveform that is symmetric about the crest and propagates without changing shape. The theories differ in their functional formulation and in the degree to which they satisfy the nonlinear kinematic and dynamic boundary conditions at the wave surface.

Linear wave theory [10] is applicable only when the linearization of the free surface boundary conditions is reasonable, i.e. strictly speaking only when the wave amplitude and steepness are infinitesimally small. Stokes' fifth-order theory [31] is a fifth-order expansion in the wave steepness about mean water level that satisfies the free surface boundary conditions with acceptable accuracy over a fairly broad range of applications, as shown in Figure A.3, which is adapted from reference [12]. Chappelear's theory[32] is similar to Stokes' fifth-order theory, but determines the coefficients in the expansion numerically through a least

squares minimization of errors in the free surface boundary conditions, rather than analytically. Extended velocity potential theory (EXVP-D)[33] satisfies the dynamic boundary condition exactly and minimizes the errors in the kinematic boundary condition. Stream function theory [34] satisfies the kinematic boundary condition exactly and minimizes the errors in the dynamic boundary condition.

When Stokes' fifth-order theory is not applicable, stream function theory may be used. Selection of the appropriate solution order may be based either on the percentage error in the dynamic and kinematic boundary conditions, or on the percentage error in the velocity or acceleration compared with the next higher order. These two methods provide comparable solution orders over most of the feasible domain, but differ in the extremes for $H > 0{,}9\ H_b$ (where H_b is the breaking wave height) and $d/gT_i^2 < 0{,}003$. In these extremes, the theories have not been well substantiated with laboratory measurements and should therefore be used with caution. In particular, the curve for long-crested breaking wave height H_b shown in Figure A.3 is not universally accepted.

As an alternative to periodic wave theories, representative waves from a random sea derived with wave theories such as New-wave theory may be used. New-wave theory (see for example reference [35]) is based on a mathematical derivation of the characteristics of the most probable maximum wave in a linear random sea-state. The New-wave surface has the shape of the autocorrelation function. New-wave includes the continuous spectrum of wave frequencies in a random sea; it is not based on discrete harmonics of the fundamental frequency. To ensure approximate parity of actions caused by different design waves, the crest elevation in New-wave shall then be taken as 5/9 times the wave height used in Stokes 5th order or stream function theory. The kinematics of each wave frequency are computed using linear wave theory, summed and subsequently delta-stretched.

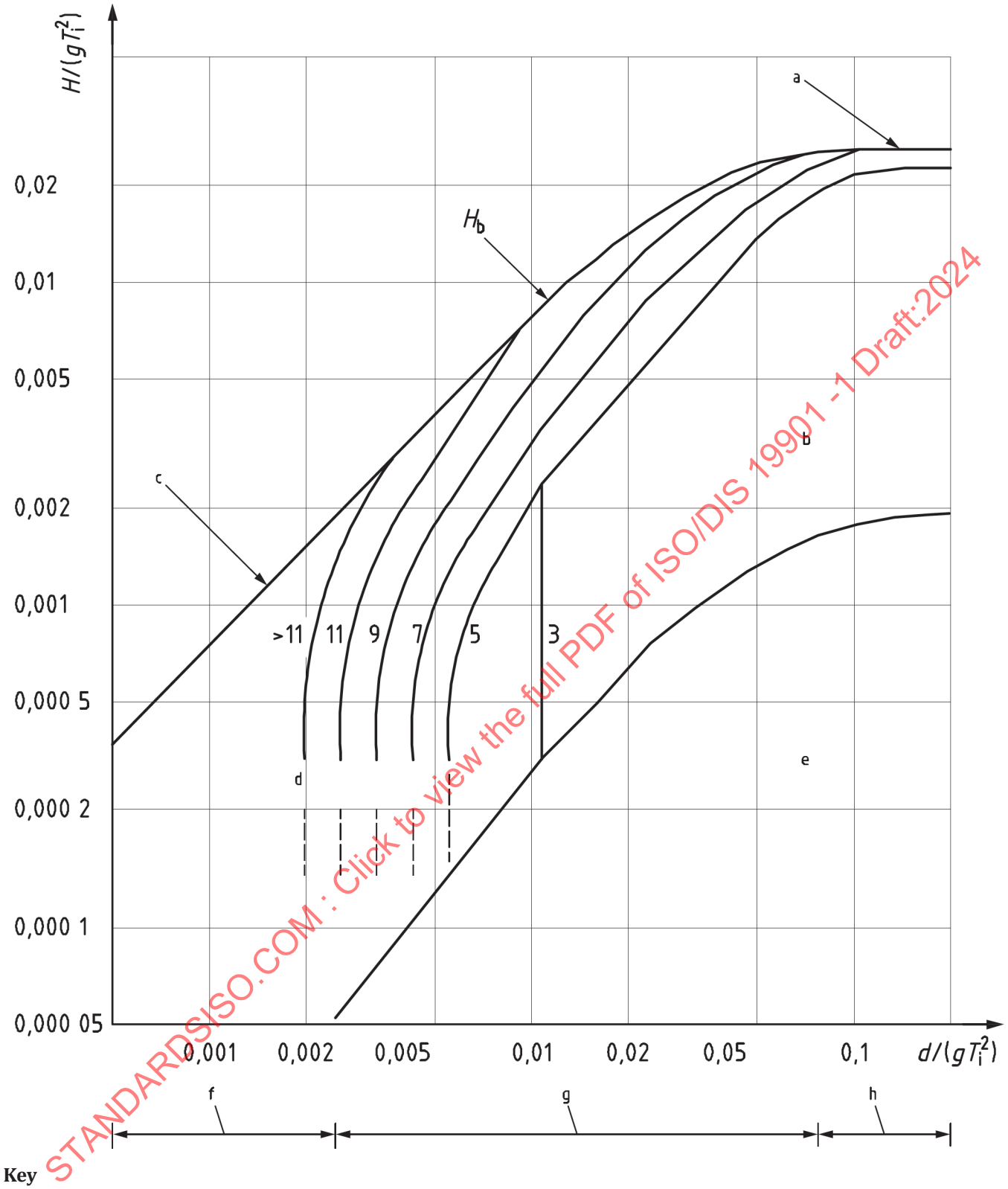

Key

a	Deep water breaking limit $H/\lambda = 0{,}14$	e	Linear/Airy or third-order stream function
b	Stokes' fifth-order, New-wave or third-order stream function	f	Shallow water
c	Shallow water breaking limit $H / d = 0{,}78$	g	Intermediate depth
d	Stream function (showing order number)	h	Deep water

Figure A.3 — Regions of convergence of alternative wave theories

Delta stretching[36] provides a simple empirical correction to extend the kinematics obtained from linear theory into the wave crest above the still water level. When the local water surface elevation is above still water level and the vertical coordinate being considered, z, is above the stretching depth, d_s (the distance below the still water level at which the stretching process begins), then z in the equations for linear wave kinematics should be replaced by the stretched vertical coordinate z_s:

$$z_s = F_s\,(d_s + z) - d_s = (F_s - 1)\,d_s + F_s\,z \tag{A.40}$$

where

z is defined as the vertical coordinate with $z = 0$ at the still water level;

F_s is a stretching factor defined by:

$$F_s = \frac{d_s + a\eta}{d_s + \eta} \tag{A.41}$$

where

a is a stretching parameter ($0 < a < 1{,}0$);

η is the water surface elevation at the horizontal location of interest.

The stretching depth (d_s) is typically set to one-half of the significant wave height or half of the crest elevation, and the stretching parameter a typically equals 0,3. The stretching factor F_s is always smaller than 1,0 and consequently $z_s < z$.

In the use of New-wave theory, the kinematics are evaluated at only one instant during the wave evolution and are kept constant as the wave propagates through the structure. New-wave is compatible with random directional wave models and produces results for global direct actions on fixed steel structures similar to those calculated by time-domain simulations.

Another form of stretching is linear or Wheeler stretching, see A.9.4.1.

A.5.4.3.1 Non-Breaking Waves

Wave breaking is an inherently stochastic process. Its occurrence is a function of the water depth, the wave steepness, the wind, and the current.

Numerous studies have been completed into the onset of wave breaking. These have used a wide range of parameters to describe the process and have arrived at a number of slightly different conclusions.[37,38] To generalise, the occurrence of deep water wave breaking should be considered when the nonlinear wave steepness, ηkL is greater than 0,30, where kL is a representative local wave number. As the water depth reduces, this steepness will also reduce; the occurrence of wave breaking being controlled by a combination of steepness and effective water depth. In terms of sea-state parameters, wave breaking will be dependent upon both the sea-state steepness (S1) and the Ursell number (Ur). Alternatively, these may be combined into a single parameter, μ, defined in terms of the (α, β) parameters employed in reference [39] crest height model such that:

$$\mu = 16.\frac{\alpha^3}{\beta}\text{“}\left(\frac{3}{\beta}\right) - \frac{1}{4}\sqrt{\frac{\pi}{2}} \tag{A.42}$$

where Γ is the incomplete gamma function. Adopting this approach, wave breaking becomes important for sea-states in which μ>0,065.

The horizontal velocities in the crest of a breaking wave can be in excess of 1,2 times the phase speed. As waves evolve nonlinearly up to and including the occurrence of wave breaking, the local crest kinematics increase (see comments above), but the phase velocity reduces. Both effects are a direct consequence of the

transfer of energy into the higher frequencies. As such, they may only be described by a fully nonlinear wave model, CFD and/or laboratory data, and should be expressed in an Eulerian frame of reference.

2nd Order Irregular Wave Theory – for application in deep-intermediate water depths:

Second-order models have been shown to be an accurate method of predicting the velocity field under irregular waves in deep and intermediate water depths down to kp.d of 1,2,[40] provided they are non-breaking. These may be estimated following reference [41]. If the waves are breaking, fully nonlinear calculations are required.

Molin Stretching – for application in intermediate-shallow water depths:

According to a recent review of the kinematics models proposed in DNV RP C205, some traditional 'stretching' methods may not provide satisfactory results. These include the methods proposed by Wheeler[43] and Grue et al,[44] which have been used to extrapolate conditions above still water level without introducing high-frequency contamination. "High-frequency contamination is the erroneous prediction of kinematics from linear superposition due to the extrapolation of high-frequency components into the crest of a large wave; the latter being significantly larger than the amplitude of the individual components"[42].

Stretching methods, involve transformation of the vertical coordinate, z, such that the velocity predicted by linear superposition at MWL is stretched to the crest elevation. This reduces the predicted velocities throughout the water column, but most noticeably around and above the MWL. The transformation works by replacing z in:

$$u(x,z,t)=\sum_i a_i\omega_i \frac{\cosh(k_i(z+d))}{\sinh(k_i d)}\cos(k_i x-\omega_i t+\theta_i) \tag{A.43}$$

with z', as follows:

$$z'=d\frac{(z-\eta)}{(d+\eta)} \tag{A.44}$$

such that

$$u(x,z,t)=\sum_i a_i\omega_i \frac{\cosh\left(k_i d\frac{z+d}{d+\eta}\right)}{\sinh(k_i d)}\cos(k_i x-\omega_i t+\theta_i) \tag{A.45}$$

The approach has been shown to under-predict kinematics in large wave crests[42] and improvements have been suggested both by Donelan et al.[45] and Molin.[46] Karmpadakis et al.,[42] show that both approaches produce satisfactory predictions of kinematics through the water column, particularly in the crests of large waves, and that the model of Molin (2002) was marginally superior. Molin's[46] approach involves a modified Wheeler stretch such that the vertical elevation z is replaced in Equation A.43 by:

$$z_i'=d\frac{(z-\eta_i)}{(d+\eta_i)} \tag{A.46}$$

This transformation implies that the velocity of the ith component will be stretched only up to the surface elevation of the components with a lower frequency than component i. As such, the calculation for the velocities becomes:

$$u(x,z,t)=\sum_i a_i\omega_i \frac{\cosh\left(k_i d\frac{z+d}{d+\eta_i}\right)}{\sinh(k_i d)}\cos(k_i x-\omega_i t+\theta_i) \tag{A.47}$$

In addition to the conclusions drawn by Kampadakis et al., de Lutio[47] independently demonstrated that the Molin formulation compared most favourably with experimental measurements of kinematics under large uni-directional waves in intermediate water depths

A.5.4.3.2 Higher Order Stream Function Theory – For application in shallow water depths.

Regular wave theories have been routinely used to describe the kinematics under large irregular waves. Given the limitations discussed above regarding irregular wave models, the ease of application of regular wave theories makes them an attractive alternative.

Typically, regular wave solutions are not applicable in broad-banded sea-states as they neglect the distribution of energy across the frequency range. When waves propagate into shallower water, frequency dispersion reduces and, in the limit, as $d \to 0$, all components travel with the same phase velocity, which depends only on the water depth. As such, the argument can be made that the kinematics of large waves in low effective water depths may be adequately described by regular wave theories because the waves are non-dispersive.

Kampakardis et al.[42] made comparisons between Stokes 5th, Cnoidal 5th and Stream function theories and laboratory data and showed that over the range that Stokes 5th waves are valid, Stream function gave comparable results and that Stream function performed better than Cnoidal 5th waves over their valid range of applicability. Stream function allows for the inclusion of a much broader range of harmonics which means the kinematics predictions will be superior.

A.5.4.3.3 Directional Wave Spreading

Most periodic wave theories do not account for wave directional spreading in their kinematics, however directional spreading may be approximated in periodic waves by multiplying the horizontal velocities and accelerations by a wave directional spreading factor φ (see A.8.3.2). However, Latheef et al[48] have shown that:

— The most severe sea-states will be less directionally spread than those for which field data is commonly available

— The largest waves within a given sea-state will be less spread than the sea-state as a whole.

A.5.4.4 Intrinsic, apparent and encounter wave periods

The correct period to be used in all periodic wave theories to determine the wavelength and all wave kinematics is the intrinsic period. If the wave period is derived from measurements taken by fixed (rather than drifting) instruments, the measurements are of the apparent wave period. If the wave period is based on hindcasts of waves with a model that is calibrated to measurements taken by fixed instruments, and no adjustments are made to the model to account for the presence of current, then again the wave period represents the apparent wave period. In both cases the intrinsic wave period should be calculated from the apparent wave period. These are the usual cases for offshore structures covered by this part of ISO 19901. If the wave hindcast model already accounts for the Doppler effect on the wave periods due to currents, no adjustment is required.

In calculating wave particle kinematics, some computer programs adjust the wave period/length internally to account for currents. Other programs require the user to manually adjust the wave period before using it to compute kinematics. The user should ensure that the correct procedure is applied.

For a uniform current profile over the water depth, the basic problem is formulated by the relationship between speeds in the apparent and the intrinsic coordinate systems:

$$\begin{aligned} c_{\mathrm{a}} &= c_{\mathrm{i}} + V_{\text{in-line}} \\ c_{\mathrm{a}} &= \frac{\lambda}{T_{\mathrm{a}}} \\ c_{\mathrm{i}} &= \frac{\lambda}{T_{\mathrm{i}}} \\ V_{\text{in-line}} &= U_{\mathrm{c}} \cos\theta_{\mathrm{c}} \end{aligned} \tag{A.48}$$

where

a is a subscript for an apparent property;

i is a subscript for an intrinsic property;

c is the wave celerity (the wave phase speed);

λ is the wavelength;

T is the wave period;

$V_{\text{in-line}}$ is the component of the current velocity in-line with the direction of wave propagation;

U_c is the free-stream steady current velocity, not reduced by structure blockage;

θ_c is the direction of the current velocity with respect to the direction of wave propagation.

This results in the relationship between the apparent and intrinsic periods:

$$\frac{\lambda}{T_a} = \frac{\lambda}{T_i} + V_{\text{in-line}} \tag{A.49}$$

Through multiplication by the wave number $k = 2\pi/\lambda$, Formula (A.49) may be rewritten in terms of the apparent and intrinsic frequencies:

$$\omega_a = \omega_i + k\, V_{\text{in-line}} \tag{A.50}$$

where ω is the wave circular frequency, $\omega = 2\pi/T$.

The wavelength, which is unaffected by the frame of reference, and the intrinsic period are coupled through the dispersion equation, which for first and second order waves is

$$T_i^2 = \frac{2\pi\lambda}{g\tanh(2\pi d/\lambda)} = \frac{4\pi^2}{kg\tanh(kd)} \tag{A.51}$$

where:

d is the water depth;

g is the acceleration due to gravity.

For higher-order waves, the dispersion relationship is determined through numerical simulations.

$V_{\text{in-line}}$ is positive when wave propagation and the in-line component of the current velocity are in the same direction ($-90° < \theta_c < +90°$); in these cases the apparent frequency is higher than the intrinsic frequency.

Conversely, $V_{\text{in-line}}$ is negative when wave propagation and the in-line component of the current velocity are in opposite directions ($\theta_c > +90°$ or $\theta_c < -90°$) and the apparent frequency is lower than the intrinsic frequency. For negative values of $V_{\text{in-line}}$ (opposing currents), the condition $c_i + V_{\text{in-line}} > 0$ should be satisfied — otherwise, the waves move faster downstream by the current than they can propagate forward. For the special case of $c_i + V_{\text{in-line}} = 0$ and $\theta_c = 0$, standing waves occur.

When the intrinsic period T_i [or frequency ω_i] is known, the wavelength λ and the wave number k are also known [see Formula (A.33)], and there is a unique apparent period T_a [or frequency ω_a] associated with T_i [ω_i] for each current velocity. When the apparent wave period T_a [ω_a] is known, there is only a unique intrinsic period T_i [ω_i] associated with T_a [ω_a] when the current velocity is in the direction of wave propagation ($V_{\text{in-line}} > 0$). For opposing current velocities, i.e. $-c_i < V_{\text{in-line}} < 0$, there are in principle two values of T_i [ω_i] that correspond with each T_a [ω_a]. However, the second solution is associated with excessively short, unrealistic waves and may be ignored.

Formulae (A.48) to (A.51) directly provide T_a from a given T_i, but should be solved iteratively to determine T_i from a given T_a. For the special case of a uniform current profile, the solution to these equations is provided in non-dimensional form in Figure A.4. This figure gives the ratio of T_i to T_a as a function of $V_{\text{in-line}}/gT$ for constant values of $d/gT^2 > 0{,}01$. Figure A.4 may be used with $T = T_a$ to determine T_i or with $T = T_i$ to determine T_a. For smaller values of d/gT^2, shallow-water depth approximations apply and the equation

$$\frac{T_i}{T_a} = 1 + \frac{V_{in-line}}{\sqrt{gd}}$$

may be used.

While strictly applicable only to a current that is uniform over the full water depth, Figure A.4 provides acceptable estimates of T_i/T_a for "slab" current profiles that are uniform over the top 50 m or more of the water column. For non-uniform current profiles a weighted, depth-averaged in-line current speed may be used, as shown in reference [29]:

$$V_{\text{in-line}} = \frac{2k}{\sinh(2kd)} \int_{-d}^{0} U_c(z) \cos\theta(z) \cosh[2k(z+d)]\, dz \qquad \text{(A.52)}$$

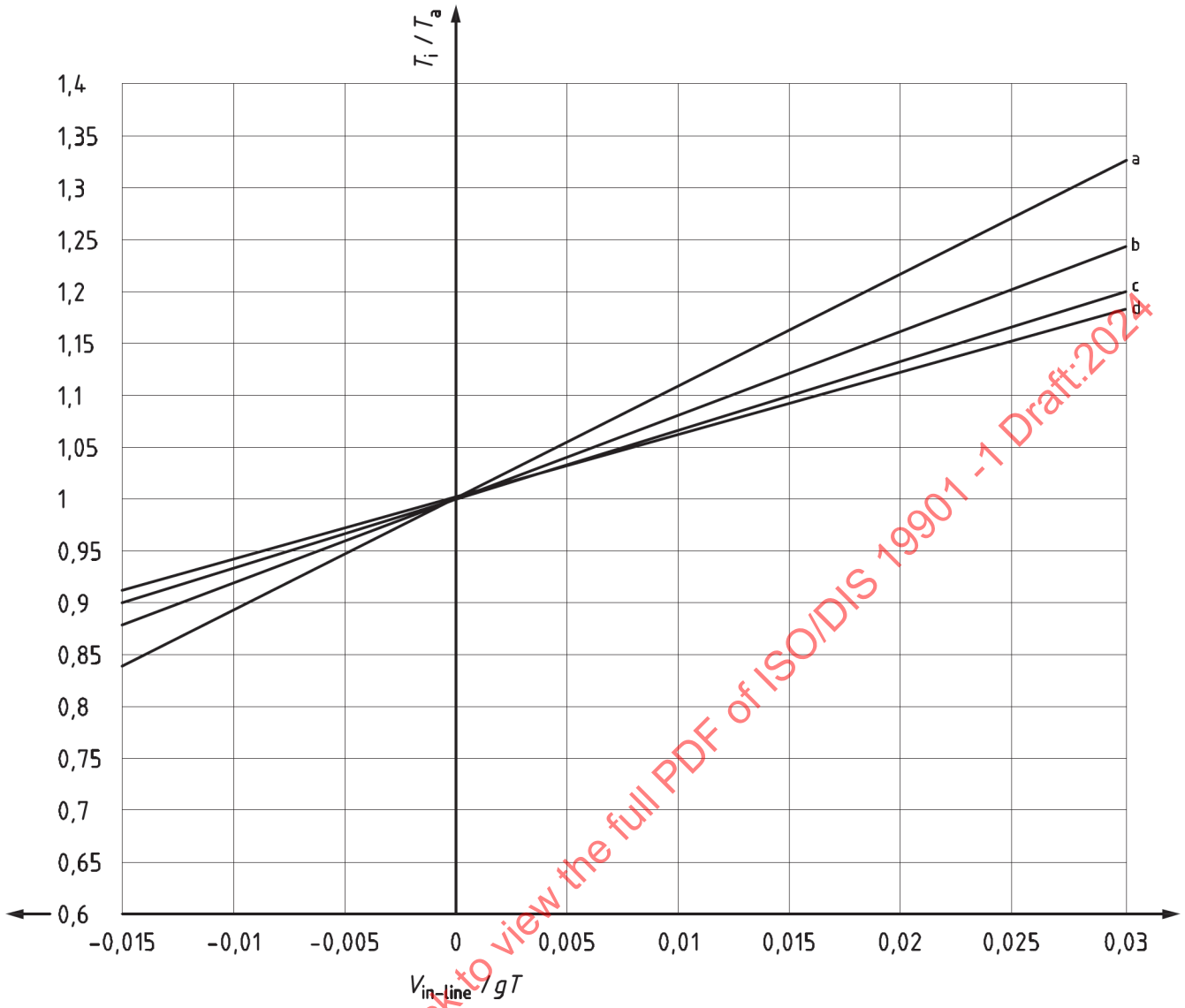

Key

a $d/(gT^2) = 0{,}01$

b $d/(gT^2) = 0{,}02$

c $d/(gT^2) = 0{,}04$

d $d/(gT^2) = 0{,}10$

NOTE Either $T = T_a$ or $T = T_i$ may be used to calculate $d/(gT2)$ and $V_{in\text{-}line} / gT$.

Figure A.4 — Doppler shift in wave period due to steady current — Relationship between intrinsic and apparent periods

Spatial relationships change in a similar manner as the temporal relationships. The relationship between the coordinate (x) in the direction of wave propagation in the apparent reference frame and the intrinsic reference frame is:

$$x_a = x_i + V_{\text{in-line}}t \tag{A.53}$$

so that the space- and time-dependent argument ($kx_i - \omega_i$) of the harmonic function in all wave equations transforms, using Formulae (A.53) and (A.50), into:

$$kx_i - \omega_i t = kx_a - (\omega_i + kV_{\text{in-line}})t = kx_a - \omega_a t \tag{A.54}$$

The transformation between encounter periods as measured from a moving vessel and intrinsic periods follows similar principles.

In wave spectra formulations (see A.8.3), the frequency parameter is the intrinsic frequency. However, a stationary structure (fixed or floating) in a wave field with current responds to the apparent frequency. To be able to perform the response calculations, the wave frequency spectrum formulation should therefore be transformed into the apparent frequency. As the wave energy per frequency band is independent of the reference frame, $S(\omega_i)d\omega_i = S(\omega_a)d\omega_a$ and hence the wave spectrum in the apparent frequency becomes $S(\omega_a) = S(\omega_i)d\omega_i/d\omega_a$. The coordinate transformations are carried out using Formula (A.50), taking due account of the fact that the wave number k is a function of the intrinsic wave frequency ω_i through Formula (A.51). However, the wave actions on a spatially distributed structure cannot be determined accurately using this spectrum as both the wavelength and the kinematics are a function of the intrinsic period, not the apparent period. An approach to addressing this issue is presented in reference [49].

A.5.5 Maximum height of an individual wave for long return periods

The long-term maximum height H_N of an individual wave with a return period of N years can be estimated in several ways. The method used should account for the long-term uncertainty in the severity of the environment and the short-term uncertainty in the severity of the maximum wave of a given sea state or storm.

The statistically correct methods are based on storms. Storms are obtained from a time series of significant wave height by breaking it into events that have a peak significant wave height (Hsp) above some threshold.

The long-term uncertainty in the severity of the environment is treated using the probability distribution of the severity of the storm, measured in terms of either its peak significant wave height or the most probable maximum value of the individual waves in the storm (Hmp). The uncertainty in the height of the maximum wave of any storm is estimated as a probability distribution conditional on Hsp or Hmp. Convolution of the two distributions gives the distribution for any random storm and, thereby, the complete long-term distribution for the heights of individual waves. For further information, see reference [3].

A similar method has been applied using sea states rather than storms as the independent variable. It is recognized that this method is not statistically robust because successive sea states are not independent. It involves analysis of many sea states that do not contribute to the final result and can give a false confidence in the results, as the amount of independent input data is much less than it appears. Despite these known flaws, this method often provides a useful first estimate of conditions in an area when only a short (e.g. 1 year to 2 years) measured dataset of Hs is available (see, for example, reference [50]).

An approximation that is sometimes used to generate H_N is to multiply Hs_N, an estimate of the N-year return period Hs, by a factor that relates to the ratio of the most-probable highest wave in a sea state to the significant wave height Hs_N. However, this method underestimates H_N because it ignores the contribution from sea states that are lower but more frequent than Hs_N, as well as sea states that are higher but less frequent than Hs_N. The accuracy of the method also depends on the mutual cancellation of errors in all the steps leading to the final answer. When this method is used, the individual wave heights are generally assumed to obey a Rayleigh or Forristall[51] distribution, see below, and the sea state is assumed to have a duration of 3 h. Although the method has been applied in the past with some success, its use demands extreme care and should be avoided as better methods are now available (see, for example, references [3] and [10] for a discussion of various methods).

The classical description of the distribution of crest to trough heights (H) in narrow-banded seas is the Rayleigh distribution,[52] which in its cumulative probability form is given by

$$P\left(H \le H^*\right) = 1 - \exp\left[\frac{-2\left(H^*\right)^2}{\left(H_s\right)^2}\right] \quad \text{(A.55)}$$

where H* is any desired value of the individual wave height.

In practice, most seas are not narrow-banded and using the Rayleigh distribution would tend to over-predict the height of waves. To take account of the finite bandwidth, a number of empirically derived distributions have been proposed. The distribution proposed by Forristall,[51] which was empirically derived using hurricane wave data from the Gulf of Mexico, is often used:

$$P(H \le H^*) = 1 - exp\left[\frac{-(4H^*/H_s)^{\alpha}}{\beta}\right] \quad \text{(A.56)}$$

where

α 2,126

β 8,42

NOTE 1 When α = 2 and β = 8, the Forristall distribution reverts to the Rayleigh form.

NOTE 2 Though the above coefficients were developed using hurricane data, Krogstad's distribution based on North Sea storms is virtually the same[53]

The probability distributions for the maximum individual wave height in a stationary sea-state can be established by raising Equation (A.55) or Equation (A.56) to a power equal to the number of waves in the interval. The probability distribution for the maximum individual wave height conditional on Hsp or Hmp, can be determined by combining the distributions for each of the stationary sea-states of which the storm is composed.

In deep or intermediate water depths where the spectra are broad banded, such that the JONSWAP gamma parameter is close to one, the Forristall distribution[51] generally provides a good estimate of the wave height distribution. However, design sea states are often more narrow-banded than this with gamma values in excess of one; based on results from laboratory experiments, in these situations the Forristall distribution may not provide the best characterization. Alternative distributions that may be applied in these situations are those of Boccotti,[62] Naess[235] and Tayfun.[236] For very narrow-banded seas such as those dominated by long-period swell, the Rayleigh distribution may provide the best characterization of waves. In shallow water the Forristall distribution tends to be conservative for large sea states as it does not include the effects of wave breaking.

A.5.6 Fully nonlinear wave models

The fully nonlinear modelling of random, directional waves has been an active area of research for several years and some methods are now applicable for realistic sea-states. Examples that might be considered for engineering application are those in references [54-58]. Though the methods offer the advantages of realism, there are the following difficulties and limitations:

a) The models are slow even on the fastest computers. Computational effort may be significantly reduced by calculating New-waves rather than complete, random sea-states.

b) Some of the methods use Fourier models to describe the free-surface. This limits the validity of results as waves become steep-fronted at the crest at the onset of breaking. Others can restrict the freedom of motion of surface particles, with similar consequences.

c) The overall recipe for calculation of actions based on regular wave or linear, random theory may have been subject to calibration against offshore measurements. When this is the case, actions calculated

from the fully nonlinear methods should be tested either against the measurements or against the conventional method in the regime of the measurements.

Wave models based on expansions in wave slope might also be considered although, as perturbation methods, they are not fully nonlinear.[58],[59] There is some indication that schemes valid to third-order, including quartet resonance effects, capture much of the important nonlinearity. However, as a wave slope expansion, they may fail, at least locally, as a wave becomes steep-fronted.

Linear spectral representations ignore the nonlinear interactions between waves of different frequencies and directions, whereas periodic wave representations ignore the irregular nature of waves. Extension of spectral representations to second-order has been used in practice (see reference [60]).

A.5.7 Wave crest elevation

The long-term distribution of extreme and abnormal crest elevations may be established from a long time series of sea-state parameters and a short-term distribution of crest elevations conditional on storm sea-states. The statistically correct approach would use storms as the independent variable. The methods described in A.8.5 for wave height are equally useful for obtaining design values of crest elevation and total surface elevation.

Research (e.g. ShortCrest,[322] and LOADS[61,65,233]) has shown that the Forristall second order distribution[39] for the probability of crest heights in a sea-state to be inappropriate for very steep and shallow water sea-states. In these circumstances, non-linear processes can be significant, and this can result in either an increase in crest heights or, where wave breaking is significant, a decrease in the largest crests[48,61].

However, the description of probability distributions that reflect the higher order physics and breaking processes is not straightforward, and the spreading (and to a lesser extent peakedness) of the sea-states plays a role. For this reason, it is important that the underlying datasets that are used for the EVA reflect the real characteristics of the directional wave spectrum reasonably well. If there is doubt as to the accuracy, it would be prudent either to select conservative values for the analysis or use measured datasets to allow for a reasonable probabilistic model to be developed for the key sea-state parameters.

Wave characteristics will change with region and with storm type:

— in tropical cyclones where large sea-states are typically highly spread, the Forristall 2nd order distribution may be representative;

— for extra-tropical storms, there may be an under-estimation on the order of 5 % by using the Forristall 2nd order distribution and ignoring higher-order nonlinearity;

— for swell-dominated locations such as offshore West Africa, the Forristall 2nd order distribution may be over-estimate the crest heights, as the sea-states can be very linear and the Rayleigh distribution may be more appropriate.

It should be noted that the crest elevation estimates derived using distributions derived from measurements at a single point effectively only reflect the risk of exceedance at a single point.[63,64] However, as described by Forristall,[63] when the true area of exposure to wave crests is considered (i.e. the full platform-deck area), the probability of having the point estimate exceeded somewhere locally within the deck is naturally higher than the probability of having it exceeded just at one point, since the potential crest encounter area is larger than one point. For example, for a 1,500 m^2 deck area, the local crest estimate could exceed the point crest estimate by 10 % for the same probability of occurrence. The local crest height in shallow water will, however, be limited due to wave breaking effects.

For gently-sloping seabeds of gradient less than 1 in a 100, in shallow water, the Forristall 2nd order distribution can be used for a conservative estimate. Other more accurate distributions are available, such as the LOADS distributions, however should only be applied if verified against site-specific measurements or tank testing.

A.6 Currents

A.6.1 General

For bottom-founded structures, the total current profile associated with the sea-state producing extreme or abnormal waves should be specified for the design of the structure. For floating structures, the selection of an appropriate combination of currents, waves and winds is often less obvious and needs careful consideration.

A.6.2 Current velocities

The current flow at a particular site varies both in time and with depth below the mean sea surface. The characteristics of the extreme or abnormal current profile that need to be estimated for the design of offshore structures are particularly difficult to determine, since current measurement surveys are relatively expensive and consequently it is unlikely that any measurement program will be sufficiently long to capture a representative number of severe events. Furthermore, current (hindcast) modelling is not as advanced as wind and wave modelling. Also, extrapolation of any dataset demands that account be taken of the three-dimensional nature of the flow.

Site-specific measurements of currents at the location of a structure may be used either as the basis for independent estimates of likely extremes or to check the indicative values of the various components of the total current.

Information on the frequency of occurrence of total current speed and direction at different depths for each month and/or each season is normally useful for planning operations. For most design situations in which waves are dominant, estimates of the extreme or abnormal residual current and total current may be obtained from high-quality site-specific measurements; these should extend over the water profile and over a period that captures several major storm events that generated large sea-states. Current models may be used in lieu of site-specific measured data. The period over which the current model is run should be adequate to allow tidal decomposition to be carried out and the residual current to be separated out of the total current where appropriate. Consideration should be given to long-period, large-scale environmental fluctuations, which may affect the residual current climate. Efforts should be made to ensure that if a current model is used it is validated against nearby measured data.

A.6.3 Current profile

The characteristics of the current profile over depth in different parts of the world depend on the regional oceanographic climate, in particular the vertical density distribution and the flow of water into or out of the area. Both of these controlling aspects vary from season to season. Typically, shallow-water current profiles in which tides are dominant may often be characterized by simple power laws of velocity versus depth, whereas deep-water profiles are more complex and may even show reversals of the current direction with depth. Such characteristics of the current flow may be particularly important to consider in the design of deep-water structures and parts of the system such as risers and mooring systems. Near sea-bed current profiles require special attention and measurement where they are important for the specific design or assessment condition.

The power law current profile given in Formula (A.57) may be used where appropriate (e.g. in areas dominated by tidal currents in relatively shallow water, such as the southern North Sea):

$$U_c(z) = U_{c0}\left(\frac{z+d}{d}\right)^{\alpha} \tag{A.57}$$

where

$U_c(z)$ is the current speed at elevation z ($z \leq 0$);

U_{c0} is the surface current speed (at $z = 0$);

z is the vertical coordinate, measured positively upwards from still water level;

d is the still water depth;

α is an exponent (typically 1/7).

Other current profiles in common use are

— a linear distribution between the surface current U_{c0} and a bottom current of half the surface current ($U_{c0}/2$),

— a bilinear distribution with parameters that are determined for the location concerned, and

— a slab profile [see Figure A.5 b)] where a uniform current occurs over the upper part of the water column with zero current over the lower part.

For deep water, design current profiles may be derived from long-term measured current-profile datasets through a two-stage process. In the first stage, the data are parameterized using empirical orthogonal functions; in the second stage, the design current profile with the required return period is selected through a process involving an inverse first-order reliability method (FORM) procedure. The method is described in reference [66].

When a sufficiently long data series is available, with simultaneous data at different water depths, an alternative approach to deriving an N-year current profile commences with the estimation of the N-year current speed at a given reference depth. The conditional mean speed (given the extreme speed at the reference depth) is then selected for other depths. The process is repeated for differing reference depths, with the most onerous profile (for the particular application) being selected.

For some applications, an approach using a response function such as the integrated drag loading on a vertical cylinder may be used, as described in A.5.3 c).

A.6.4 Current profile stretching

A.6.4.1 General

References [67] and [68] show that waves alternately stretch and compress the current profile under crests and troughs, respectively. Stretching means that, in the presence of waves, the instantaneous current speed $U_c(z)$ of a water particle calculated at depth z (measured positively upwards from still water level for $-d \leq z \leq 0$) is effective at a stretched vertical coordinate z_s. In the design data, the current profile $U_c(z)$ is specified over the full water column between the sea floor at $z = -d$ and the still water level at $z = 0$. Both linear and nonlinear stretching methods are used.

In linear stretching, the relationship between z_s and z is proportional to the ratio of the instantaneous height of the water surface elevation and the still water depth. A stretching factor F_s may be introduced, in a manner analogous to the delta stretching procedure for wave kinematics. For current stretching, F_s is defined as:

$$F_s = \frac{d+\eta}{d} \tag{A.58}$$

where

η is the instantaneous height of the water surface elevation (measured upwards from still water level);

d is the still water depth.

The stretched vertical coordinate may then be expressed as

$$z_s = F_s\,(d + z) - d \tag{A.59}$$

where

z_s is the stretched elevation (measured upwards from still water level);

z is the original elevation (measured upwards from still water level).

For current stretching, the stretching factor F_s is larger than 1,0 and consequently $z_s > z$.

In nonlinear stretching, the elevations z_s and z are related through linear (Airy) wave theory as:

$$z_s = z + \eta \frac{\sinh\left[k_{nl}(z+d)\right]}{\sinh(k_{nl}d)} \tag{A.60}$$

where, additionally,

k_{nl} is the nonlinear wave number:

$$k_{nl} = \frac{2\pi}{\lambda_{nl}}$$

λ_{nl} is the wavelength for the regular wave under consideration for water depth d and wave height H (calculated using nonlinear wave theory and the intrinsic wave period).

Formula (A.60) provides a nonlinear stretching of the current, with the greatest stretching occurring high in the water column, where the particle orbits have the greatest radii. Figure A.5 illustrates a comparison of linear and nonlinear stretching for sheared and slab current profiles.

Nonlinear stretching is the preferred method. For slab or power-law current profiles, simple vertical extension of the current profile from the still water level to the instantaneous wave surface is a good approximation to nonlinear stretching. For other current profiles, linear stretching is an acceptable approximation.

Another approximate model is the linearly stretched model described by Formula (A.60), adjusted such that the total momentum in the stretched profile from the sea floor to the wave surface equals that in the specified profile from the sea floor to the still water level. However, this procedure is not supported by the theoretical analyses in references [67] and [68].

If the current is not in the same direction as the wave, the methods discussed above may still be used, with one modification: both the in-line and the normal components of the current need to be stretched, but only the in-line component used to estimate T_i for the Doppler-shifted wave.

While no exact solution has been developed for irregular waves, the wave/current solution for regular waves may be logically extended. In the two approximations described above for regular waves, the period and length of the regular wave are replaced by the period and length corresponding to the spectral peak frequency.

A linearly stretched current profile is an acceptable approximate model for many applications. The method is exactly analogous to the stretching of linear wave kinematics as applied by Wheeler[69].

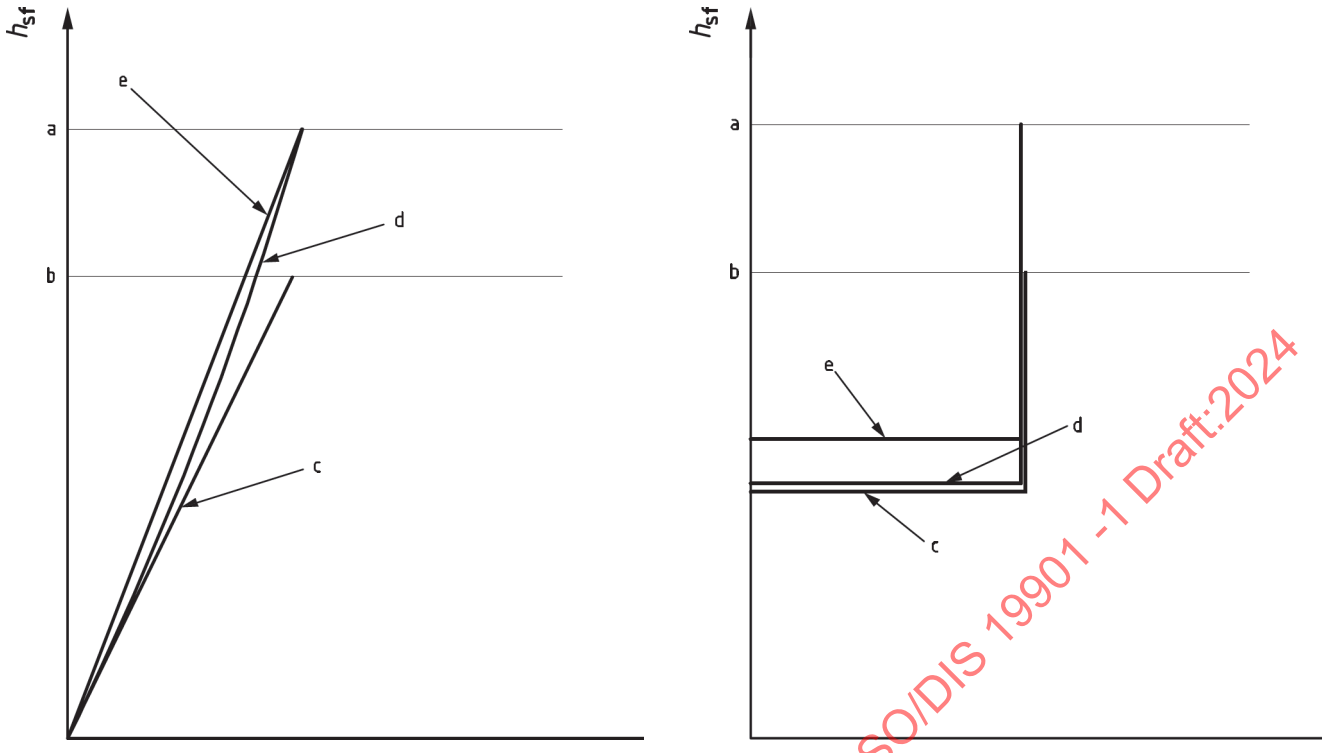

a) Shear profile **b) Slab profile**

Key

h_{sf}	height above sea floor	c	Input current profile.
U_c	current speed	d	Nonlinear stretch current profile.
a	Wave crest.	e	Linear stretch current profile.
b	Still water level.		

Figure A.5 — Linear and nonlinear stretching of current profiles

A.6.4.2 Effect of current profile stretching on hydrodynamic actions

Reference [67] reports that a model that combined Doppler-shifted wave kinematics with a nonlinearly stretched current profile gave the best estimate of global hydrodynamic actions on a space-frame structure. These are within a few percent of those produced by the exact solution on a typical drag-dominant fixed structure subjected to representative waves and current profiles.

In most cases, simple vertical extrapolation of the input current profile above mean water level produces reasonably accurate estimates of global hydrodynamic actions on drag-dominated fixed structures. In particular, for a slab profile thicker than approximately 50 m, vertical extrapolation produces nearly the same result as nonlinear stretching, as illustrated in Figure A.5. However, if the specified profile $U_c(z)$ has a very high speed at the still water level, sheared to much lower speeds just below still water level, the global action may be overestimated (by approximately 8 % in a typical application).

A.6.5 Current blockage

Current blockage refers to the global distortion of the current field in and around non-solid structures. These are structures with a configuration that is to some extent transparent to the current and which thus allow partial flow at a reduced velocity through the structure. Taking account of current blockage may be of interest for the design of space-frame-type structures, both fixed and floating (e.g. semi-submersibles and TLPs), especially when they accommodate a large number of conductors or risers.

For fixed steel structures, reference should be made to ISO 19902.

A.7 Other environmental factors

A.7.1 Marine growth

No guidance is offered. Some information is included within regional annexes. See reference [70].

A.7.2 Tsunamis

For a given location, the frequency of earthquake events is generally very low and in particular the frequency of occurrence of a tsunami at a site is even lower, since only a very few earthquakes give rise to tsunamis. In comparison to earthquake data, the data on tsunamis are limited. Historical records should be examined to see if any tsunamis have occurred at or near a particular location, and consideration should also be given to possible source events and possible magnitudes. Tsunami waves undergo strong refraction, so consideration should be given to the exposure of a site to the possible directions of tsunami wave approach and the resulting associated currents. Detailed tsunami studies consider potential source zones which may generate tsunami waves, model transoceanic propagation and local refraction. Historic run-up events may be used for model validation, and modelling potential source zone events may lead to extreme-value estimates.

For the majority of offshore structures, the environmental actions are dominated by extreme wind waves. Most structures are effectively in deep water with regard to tsunami wave physics, which are at most a few tens of centimetres in height. While tsunami waves do not generally govern the design of fixed offshore structures, their very long periods may result in substantial actions on moored floating structures in water shallower than 100 m. It is prudent to be aware of the potential impact of tsunamis on moored floating structures that form part of an offshore field development.

Tsunami heights may radically increase due to shoaling and refraction, so special care should be taken at shallow-water sites near complicated bathymetry that may lead to a caustic (focal point for wave energy) or near semi-enclosed features such as bays. Coastal facilities are likely to be at the greatest risk due to the run-up of the tsunami and the potential for inundation of the facility and processing plant. Tsunamis approaching the coastline often scour the seabed, transporting large amounts of sediment shoreward and dumping it onshore, thereby increasing their destructiveness. It is prudent to perform an inspection if a tsunami passes over a pipeline.

Where tsunamis have a high probability of occurrence and significance (exceeding the generally accepted risk level in the design), the effects on structures should be assessed. Where possible, offshore structures should be designed against potential tsunamis or they should be located to minimize the consequences of impact.

Detailed procedures for seismic design are described in ISO 19901-2, which provides guidance and methods for determining the magnitude and probability of earthquake events.

A.7.3 Seiches

The effect of seiches may be important to consider for the design of loading and offloading facilities, as well as for operations (e.g. of tankers) in relatively shallow water locations.

A.7.4 Sea ice and icebergs

Where data are being collected on sea ice and icebergs, the following should be considered:

— The type of sea ice expected to occur is a measure of its age, whether first-year, multi-year or of glacial origin. Distribution statistics reflect the variations that occur in the thickness, consolidation and concentration of ice types during a season, both seasonally and from year to year.

— Sea-ice keels may create gouges in the seabed in relatively shallow or intermediate water depths (typically less than 25 m water depth).

— Characterization of year-round regional ice cover includes the occurrence and distribution of ice concentrations, thicknesses, floe sizes and types present during freeze-up, winter, break-up and open water seasons.

— Probability of occurrence of specific ice features, such as multi-year hummock fields and ice islands. In areas where ice of glacial origin is to be expected, the annual and seasonal variation in the flux, concentration and size of icebergs is relevant.

— The probability distributions or extreme values of the velocity of pack ice, ice floes, and discrete ice features (such as icebergs, “bergy bits”, “growlers” and ice islands) and seasonal variations of these distributions are relevant.

If sea ice or icebergs are possible and could be in excess of that which may be accommodated in a structure's design, an emergency preparedness system should be established. Solutions based on the relocation of the structure or the towing away of the ice feature may be chosen; in such cases the emergency preparedness should be reliable and planned in relation to the time required to relocate the structure or to tow the ice feature away.

A.7.5 Snow and ice accretion

Snow may settle on both horizontal surfaces and, if the snow is sufficiently wet, on non-horizontal windward parts of a structure. On vertical surfaces, it is only likely to stay in position as snow for a few hours, although it may freeze and remain as ice. It may therefore affect all exposed areas above the splash-zone. On horizontal surfaces, dry snow is blown off as soon as any thickness accumulates, while wet snow may remain in position for several hours.

In areas that are affected by icing, consideration should be given to the possibility of topsides icing from freezing sea-spray and freezing atmospheric vapour.

Ice may form on the topsides of a structure through a number of mechanisms:

— freezing of old wet snow;

— freezing sea spray;

— freezing fog and super-cooled cloud droplets;

— freezing rain.

In the absence of specific information, new snow may be assumed to have a density of 100 kg/m^3 and the average density of ice formed on the structure may be taken to be 900 kg/m^3.

A.7.6 Thunderstorms and Lightning

No guidance offered.

A.7.7 Rainfall

No guidance offered.

A.7.8 Squalls and Downbursts

Refer to section A.7.3.4 for further guidance.

A.7.9 Internal Waves and Solitons

No guidance offered.

A.7.10 Shelf Waves and Eddies

No guidance offered.

A.7.11 Infragravity Waves

No guidance offered.

A.7.12 Seawater Temperature

No guidance offered.

A.8 Collection of metocean data

A.8.1 General

Table A.4 provides a range of potential applications of metocean information collected as part of a metocean data collection system.

Table A.4 — Potential application of metocean information

Application	Comments
Bridge and flotel disengagement	Bridge and/or flotel disengagement are required once predefined wind/wave criteria are exceeded.
Installation	Wind and wave data are usually needed for setting deck and modules, and currents may be important for running risers and stabbing tension leg platform tendons.
Crane operations	Wind and waves (or vessel heave) have an impact on safety margins for crane operations.
Diving operations	May depend on a number of metocean parameters.
Evacuation	Meteorological and oceanographic data are vital for decisions regarding time of evacuation and selection of evacuation means.
Helicopter operations	Dependent on a number of metocean parameters, principally winds and visibility
Maintenance	Maintenance operations, especially outdoor work above the open sea, are often subject to restrictions on weather and sea-state.
Marine operations	Most marine operations need reliable metocean information
Production shut-down	May depend on a number of metocean parameters, mainly waves and wind
Remotely operated vehicle operations	May depend on a number of metocean parameters, mainly waves and ocean currents
Search and rescue/man overboard (SAR/MOB)	Accurate metocean information may be crucial for effective and safe SAR and MOB operations.
Tanker loading	Tanker loading operations are sensitive to sea-state and wind conditions, in particular during docking operations.
Verification studies	A number of long-term metocean parameters may be required for verification of offshore structures. Verification studies may depend on special metocean parameters or installation of standard instruments in special locations.

A.8.2 Common requirements

A.8.2.1 General

No guidance is offered.

A.8.2.2 Instrumentation

The required measurement uncertainty of metocean recordings should be chosen in accordance with Table A.5, which is based on information presented in Annex 1.B, pp 19-24, Chapter 1, of WMO-No. 8:2008.

Table A.5 — Recommended instrument accuracy and typical operational performance

(1) Variable	(2) Range	(3) Reported resolution	(4) Mode of measurement/ observation	(5) Required measurement uncertainty	(6) Sensor time constant	(7) Output averaging time	(8) Typical operational performance	(9) Remarks
1 Temperature								
1.1 Air temperature	−40 °C to +40 °C	0,1 K	I	0,1 K	20 s	1 min	0,2 K	Operational performance and effective time constant may be affected by the design of thermometer solar radiation screen.
1.2 Extremes of air temperature	−40 °C to +40 °C	0,1 K	I	0,1 K	20 s	1 min	0,2 K	
1.3 Sea-surface temperature	−2 °C to +40 °C	0,1 K	I	0,1 K	20 s	1 min	0,2 K	
2 Humidity								
2.1 Dewpoint temperature	< −60 °C to +35 °C	0,1 K	I	0,1 K	20 s	1 min	0,5 K	If measured directly. Tending to ±0,1 °C when relative humidity nearing saturation.
2.2 Relative humidity	5 % to 100 %	1 %	I	±3 %	40 s	1 min	±3 % to 5 %	Solid state sensors may show significant temperature and humidity dependence. / Humidity nearing saturation.
3 Atmospheric pressure								
3.1 Pressure	920 hPa to 1 080 hPa	0,1 hPa	I	0,1 hPa	20 s	1 min	0,3 hPa	Range to sea level. Accuracy seriously affected by dynamic pressure due to wind and temperature co-efficient of transducer.
3.2 Tendency	Not specified	0,1 hPa	I	0,2 hPa			0,2 hPa	Difference between instantaneous values.
4. Clouds								
4.1 Cloud amount	0/8 to 8/8	1/8	I	1/8	n/a		2/8	Period (30 s) clustering algorithms may be used to estimate low cloud amount automatically.
4.2 Height of cloud base	0 m to 30 km	10 m	I	10 m for ≤ 100 m 10 % for > 100 m	n/a		≈10 m repeatability*	*Accuracy difficult to determine since no definition exists for instrumentally measured cloud base height.
5. Wind								

NOTES

1 Column 1 gives the basic variable.

2 Column 2 gives the common range for most variables; limits depend on local climatological conditions.

3 Column 3 gives the most stringent resolution as determined in WMO-No. 8.

4 In column 4:

I: Instantaneous. In order to exclude the natural small-scale variability and the noise, an average value over a period of 1 min is considered as a minimum and most suitable; averages over periods of up to 10 min are acceptable.

A: Averaging. Average values over a fixed time period, as specified by the coding requirements.

Table A.5 *(continued)*

(1) Variable	(2) Range	(3) Reported resolution	(4) Mode of measurement/ observation	(5) Required measurement uncertainty	(6) Sensor time constant	(7) Output averaging time	(8) Typical operational performance	(9) Remarks
5.1 Speed	0 m/s to 60 m/s	0,5 m/s	A	0,5 m/s for ≤ 5 m/s 10 % for > 5 m/s	Distance-constant. 2 m to 5 m	2 min and/or 10 min	0,5 m/s for ≤ 5 m/s 10 % for > 5 m/s	Average over 2 and /or 10 min. Nonlinear devices. Care needed in design of averaging process.
5.2 Direction	0° to 360°	1°	A	5°	1 s	2 min and/or 10 min	5°	
5.3 Gusts	0 m/s to 75 m/s	0,1 m/s	A	10 %		3 s	0,5 m/s for ≤ 5 m/s 10 % for > 5 m/s	Highest 3 s average should be recorded.
6. Visibility								
6.1 MOR	< 50 m to 70 km	10 m	I	50 m for ≤ 500 m 10 % for > 500 m and ≤ 1500 m 20 % > 1500 m	< 30 s	1 min and 10 min	The larger of 20 m or 20 %	Achievable instrumental accuracy may depend on the cause of obscuration. Quantity to be averaged: extinction coefficient (see WMO-No 8, Part III, Chapter 3, section 3.6). Preference for averaging logarithmic values.
6.2 RVR	10 m to1500 m	1 m	A	10 m for ≤ 400 m 25 m for > 400 m to ≤ 800 m 10 % for > 800 m	< 30 s	1 min and 10 min	The larger of 20 m or 20 %	Should be in accordance with WMO-No.49, Volume II, Attachment A (2004 ed.) and ICAO Doc 9328-AN/908 (2nd ed., 2 000)
7. Waves								
7.1 Time series of sea surface elevation	–15 m to +20 m	0,1 m	I		0,5 s	n/a	±0,2 m for ≤ 5 m ±4 % for > 5 m	Length of time series 17 min (typical). Sampling frequency 2 Hz.
7.2 Variables from time series (zero crossing analysis)							Depends on averaging time and sea regularity as well as intrinsic instrument accuracy	
7.2.1 Significant wave height (H_s)	0 m to 20 m	0,1 m	A	0,5 m for ≤ 5 m 10 % for > 5 m	0,5 s	20 min (typical)		
7.2.2 Average zero crossing period (T_z)	3 s to 30 s	1 s	A	0,5 s	0,5 s	20 min (typical)		
7.2.3 Maximum wave height (H_{max})	0 m to 35 m		I		0,5 s	20 min (typical)		Observed value at location of sensor. New value every 30 min (typical).

NOTES

1 Column 1 gives the basic variable.

2 Column 2 gives the common range for most variables; limits depend on local climatological conditions.

3 Column 3 gives the most stringent resolution as determined in WMO-No. 8.

4 In column 4:

I: Instantaneous. In order to exclude the natural small-scale variability and the noise, an average value over a period of 1 min is considered as a minimum and most suitable; averages over periods of up to 10 min are acceptable.

A: Averaging. Average values over a fixed time period, as specified by the coding requirements.

Table A.5 *(continued)*

(1) Variable	(2) Range	(3) Reported resolution	(4) Mode of measurement/ observation	(5) Required measurement uncertainty	(6) Sensor time constant	(7) Output averaging time	(8) Typical operational performance	(9) Remarks
7.3 Wave spectrum						Minimum 17 min	Depends on averaging time and sea regularity as well as intrinsic instrument accuracy.	Instruments may include wave buoys, altimeter, microwave doppler radar, HF radar, navigation radar etc. (1 Hz sampling frequency is sufficient).
7.3.1 1-D spectral density		0,1 $m^2 \cdot Hz^{-1}$	I				Should be sufficient to achieve 7.4 requirements.	
Frequency	0,035 Hz to 0,3 Hz	< 0,01 Hz						
7.3.2 2-D spectral density		0,1 $m^2 \cdot Hz^{-1} \cdot rad^{-1}$					Should be sufficient to achieve 7.4 requirements.	
Frequency	0,035 Hz to 0,3 Hz	< 0,01 Hz						
Direction	0° to 360°	10° (see remark)						2-D spectrum may be based on parameterized directional distribution and reported as direction and spread parameters.
7.4 Variables from wave spectrum							Depends on averaging time and sea regularity as well as intrinsic instrument accuracy.	
7.4.1 Significant wave height (H_{mo})	0 m to 20 m	0,1 m	A		0,5 s	20 min	0,5 m for ≤ 5 m; 10 % for > 5 m	
7.4.2 Average period (T_{m02})	3 s to 30 s	0,1 s	A		0,5 s	20 min	0,5 s	
7.4.3 Peak period (T_p)	3 s to 30 s	0,1 s	A		0,5 s	20 min	0,5 s	Period of peak of frequency spectrum.
7.4.4 Mean direction	0° to 360°	10°	A		0,5 s	20 min	20°	May be spectrally averaged or based on angular harmonics.
7.4.5 Direction spread	0° to 360°	10°	A					
8 Ocean currents								
8.1 Current speed	0 $cm \cdot s^{-1}$ to 250 $cm \cdot s^{-1}$	1 $cm \cdot s^{-1}$	A	1 $cm \cdot s^{-1}$ to 10 $cm \cdot s^{-1}$	1 s	5 min to 20 min	2 $cm \cdot s^{-1}$ to 10 $cm \cdot s^{-1}$	Achievable accuracy affected by type of measurement; direct or acoustic doppler profilers
8.2 Current direction	0° to 360°	1°	A	±5°	1 s	5 min to 20 min	±5°	
9 Water level	±3 m	1 cm	I	±1 cm		10 min	±5 cm	

NOTES

1 Column 1 gives the basic variable.

2 Column 2 gives the common range for most variables; limits depend on local climatological conditions.

3 Column 3 gives the most stringent resolution as determined in WMO-No. 8.

4 In column 4:

I: Instantaneous. In order to exclude the natural small-scale variability and the noise, an average value over a period of 1 min is considered as a minimum and most suitable; averages over periods of up to 10 min are acceptable.

A: Averaging. Average values over a fixed time period, as specified by the coding requirements.

Table A.5 *(continued)*

(1) Variable	(2) Range	(3) Reported resolution	(4) Mode of measurement/ observation	(5) Required measurement uncertainty	(6) Sensor time constant	(7) Output averaging time	(8) Typical operational performance	(9) Remarks
10 Temperature profile	−2 °C to +25 °C	0,1 K	I	0,01 K	0,5 s	1 s	0,05 K	Achievable accuracy according to commonly used CTD sensors
11 Salinity profile	0 to 40 PSU	0,1	I	±0,01 PSU	0,5 s	1 s	±0,05 PSU	As per temperature profile unit: PSU (Practical Salinity Unit) according to PSS78.
12 Oxygen	0 ml/l to 15 ml/l	0,1 ml/l	I	±5 %	0,5 s	1 s	±5 %	

NOTES

1 Column 1 gives the basic variable.

2 Column 2 gives the common range for most variables; limits depend on local climatological conditions.

3 Column 3 gives the most stringent resolution as determined in WMO-No. 8.

4 In column 4:

I: Instantaneous. In order to exclude the natural small-scale variability and the noise, an average value over a period of 1 min is considered as a minimum and most suitable; averages over periods of up to 10 min are acceptable.

A: Averaging. Average values over a fixed time period, as specified by the coding requirements.

A.8.3 Meteorology

A.8.3.1 General

Details on instrument accuracy and calibration are found in WMO-No. 8, Parts I and III.

A.8.3.2 Weather observation and reporting for helicopter operations

Experience has shown that the best quality wind measurements are achieved if the location of the wind sensor is selected to minimize the influence from the construction itself (living quarters, cranes, etc.). This means that the top of derrick or mast is the best choice in most cases.

The measurement of these parameters does not replace the need for an easily perceptible wind sock or cone.

The observations should be recorded in accordance with WMO-No. 306, Section A, pp 25-36.

In addition to METAR, a code for special reports is specified in WMO-No. 306, under code FM 16-XV Ext. SPECI.

The criteria for, and frequency of, issue of METARs and SPECIs is the responsibility of the relevant aviation regulations. International recommendations may be found in WMO-No. 842 (Chapter 4).

A.8.3.3 Weather observation and reporting for weather forecasting services

No guidance is offered.

A.8.3.4 Weather observation and reporting for climatological purposes

No guidance is offered.

A.8.4 Oceanography

A.8.4.1 General

No guidance is offered.

A.8.4.2 Measurements and observations

Ocean currents should be measured at fixed depths (or bins), and include at least three depths in shallow waters: near-surface, mid-depth and near-bottom.

For measurements in deeper waters, the following depths should be considered in addition to near-surface and near-bottom: 50 m, 100 m, 150 m, 200 m, 300 m and every 200 m thereafter to 3 m above the seabed.

The mean speed and direction of ocean currents should be recorded at least once per hour. Measurements of sea temperature and salinity should be performed as an integrated activity. If Nansen bottles or similar equipment are used, data should be recorded at standard depths: 0 m, 5 m, 10 m, 20 m, 30 m, 50 m, 75 m, 100 m, 125 m, 150 m, 200 m, 250 m, 300 m, 400 m, 500 m, 600 m, 800 m, etc.

If a conductivity-temperature-depth sensor (CTD) is used for measuring temperature and salinity, data should be stored for at least every 50 kPa (0,5 bar).

Oxygen content, if required, should be measured at a subset of the temperature/salinity depths given above. However, the number of depths may be considerably reduced.

The observation of sea ice and icebergs (dimensions and drift), may be performed by combining e.g. manual observations, instrument recordings and remote sensing.

A.8.5 Data quality control

No guidance is offered.

A.9 Verification of Weather Forecast Information

A.9.1 General

In the following sections the different types of weather forecast are introduced, followed by recommendations on suitable verification data, and the techniques used to verify the various types of forecast. Finally, guidance on forecast improvement – which should be undertaken following forecast verification - is also provided.

A.9.2 Forecast Categories

Guidance is provided for the verification of deterministic and ensemble forecasts at a single location. Although forecasts may be provided and verified over an area, such verification represents a special case, making use of image analyses, feature identification and filtering methods and is not covered by the guidance; further information may be found in chapter 6 of reference [71].

Ensemble forecasts, which are recommended for operational planning, allow the user to quantify the forecast probability of a critical threshold being exceeded, whereas in a deterministic forecast the threshold is either exceeded or it is not. If deterministic forecasts must be used then an Alpha factor [72] may be employed, which reduces the operational limit to attempt to account for uncertainty in the deterministic forecast. For higher-risk operations, the Alpha factors should be assessed to ensure that these adequately reduce the operational limits to account for the forecast uncertainty; reference [72] provides guidance on how to quantify the relative risk level of a given operation. Note that the Alpha factors in reference [72] were derived specifically for European waters.

Ensemble and deterministic forecasts usually contain predictions of continuous variables – for example, temperature, wind speed, current speed, significant wave height, mean zero-crossing period. A binary forecast is one which provides information on threshold exceedance (rain / no rain; storm / no storm; fog / no fog, etc.) whereas a multi-category forecast provides similar information but split over more than two categories (no rain / light rain / heavy rain, for example). Many of the existing verification approaches are tailored towards binary or multi-category forecasts. Forecasts of continuous variables may be manipulated to generate binary or multi-category forecasts, allowing a full set of verification techniques to be applied to the forecast.

A.9.2.1 Forecast Model Limitations

Forecast models, no matter how accurate, may not have sufficient resolution to capture events at all scales. Examples of phenomena which may not be represented due to forecast resolution limitations are:

— Squalls: in tropical regions squalls may cause operational hazards but are too localised to be represented in the regional forecast models;

— Sting jets: rapidly deepening extra-tropical low pressure systems may enhance wind speeds in certain areas of the storm [73]. Again, the length scales involved are typically beyond the resolution of standard forecast models;

— Topographic shielding: forecasts for larger wind farm arrays may need to take into account the presence of the turbines to accurately predict the wind fields at all locations. In coastal regions, land-sea breezes and topography may degrade the quality of a regional forecast model;

— Tropical cyclones,

— Polar Lows, and

— Current eddies.

These limitations will be revealed through the presence of bias between the forecast model output and appropriate verification data (see Section A.12.3), over an historical period. Opportunities to reduce these biases are available through, for example, high-resolution down-scaling; however, this may be computationally prohibitive, particularly for ensembles, and may be limited in providing reliable estimates of timing and location of mesoscale phenomena such as sting jets, eddies, and squalls.

A.9.3 Verification Data

Forecasts are typically verified against some other source of data – usually measurements, or perhaps a different benchmark forecast or hindcast model. Verification data should be properly prepared prior to its use in assessing forecasts:

— Verification data must be representative of the same location, parameter and time as the forecast data. For example, winds should be for the same height and averaging period, sea-state parameters should represent the same averaging period (see section A.5.4), whereas parameters such as rainfall, wave power or solar irradiance should be calculated over the same duration and area scales. Checks should also be made to ensure that forecast and verification data are presented in the same time-zone [UTC, for example].

— Measurements must be quality-controlled to ensure that erroneous data have been removed, and full consideration should be given to the accuracy of the instrumentation and data processing methods used to make the measurements. This is also important when generating long-term archives of measured data where changes in instrumentation or siting may affect the statistics.

— Some parameters may need to be categorised before forecast verification may take place. For example, cloud cover may be reported in the forecasts in octas but measured in fewer categories. Similarly, care should be taken to ensure any comparison is not affected by the type of sensor used to measure the parameter. For example, the maximum values of cloud height or visibility are particularly dependent on the limits of the sensors and may need to be categorised prior to undertaking forecast verification. Manipulation of the forecasts and measurements could involve generating a binary category (poor visibility/good visibility) or multi-category (low/medium/high cloud), or perhaps using a combination of the two parameters to assess flying conditions (CAVOK[74]). Consideration should also be given to how rapidly in time or location a parameter varies. For example, cloud height and visibility may change rapidly and so some adjustment to the forecast and verification data may be required – perhaps to calculate the daily minimum visibility or to estimate if there was fog on a given day.

— Phenomena may exist that are not resolvable by the forecast model (see discussion in Section A.12.2.1) and so consideration should be given to which aspects of the forecast may be verified, and which sources of data are suitable for this verification. There is little point in attempting to verify a forecast that cannot resolve certain phenomena, using measurements which contain these phenomena. Instead, either the verification should proceed using data without these phenomena, or re-forecasting using a higher-resolution model is required.

In summary: data used to verify forecasts must: be representative of the time, location and parameters of interest; have undergone quality control to remove errors; contain examples of events that are of interest.

A.9.4 Verification

The following subsections describe the verification of:

— Continuous, binary and multi-category deterministic and ensemble forecasts;

— Forecast timings;

— Forecasts of extreme or rare events; and,

— Forecasts in particularly challenging locations.

It is assumed that suitably prepared data (see Section A.12.3) are available against which the forecast performance may be assessed. These data may be measured, modelled or from a benchmark forecast and for ease of discussion they will be termed “observations”.

Rather than consider each forecast in its entirety, verification typically proceeds by focusing on each forecast horizon in turn and using historical observations to quantify the performance at that horizon; the analyses are completed across all relevant horizons.

A.9.4.1 Deterministic Forecast Verification

This section provides guidance on the verification of continuous forecast variables and binary or multi-category forecasts.

A.9.4.1.1 Continuous Variables

The performance of forecasts of continuous variables is typically quantified via the following:

— Bias: the difference between the means of the forecast and observations;

— Mean absolute error or mean squared error: the mean of the absolute or squared difference between forecast and observations; and,

— Correlation: the covariance of the forecast and observed data, divided by the product of their standard deviations.

Plots of bias and the mean absolute or squared error for each forecast horizon provide insight on forecast performance with increasing horizon; the mean squared error is more sensitive to larger forecast errors. The correlation has the benefit of being unaffected by any forecast bias or differences in forecast and observed units.

Examples of bias and mean absolute error against forecast horizon for various different forecast providers (labelled FX_A, FX_B, …, FX_H) are shown in Figure A.12.1. At almost every horizon, FX_C performs worst, while FX_D and FX_G perform best. Visual comparisons such as these are useful when comparing forecasts from different models.

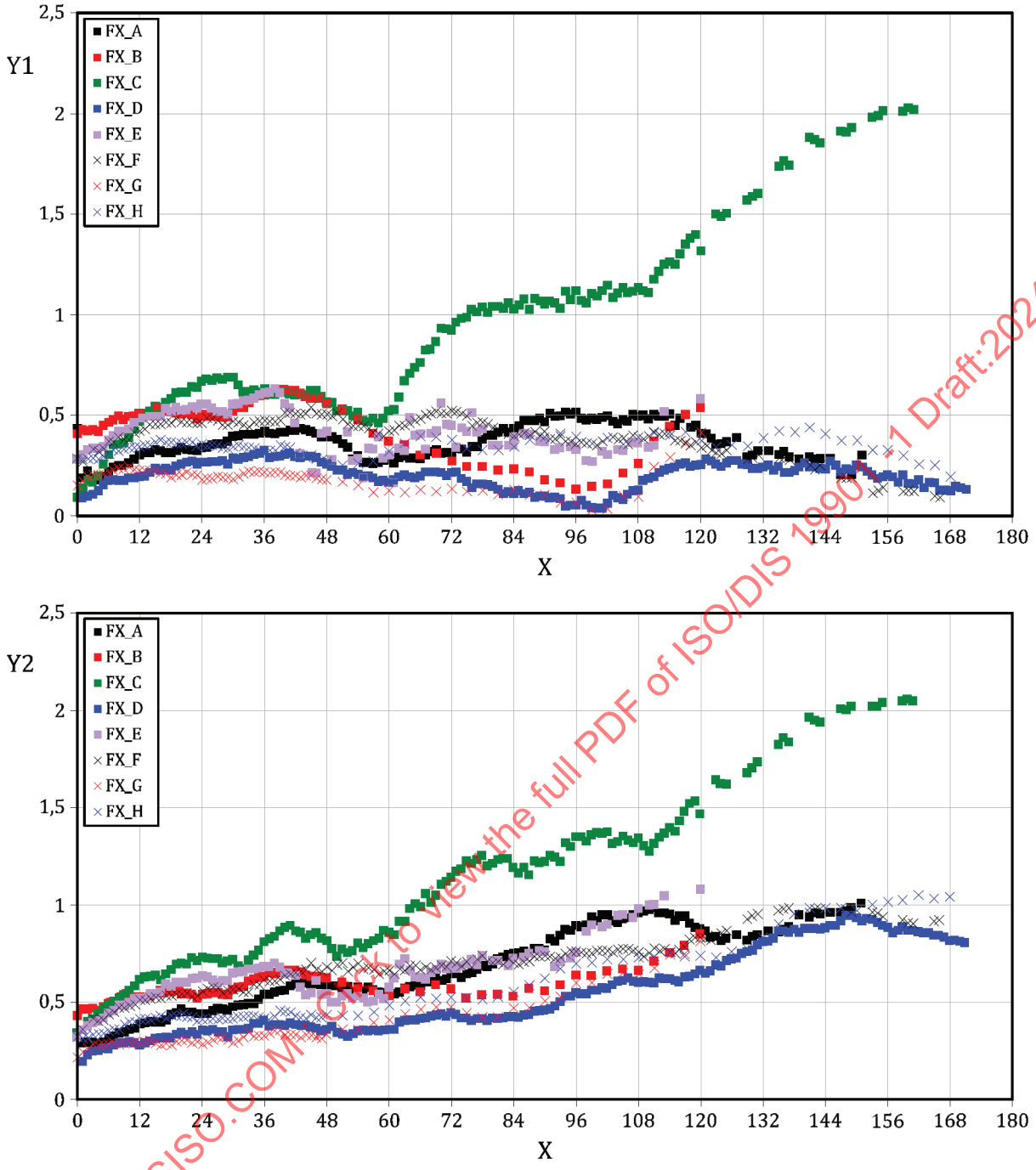

Key

X forecast horizon (hours)

Y1 bias (m) Y2 MAE (m)

Figure A.12.1 — Example of bias (top) and mean absolute error (bottom) for Hs plotted against forecast horizon for various forecasters

Although it is possible to also quantify the performance of forecasts of continuous variables via skill measures, these are more typically derived for binary or multi-category forecasts (or continuous forecasts that have been manipulated into binary or multi-categories) and are discussed in Section A.12.4.1.2. Further details of skill scores derived directly from forecasts of continuous variables may be found in reference [75].

Additional Verification techniques:

While the techniques discussed above provide statistics of forecast performance, the following plots are also useful when undertaking forecast verification of continuous variables as they are easy to interpret and offer a visual indication of forecast performance. Unless otherwise stated, each plot provides information for a single forecast horizon.

— Forecast-observation scatter plots, either based on all data or above a threshold

— Forecast-observation quantile-quantile plots, either based on all data or above a threshold

— Taylor diagrams[76]

These may be used to display the mean squared error, correlation and variance on a single plot, and may either compare different forecast models or different horizons against observations.

— Forecast-observed time-series plots; and

— Forecast observation exceedance plots.

Example scatter and exceedance plots for various forecast horizons are shown below in Figure A.12.2 and Figure A.12.3, and highlight the gradual degradation in performance with increasing horizon.

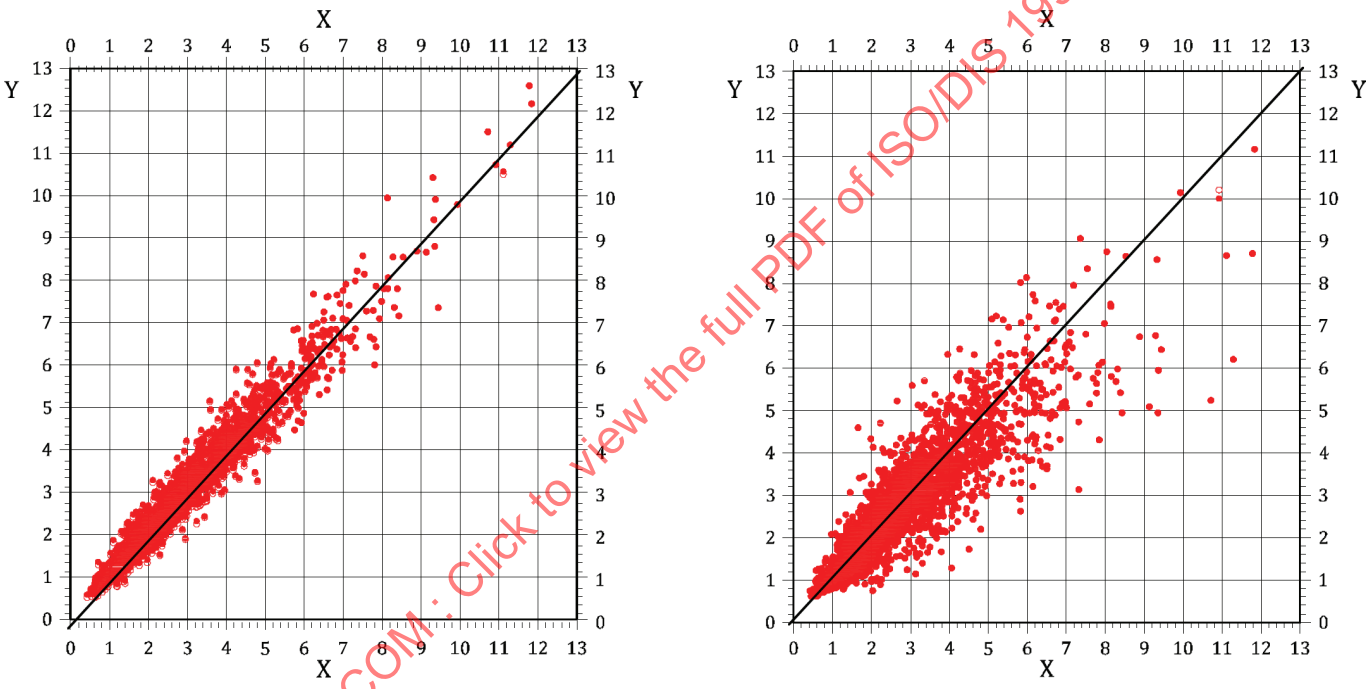

Key

X observed Hs (m) Y forecast Hs (m)

Figure A.12.2 — Example observed-forecast Hs scatter plots for 1 and 5 day horizons. 1:1 reference line is shown in black.

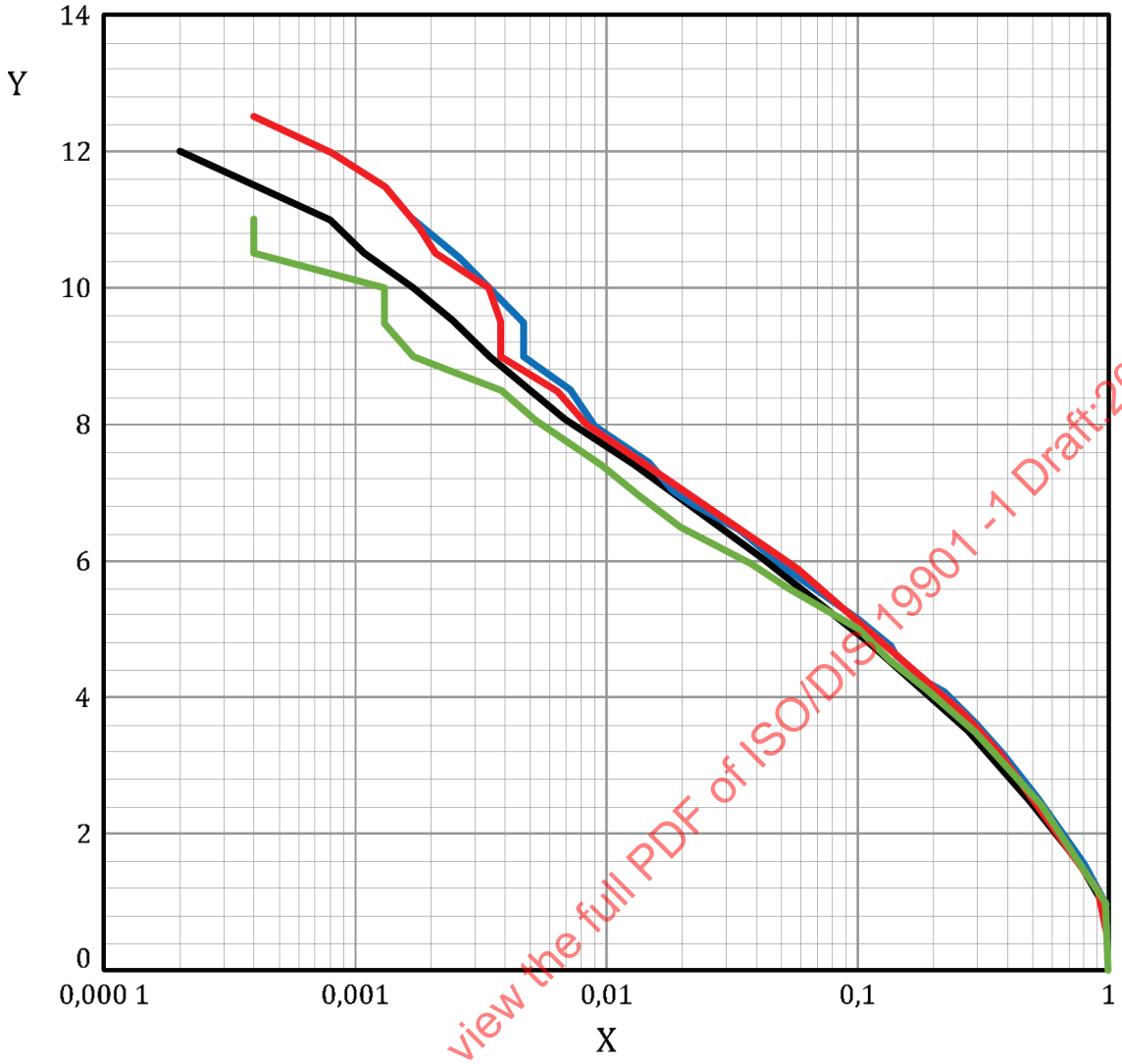

Key

X	probability of exceedance	Y	Hs (m)
	observations		3 days
	1 day		5 days

Figure A.12.3 — Example Hs exceedance plots for observations and various forecast horizons.

A.9.4.1.2 Binary or multi-category

For binary forecasts, the bias is calculated as the ratio between the number of times an event was forecasted and the number of times an event occurred. However, this does not imply any skill since the statistics are based on the marginal occurrence rates and the forecast could never correctly predict an event and still achieve a perfect score of 1. For multi-category forecasts the bias may be calculated separately for each category.

Skill scores for binary events are typically compared against theoretical limits – for example, a perfect forecast or a random forecast. Numerous skill scores exist even for binary forecasts where only four outcomes are possible; for multi-category events the number increases, as does the complexity of their

derivation. A comprehensive discussion of the various skill measures is provided in reference [71], with the following list representing the most commonly used binary forecast skill measures.

— Proportion of correct forecasts – i.e. forecasts which correctly predicted an event would occur, or correctly predicted an event would not occur, divided by the total number of forecasts [(Hits + CorrectRejections)/ NumberOfForecasts].

— Care should be taken for rarely-occurring events since the proportion correct may be improved by never forecasting an event.

— False Alarm Rate [FAR] and Hit Rate [HR] – often plotted on a diagram with false alarm rate on the x-axis and hit rate on the y-axis, with the no-skill line being a line through the origin of gradient 1. Points lying above the line indicate an improvement over the no-skill line, with points from a perfect forecast lying at the upper-left corner of the plot.

— HR: proportion of events occurring which were also forecast as events: [Hits/(Hits + Misses)]

— FAR: proportion of non-events which were incorrectly forecast as events: [FalseAlarms/(FalseAlarms + CorrectRejections)]

— Critical Success Index – defined as the ratio between the number of correctly forecast events to the total number of events, excluding correct rejections [Hits/(Hits + FalseAlarms + Misses)].

— Pierce Skill Score[77] – defined as the difference between the Hit Rate and False Alarm Rate [HR-FAR], often plotted against bias.

— Other measures of skill compare the forecast performance against a random forecast. For example:

  Heidke Skill Score[78]

  Gilbert Skill Score[78,79].

The False Alarm Rate and Hit Rate plot is one of the most useful binary skill scores because it is simple to generate and easy to interpret. Results for multiple forecast horizons or from different forecasters may be shown on a single plot to explore the variation in forecast skill. An example plot in Figure A.12.4 compares FAR and HR from different forecast providers (labelled FX_A, FX_B, …, FX_E) for various horizons. The plot shows, for example, that FX_B tends to raise fewer false alarms than FX_E but also has a lower hit rate for most events; FX_C performs well – with a high hit rate and low false alarm rate.

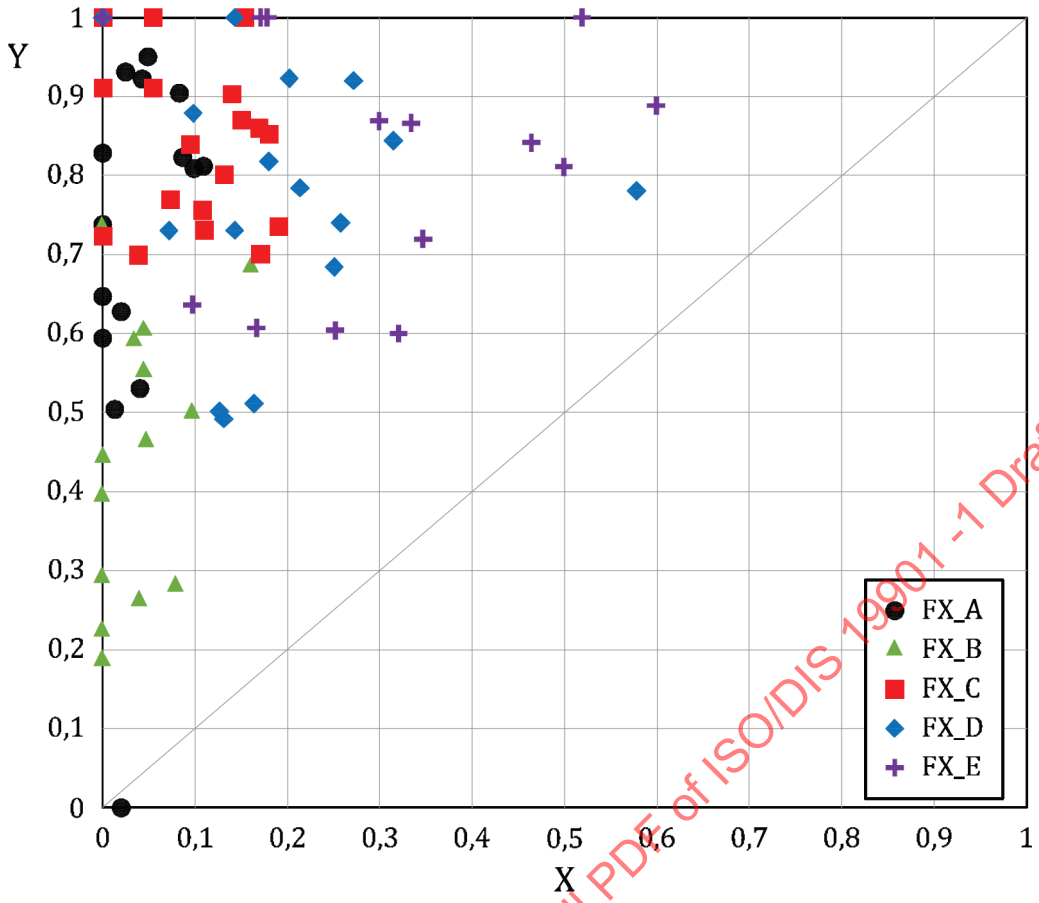

Key

X false alarm rate Y hit rate

Figure A.12.4 — False Alarm Rate and Hit Rate for various forecasters and horizons.

For multi-category forecasts, the derivation of skill scores becomes more complex, requiring the development of a scoring matrix based on the probability of occurrence of each event category. Once this is developed, various skill scores may then be derived. Full details are provided in reference [75] and summarised in chapter 4 of reference [71].

Note that care must be taken when deriving skill scores for extreme or rare events since many tend towards a limiting value as the event rate approaches zero; Section A.12.4.4 discusses verification of extreme or rare events.

A.9.4.2 Ensemble Forecast Verification

Ensemble forecasts may be verified using either a “discrete” or “probabilistic” approach, both of which are discussed in the following sections. The former treats each member of the ensemble as a discrete sample from an underlying probability distribution, while the latter attempts to define the underlying probability distribution using the ensembles. In either case, it is important to first identify if the ensembles are reliable, i.e. if they represent the true range of possible outcomes. Comparison of the ensemble probability distribution with that of the observations may determine if the ensembles show bias, underdispersion or overdispersion. This important step, together with a summary of verification techniques, is discussed in the following sections.

A.9.4.2.1 Discrete Samples

To determine the reliability of ensembles treated as discrete samples, the position of the observation relative to the ensembles may be calculated (via its rank) and plotted as a histogram. The shape of the rank histogram provides information on ensemble bias (via the slope of the histogram) and dispersive behaviour

(via under or over-population of the lowest and highest ranks). Un-biased forecasts which capture the full range of possible outcomes would be represented as a flat histogram. The statistical significance of any deviation from this flat histogram may be determined via goodness of fit tests. A separate rank histogram may be generated for all relevant horizons. The rank approach may be extended to multiple dimensions, such as different forecast parameters, or different forecast locations; full details may be found in chapter 8 of reference [71].

An example rank histogram is shown in Figure A.12.5 based on 2100 forecasts each with 21 ensembles. The blue dashed line indicates the expected distribution from a perfect forecast while the green bars indicate the number of times the observation corresponded with a particular ensemble rank. The plot indicates that the forecasts appear to be un-biased but show overdispersion since the observed value is typically less extreme than the forecasts and so the highest and lowest ranks are underpopulated.

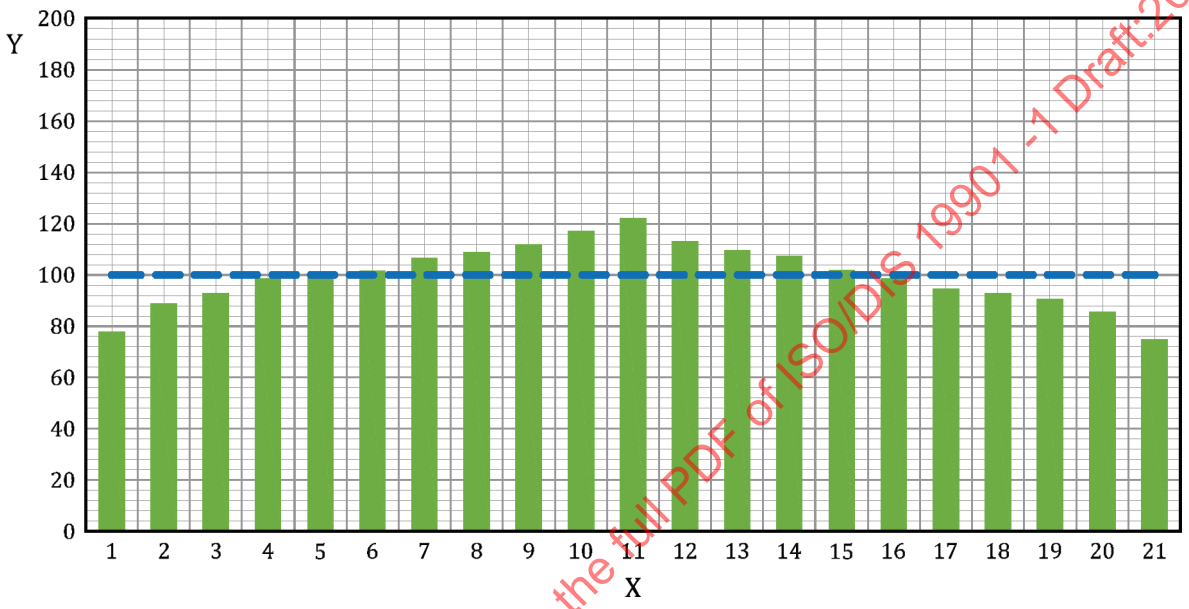

Key

X	rank of observation relative ensembles	Y	frequency
Blue dashed line	Expected distribution from perfect forecast	Green bars	Distribution of the rank of the observation relative to the ensembles

Figure A.12.5 — Example rank histogram from 21-member ensemble.

While the rank histogram may provide information on the presence of bias and dispersion of the ensembles, it does not assess if the Nth percentile ensemble truly represents the Nth percentile of the observed data. This may be tested via the Conditional Exceedance Probability [CEP] - see reference [80]. The CEP provides information on how likely the forecast is to be exceeded by the observed data, as a function of the forecast value. For example, a perfect forecast would show the 95 percentile ensemble being exceeded only 5 % of the time, regardless of if the forecast predicts a low or high value of the parameter. The CEP plot therefore reveals any conditional bias in the ensemble, and also determines if the Nth percentile ensemble truly reflects the Nth percentile of the observed data.

Figure A.12.6 shows an example CEP plot for a median ensemble. The grey line is included for reference and shows the marginal long-term distribution of Hs based on the observations; the blue dashed line shows the exceedance for the median ensemble based on a perfect forecast; the green line shows the exceedance of the median ensemble forecast value, conditional on that forecast value, i.e. given that the median ensemble forecasts a value of X, what is the probability that the corresponding observation exceeds X. For median ensemble forecast Hs below around 3 m, the median ensemble probability of exceedance is less than 0,5, indicating that the forecasts from that ensemble are bias high; for forecast Hs above 3 m, the median ensemble probability of exceedance is greater than 0,5, indicating the forecasts from that ensemble are bias low. For a perfect forecast, the green line would overlay the blue dashed line.

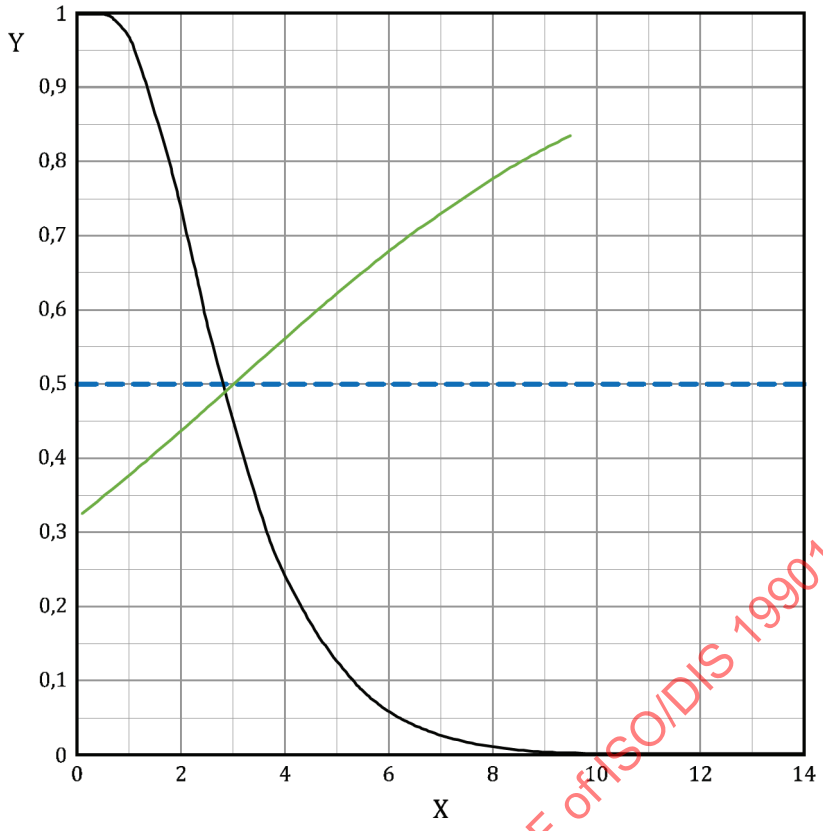

Key

X	Hs (m)	Y	conditional exceedance probability
Green line	Probability that the observations exceed the forecast ensemble being considered (median), conditional on the forecast value of Hs		
Blue dashed line	Results for the ensemble from a perfect forecast		
Grey line	For reference, the marginal long-term Hs exceedance based on observations		

Figure A.12.6 — Example CEP plot

Any of the methods applied to deterministic forecasts (discussed in Section A.12.4.1) may be applied to each member of an ensemble. However, this may generate an overwhelming quantity of results and it is more practical to adopt the approach discussed in the following section, whereby the ensembles are treated as probability distributions at different forecast horizons.

A.9.4.2.2 Probability Distributions

The first task in treating ensemble forecasts as probability distributions is to fit an appropriate distribution to the forecast values, with each horizon being considered separately. Typically this is done by fitting a single overall distribution across all of the ensemble values or via a kernel dressing approach, where each ensemble value is represented by a probability distribution of fixed width – representing the uncertainty in that forecast value. The choice of distributions to apply to the kernel dressing or single overall distribution approaches is dependent on the parameter being considered, although Gaussian and Gamma distributions are typically used; further information may found in chapter 8 of reference [71] and in references [81-87].

Figure A.12.7 shows an example of the Kernel dressing approach: each of the discrete ensemble forecast values (green diamonds) are represented by a Gaussian distribution (black lines) which are summed to generate the overall probability distribution (blue dashed line).

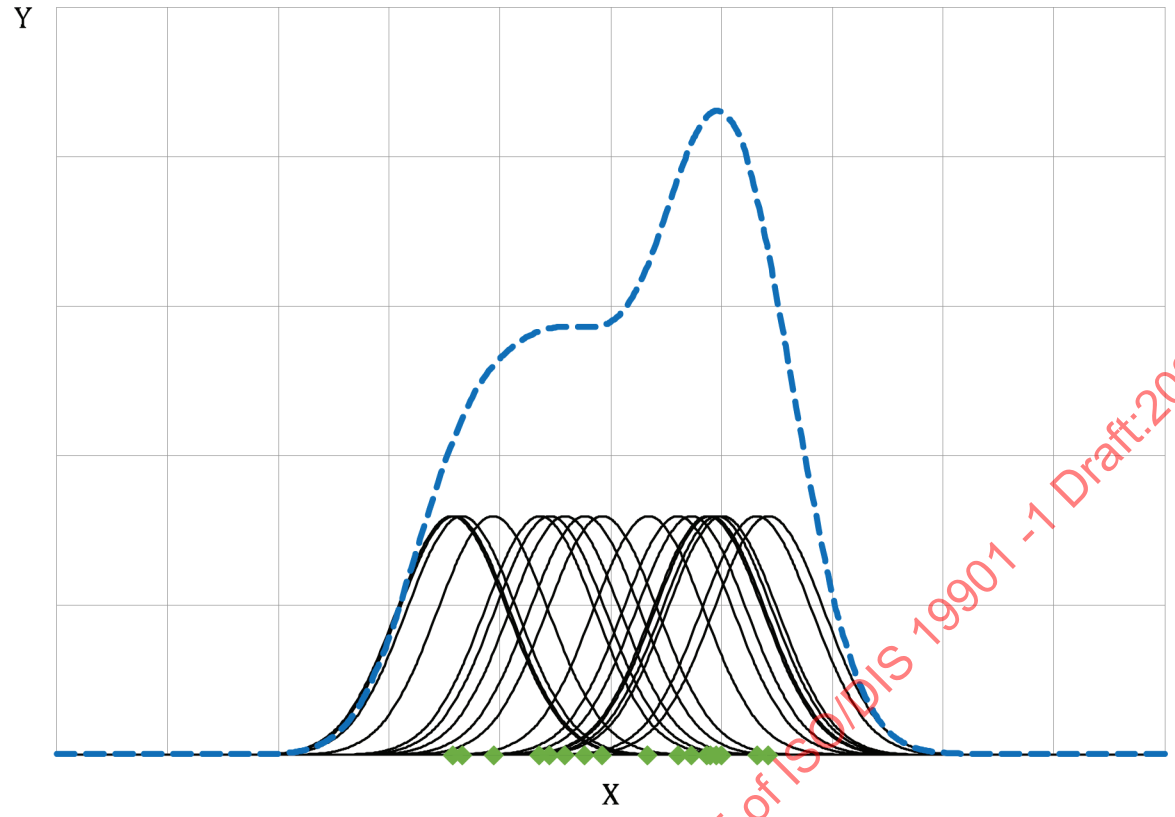

Key

X	value	Y	probability density
◆	individual ensemble member predictions at a given forecast horizon		
———	kernels fit to each ensemble prediction		
- - -	the combined distribution		

Figure A.12.7 — Schematic showing Kernel dressing approach

Once the probability distribution has been generated from the ensemble values, the forecasts may be verified - as discussed in the following sections for both continuous and binary or multi-category forecasts. Binary and multi-category forecasts may be derived directly from the ensemble probability distributions (at a given time horizon) by assigning the relevant probability into each category – for example, the probability of rainfall, or the probability of temperatures between two limits.

A.9.4.2.2.1 Continuous Variables

Although performance measures for continuous forecasts do exist, such as the Continuous Ranked Probability Score (CRPS), accuracy and skill measures for continuous variables are typically determined by first categorising the forecasts into binary or multi-category events, and applying the techniques discussed in the following sections. For a comprehensive discussion of the CRPS, see reference [88].

A.9.4.2.2.2 Binary and Multi-category

The bias is calculated as the ratio of the ensemble event probabilities and the observed event probabilities; this does not imply any skill since the statistics are based on the marginal occurrence rates. For multi-category forecasts the bias may be calculated separately for each category and may be presented using a reliability diagram, see chapter 7.4.4 of reference [89].

For binary forecasts, the accuracy may be measured via the mean squared difference between the forecast and observed event probabilities; note that this is often termed the Brier Score.[90] Hit Rate and False Alarm

Rate may also be calculated for an event based on a probability limit, above which the forecast is deemed to predict an event: for example, the probability of exceedance of the event threshold is larger than, say, 0,8. Once set, this threshold may be used to derive the Hit Rate (probability that the forecasts exceed the event threshold, given that the event occurred) and the False Alarm Rate (probability that the forecasts exceed the event threshold, given that the event did not occur).

For multi-category forecasts, the Brier Score may be generalised to the Ranked Probability Score[91] which depends on the squared difference of probabilities in each of the categories. The Hit Rate may also be extended to generate a separate statistic for each category.

The Brier Score or the Ranked Probability Score for the forecast may be compared against some benchmark – such as climatology - to determine the corresponding Skill Score.

A.9.4.3 Verification of Forecast Timing

The ability of a forecast to accurately capture the timing of events is important since even a forecast which perfectly captures the severity of an event may be misleading if the event timing is wrong. Performance statistics may be generated by calculating the difference in timing between the forecast and observed events – perhaps separately for the event threshold up-crossing, event peak, and threshold down-crossing. Note that this approach requires that the event occurs in both the forecast and observed data and so the skill of the forecast in predicting events should be assessed. Any offset between the forecast and observed timings may be treated in a similar manner as offsets between forecast and observed parameter values. Statistics may be derived such as bias, mean squared error, or via categories (e.g., storm timing within 6 hours of observed event). Given sufficient data, the timing errors may be presented as a function of storm peak value to determine the forecast performance for more severe events. However, care must be taken when interpreting statistics based on very few events.

A.9.4.4 Verification of Extreme or Rare Events

The techniques discussed in Section A.12.4.1.2 relating to forecast skill for binary events may be applied to extreme or rare events. However, many of these scores approach their limiting values (degrade) as the number of events reduces. An important question to answer is whether this degradation occurs faster or slower than it would for some benchmark forecast.

To answer the question, a model may be fit to the joint distribution of measured and forecast data and this model may be used to estimate the four different binary forecast outcomes (hit, miss, false alarm, or correct rejection) as a function of the number of observed events. These outcomes may be used to estimate various forecast skill scores (see Section A.12.4.1.2) for events which may be beyond the limits of the data, while the model parameters themselves indicate if the degradation is faster or slower than would occur for a random forecast. This approach is discussed in chapter 10 of reference [71] and in reference [92].

The model must be fit sufficiently far into the tail of the joint measured-forecast distribution, but must maintain sufficient points to produce a reasonable fit; discussion of this is provided in the references given in the paragraph above, which also recommend providing confidence intervals for the model-derived skill scores using a bootstrapping approach.

It should be noted that the measurements of extreme or rare events may have relatively large associated errors which may have a corresponding effect on the calculated forecast skill and so particular care must be taken when choosing and preparing these measurements.

A.9.4.5 Forecast Verification in Challenging Locations: Multi-Mode Seas

A specific forecast verification challenge occurs in regions where multiple wave modes (e.g. wind-sea and swell or multiple swell systems) exist. Vessel response may be significant in even relatively calm seas if the different modes are close to critical periods or are from multiple directions and forecasts that provide only the total wave parameters (i.e. integrated parameters derived from the total wave spectrum) will not be appropriate.

One approach is to receive forecast directional wave spectra which may be verified against measured directional wave spectra, to assess whether the model is capturing sufficient energy by frequency and

direction. This could be done on a cumulative basis (i.e. summed measured spectra over a continuous period compared with summed forecast spectra over the same period), or on a discrete basis by considering events of interest (e.g. long period swell energy events). However, given the different approaches to spectral partitioning, often combined with a lack of measured directional wave data, it may not be possible for the forecasts to be directly verified in this manner.

Another, more accurate alternative is to use forecast directional wave spectra to simulate vessel responses; the forecast responses may then be compared with the measured response of the vessel. This assumes that the vessel Response Amplitude Operators [RAOs] may be provided to the forecasters and may be incorporated within the forecast model, and that suitable measurements of vessel response exist. By taking this approach, a multi-dimensional verification problem is reduced to one based on (typically) three parameters – heave, pitch and roll (or whatever the key response - or load - of interest is).

A.9.5 Forecast Improvement

The forecast verification measures discussed in the previous sections should be used to improve the forecasts. This may be done either by making changes to the underlying forecast model, or by post-model adjustment of the forecasts to account for known, quantified deficiencies (e.g. bias). Significant resources are required to update and improve the underlying forecast models and so this tends to occur relatively infrequently and so it is usually the latter approach – post-model adjustment to the forecasts - that is taken.

Ensemble forecasts provide the best opportunity for forecast improvement since they may be verified to determine bias and any under- or over-dispersion – both of which may be accounted for. By contrast, only bias removal may be used to improve a deterministic forecast, without making adjustments to the underlying forecast models.

Full details of the methods used to improve ensemble forecasts are provided elsewhere, for example reference [87]. In summary, the methods attempt to generate a bias correction and width adjustment of the kernel distributions (at a given forecast time horizon) which are used to transform the ensemble values into a probability distribution (see Section A.12.4.2.2). The adjustments are determined by using an appropriate skill score and choosing parameters which maximise the improvement of the skill score. They may be developed separately for different forecast parameters and conditionally on the parameter magnitude. They may also be drawn randomly from a pool of parameters to reflect uncertainty in the corrections.

The figure below shows an example of forecast improvement at a single forecast horizon. The original forecast information is presented as per Figure A.12.7: each of the discrete ensemble forecast values (green diamonds) are represented by a Gaussian distribution (black lines) which are summed to generate the overall probability distribution (blue dashed line). A transformation, such as the ones discussed above, is applied to the forecast, which shifts the resulting probability distribution (red line) to the mean of the transformed values (open red squares), which better represent the observed data (vertical dashed line).

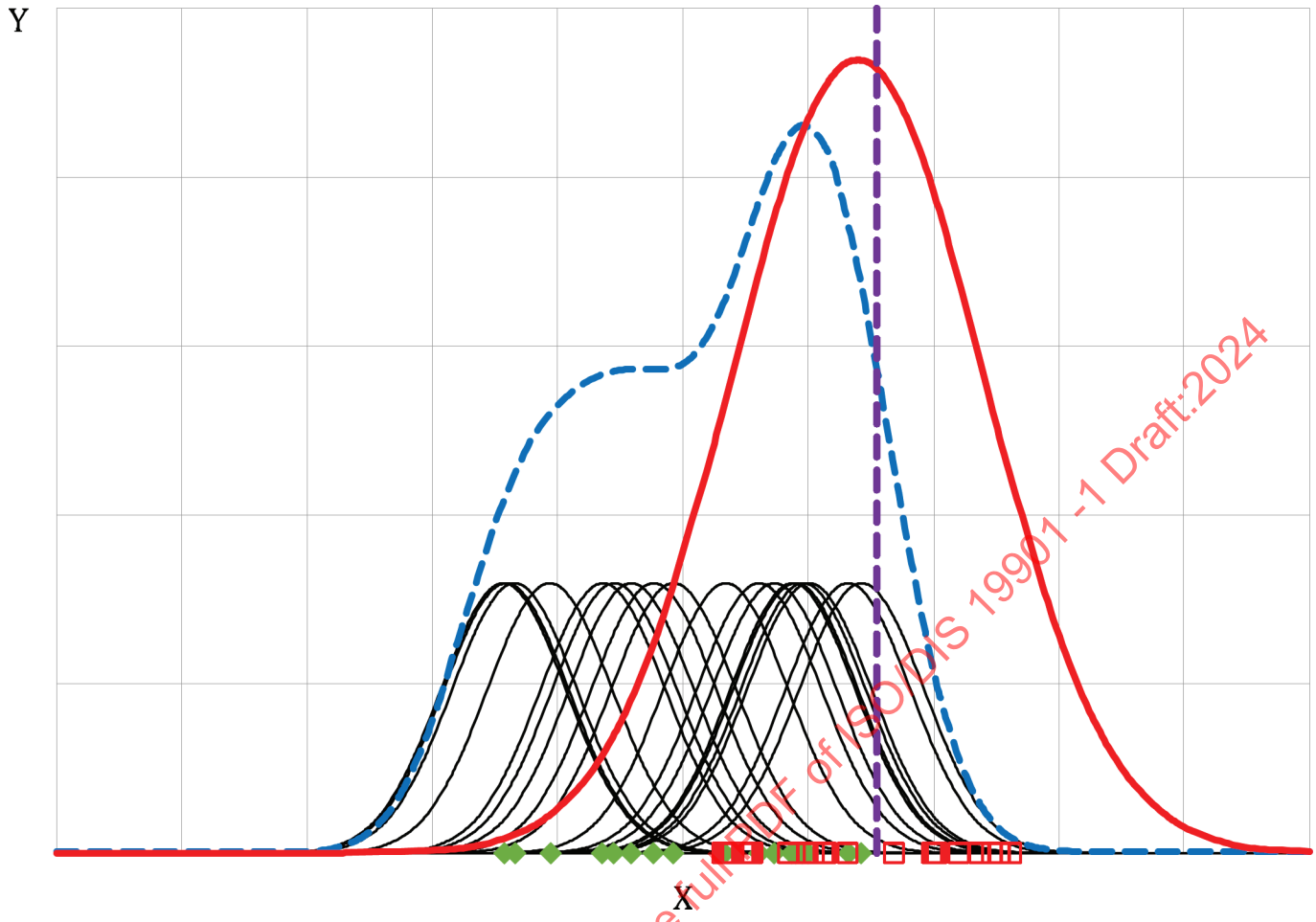

Key

X value Y probability density

Figure A.12.8 — Schematic showing improvement to ensemble forecast model uncertainty through use of kernel dressing.

The steps outlined above allow ensemble forecasts to benefit from any verification that has been performed either by the forecast provider or by the users of the forecast, without having to wait for improvements to be implemented in the underlying forecast model. However, it is important that forecast providers are made aware of any forecast shortcomings and are encouraged to address these to make improvements to their models.

For high-risk operations (defined in reference [72]), any forecast improvement may be determined prior to the operation commencing by using historical ensemble forecast data and comparing it with historical measurements; historical forecast model data are available from large regional forecast providers. Any improvements to the forecast may then be implemented before the operation takes place.

Annex B
(informative)

Northwest Europe

B.1 Description of region

The geographical extent of the region of northwest Europe is bounded by the continental shelf margins of Europe, as shown in Figure B.1. The region is diverse, stretching from the sub-arctic waters off Norway and Iceland to the Atlantic seaboard of France and Ireland in the south, and includes:

— the waters off Norway, part of which are within the Arctic Circle,

— the Baltic Sea,

— the North Sea,

— the Irish Sea,

— the English Channel,

— the northern half of the Bay of Biscay,

— the waters off the west coasts of Ireland and Scotland, and

— the waters off the Faroe Islands.

B.2 Data sources

Measured data are available from many stations throughout the area. Sources for measured data may be identified through the International Oceanographic Data and Information Exchange,[93] which is part of UNESCO[1]). Links will be found to national oceanographic data centres, which in turn provide links to specialist institutes and other organizations within each country. Data may also be obtained from commercial organizations. In addition to measured data, in recent years a number of joint industry-sponsored hindcast studies have been performed (see for example, references [94] and [95]). These have resulted in extensive (but usually proprietary) datasets for the companies involved; however, a published report[96] provides useful information derived from the NEXT hindcast study[94].

B.3 Overview of regional climatology

The conditions experienced within the region vary from arctic to temperate. The north of Norway experiences very cold winters, with low temperatures and associated ice in various forms. However, ice occurs very rarely in the southwest of the region.

In all parts of the region, extremes of wind and wave are most likely to occur during the passage of a vigorous frontal depression. Depressions are areas of low atmospheric pressure and cyclonic airflow; they vary from nebulous, with light winds, to intense and stormy with a large area of strong winds. Together with associated frontal systems, they cross the area throughout the year, generally from west to east. They may move rapidly, with speeds of translation of 5 m/s to 15 m/s, and a wide range of conditions may be experienced at any one site. Depressions are larger than tropical cyclonic storms such as hurricanes. Another type of depression is called a “polar low”. Such depressions do not have fronts and are less common than frontal depressions and generally less intense.

1) United Nations Educational, Scientific and Cultural Organization.

B.4 Water depth, tides and storm surges

Water depths in the area are shown in Figure B.2. Much of the water around the British Isles and in the North Sea and Baltic Sea is less than 200 m deep. However, there is a deep trench adjacent to the southern coast of Norway where water depths in excess of 1 000 m occur. Off the continental shelf, the Norwegian Sea is deep water, while the Barents Sea is approximately 500 m deep. The Faroe-Shetland Channel is approximately 1 000 m deep.

Tides in the region are semi-diurnal, with two high and two low tides per day. Largest tidal ranges occur on the eastern side of the Irish Sea, the east coast of the UK, in the English Channel and around the Brest Peninsula.

The highest storm surges occur in the southeastern part of the North Sea. Storm surges also affect areas with large tidal range.

B.5 Winds

The airflow in depressions is cyclonic, which is anti-clockwise in the northern hemisphere. The fronts associated with depressions occur in troughs of low pressure within the depression, and are often marked by a change of wind direction and/or speed.

Intense depressions generate sustained winds with speeds in excess of 33 m/s, which is hurricane force. The strongest winds tend to blow from between southwest and northwest, with the lightest winds being those from the northeast. Topography and unstable atmospheric conditions may modify wind speed and direction. A warmer sea overlain with cooler air produces unstable atmospheric conditions conducive to squalls and turbulent airflow.

B.6 Waves

The region includes semi-enclosed seas, i.e. the Irish Sea, the English Channel, the North Sea and the Baltic Sea, as well as areas of ocean. While strong winds may occur over the whole region, the nature of waves varies according to the water depth and fetch over which they have been generated. Where fetch is restricted, storm waves are shorter, steeper and lower than in the deep ocean. The oceanic area is subject to swell waves that have moved out of the area in which they were generated. These swell waves may occur without any wind and may have wave periods of 20 s or more. Swell may penetrate to all but the most sheltered locations.

B.7 Currents

The seas of the region contain extensive areas of shallow water, channels and headlands that experience strong tidal currents on a daily basis.

Periodically, strong currents may also occur in association with storm surge. This is water flow induced by meteorological forcing such as wind and atmospheric pressure.

Significant eddies occur in a permanent current along the coast of Norway.

In the oceans, the continental shelf edge is subject to particularly complex processes that have been the subject of extensive study. The area west of the Shetland Islands experiences strong currents at all depths, due to the topography of the sea floor and the interaction of water masses with differing characteristics. Other sections of the continental shelf edge have yet to be studied in detail. A comparison of the area to the west of Shetland with the northern North Sea, together with a discussion of the background to the complex current regime in the area, may be found in reference [97].

B.8 Other environmental factors

B.8.1 Marine growth

Marine growth, or fouling, occurs in both hard and soft forms and also as seaweed or kelp. Hard fouling consists of mussels, barnacles and tubeworms, whereas soft fouling consists of organisms such as hydroids, anemones and coral. Different types of marine growth occur at different water depths and in different parts of the region. An anti-fouling coating may delay marine growth, but significant fouling is likely within 2 years to 4 years.

Estimates of marine growth on offshore structures in UK waters are given in references [70, 98]; the information from reference [98] is summarized in Table B.1.

Table B.1 — Terminal thickness of marine growth — UK sector

Depth	Type of growth		
	Hard	Soft	Algae/Kelps
0 m to 15 m	0,2 m	0,07 m	3,0 m
15 m to 30 m	0,2 m	0,3 m	unknown
30 m to sea floor	0,01 m	0,3 m	no growth

Unless more accurate data are available, or if regular cleaning is not planned, the thickness of marine growth for areas offshore Norway may be assumed to be those shown in Table B.2 (reference [99]). The thickness of marine growth may be assumed to increase linearly over a period of two years after the structure has been placed offshore.

Table B.2 — Estimated maximum thickness of marine growth — Areas offshore Norway

Depth from mean water level m	Thickness of marine growth at latitude	
	56° N to 59° N	59° N to 72° N
Above +2	0,00 m	0,00 m
+2 to −40	0,10 m	0,06 m
Below −40	0,05 m	0,03 m

B.8.2 Sea ice and icebergs

The Barents Sea is the most northerly sea in the region, and there is a large variation of ice conditions from year to year. The ice usually reaches its maximum extension in April; when in the eastern part it reaches the Russian mainland. The minimum extension is usually in August, when an ice border may typically be seen at 80° N. The icebergs that drift in the Barents Sea originate from the glaciers at Svalbard and Franz Joseph Land and Novaya Zemlya. Reference [100] provides a good general overview of the meteorological and oceanographic conditions pertaining to the Barents Sea area.

Actions from sea ice and icebergs should be taken into account when structures are located in areas near shore, in Skagerrak, in the northern and western parts of the Norwegian Sea and in parts of the Barents Sea.

Figure B.3 shows the occurrence of first-year ice in the region, based on satellite observations, with an annual probability of exceedance of 10^{-2}. For planning of operations, the monthly extreme ice limit with annual probability of exceedance of 10^{-2} may be used; however, these data should be used with caution and allowance made for ice concentrations below some 10 % to 20 %, which cannot be detected by satellite. Monthly values for the extreme ice limit with an annual probability of exceedance of 10^{-2} may be found in reference [100]. These values may be used in evaluations during an early phase of exploration.

To calculate the actions caused by ice, values for thickness and dimensions of ice floes that are representative of the area should be selected. The mechanical properties of the ice may be assumed to be similar to those in other arctic areas.

Regions where collision between icebergs and a structure may occur with an annual probability of exceedance of 10^{-2} and 10^{-4} in the Barents Sea are shown in Figure B.4. Icebergs were observed in considerable numbers off the East Finnmark coast in 1881 and in 1929.

B.8.3 Snow and ice accretion

The incidence of snow and ice varies considerably between the southwestern and northeastern limits of northwest Europe. In the southwest, snow and ice occur infrequently, while in the northeast, snow and ice are important design parameters.

Estimates of extreme snow accumulations on offshore structures in UK waters are given in reference [98]; typical values are given in Table B.3. The pressure due to wet snow has been calculated as being in the range of 0,15 kPa to 0,24 kPa.

Table B.3 — Accumulation of ice — Offshore structures in UK sector

Cause of ice	Thickness mm	Density kg/m^3
Wet snow	10 to 30	900
Sea spray	5 to 25	850

Useful information about the occurrence of snow and ice accretion off Norway may be found in reference [99]. For areas on the Norwegian continental shelf where more accurate meteorological observations have not been made, the characteristic pressure due to snow may be assumed to be 0,5 kPa.

In the absence of a more detailed assessment, values for the thickness of ice accretion caused by sea spray and precipitation may be taken from Table B.4. The thicknesses and densities should be calculated separately for ice created from sea spray and ice created from precipitation, and both should be applied. When calculating wind, wave and current actions, increases in dimensions and changes in the shape and surface roughness of the structure as a result of ice accretion should be considered by assuming that:

— ice from sea spray covers the whole circumference of the element, and

— ice from precipitation covers all surfaces facing upwards or against the wind (for tubular structures it may be assumed that ice covers half the circumference).

An uneven distribution of ice should be considered for buoyancy-stabilized structures. The effects of ballast water, firewater, etc., which may freeze should also be taken into account.

Table B.4 — Ice accretions — Annual probability of exceedance of 10^{-2}

Height above sea level m	Ice created from sea spray			Ice created from precipitation	
	Thickness mm		Density kg/m^3	Thickness mm	Density kg/m^3
	56° N to 68° N	North of 68° N			
5 to 10	80	150	850	10	900
10 to 25	Linear reduction from 80 to 0	Linear reduction from 150 to 0	Linear reduction from 850 to 500	10	900
Above 25	0	0	—	10	900

B.8.4 Air temperature, humidity, and visibility

In winter, typical air temperatures range from −4 °C in the Barents Sea to +10 °C south of Ireland. Absolute minima are considerably lower. In summer, typical air temperatures range from 6 °C in the Barents Sea to 18 °C south of Ireland. Absolute maxima are considerably higher.

High humidity occurs when relatively warm air is cooled by the sea. This leads to reduced visibility or fog. Fog is more common in winter than in summer, with the North Sea experiencing more fog than most other areas.

Details of the meteorology of all sea areas are found in navigational publications such as *Pilots*. Such documents are published in many countries.

B.8.5 Sea water temperature and salinity

In winter, sea surface temperature ranges from about 0 °C in the Barents Sea to 12 °C south of Ireland. In summer, the corresponding range is from about 8 °C to 18 °C. Both lower temperatures in winter and higher temperatures in summer are regularly attained locally.

Mean salinity is fairly constant at 35 PSU, but lower salinity occurs around the coasts of Norway and in particular in the Baltic Sea where the surface water is much less saline.

B.9 Estimates of metocean parameters

B.9.1 Extreme metocean parameters

In the northwest European region, there is a high (but not perfect) correlation between severe wind and wave events. Storm surge events are also associated with strong winds as well as with low atmospheric pressure. Tides are forced by astronomical influences, and as such are independent of meteorology.

Actions on a structure are due to the combined action of wind, waves and current. However all structures react differently, and without detailed knowledge of a structure it is not possible to define how wind, waves and current should be characterized and combined to generate actions.

Metocean parameters for several locations in the region are provided in Tables B.5 to B.12. The wind, wave and current values are independently derived marginal parameters; no account has been taken of conditional probability. This information should not replace the detailed, site-specific parameters which should be obtained for the design or assessment of a particular structure that is to be constructed for, or operated at, a particular site.

Table B.5 — Indicative values of metocean parameters — Sites in Celtic Sea

Metocean parameter	Return period N years				
	1	5	10	50	100
10 min mean wind speed (m/s)	27	31	32	35	37
Significant wave height (m)	9,4	11,8	12,8	15,4	16,8
Spectral peak period [a] (s)	13,9	15,6	16,3	17,9	18,7
Surface current speed (m/s)	0,89	0,92	0,94	0,98	1,00
[a] Assume the spectral peak period may vary by ±10 % around these central estimates.					

Table B.6 — Indicative values of metocean parameters — Sites in southern North Sea

Metocean parameter	Return period N years				
	1	5	10	50	100
10 min mean wind speed (m/s)	27	31	32	35	36
Significant wave height (m)	6,0	7,1	7,5	8,6	9,0
Spectral peak period [a] (s)	11,3	12,3	12,6	13,6	13,9
Surface current speed (m/s)	1,17	1,23	1,25	1,31	1,33
[a] Assume the spectral peak period may vary by ±10 % around these central estimates.					

Table B.7 — Indicative values of metocean parameters — Sites in central North Sea

Metocean parameter	Return period *N* years				
	1	**5**	**10**	**50**	**100**
10 min mean wind speed (m/s)	31	33	34	36	39
Significant wave height (m)	9,8	11,2	11,8	13,1	13,6
Spectral peak period [a] (s)	13,6	14,6	15,0	15,7	16,0
Surface current speed (m/s)	0,88	0,90	1,00	1,00	1,00
[a] Assume the spectral peak period may vary by ±10 % around these central estimates.					

Table B.8 — Indicative values of metocean parameters — Sites in northern North Sea

Metocean parameter	Return period *N* years				
	1	**5**	**10**	**50**	**100**
10 min mean wind speed (m/s)	35	39	40	43	45
Significant wave height (m)	12,0	13,6	14,3	15,7	16,4
Spectral peak period [a] (s)	14,6	15,5	15,9	16,7	17,0
Surface current speed (m/s)	0,60	0,65	0,70	0,85	0,90
[a] Assume the spectral peak period may vary by ±10 % around these central estimates.					

Table B.9 — Indicative values of metocean parameters — Sites west of Shetland

Metocean parameter	Return period *N* years				
	1	**5**	**10**	**50**	**100**
10 min mean wind speed (m/s)	35	39	40	43	45
Significant wave height (m)	13,2	15,0	15,7	17,3	18,0
Spectral peak period [a] (s)	16,2	17,1	17,4	17,9	18,2
Surface current speed (m/s)	1,64	1,78	1,80	1,95	2,00
[a] Assume the spectral peak period may vary by ±10 % around these central estimates.					

Table B.10 — Indicative values of metocean parameters — Sites at the Haltenbank

Metocean parameter	Return period *N* years				
	1	**5**	**10**	**50**	**100**
10 min mean wind speed (m/s)	32	35	34	36	37
Significant wave height (m)	11,6	13,3	13,9	15,7	16,4
Spectral peak period [a] (s)	15,9	16,8	17,2	17,9	18,2
Surface current speed (m/s)	0,80	0,85	0,95	1,00	1,05
[a] Assume the spectral peak period may vary by ±10 % around these central estimates.					

Table B.11 — Indicative values of metocean parameters — Sites in Barents Sea

Metocean parameter	Return period N years				
	1	**5**	**10**	**50**	**100**
10 min mean wind speed (m/s)	33	35	36	39	40
Significant wave height (m)	10,0	11,9	12,2	14,0	14,5
Spectral peak period [a] (s)	14,7	15,9	16,0	17,1	17,4
Surface current speed (m/s)	0,90	0,95	0,97	1,00	1,05
[a] Assume the spectral peak period may vary by ±10 % around these central estimates.					

Table B.12 — Temperature ranges — Sites in North Sea, eastern North Atlantic and Norwegian Sea

Area	Air temperature	Sea surface temperature	Sea floor temperature
	°C		
Celtic Sea	−4 to +27	−4 to +22	—
Southern North Sea	−6 to +26	0 to +22	+4 to +15
Central North Sea	−6 to +24	+1 to +21	+4 to +11
Northern North Sea	−7 to +22	+2 to +19	+3 to +13
West of Shetland	−5 to +22	+3 to +19	−2 to +12
Haltenbank	−9 to +18	+5 to +17	+5 to +9
Barents Sea	−18 to +18	+2 to +14	−1 to +7

B.9.2 Long-term distributions of metocean parameters

Scatter diagrams of significant wave height versus zero-crossing period for sites in the North Sea, eastern North Atlantic and Norwegian Sea are available for UK operating areas from reference [96].

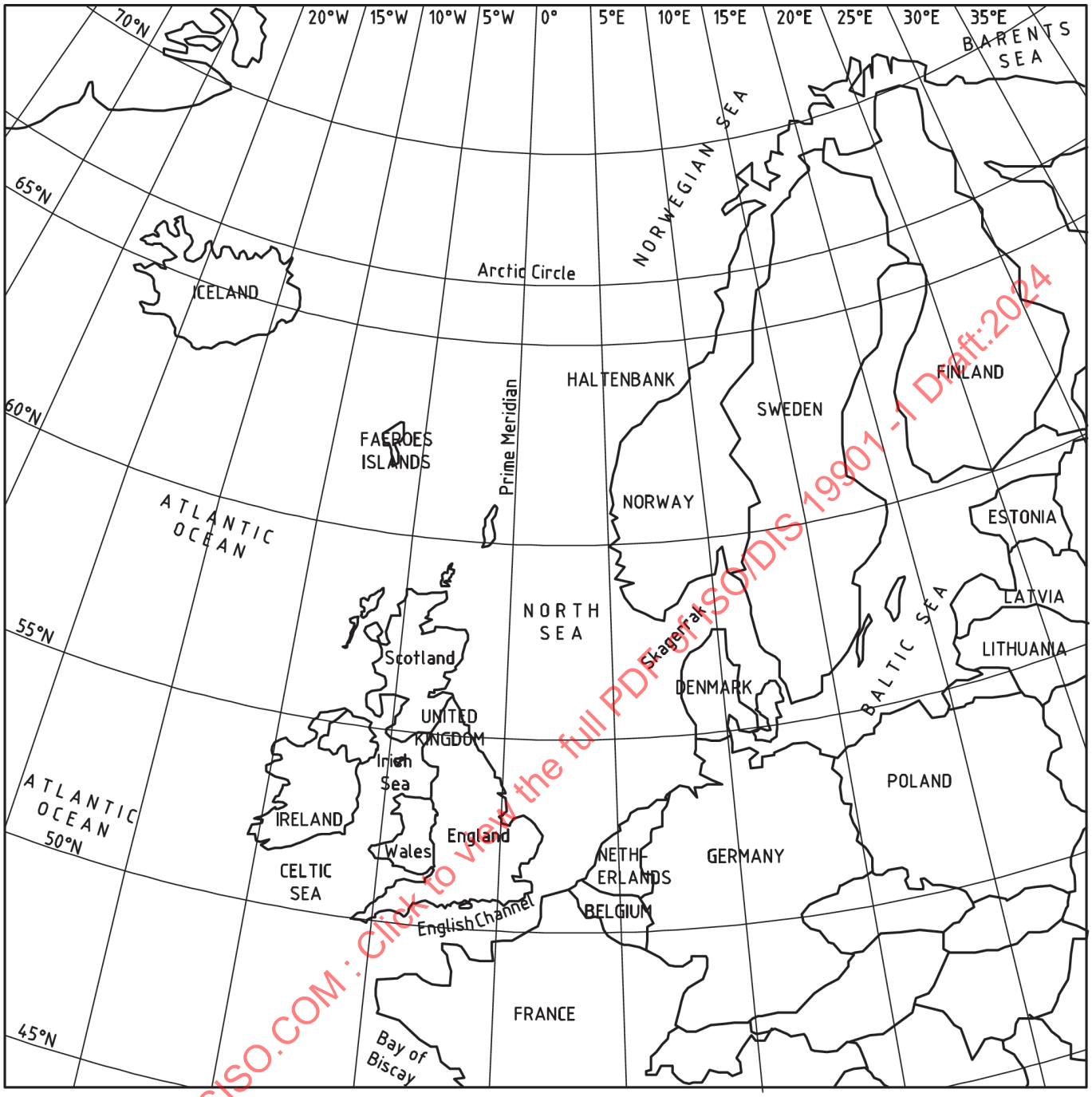

Figure B.1 — Map of northwest Europe region

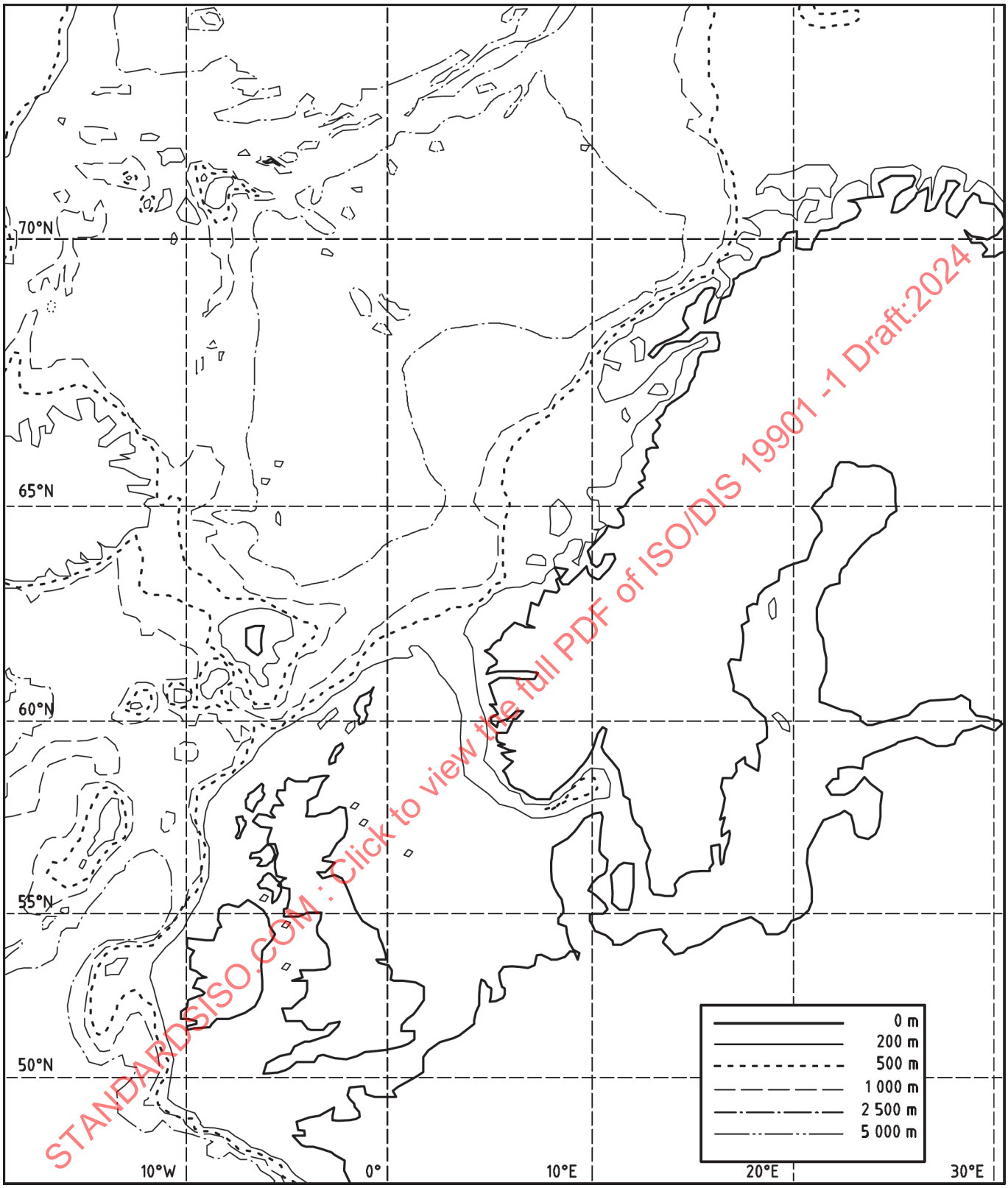

Figure B.2 — Water depths — Northwest Europe region

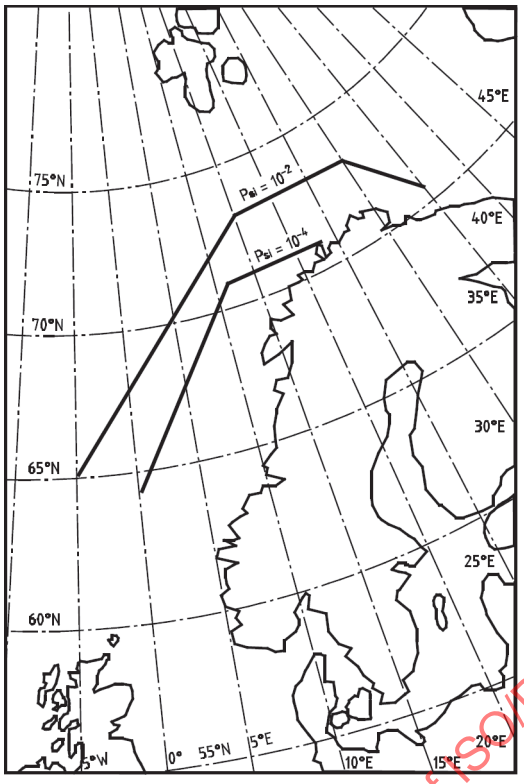

Figure B.3 — Limit of sea ice — Northwest Europe region — Annual probabilities of exceedance of 10^{-2} and 10^{-4}

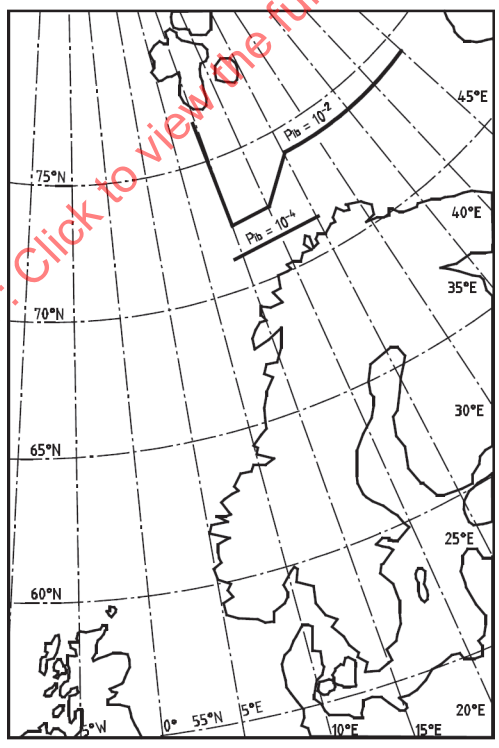

Figure B.4 — Limit for collision with icebergs — Northwest Europe region — Probabilities of exceedance of 10^{-2} and 10^{-4}

Annex C
(informative)

West Coast of Africa

C.1 Description of region

The geographical extent of this region are the waters off West Africa from the Ivory Coast to Namibia, see Figure C.1. Insufficient data are available to provide guidance for other waters off West Africa.

The continental shelf is relatively narrow throughout most of the region, with a distance from the coast to the 200 m depth contour generally less than 100 km. The continental shelf is generally narrower near the equator (e.g. offshore the Ivory Coast to Nigeria) and wider in the south (e.g. offshore Namibia), although there are fluctuations along the entire coast.

A large number of rivers discharge into the area, the most significant being the Congo and the Niger.

C.2 Data sources

Publicly available measured and modelled data are generally scarce across the region. The principal metocean hindcast dataset for the region is WANE (West Africa normals and extremes).[101] The WANE hindcast model does not represent squalls, which dominate the extreme wind conditions. Detailed squall criteria have so far been derived from a small number of proprietary measured datasets. Strategic measurement programs that provide improved measurement of squalls are likely to be a focus of future joint industry projects.

A description of the environmental conditions offshore West Africa is available in reference [102]. Much of the information in this clause has been derived from this source and from the Admiralty Pilots[103].

C.3 Overview of regional climatology

The northern-hemisphere summer is defined as July through to September, while the southern-hemisphere summer is defined as November to February.

Compared to regions such as the Gulf of Mexico and West of Shetlands, the climate offshore West Africa is often considered benign. The persistent southeasterly trade winds dominate the normal wind regime, while extreme winds are caused by squall events. Normal and extreme wave conditions are dominated by two sources of swell: those coming from the southeast and those from the southwest sectors. The long periods associated with some of the swell have specific consequences for design. A distinct sea wave component is usually also present.

The long-term current conditions are dominated by large-scale circulation patterns. On shorter time scales a wide range of oceanographic processes, including mesoscale activity, river outflow, inertial currents and internal waves, complicate the current regime.

Hot and humid conditions prevail across the region, particularly near the equator. The region encounters a wide geographical variation in rainfall, with the most intense rainfall being caused by thunderstorms and squalls near the equator. Visibility is reduced by a variety of factors across the region.

C.4 Water depth, tides and storm surges

There are three major deep ocean basins in the region, all over 5 000 m deep: the Guinea basin, the Angola basin and the Cape basin. The Guinea and Angola basins are separated by a gently sloping ridge along which exist numerous seamounts and, further inshore, an island chain. The much steeper Walvis Ridge separates

the Angola and Cape basins. Between these ridges the continental slope (from the 200 m to 5 000 m depth contours) varies in width from approximately 100 km offshore Ghana to over 600 km offshore Angola.

Equatorial and southwest Africa experience a semi-diurnal tidal regime. Tidal ranges are relatively small at the coast, with spring tidal ranges around 2 m and neap tidal ranges less than 1 m. The tidal range decreases rapidly further away from the shore, with a spring tidal range usually less than 1 m in deep water. Storm surges are small throughout the region.

C.5 Winds

The normal wind regime is dominated by persistent southerly trade winds, driven by large-scale atmospheric pressure systems. The trade winds are strongest in southern parts of the region where they typically range from 5,5 m/s to 7,5 m/s, and weakest in the north where they vary between 2,5 m/s to 5,0 m/s. The strongest winds generally occur during the northern-hemisphere summer and the weakest winds generally occur in the northern-hemisphere winter. These seasonal variations follow fluctuations in the latitude of the northernmost boundary of the "south-easterly trade wind regime", from about 15° N in the northern-hemisphere summer to about 7° N in the northern-hemisphere winter.

In the southern part of the region, the trade winds blow predominately from the southeast, but the direction slowly shifts until it reaches southwesterly off Nigeria.

Apart from the seasonal changes, the strength of the trade winds is fairly constant. However, there may be a significant diurnal variation in wind speed in near-shore locations influenced by sea breezes. This diurnal variation is reduced further from the shore.

Fully developed tropical or extra-tropical revolving storms (e.g. tropical cyclones) are very rare or non-existent in the region, and extreme winds are caused by squall events. Squalls are associated with the leading edge of multi-cell thunderstorms. Thunderstorms and squalls are most frequent in equatorial West Africa, and typically stronger offshore Nigeria than offshore Angola, with around 15 to 30 significant events per year. Depending on location, there are clearly defined squall seasons that may be explained by the seasonal migration of the inter-tropical convergence zone (ITCZ). Squall activity is observed when the ITCZ and associated cumulonimbus formations are in the region. There is one clearly defined squall season in Angola during the northern-hemisphere winter. There are two peak squall seasons offshore Nigeria due to two passages of the ITCZ: on the way north in northern-hemisphere spring, then again on the way south in the northern-hemisphere autumn. Squalls occur for a much larger part of the year in Nigeria than in the other regions, with only a brief minimum around August.

The rapidly varying wind speed and direction associated with squalls, and large variations between the characteristics of different squalls, may lead to considerable variations in vessel or offshore structure response. Further measurements are required to better define squall characteristics, including spatial variations in the wind field, rates of increase and decay, variations in wind direction, and improved extreme value estimates. These are likely to be considered as part of a future joint industry project.

Thunderstorms and squalls are responsible for the strongest winds, but are thought to generate only weak currents and low wave heights due to the limited fetch and duration.

C.6 Waves

The wave climate offshore West Africa is dominated by swell from two distinct sources:

— high-latitude extra-tropical storms in the South Atlantic generate swell from the southwest; and

— episodic increases in the trade winds offshore South Africa generate swell from the southeast.

Wind seas are driven by the local winds.

The swell is greatest in southern parts of the region, where extreme significant wave heights may be about 9 m.[104] Wave heights decrease further north due to dissipation, where extreme values of about 3 m to 4 m are more typical. It is in these more northern regions that locally-generated wind seas may become just as important as the swell component, at least for structural designs that are governed by drag.

Swell waves from distant storms may be associated with long peak periods, sometimes in excess of 20 s. Such long-period waves may be critical for the operability of some vessels. Longer period swells are generally encountered in northern parts of the region, due to the longer propagation distance from the source.

The wave spectrum is often characterized by at least two peaks, a swell component and a locally-generated wind seas component, the latter having significant wave heights of about 1 m.[105] Owing to the presence of both sea and swell, it is not appropriate to represent the sea-state offshore West Africa using a spectral model with just one peak. Use of a bimodal Ochi-Hubble spectra is recommended; however, the latest results from research into appropriate spectral models of the wave climate offshore West Africa under the joint-industry West Africa squall project (WASP) should be considered.

As swell approaches the coast in some parts of the region, particularly along the coast of South-West Africa, it may be transformed into a phenomenon called rollers. These are large steep waves that are likely to affect both floating structures in near-shore regions and coastal infrastructure.

C.7 Currents

The long-term current conditions offshore West Africa are controlled by the large-scale anti-clockwise surface circulations of the South Atlantic Ocean. These currents undergo seasonal variations in intensity and extent, but are generally less than 0,5 m/s. Although they usually only impact the deep ocean, the key characteristics are described here, mostly derived from an excellent review conducted as part of the WAX project[106].

The Benguela Current flows northwards along the coast of Namibia and separates from the coast to form part of the South Equatorial Current that turns westwards near the equator to flow across the Atlantic Ocean. The Benguela Current only affects the southern-most deep water parts off Namibia.

The other energetic (peaks of the order of 0,50 m/s) current system in the region, the Guinea Current, flows eastward along the Ivory Coast to Nigeria in the upper part of the water column, below which the Guinea Undercurrent flows towards the west.

Other current systems in the region are weak (0,1 m/s) but may be persistent. The Equatorial Undercurrent flows eastwards along the equator underneath the South Equatorial Current, and splits into two branches when it reaches the West Afrimay coast. The northern branch enters the Gulf of Guinea and the southern branch feeds the southward-flowing Gabon-Congo Undercurrent, and then surfaces to form part of the southward-flowing Angola Current. Throughout most of the region, the current direction often reverses, through a vertical section, leading to complex current profiles with strong shear.

The large-scale circulation patterns described above are characterized by significant meanders, and numerous eddies are formed either side of the main flow. This mesoscale activity is found throughout the region and may be associated with stronger-than-average currents flowing in directions different to that of the larger scale flow.

Strong currents have been encountered near the Congo River, and these may extend perhaps 50 km north of the mouth of the river. These strong currents are confined to the uppermost few metres of the water column, but may be responsible for extreme current conditions.

Perhaps of wider impact is the effect of the major rivers on the near-surface salinity. Significantly fresher water may be observed several hundred kilometres from the mouths of the Congo and Niger. The stratification means that strong (1 m/s) inertial currents may be generated in the upper water column (approximately the top 30 m) by local winds.

Tidal currents are generally less than 0,1 m/s throughout the region, although local intensification exists in some areas due to seabed features. In such regions the tidal currents are likely to generate internal waves at the tidal period, called internal tides. These manifest themselves as currents that vary in time at the semi-diurnal tidal period, but flow in opposite directions in different depths of the water column. Shorter-period internal waves (solitons) have been reported in some parts of West Africa. Although the currents associated with these internal waves are unlikely to be much higher than 0,5 m/s in the region, they cause rapid changes in current speed and direction over periods as short as half an hour, so may be significant for design and operation of marine equipment.

Strong inertial currents have been observed in some deep-water areas offshore West Africa. The direction of these currents rotates through 360° once every inertial period (the natural period of large-scale oscillations in the ocean). The inertial period is infinite at the equator and decreases with latitude. Inertial currents are particularly notable offshore southern Namibia where the inertial period is close to 24 h, allowing a near-resonant response to diurnal variations in wind forcing. The vertical structure of inertial currents may be complex, with one or more peaks in the current speed that move vertically through the water column with time.

The description given in this subclause only provides a very general overview of current conditions likely to be experienced offshore West Africa. The processes that drive ocean currents are considerably more numerous and complex than those that drive wind and waves, and site-specific measurements may be required to derive criteria for engineering design, particularly in deeper waters.

C.8 Other environmental factors

C.8.1 Marine growth

Warm water conditions coupled with an abundance of nutrients are likely to lead to extensive marine growth. The rate of growth and the particular marine species are likely to vary considerably over the region, but a typical thickness of about 0,1 m may be expected in the upper 50 m of the water column, and up to about 0,3 m above mean sea level in the splash zone.

C.8.2 Tsunamis

West Africa is not considered one of the high-risk areas for tsunami activity, although future events may never be completely discounted. An online tsunami database[108] contains details of only two distinct tsunami events anywhere in the region, both of which affected the coastal regions of Ghana. The first event in 1911 was associated with a wave of height 1,5 m, and the second event in 1939 with a height of 0,6 m.

C.8.3 Sea ice and icebergs

Sea ice does not develop within the region, and iceberg drift is not a design consideration. Icebergs have been sighted as far north as 35° S, and are possible around the Cape of Good Hope[103].

C.8.4 Snow and ice accretion

As with sea ice, snowfall and ice accumulation on structures are not design considerations.

C.8.5 Air temperature, humidity, pressure and visibility

High air temperatures are encountered throughout the region, particularly close to the equator. In equatorial West Africa, daily temperatures range between 23 °C and 33 °C in the northern-hemisphere summer, and 20 °C to 25 °C in the northern-hemisphere winter. In southwest Africa, daily temperatures range between 26 °C and 31 °C in the southern-hemisphere summer and 20 °C to 27 °C in the southern-hemisphere winter. These figures were derived from a climate summary[107] containing data from onshore meteorological stations and some offshore measurements.

The amount of rainfall varies considerably over the region, with very high values near the equator (annual total up to about 4 000 mm) and low rates in the south (annual total as low as 40 mm). The most intense rainfall is usually associated with thunderstorms and squalls.

The relative humidity is highest in equatorial regions, where values often exceed 90 %, and generally decreases towards the south. Warm air temperatures combined with high humidity represent a potential hazard to personnel. The humidity varies throughout the day, with a maximum generally occurring in the morning and a minimum during the afternoon. Seasonal variations also exist in many parts of the region, with a maximum in the southern-hemisphere summer and a minimum in the southern-hemisphere winter. Large fluctuations in humidity may be caused locally by changes in the wind direction, with much lower values associated with dry winds blowing from the interior.

A high pressure system is usually located in the southeast Atlantic close to 30 °S 10 °W, driving the southeasterly trade winds that prevail over the region. The position of this high leads to generally higher atmospheric pressures in the south and lower pressures in equatorial regions. Seasonal variations in mean atmospheric pressure are typically between 101,0 kPa (1 010 mbar) and 101,4 kPa (1 014 mbar) near the equator and between 101,4 kPa (1 014 mbar) and 102,2 kPa (1 022 mbar) in the south. The atmospheric pressure is higher over the entire region during the southern-hemisphere summer than during the southern-hemisphere winter. Atmospheric pressure undergoes significant diurnal variations in many parts of the region.

Air temperatures, humidity and pressure all undergo rapid changes during the passage of thunderstorms and squalls.

Visibility is reduced by fog along many parts of the coast, particularly in areas to the south influenced by the cold water of the Benguela Current. Low visibility is also caused by dust (windborne sand) or heavy rain, particularly near the equator, offshore Namibia and most notably in the Bight of Biafra.

C.8.6 Sea water temperature and salinity

Sea-surface temperatures are warmest near the equator, where they typically range between 24 °C and 28 °C over the year, and cooler in the south where seasonal variations between about 13 °C and 16 °C occur. Temperatures across the region are warmer during the southern-hemisphere summer and cooler during the southern-hemisphere winter.

Cold water transported into the region by the Benguela Current is a major influence on sea-surface temperature in southern regions. Localized decreases in surface temperatures occur along several areas of the continental slope throughout West Africa, due to upwelling of cooler deep waters. The water column is generally stratified throughout the year, with temperatures less than 15 °C at 200 m depth.

Sea-surface salinities in the open ocean are generally between 35 PSU and 3 PSU, but there are very significant reductions in salinity in areas influenced by river discharge, where salinity may be as low as 28 PSU. The Congo River provides one of the largest inputs of fresh water into an ocean anywhere in the world.

C.9 Estimates of metocean parameters

C.9.1 Extreme metocean parameters

Indicative extreme values of wind, wave and current parameters are provided in Tables C.1 to C.4 for various return periods and for four locations offshore West Africa. The wind, wave and current values are independently derived marginal parameters; no account has been taken of conditional probability. Table C.5 gives extreme values for other metocean parameters. As for all indicative values provided within this annex, these figures are provided to assist preliminary engineering concept selection; they are not suitable for design of offshore structures.

Extreme wave conditions offshore Nigeria are caused by swell from distant storms, and Nigerian wave spectra tend to be more narrow-banded compared to most extreme conditions in other parts of the world. The Rayleigh distribution assumes narrow-band conditions, whereas the Forristall distribution is a modified Rayleigh distribution which takes account of the wider band conditions within storms. The Rayleigh distribution leads to a higher ratio of H_{max}/H_s, typically by about 10 %.[28] Calculations of the short-term statistics from offshore Nigeria hindcast spectra[28] show that their distribution is close to halfway between Rayleigh and Forristall, which results in individual wave height around 5 % lower than would be predicted by the Rayleigh distribution. In addition, account is made of short-term variability, i.e. the possibility that the maximum individual wave could occur in a sea-state other than the maximum sea-state. The net result of the computations is that the ratio H_{max}/H_s tends to a value of 2,0 rather than 1,9.

Structures may be sensitive to different combinations of sea and swell heights as well as spectral peak periods and spectral widths. A representative combination of wave/swell parameters should be defined for the location of interest, and the largest action effects for the component being designed should be determined. A combination of 100 % wind waves with no swell and, separately, 100 % swell with no wind waves is a useful combination to test on structures. For swell, the longer T_p range should be used, and for wind waves the shorter T_p range.

Table C.1 — Indicative wind, wave and current parameters — Shallow water sites off Nigeria

Metocean parameter		Return period *N* years				
		1	**5**	**10**	**50**	**100**
Nominal water depth		30 m				
Wind speed at 10 m above MSL (m/s)						
	10 min mean [b]	19	23	25	29	31
	1 min mean [b]	23	27	29	35	38
	3 s gust [b]	26	31	34	39	42
Wave height (m)						
	Maximum	4,8	5,5	5,8	6,5	6,8
	Significant	2,3	2,7	2,8	3,2	3,3
Wave direction (from)		SSW				
Spectral peak period (s)						
	For swell	15 to 17	15 to 17	15 to 17	15 to 17	15 to 17
	For wind seas	7 to 8	7 to 8	7 to 8	7 to 8	7 to 8
Current speed (m/s)						
	Surface [a]	0,9	1,0	1,0	1,1	1,1
	Mid-depth	0,8	0,9	0,9	1,0	1,0
	1 m above sea floor	0,5	0,6	0,6	0,7	0,7

[a] These extreme values exclude any effect from river plumes.

[b] These extremes are associated with the passage of squall

Table C.2 — Indicative wind, wave and current parameters — Deep water sites off Nigeria

Metocean parameter		Return period *N* years				
		1	**5**	**10**	**50**	**100**
Nominal water depth		1 000 m				
Wind speed at 10 m above MSL (m/s)						
	10 min mean [b]	19	23	25	29	31
	1 min mean [b]	23	27	29	35	38
	3 s gust [b]	26	31	34	39	42
Wave height (m)						
	Maximum	5,7	6,4	6,8	7,5	7,7
	Significant	2,7	3,2	3,4	3,7	3,8
Wave direction (from)		SSW				
Spectral peak period (s)						
	For swell	14 to 16	15 to 17	16 to 18	17 to 19	17 to 19
	For wind seas	7 to 8	7 to 8	7 to 8	7 to 8	7 to 8
Current speed (m/s)						
	Surface [a]	1,1	1,2	1,2	1,3	1,4
	Mid-depth	0,3	0,3	0,3	0,3	0,4
	1 m above sea floor	0,2	0,2	0,2	0,2	0,2

[a] These extreme values exclude any effect from river plumes.

[b] These extremes are associated with the passage of squall

Table C.3 — Indicative wind, wave and current parameters — Sites off northern Angola

Metocean parameter		Return period *N* years				
		1	**5**	**10**	**50**	**100**
Nominal water depth		1 400 m				
Wind speed at 10 m above MSL (m/s)						
	10 min mean	16	20	21	25	26
	3 s gust	19	23	25	29	31
Wave height (m)						
	Maximum	7,9	8,6	8,8	9,5	9,9
	Significant	4,0	4,3	4,4	4,7	4,9
Wave direction (from)		SSW				
Spectral peak period (s)						
	For swell	13 to 17	13 to 17	13 to 17	13 to 17	13 to 17
	For wind-seas	7 to 8	7 to 8	7 to 8	7 to 8	7 to 8
Current speed (m/s)						
	Surface [a]	0,9	1,0	1,0	1,2	1,2
	Mid-depth	0,2	0,3	0,3	0,3	0,3
	1 m above sea floor	0,2	0,3	0,3	0,3	0,3

[a] These extreme values exclude any effect from river plumes.

Table C.4 — Indicative wind, wave and current parameters — Sites off southern Namibia

Metocean parameter		Return period *N* years				
		1	**5**	**10**	**50**	**100**
Nominal water depth		200 m				
Wind speed at 10 m above MSL (m/s)						
	10 min mean	20	20	26	29	31
	3 s gust	25	27	32	36	39
Wave height (m)						
	Maximum	12,7	13,7	16,0	19,0	20,0
	Significant	6,8	7,4	8,7	10,0	10,6
Wave direction (from)		SSE/SW				
Spectral peak period (s)						
	For swell	11 to 14	12 to 15	13 to 16	14 to 17	14 to 17
	For wind-seas	7 to 8	7 to 8	7 to 8	7 to 8	7 to 8
Current speed (m/s)						
	Surface [a]	1,1	1,2	1,2	1,3	1,4
	Mid-depth [b]	0,3	0,3	0,3	0,3	0,5
	1 m above sea floor	0,3	0,3	0,3	0,4	0,5

[a] These extreme values exclude any effect from river plumes.

[b] Mid-depth currents off southern Namibia are below the seasonal thermocline where currents may be stronger.

Table C.5 — Indicative extreme values for other metocean parameters

Metocean parameter		Nigeria		Northern Angola	Southern Namibia
		Shallow water	Deep water		
Mean spring tidal range (m)		1,9	1,5	1,4	2,0
Sea water temperature (°C)					
	Minimum near surface	22	25	17	9
	Maximum near surface	32	31	28	28
	Minimum near bottom	20	4	4	4
	Maximum near bottom	30	4	4	—
Air temperature (°C)					
	Minimum	18	20	17	8
	Maximum	33	33	35	26

C.9.2 Long-term distributions of metocean parameters

Recorded wave spectra offshore West Africa are complex and present simultaneous long-period swell components, with various peak periods and directions, generated by storms in different parts of the Atlantic Ocean. *In situ* wave measurements also indicate that mixed swell and wind sea conditions are quasi-permanent. As a minimum for design purposes, one swell component should be superimposed on a wind-sea component. A refinement considers two swell partitions superimposed on a wind sea.

Wave-scatter diagrams for two areas offshore West Africa are provided in Tables C.6 and C.7, showing combinations of total significant wave height and associated spectral peak wave periods of combined wind seas and swell conditions. The information in these tables was generated from the WANE hindcast model. [101,104] It should be noted that a significant proportion of the wave energy in any given sea-state offshore West Africa consists of long-period swell. These tables are not always conservative for certain applications to dynamically responding structures, therefore designers should also test against the appropriate dual-peaked cases such as those given in Table C.8.

Table C.6 — Percentage occurrence of total significant wave height *vs.* spectral peak period — Offshore Nigeria location

Significant wave height m	Peak period s													
	0 to 1,99	2 to 3,99	4 to 5,99	6 to 7,99	8 to 9,99	10 to 11,99	12 to 13,99	14 to 15,99	16 to 17,99	18 to 19,99	20 to 21,99	22 to 23,99	> 24	Total
0,00 to 0,49				0,02		0,03	0,02	0,03						0,10
0,50 to 0,99			0,50	5,37	2,55	3,48	3,14	2,46	0,64	0,13	0,05	0,02		18,34
1,00 to 1,49			0,34	11,01	16,65	9,40	11,01	8,76	2,74	0,88	0,24	0,04		61,07
1,50 to 1,99				0,08	5,85	4,67	2,76	2,95	1,19	0,33	0,09	0,03		17,95
2,00 to 2,49					0,17	0,79	0,58	0,41	0,19	0,07	0,03			2,24
2,50 to 2,99						0,06	0,08	0,04	0,05	0,02				0,25
> 3,00							0,02	0,03						0,05
Total			0,84	16,48	25,22	18,43	17,61	14,68	4,81	1,43	0,41	0,09	0	100,00

Table C.7 — Percentage occurrence of total significant wave height *vs.* spectral peak period — Offshore Angola location

Significant wave height m	Peak period s													
	0 to 1,99	2 to 3,99	4 to 5,99	6 to 7,99	8 to 9,99	10 to 11,99	12 to 13,99	14 to 15,99	16 to 17,99	18 to 19,99	20 to 21,99	22 to 23,99	> 24	Total
0,00 to 0,49				0,01	0,03	0,04	0,06	0,06						0,20
0,50 to 0,99		0,01	1,00	3,98	1,82	5,17	5,52	3,70	1,17	0,34	0,13	0,01	0,00	22,85
1,00 to 1,49			0,60	6,28	10,48	11,49	11,38	9,19	2,87	0,83	0,19	0,06	0,00	53,37
1,50 to 1,99			0,01	0,06	2,86	5,78	4,76	3,52	1,51	0,54	0,12	0,01		19,17
2,00 to 2,49					0,07	0,94	1,33	1,05	0,34	0,10	0,01			3,84
2,50 to 2,99					0,00	0,04	0,14	0,23	0,10	0,03				0,54
3,00 to 3,49								0,02	0,01					0,03
> 3,50								0,00						0,00
Total	0,00	0,01	1,61	10,33	15,26	23,46	23,19	17,77	6,00	1,84	0,45	0,08	0,00	100,00

Wind seas and swell conditions are considered as independent phenomena. In principle, any combination of wind seas and swell H_s—T_p classes is possible, and all permutations, with their joint frequency of occurrence, should be considered for engineering purposes.

Sea-states offshore West Africa may be represented by the dual-peaked Ochi-Hubble spectra. Table C.8 provides an example of a scatter diagram for offshore Angola.

For the purposes of defining bimodal spectra representing combined swell and wind sea conditions, the total significant wave height H_s and the associated spectral peak period T_p should be divided into a swell part and a wind sea part. This may be achieved by inspection of a frequency table of the joint occurrences of H_s and T_p. The low wave heights associated with the wind sea component permit selection of relatively few significant wave height classes for wind seas. The frequency of occurrence of swell H_s with associated T_p should be calculated, conditional on the value of the wind sea H_s with its associated T_p, to determine the frequency of occurrence of each combined wind sea/swell bimodal sea-state. The resolution of the swell H_s class will determine the number of combinations of wind sea and swell H_s and T_p available for engineering purposes.

The example in Table C.8 provides information on the joint frequency of occurrence of swell and wind sea conditions, giving the significant wave height, the peak period, the associated parameter γ and the direction of swell (θ_1) and wind sea (θ_2) for a site offshore Angola.

For the example data in Table C.8, the values from any row may be used to construct a bimodal Ochi-Hubble spectrum. Sea-states should be assumed to be representative of a duration of 3 h. The values of percentage occurrence in Table C.8 may be used to define the fatigue wave climate.

Table C.8 — Example of wind sea-states used for combined wind sea/swell bimodal sea-states — Offshore Angola

No.	% occurrence	H_{s1} m	T_{p1} s	H_{s2} m	T_{p2} s	$\gamma 1$	$\gamma 2$	θ_1 (towards)	θ_2 (towards)
291	15,3	0,91	12	0,76	7,7	7,0	2,1	27	21
231	12,1	0,61	11	0,70	7,2	7,3	1,6	25	23
208	10,9	0,61	12	0,70	7,7	7,3	1,8	29	19
154	8,1	0,91	11	0,76	7,2	7,1	1,8	22	23
117	6,1	1,22	12	0,82	8,1	7,4	2,9	27	22
103	5,4	0,61	10	0,73	6,3	5,4	1,4	21	27
94	4,9	0,91	13	0,76	8,4	7,5	2,3	30	18
90	4,7	1,22	13	0,85	8,2	7,2	2,2	32	21

Table C.8 *(continued)*

No.	% occurrence	H_{s1} m	T_{p1} s	H_{s2} m	T_{p2} s	$\gamma 1$	$\gamma 2$	θ_1 (towards)	θ_2 (towards)
72	3,8	0,61	13	0,79	7,9	7,1	2,2	33	19
65	3,4	0,91	14	0,88	8,7	7,5	2,4	33	17
63	3,3	0,61	14	0,79	8,9	7,7	2,3	35	18
52	2,7	1,52	13	0,91	8,7	8,1	2,4	29	22
47	2,5	1,22	14	0,98	9,4	8,3	2,7	31	21
37	1,9	1,52	14	0,98	9,4	7,3	3,1	32	19
36	1,9	1,22	11	0,88	7,7	7,5	2,0	21	22
35	1,8	0,91	10	0,76	5,9	4,0	1,4	21	31
32	1,7	0,61	15	0,91	9,6	8,4	2,4	32	22
29	1,5	0,91	15	0,88	9,4	8,7	2,9	34	17
28	1,5	0,30	12	0,61	8,6	8,7	3,3	32	15
27	1,4	1,52	12	0,82	8,6	7,5	5,0	27	21
26	1,4	0,30	11	0,76	7,0	8,1	1,9	28	18
24	1,3	1,52	15	1,01	9,8	8,1	2,5	31	20
23	1,2	1,83	14	0,88	8,7	7,0	1,7	32	18
20	1,1	0,61	17	1,04	10,2	9,0	2,8	31	23

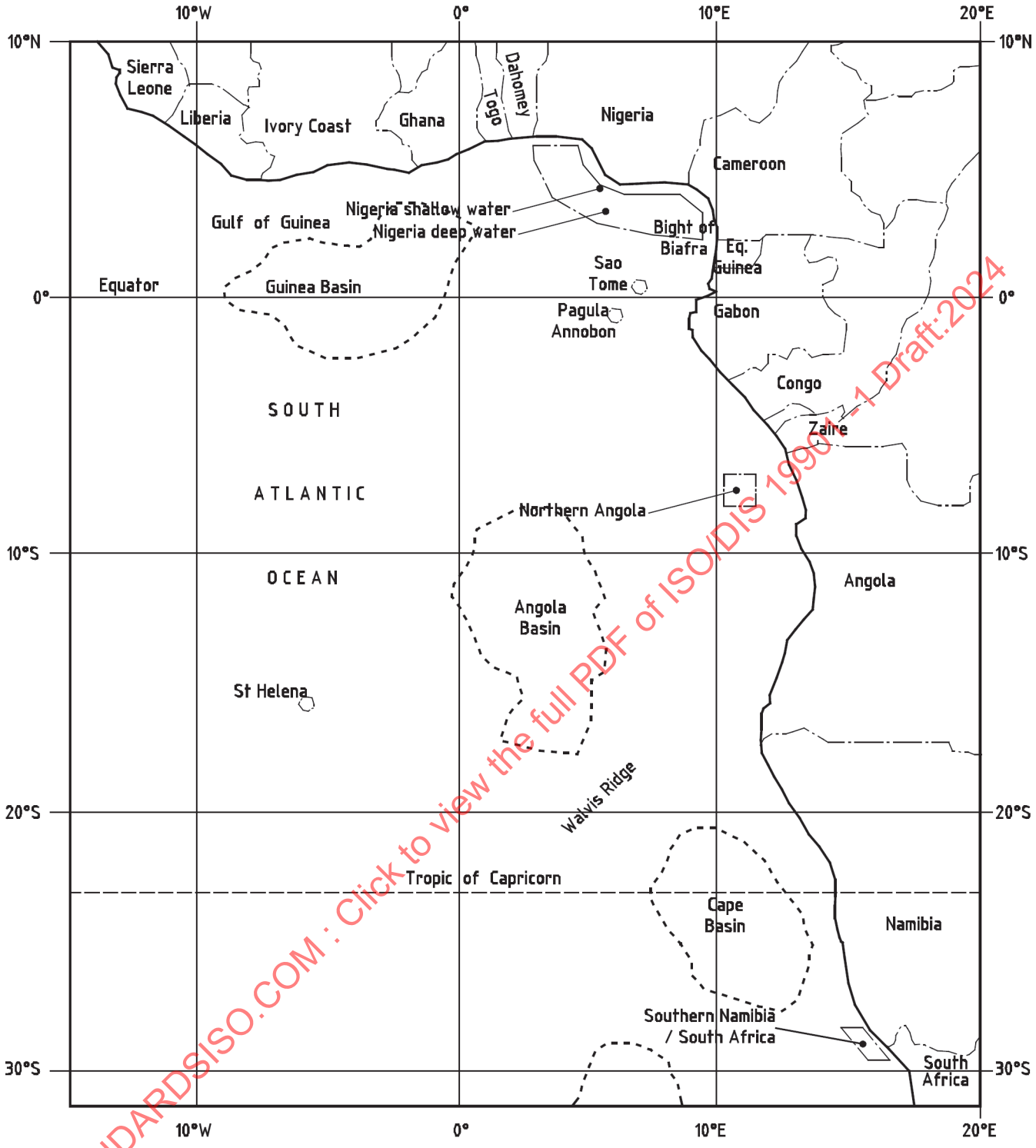

Figure C.1 — Map of west coast of Africa region — Locations of example metocean parameters

Annex D
(informative)

Offshore Canada

D.1 Description of region

D.1.1 General

The geographical scope of this annex includes current hydrocarbon-producing regions of offshore Canada: the Sable Island region offshore Nova Scotia and the Grand Banks of Newfoundland. Some areas with potential for future hydrocarbon development have also been included, such as East Coast Deepwater, the Beaufort Sea, the Gulf of St. Lawrence, offshore Labrador and Davis Strait/Baffin Bay.

This annex provides an overview of metocean design and operating conditions for areas offshore Canada where hydrocarbon production exists, as well as for certain areas where significant industry interest exists. A range of values based on existing datasets is provided to give an indication of the degree of variability that may be expected for a particular region. The numbers provided are indicative only and should be used in conjunction with site-specific or project-specific studies to develop environmental criteria to be used for design.

The current hydrocarbon production operations on the east coast of Canada are located offshore of Newfoundland and Labrador on the Grand Banks, and offshore Nova Scotia on the Scotian Shelf near Sable Island, as shown in Figures D.1 and D.2.

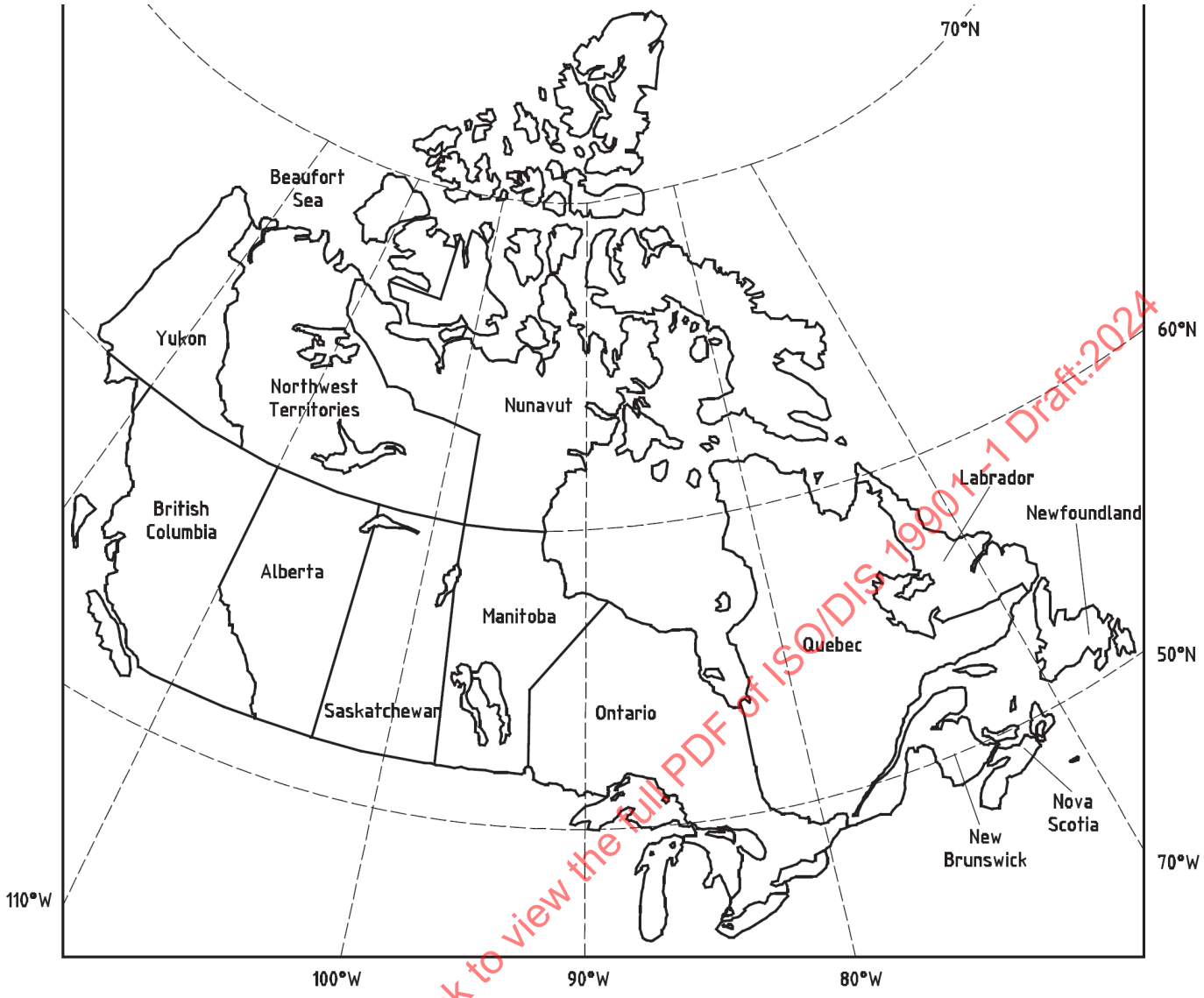

Figure D.1 — Map of Canada

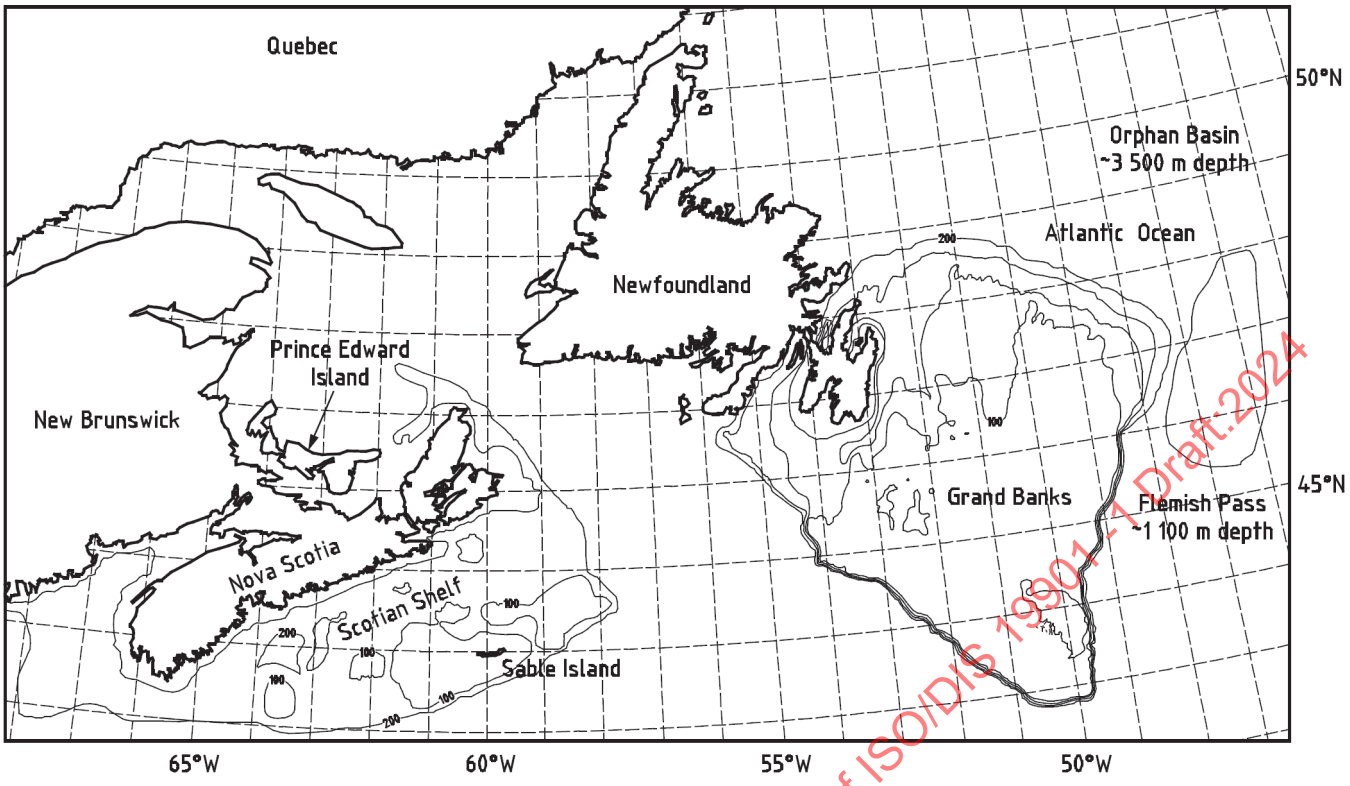

Figure D.2 — East Coast of Canada Current Regions of Oil and Gas Production Operations — Near Sable Island offshore Nova Scotia and on the Grand Banks offshore Newfoundland and Labrador

D.1.2 Grand Banks

The Grand Banks are one of the world's largest and richest resource areas, renowned for both its valuable fish stocks and petroleum reserves. Situated off the southeast coast of the island of Newfoundland, the Grand Banks are a series of raised submarine plateaus with a water depth ranging between approximately 40 m and 200 m. Grand Bank is the largest of several banks comprising the Grand Banks of Newfoundland, and lies to the east and southeast of the Avalon Peninsula. Grand Bank has a relatively flat surface that is generally less than 120 m deep. It is separated from the island of Newfoundland by the Avalon Channel which has water depths ranging up to 200 m deep.

D.1.3 Scotian Shelf

The Scotian Shelf which comprises an area of approximately 120 000 km^2, is over 700 km long and ranges in width from 100 km to 250 km. The Scotian shelf physiography consists of three physiographic zones:

a) Inner Shelf

The Inner Shelf borders mainland Nova Scotia, extending roughly 25 km offshore, with water depths less than 100 m. It is characterized by rough topography.

b) Central Zone

This zone is about 80 km to 100 km in width and lies between the Inner Shelf and Outer Shelf. It is characterized by an inner trough running parallel to the coast, and isolated banks with intervening basins and valleys. Water depth varies from less than 100 m over the banks to about 180 m in the inner trough, with some basins up to 300 m in depth.

c) Outer Shelf

This zone is bounded by the eastern shelf break and is about 50 km to 70 km wide. This shelf is characterized by broad flat banks with little relief. Sable Island Bank is the largest and most extensive

bank on the Scotian Shelf, with water depths less than 100 m. Sable Island is an arc-shaped sandbar more than 40 km long and about 1,3 km wide.

D.1.4 Deepwater

The Flemish Pass and Orphan Basin are two hydrocarbon fields located in deepwater. These fields are located beyond the Grand Banks, approximately 450 km offshore Newfoundland, as shown in Figure D.2. Water depth varies from 1 100 m to 3 500 m in the Flemish Pass and Orphan Basin, respectively.

D.1.5 Gulf of St. Lawrence

The Gulf of St. Lawrence is located at the mouth of the St. Lawrence River; it is the body of water enveloped by Quebec and the Atlantic Provinces, shown in Figure D.2. The Gulf contains channels with water depths up to 300 m.

D.1.6 Beaufort Sea

The Beaufort Sea is located along the Arctic Circle in northwestern Canada, as shown in Figure D.1. There are three main bathymetric features in the southeastern Beaufort Sea:

a) the continental shelf, which slopes gently from the coastline to water depths of approximately 100 m;

b) the continental slope, angling steeply from the edge of this shelf to depths of 1 000 m; and

c) the trench-like Mackenzie (or Herschel) Canyon, which transects a portion of the shelf[115].

D.1.7 Labrador Shelf

The Labrador shelf lies off eastern Canada, off the east coast of Newfoundland and Labrador, between about 51 N and 60 N. Along the Labrador shelf water depths are generally 300 m and less as you approach the shore, but fall off quickly to more than 3 000 m in the Labrador Sea.

D.1.8 Davis Strait/Baffin Bay

The Davis Strait and Baffin Bay are located in northeastern Canada, between the east coast of Baffin Island and the west coast of Greenland. The International Hydrographic Organization defines the boundary between Davis Strait and Baffin Bay as the 70 N line of latitude. Water depths are generally less than 500 m on the coastal shelf; in the centre of the Baffin Basin depths exceed 2 000 m.

D.2 Data sources

Data regarding metocean conditions in the region are available from a variety of sources. These include regulatory bodies, such as the Canada-Newfoundland Offshore Petroleum Board and the Canada-Nova Scotia Offshore Petroleum Board, Operators, federal government agencies and published papers.

Another source of metocean related information is the MSC50 North Atlantic Wind and Wave hindcast model.[125, 126] This model was developed for the Meteorological Service of Canada and is a 65-year (1954 to 2018) wind and wave hindcast model of the North Atlantic. It allows the estimation of extreme wind and wave parameters for the Scotian shelf and the Grand Banks of Newfoundland as well as other locations in the North Atlantic. A separate hindcast has been carried out for the Canadian Beaufort Sea, which has now been updated to cover the period 1970-2018[127].

For the offshore Newfoundland and Labrador region, environmental impact statements as well as project-specific design environmental criteria were available from the Operators as well as other related information. With respect to the offshore Nova Scotia region, environmental impact statements and development plan applications were utilized such as Sable Offshore Energy Project (SOEP) (1996),[121] Deep Panuke (2002) [114] and Cohasset/Panuke (1990)[113].

A description of observed variability in ice patterns over a 30-year period (1981 to 2010) has been published in map format by the Canadian Ice Service and used here to describe normal conditions [111].

A comprehensive listing of additional related environmental and meteorological information sources is presented in D.13.

D.3 Overview of regional climatology

D.3.1 Atlantic Canada

D.3.1.1 General

Offshore Atlantic Canada has very complex and unpredictable weather. The variable climate of the Canadian east coast is influenced by the warm Gulf Stream and the cold water of the Labrador Current (as discussed further in Section D.7). It is also influenced by seasonal changes in air masses, exchanges in energy between the atmosphere and the ocean, seasonal variations in sun radiation, the rugged coastal topography as well as the variability of the Icelandic Low and the Bermuda High, which locally control the Jet Stream and thus storm tracks. They are described further below.

D.3.1.2 Icelandic Low

The Icelandic Low is a large low-pressure system normally located near Iceland and southern Greenland. In mid-summer, when it is at its weakest, it may lie as far west as the Hudson Strait. It exerts a major influence on the tracks of lows passing through Atlantic Canada, and fosters the strong cold northwesterly Arctic air flow across the region in winter and early spring.

D.3.1.3 Bermuda High

The Bermuda High is a semi-permanent high-pressure zone with its mean centre lying east of Bermuda and southwest of the Azores. It may play a major role in the climate of eastern Canada in spring and summer, when it is most persistent. It causes air of tropical origin to penetrate the southern United States and move northward to become entrained in westerly winds. In general, this air may bring in periods of warm humid air and heavy precipitation to Atlantic Canada.

D.3.1.4 Eastern Canada weather

High winds and storms are more common in eastern Canada during the winter months. Spring and summer months have fewer, less intense storms and moderate winds, and precipitation is usually in the form of fog, drizzle or rain showers. Hurricanes and tropical storms from the south may threaten the region in the autumn. Air quality in the region is generally good, both onshore and offshore.

Eastern Canada may experience very cold winters which result in the seasonal occurrence of sea ice from Nares Strait through Baffin Bay, Davis Strait, the Labrador Sea, offshore Newfoundland and the Gulf of St. Lawrence. Under predominantly northwesterly winds and the southward-moving Labrador Current branches, sea ice and icebergs travel southwards along the Labrador coast and reach Newfoundland waters and the Grand Banks. Sea ice is encountered seasonally offshore Newfoundland and Labrador in a variety of forms and concentrations. Icebergs of sufficient draft may make contact with the seafloor and create scours on the seabed. The maximum water depth at which scours would be expected to occur is approximately 200 m. Icebergs are rare in offshore Nova Scotia, but pack ice, originating in the Gulf of St. Lawrence, may be encountered occasionally and should be considered in the design of offshore facilities.

The Grand Banks region offshore Newfoundland is considered to be a harsh environment due to the possibility of intense storms and the potential for ice (sea ice and icebergs). Superstructure icing may also occur between December and March because of the temperature and wind and wave conditions. Restricted visibility due to fog is also common, especially in the spring and summer months, when warm air masses overlie the cold ocean surface. The worst visibility conditions are experienced in July. During the winter months, restricted visibility may also be caused by snow in addition to fog and mist.

Major seasonal mean current patterns that influence the regional climatology, and the relative location of Greenland to the Canadian east coast, are shown in Figure D.3.

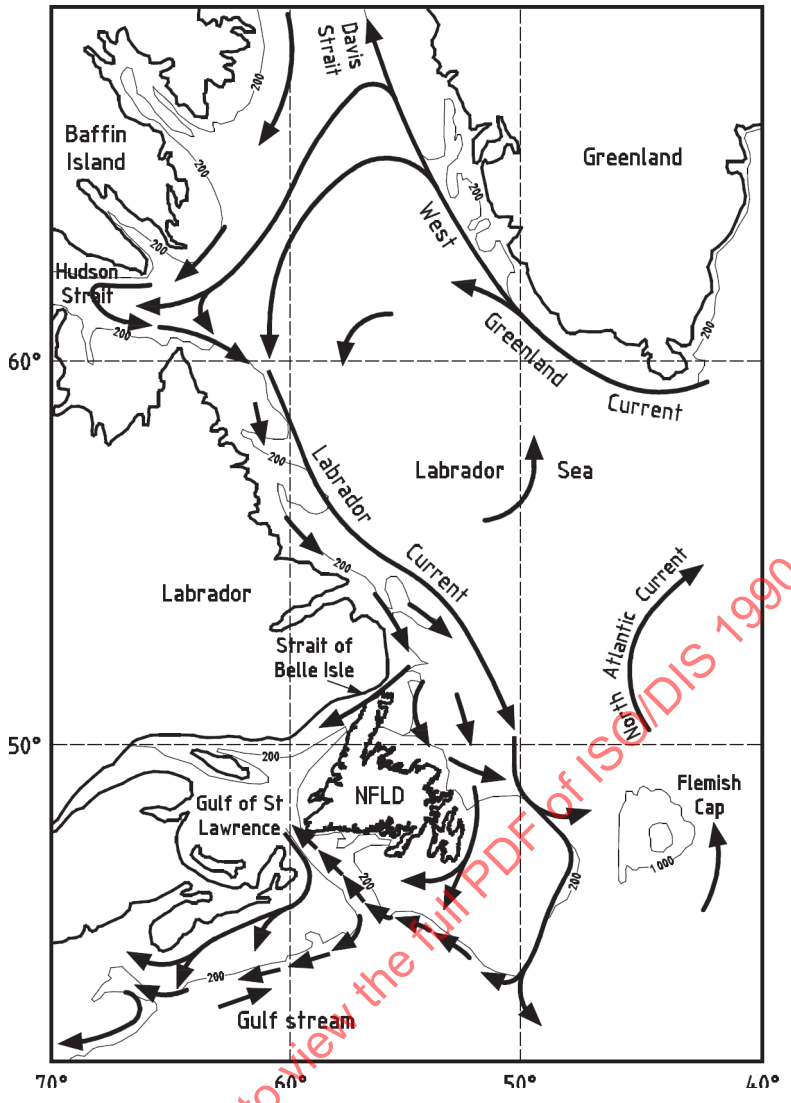

Figure D.3 — Canadian east coast ocean current regime

D.3.2 Beaufort Sea

Temperatures in the Beaufort Sea typically range up to +20 °C in the summer and typically down to below −35 °C in the winter. There are, on average, approximately 4 500 freezing-degree days in this region each year. Winds in the Beaufort Sea are influenced by the sharp thermal contrast between the land and water, and the high coastal lands.[128] The dominant wind direction ranges from northeast to southeast during any month of the year. Southerly winds are rare during the summer months. From July to September, westerly to northwesterly winds in excess of 36 km/h become persistent. Fifty percent of all strong winds with speeds exceeding 50 km/h are from the west or northwest. These winds are responsible for the multi-year ice-pack ice intrusions into the coastal waters. The average rainfall is about 150 mm per year, and the average snowfall is 750 mm each year. Poor visibility of less than 8 km occurs about 20 % of the time due to snow, fog, etc.

NOTE Due to the complexity of the heat exchange between ice, water and air and their measurement, readily available air temperature measurements are often used to quantify the effect of freezing and melting conditions. More specifically, when the mean air temperature for a day is below the freezing point temperature of water, the numerical value may be expressed as the number of Freezing Degree-Days (FDD) and, when above the freezing point temperature, expressed as the number of Melting Degree-Days (MDD). The freezing point temperature of typical marine waters is −1,8° Celsius.

D.4 Water depths

The water depths in the Arctic portion of the Canadian East Coast exhibit very deep water exceeding several hundred metres, in the central basins of Baffin Bay, Davis Strait and the Labrador Sea. The continental shelves of these deep basins extend eastward from the coast to water depths of approximately 200 m with deeper waters penetrating the shelf at the entrances to Jones Sound, Lancaster Sound and Hudson Strait.

The water depths on the Grand Banks are generally less than 200 m, as shown in Figure D.2.

The water depths in the offshore Nova Scotia area addressed in this annex range from 20 m to 80 m, whereas the waters of the Grand Banks current installations are on the order of 80 m to 130 m.

There are also deepwater locations offshore eastern Canada, such as the Flemish Pass and the Orphan Basin, which have depths of 1 100 m and 3 500 m, respectively. There are other potential deepwater hydrocarbon-producing areas offshore Newfoundland and off the Scotian Shelf.

The main characteristic of the water depths in the Gulf of St. Lawrence is the presence of channels of 300 m depth that run into the Gulf from Cabot Strait, as shown on Figure D.9. One branch runs towards the west up to the Saguenay River entrance, and others run east and north towards the strait of Belle-Isle and around Anticosti Island. The next largest feature is the southern Gulf, surrounding Prince Edward Island and the Magdalen islands, with water depths less than 100 m.

Water depth is highly variable in the Beaufort Sea. The continental shelf here has a depth of approximately 100 m. This shelf slopes down from its edge to depths of 1 000 m. The trench-like Mackenzie (or Herschel) Canyon transects a portion of the shelf.

D.5 Winds

Extreme surface winds are mainly associated with the passage of extra-tropical cyclones and their associated frontal structures. Given the large gradients in sea-surface temperature in the region and the closeness of cold and warm continental air mass source zones, the boundary layer wind shear, and hence the strength of surface winds relative to the pressure-gradient-driven free atmosphere flow, tends to be strongly modulated by the stability of the boundary layer, as evidenced by the air-sea temperature difference. The strongest surface winds tend to occur in unstable sectors of storms (air colder than the sea). Extreme winds, on the order of 25 m/s (1-h average at 10 m elevation), tend to be associated with smaller (than cyclone) scale features, such as the “surface wind jet streaks” which propagate rapidly within the broader air flows about each cyclone, within narrow frontal zones and near the cores of nascent explosively developing cyclones. At even smaller scales, convectively produced squalls may occur during seasons and in regions where cold air overlays relatively warm waters. Extreme winds in tropical cyclones are comparable to those in extra-tropical cyclones because larger-scale considerations limit the maximum intensity of tropical cyclones to a Saffir-Simpson scale intensity 2 at most (on a scale of 1 to 5). The winds vary considerably in the different regions as indicated in Table D.2.

D.6 Waves

For the areas in the Northwest Atlantic Ocean, including the Scotian Shelf, Gulf of St. Lawrence, Grand Banks and Labrador Sea, the wind fields associated with extra-tropical and tropical cyclones excite a wide range of sea-states. The resulting sea-states due to wind forcing depend on storm size, radius of curvature of the wind field, peak wind speeds, storm propagation speeds, intensity and speed of propagation of surface wind jet streaks, and proximity of land which will limit fetch for appropriate wind directions. Of course water depth is important in the shallower development areas of the Scotian Shelf for basically all return periods of interest. Indeed, on the Grand Banks, marginally shallow water may affect seas states in the most intense systems. Even relatively small-scale features, such as the small area of high winds in the right quadrant of a propagating tropical cyclone or cyclone undergoing transformation to extra-tropical stage, or a jet-stream propagating through a larger air stream, may generate enormous sea-states if the propagation speed of the wind feature and its peak wind speed allow optimum resonance coupling between the wind field and the surface waves. Extreme wave heights, with maximum individual waves up to 30 m, have been recorded in the region during previous severe storms (e.g. Hurricane Luis in 1995).

For the Arctic regions, including the Beaufort Sea in the west and Davis Strait and Baffin Bay in the east, extratropical cyclones may also affect the region in any season; smaller scale polar lows may also create high sea-states. Being semi-enclosed seas means that proximity of land which will limit fetch for appropriate wind directions. The seasonal presence of sea ice will also limit fetch which reduces ocean wave activity. Water depth is important in the shallower development areas of the Beaufort Sea for basically all return periods of interest.

It is important to note the regional variations in the extreme wave regimes of the various regions, whether due to water depth, sheltering by islands or proximity to major storm tracks. Figures D.4 to D.8 show the variations in the 100-year return period significant wave height and associated peak period for the east coast of Canada, Davis Strait and Baffin Bay and the Beaufort Sea. Other wave statistics tend to follow similar patterns. The wave hindcast models used to compute the 100-year return period waves allow for the seasonal presence of sea ice in limiting ocean wave heights[126,127].

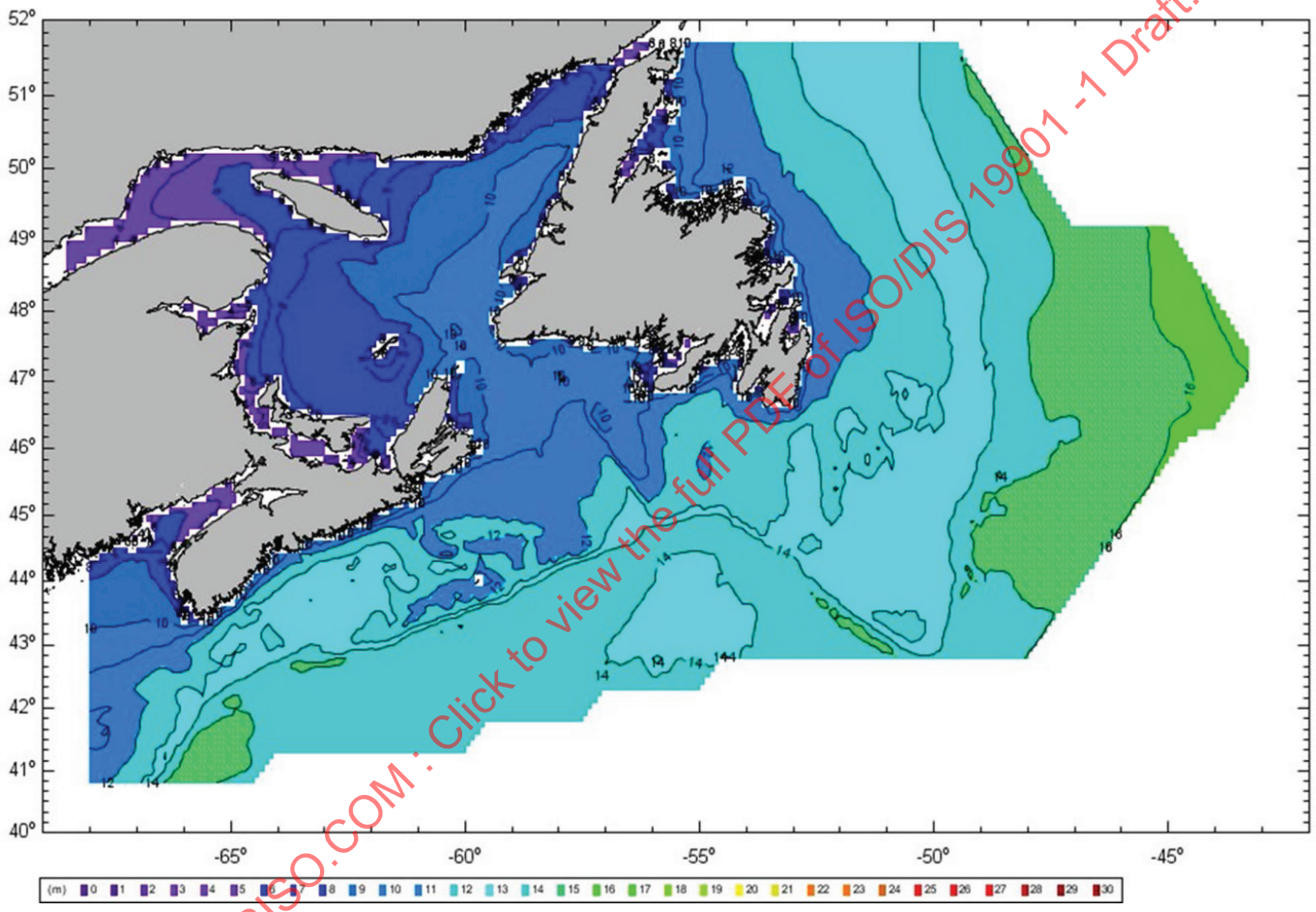

Figure D.4 — 100-year return period significant wave height (Hs) for the east coast of Canada

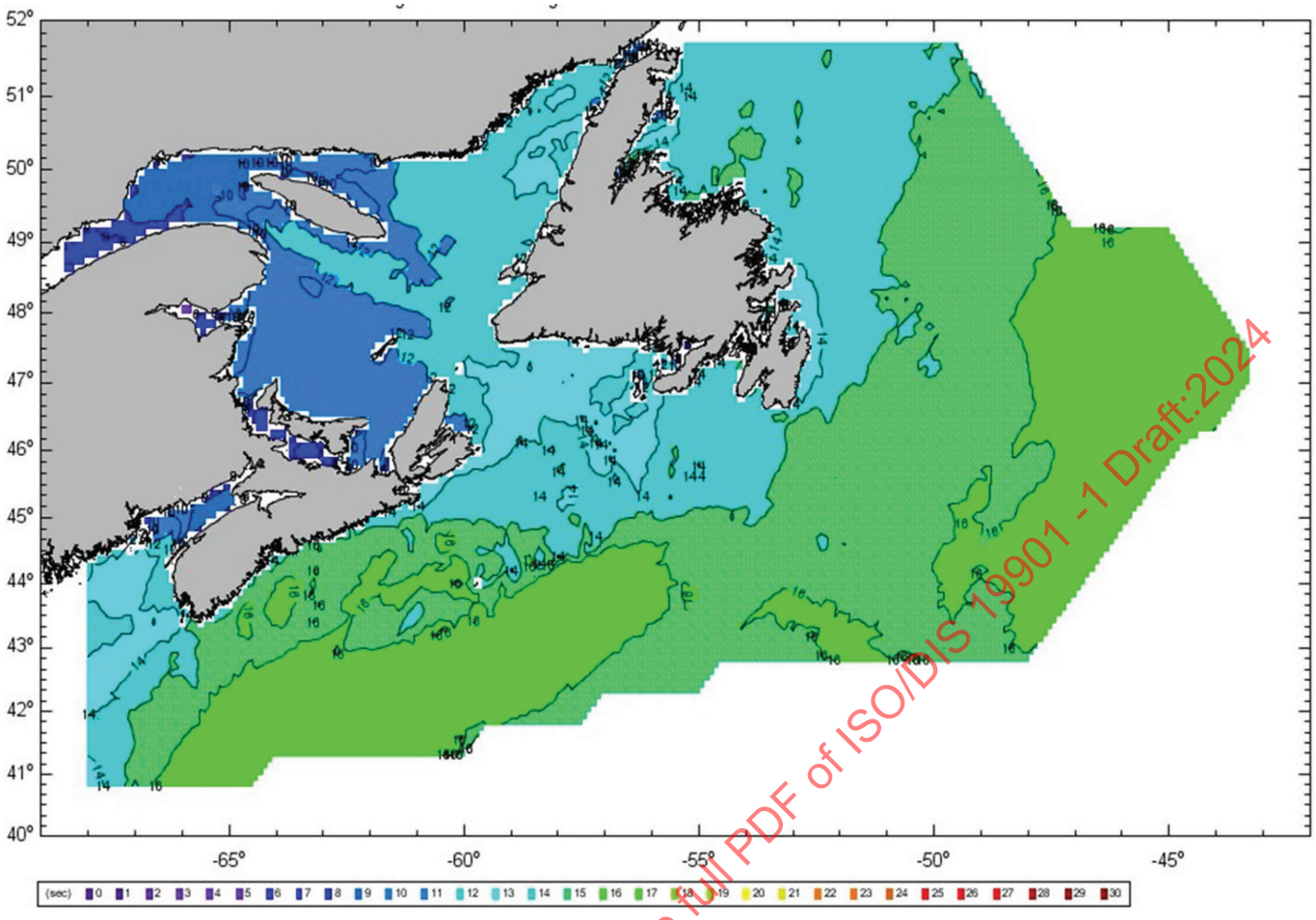

Figure D.5 — Peak Period (Tp) associated with 100-year return period significant wave height (Hs) east coast of Canada

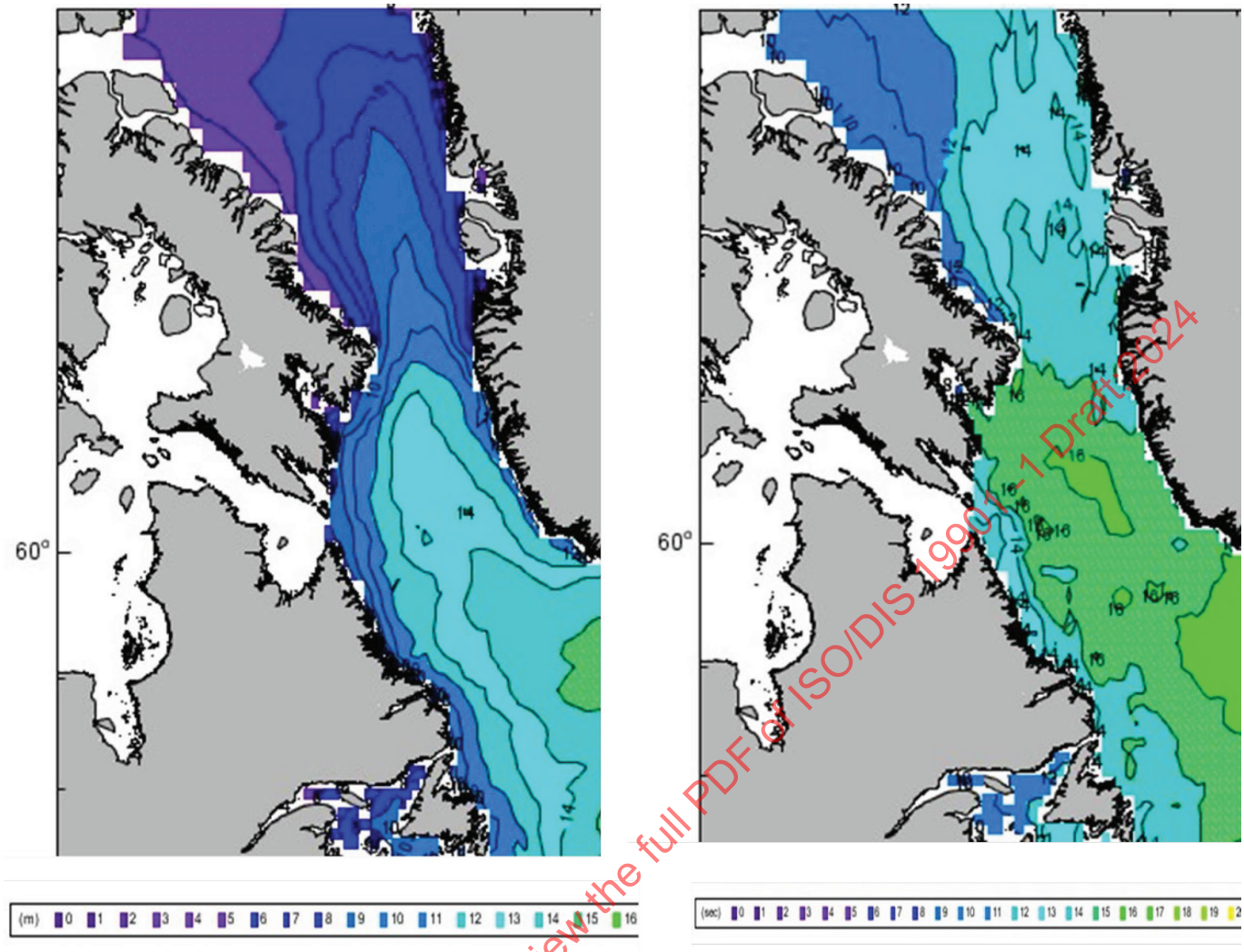

Figure D.6 — 100-year return period significant wave height (Hs) (left) and the associated peak period (Tp) (right) for offshore northeast Canada.

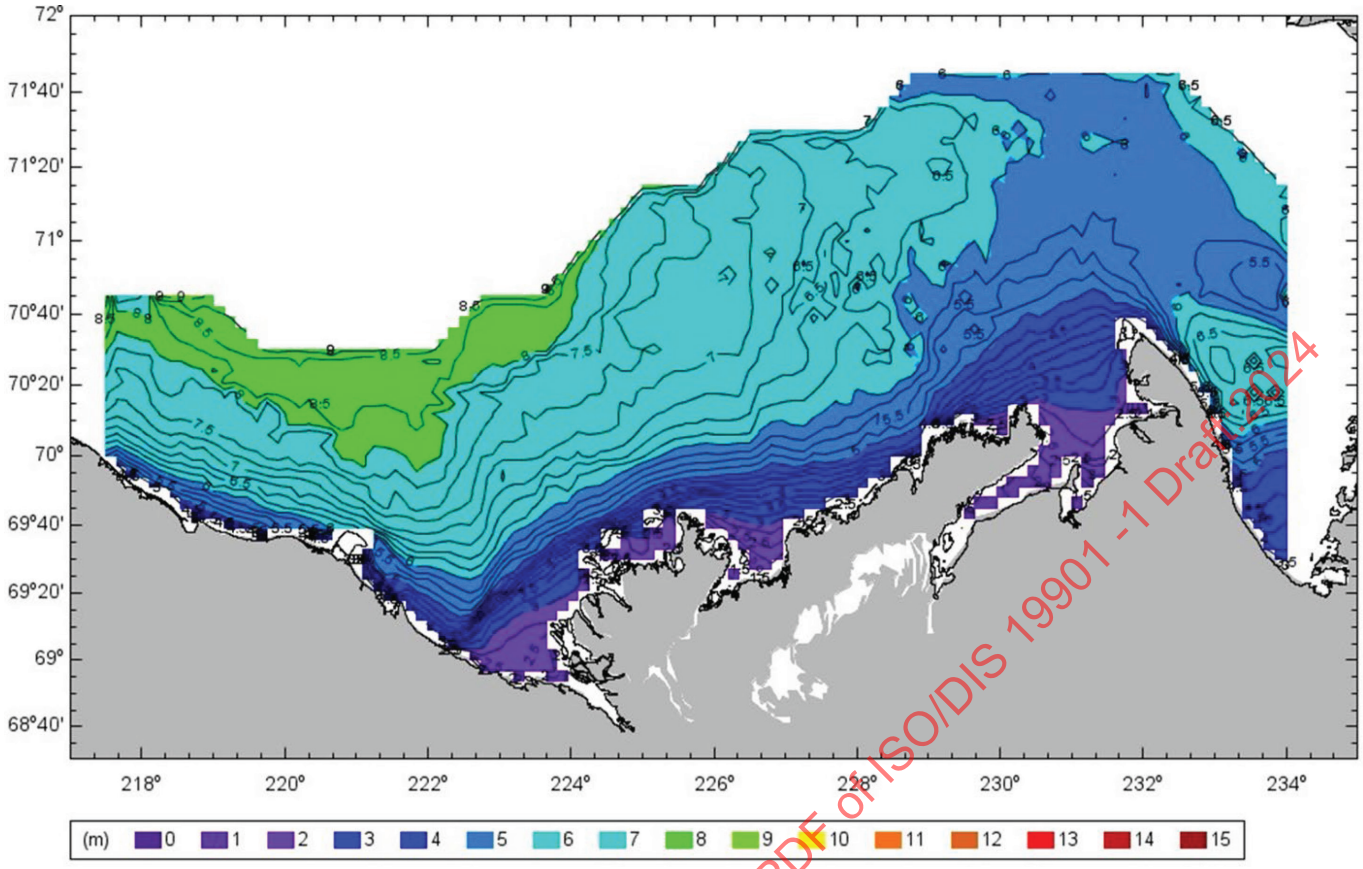

Figure D.7 — 100-year return period significant wave height (Hs) for the Canadian Beaufort Sea.

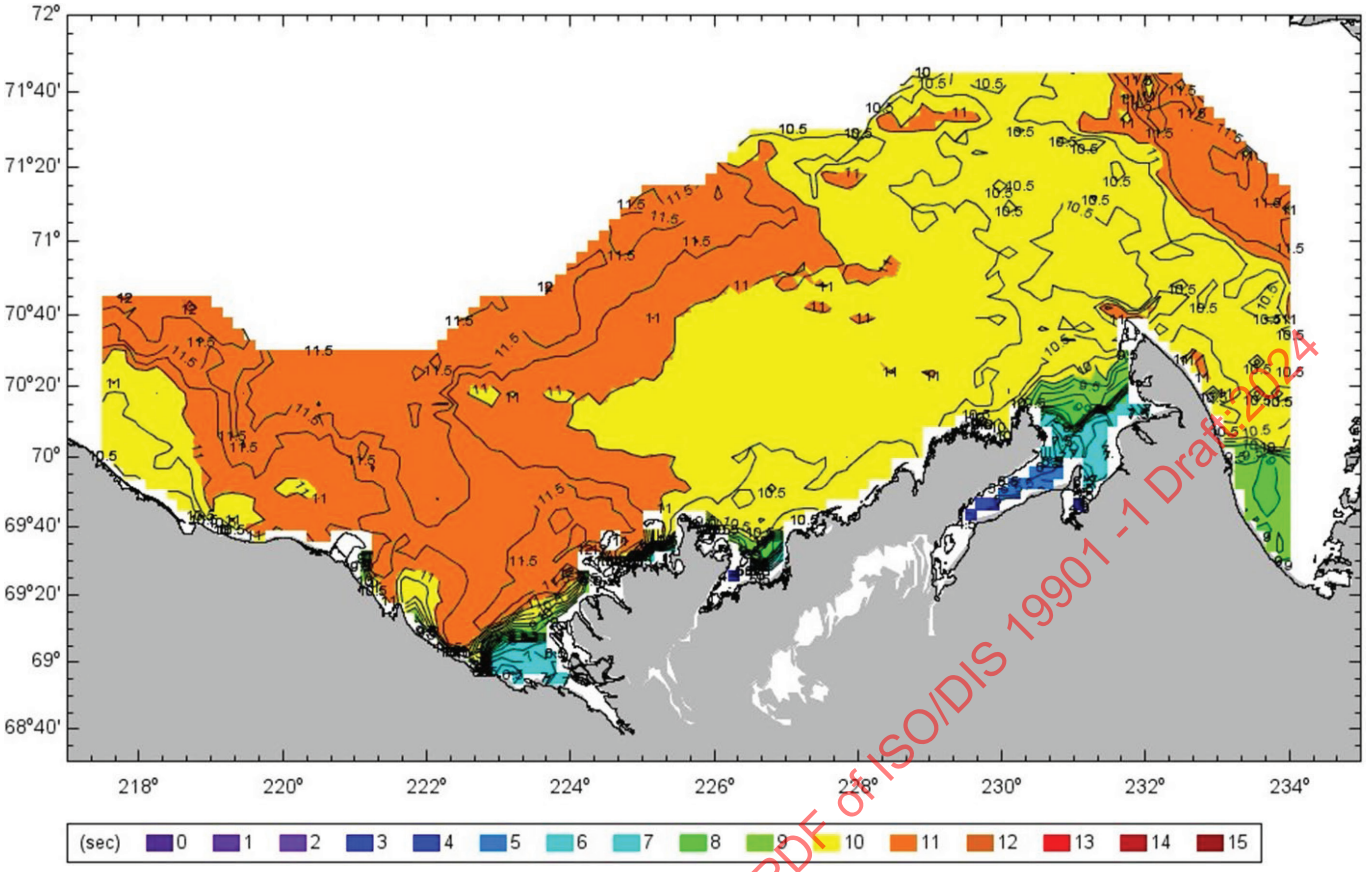

Figure D.8 — Peak Period (Tp) associated with 100-year return period significant wave height (Hs) for the Canadian Beaufort Sea.

D.7 Currents

The Labrador Current is perhaps the most dominant in the Atlantic Canada region. It plays a major role in the transport of colder water to the region, and the resultant regional current pattern is a function not only of this large current, but also of tides, encounters with ocean currents (such as the warmer eddies and meanders of the Gulf Stream) and storm winds.

The Labrador Current is also responsible for the transport of icebergs from northern areas to offshore Newfoundland. Figure D.3 shows how the Labrador Current divides into an inshore branch and an offshore branch. The offshore branch of the Labrador Current is mainly responsible for the transport of icebergs to the hydrocarbon-producing region of the Grand Banks.

The main feature in the Gulf of St. Lawrence is the Gaspé current that flows out of the St. Lawrence Estuary along the Gaspé Peninsula towards the Gulf, loosely following the 50-m isobath as shown in Figure D.9. It is driven by the freshwater outflow of the St. Lawrence River and is intensified by winds. In addition, strong tidal currents[109] are present in the Jacques Cartier Passage, north of Anticosti Island, and at the mouth of the Saguenay River.

The mean circulation pattern in the Beaufort Sea is shown in Figure D.10.[115] Offshore in the Beaufort, the surface flow is dominated by the clockwise circulation of the Beaufort Gyre. Estimates by Newton (1973) [119] indicate that flow speeds reach 5 cm/s to 10 cm/s at the southern rim of the Gyre over the western Beaufort Sea. Figure D.11 shows the pattern of the currents in the nearshore region for both northwest winds and east winds. During the summer season, measurements of currents made at the Kopanoar location indicate values of 0,3 m/s to 0,4 m/s at 5 m depth, and decreasing to 0,1 m/s to 0,2 m/s at 12 m depth [116].

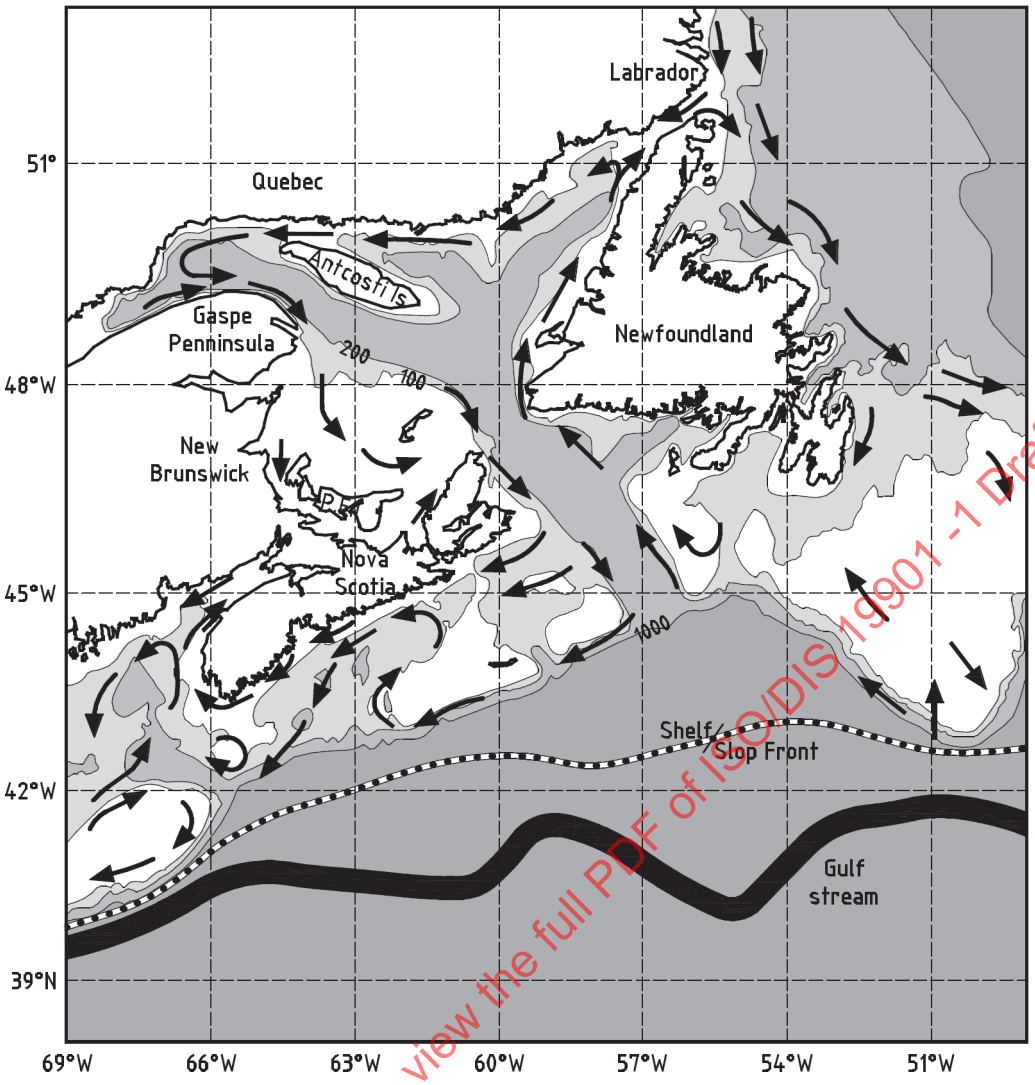

Figure D.9 — Map of the Gulf of St. Lawrence showing the general circulation pattern

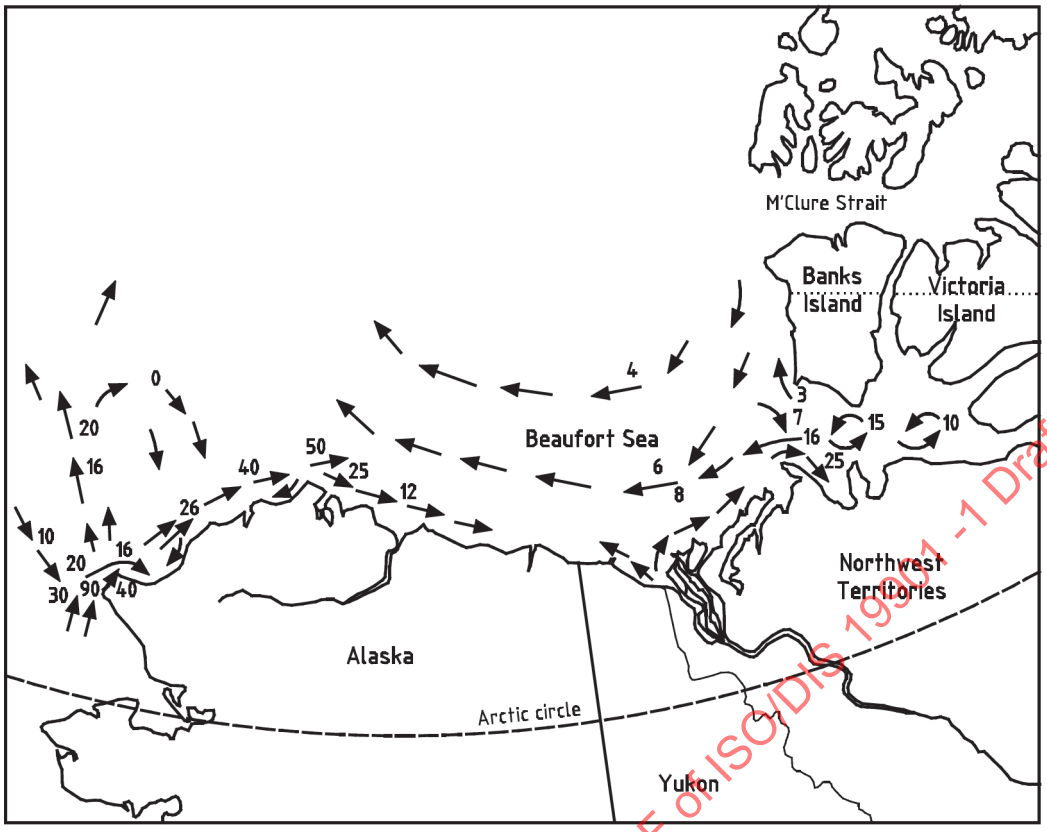

Key

20 → flow speed (cm/s)

Figure D.10 — Mean general summer circulation of the surface water in the Beaufort and Chukchi Seas[115]

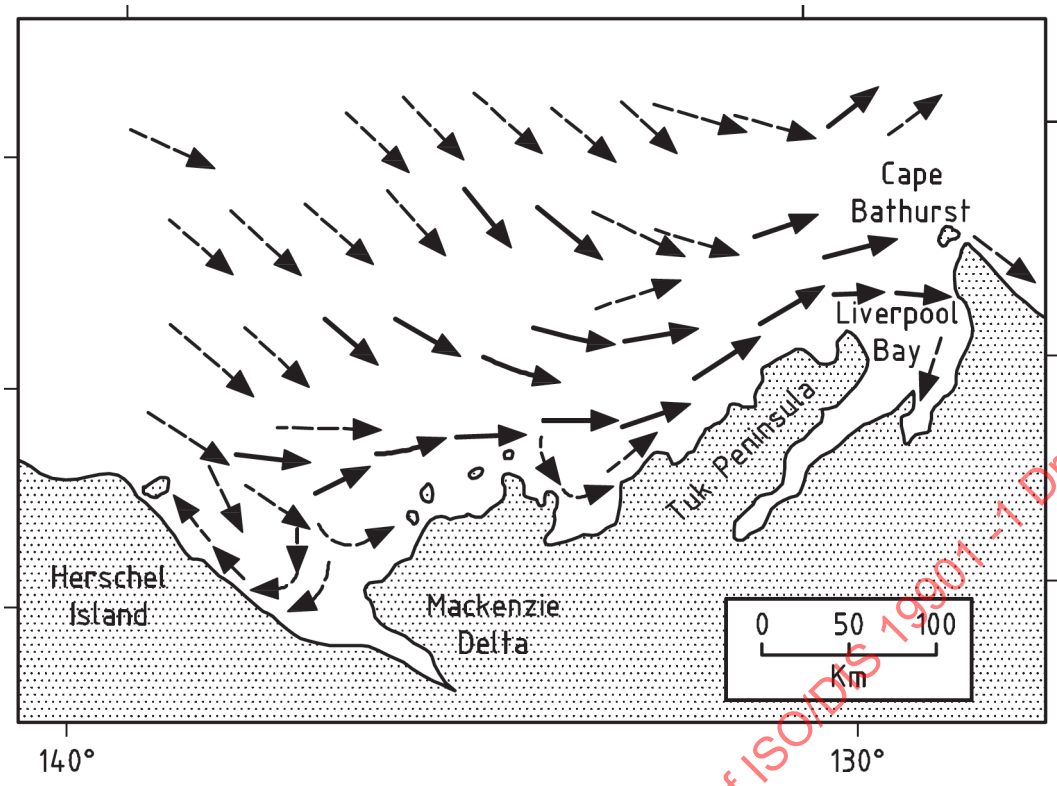

Northwesterly winds

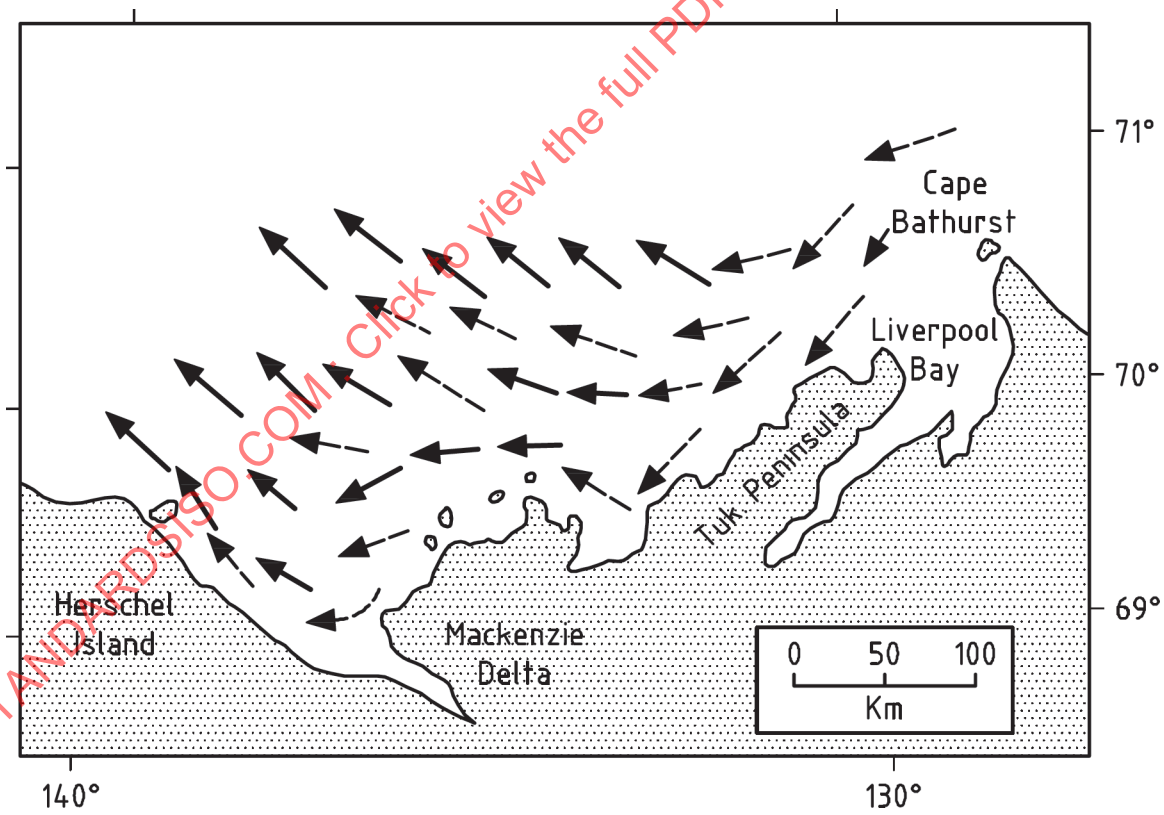

Easterly winds

Figure D.11 — Surface circulation in the southeastern Beaufort Sea for northwest and east winds from surface drift studies[118]

D.8 Sea ice

NOTE The World Meteorological Organization (WMO) Sea Ice Terminology provides an accepted description for sea ice and iceberg characterization, and these definitions will be used throughout this clause. In Canada, the Manual of Ice (MANICE)[129] provides standard procedures for observing and reporting ice conditions.

The seasonal presence of sea ice in Canadian offshore waters has a profound effect on the meteorological and oceanographic conditions. Regional information on sea ice and iceberg conditions in Canadian waters is provided in Annex B (Regional Information) of ISO 19906:2019(E) "Petroleum and natural gas industries — Arctic offshore structures". The presence of sea ice varies widely among Canadian offshore waters, as described below.

D.8.1 Canadian east coast

Freeze-up of sea ice in Canadian east coast waters[112] begins earlier in the more northerly waters offshore of Labrador, starting between Dec. 4 to Jan. 15 (Figure D.12) while further to the south on the northeast shelf and the Grand Banks, the average dates of ice freeze-up are from Jan. 29 – Feb. 26. Average freeze-up dates further to the south and to the west in the Gulf of St. Lawrence occur as early as Jan. 15 in the St. Lawrence estuary extending to Jan. 29 in the western and central portions of the Gulf of St. Lawrence and to Feb. 26 in the eastern Gulf of St. Lawrence.

Break-up of sea-ice in Canadian east coast waters begins first in the more southerly waters of the Gulf of St. Lawrence and over the Grand Banks of Newfoundland with average dates from April 2 – 16 followed by later average break-up dates of April 30 on the Northeast Newfoundland Shelf (Figure D.13). The average dates of break-up of sea ice in the waters offshore of Labrador occurs from April 30 to June 25. The average duration of sea ice cover for the waters of the Canadian east coast ranges from approximately two months in the Gulf of St. Lawrence and the Grand Banks to as much as four months for offshore of Labrador.

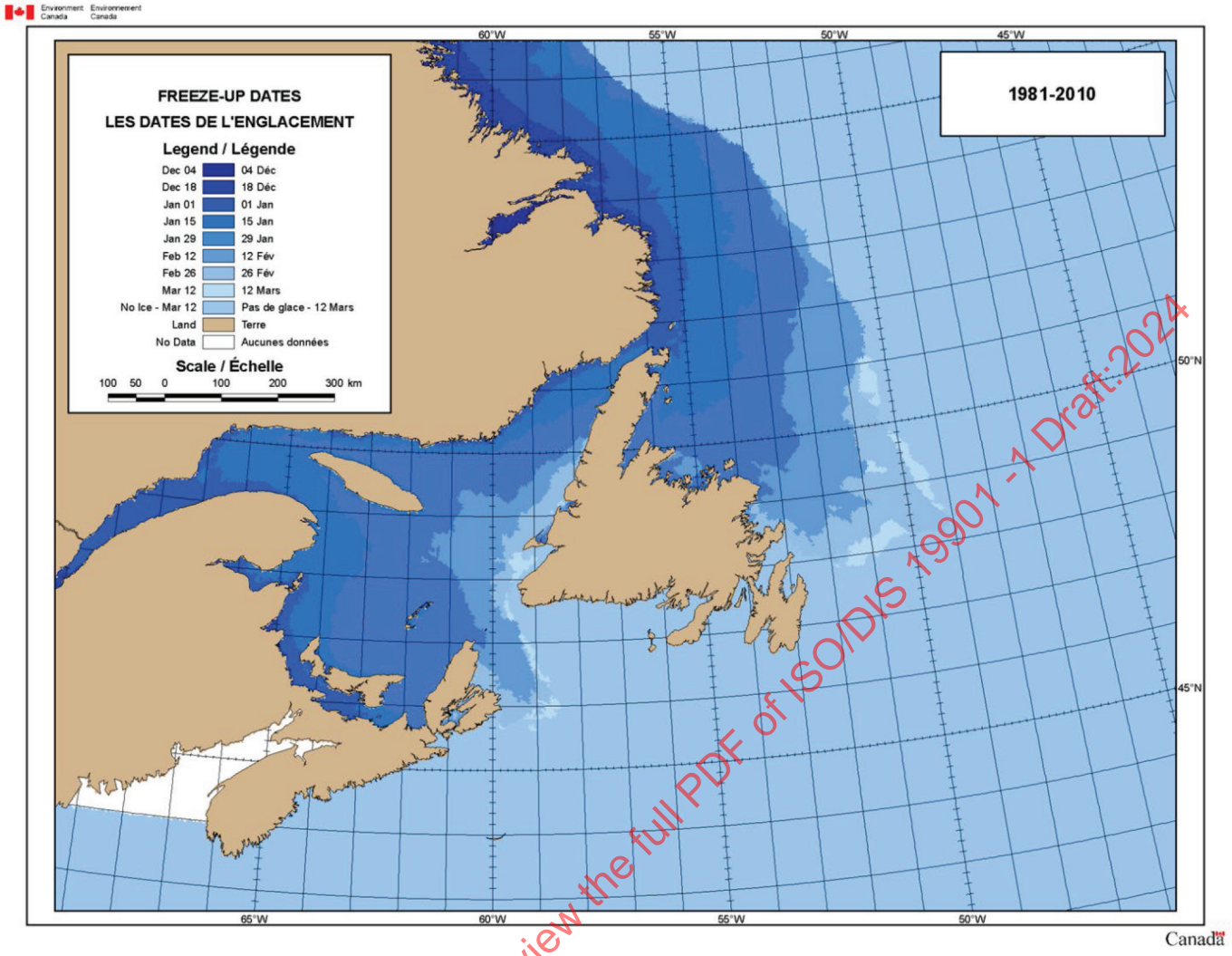

Figure D.12 — Average dates of freeze-up for sea ice in Eastern Canada offshore waters, based on 30 years of ice charts (1981-2010) [112].

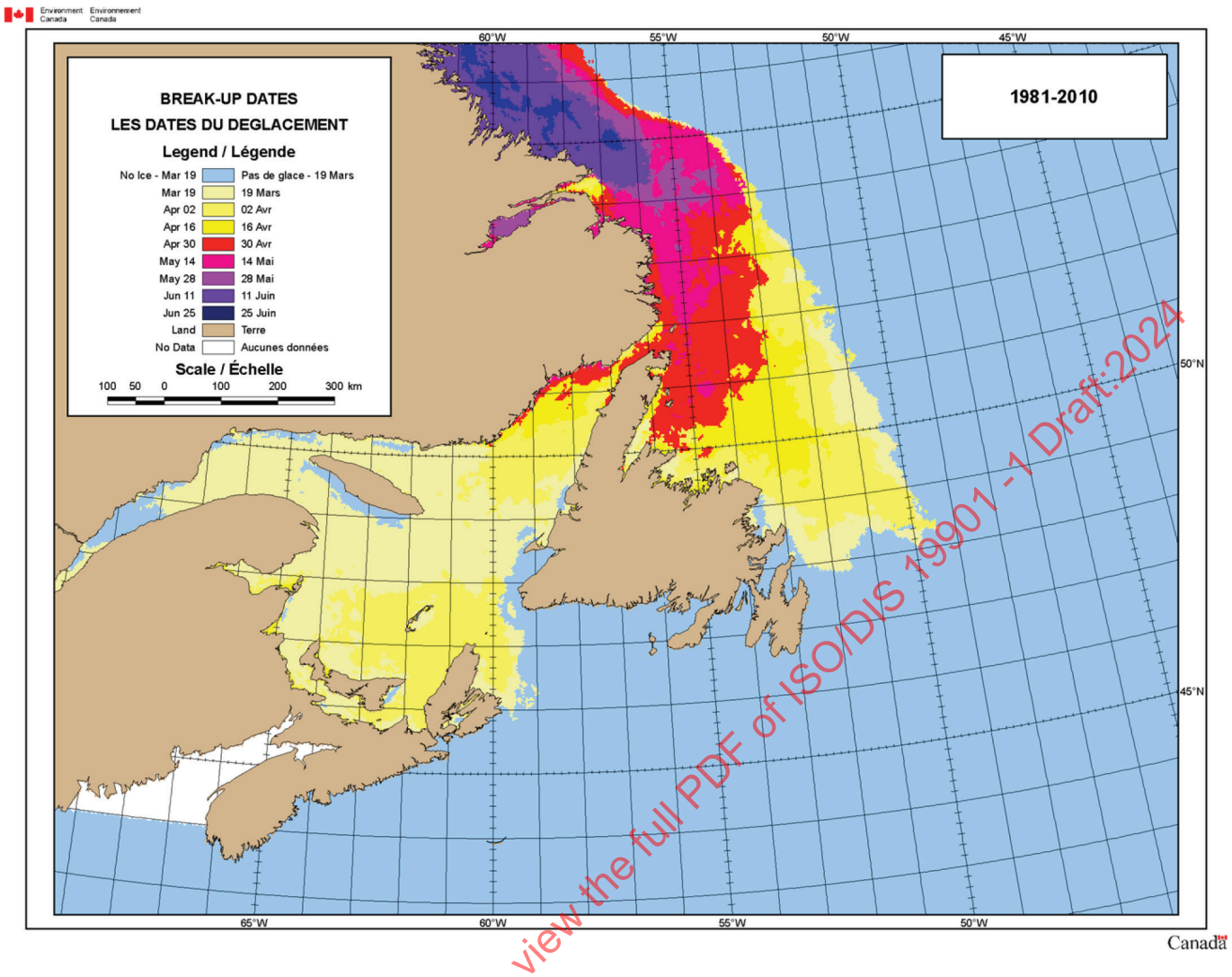

Figure D.13 — Average dates of break-up for sea ice in Eastern Canada offshore waters, based on 30 years of ice charts (1981-2010) [112].

D.8.2 Canadian eastern Arctic (Davis Strait and Baffin Bay)

Sea ice formation starts in late September to early October in north-western Baffin Bay slowly advancing southward driven by the predominantly southward drift, due to the prevailing northerly winds and the strong cold Baffin Current. By early December, freeze-up has extended through the southernmost waters of western Baffin Bay and into the western waters of Davis Strait (Figure D.14).

Break-up of the sea ice cover in the Canadian eastern Arctic occurs in western Davis Strait between June 4 and July 16 and between June 4 and August 15, on average, in Baffin Bay with the early break-up dates in south-eastern Baffin Bay and north-western Baffin Bay (Figure D.15).

The duration of the ice cover in the Canadian eastern Arctic ranges from six months in western Davis Strait to 9,5 months in western portions of central Baffin Bay.

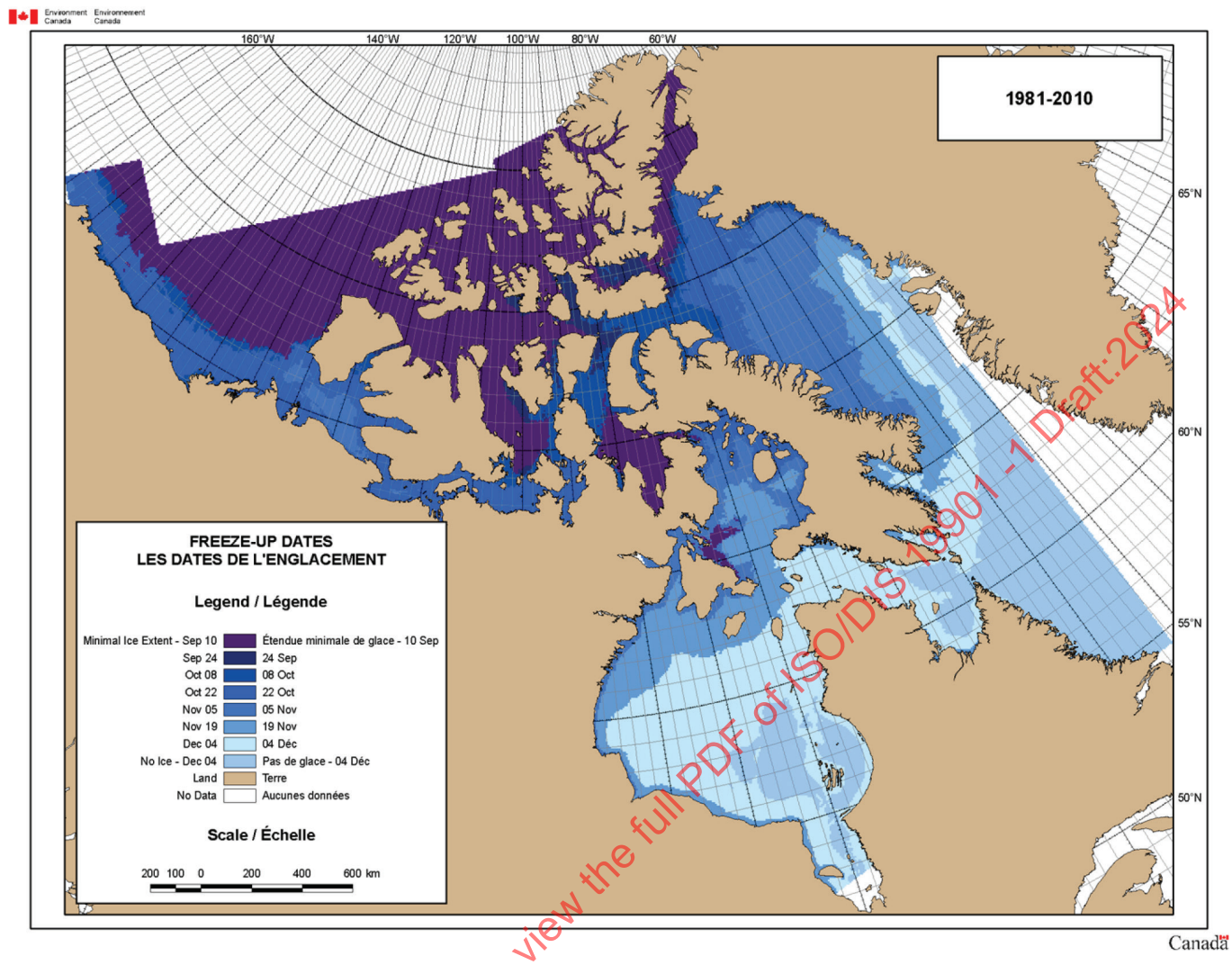

Figure D.14 — Average dates of freeze-up for sea ice in Canadian Arctic offshore waters, based on 30 years of ice charts (1981-2010) [111].

D.8.3 Canadian western Arctic (Beaufort Sea)

The duration of sea ice is generally longer in the Beaufort Sea and adjoining waters than in other Canadian offshore waters. Freeze-up occurs, on average, from Oct. 8 to Nov. 5 in the shelf and slope areas of the Beaufort Sea (Figure D.14) while break-up occurs from early June to mid-July (Figure D.15), for a total duration of 7,5 to 9 months on average. In the adjoining areas of the Canadian Arctic Archipelago, freeze-up occurs in September and break-up occurs from August to mid-September for a total duration of ice cover ranging from 10 to 11,5 months.

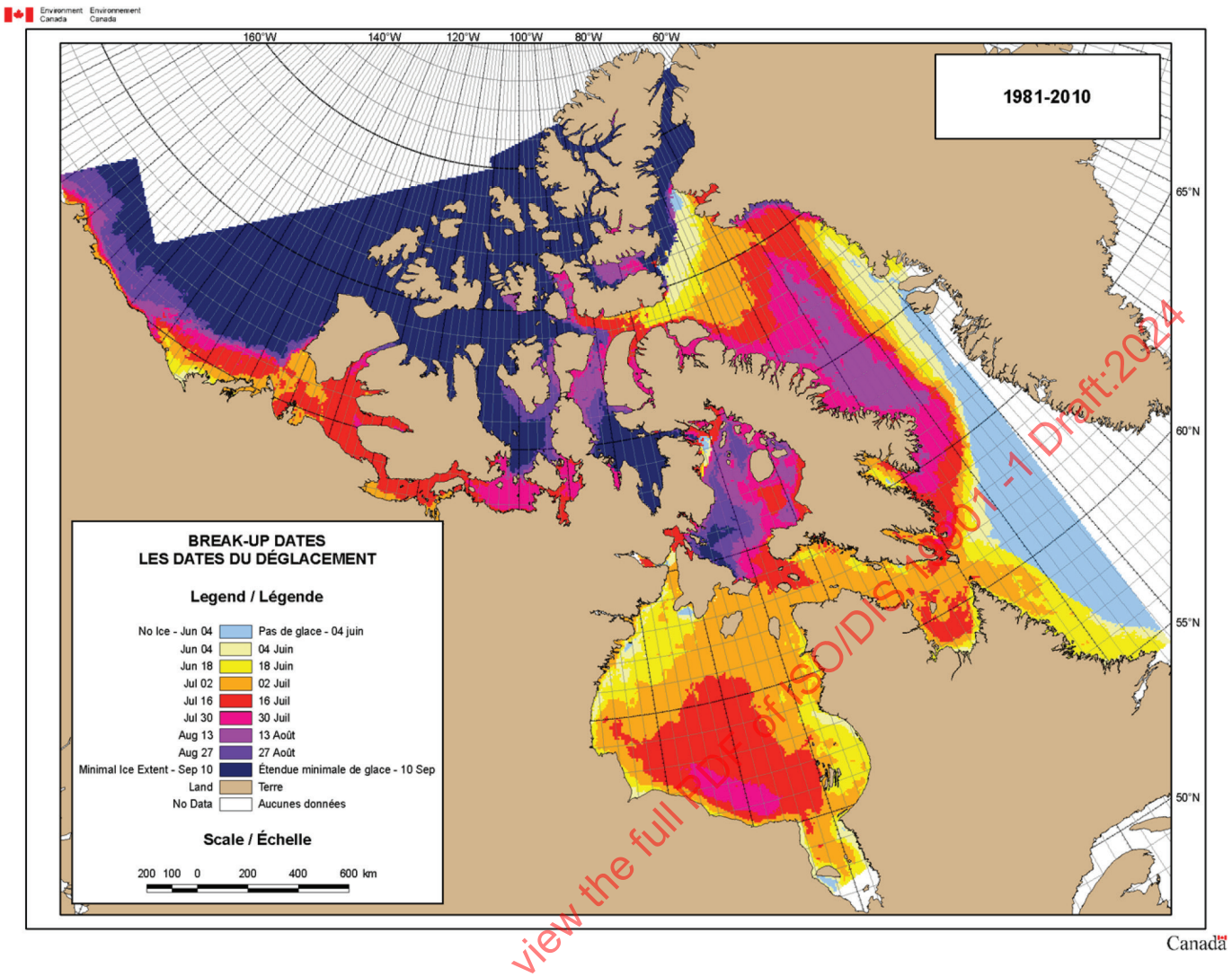

Figure D.15 — Average dates of break-up for sea ice in Canadian Arctic offshore waters, based on 30 years of ice charts (1981-2010) [111].

D.9 Other environmental factors

D.9.1 Snow and ice accretion

Installations located offshore eastern Canada may be subject to snow accumulation and superstructure icing.

The extent to which snow may accumulate and its possible effect on the structure should be considered in the design process. In the absence of specific information, new snow may be assumed to have a density of 100 kg/m^3.

Superstructure icing on fixed or floating offshore structures is a potential concern for operations in cold climates. Ice accretion may lead to several types of problems, such as safety hazards (slippery ladders, inoperable winches, ice on radar antennas, etc.). Superstructure icing is the result of both freezing sea spray and atmospheric precipitation. Ice accretion generated by wave-structure, collision-generated sea spray is the dominant source of ice accretion, due to the intensity and frequency of the spraying events. The phenomenon is seasonal, and its severity depends on the combination of wind speed, air temperature and height above sea level. The design of offshore structures should consider the possibility of superstructure icing and its overall effect on mass, structural integrity and stability. In the absence of other specific information, the ice that may form on the structure may be assumed to have a density of 900 kg/m^3.

D.9.2 Reduced flying visibility

Reduced flying visibility due to fog, snow and rain is common offshore the Canadian east coast. At a typical location on the Grand Banks, the amount of time that flying visibility is typically less than 1 km is as follows:

— from April to August: 40 %;

— from September to March: 11 %.

Based on reference [121], the frequency of reduced visibility is somewhat less in the Nova Scotia offshore area:

— from April to August: 23 %;

— from September to March: 6 %.

D.9.3 Marine growth

Installations in the Canadian offshore region should consider the potential effect of marine growth in terms of additional mass and hydrodynamic loading. If applicable, allowance should be made in the design for marine growth on vessel hulls, mooring lines, risers and other subsea equipment. The profile of marine growth thickness that may occur during the operational phase of the structure should be characterized relative to the depth of the structure below the sea surface.

D.9.4 Daylight hours

Due to the northern location of the Beaufort Sea, daylight hours for this region should be taken into account. Figure D.16 shows an illustration of the duration of sunlight at latitudes from 30° to 90°.[110] Figure D.16 also shows the duration of sunlight at Inuvik, Northwest Territories. As may be seen, the sun does not rise above the horizon for up to three months during the winter at latitudes north of the Arctic Circle. Conversely, in the summer months, the sun does not set and provides 24 h of daylight.

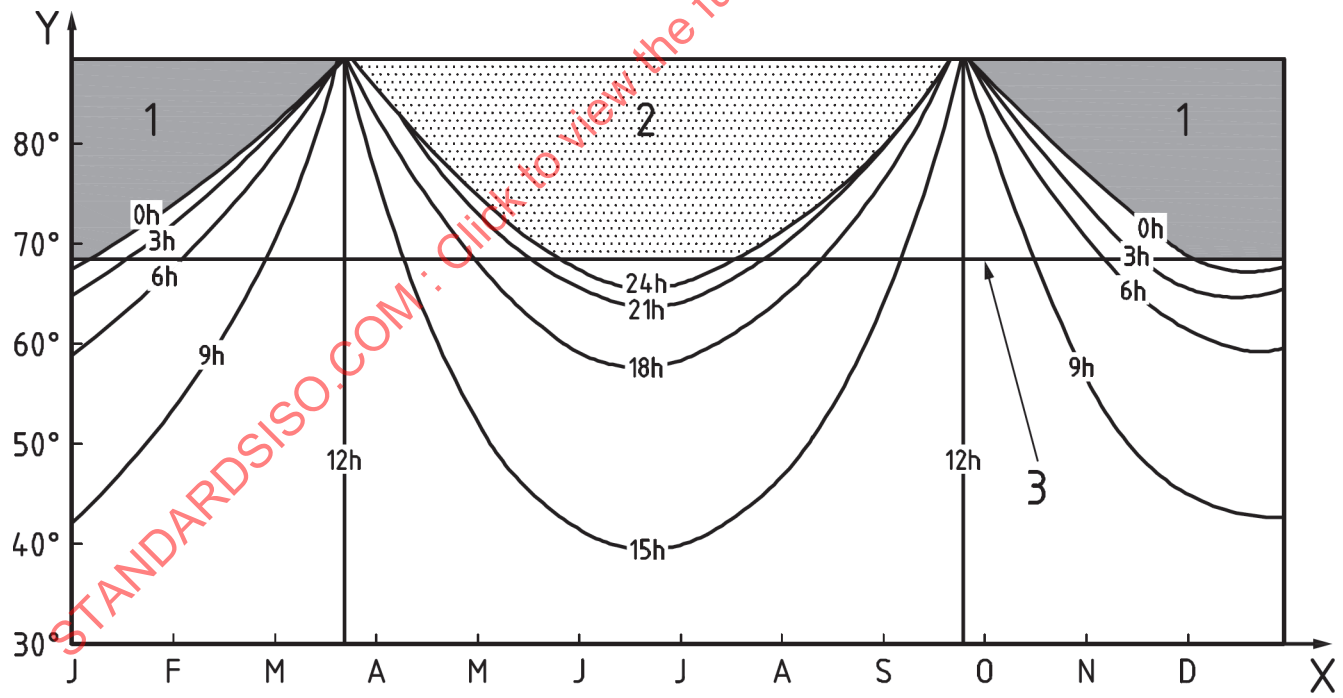

Key

X	month	Y	latitude		
1	sun below horizon	2	sun above horizon	3	the line shows daylight hours at Inuvik

Figure D.16 — Amount of daylight hours as a function of latitude [110]

D.9.5 Earthquakes

The Grand Banks is classified as an area of relatively low seismic activity, but seismic events of significant magnitude have occurred in the recent past. The consequences of earthquake damage to seabed equipment and anchor piling should be considered. The Flemish Pass prospects are located approximately 750 km northeast of the Grand Banks 1929 earthquake epicenter.

D.10 Estimates of metocean parameters

Metocean parameters for offshore Canada are provided in Tables D.1 and D.2, and wave conditions are given Table D.3. These values are indicative and are shown for illustration purposes only. This information should not replace detailed site-specific metocean parameters that should be obtained for the design or assessment of a particular structure that is to be constructed or operated at a particular site.

With respect to the offshore Nova Scotia area, site-specific conditions are highly variable depending on location and the effect of blockage from Sable Island, especially on waves and currents. Beaufort Sea waves and currents are similarly highly variable depending on depth as you get closer to the coast. Site-specific studies are particularly necessary in shallow areas to resolve local wave refraction and current intensification.

The return period for storm surges in the Gulf of St. Lawrence are calculated using the hourly observation of the water level at the station of Pointe-au-Père, Qc, for the period 1900 to 2 000.[122] The values quoted are in metres above mean sea level. Storm-surge analysis at that station is valid for the Gulf of St. Lawrence, from Rimouski to Cabot and Belle-Isle Straits. West of Rimouski towards Quebec City, the funnelling effect of the coastline and bottom topography increase the storm-surge amplitude as it progresses upstream.

No similar long series of observation is available for ocean currents as is the case with water-level observation. Time series at one station are short, one year at the most, and a station is rarely surveyed twice. Maximum speeds of currents and their variability are reported in reference [117] for a number of stations in the Gulf of St. Lawrence. These observations were used to generate the values of the currents for the return period of one year in Table D.2. The amplitudes of currents given in Table D.2 for the return periods of 5, 10, 50 and 100 years are estimated using the cited ratio for Nova Scotia and Newfoundland areas between the return period of 1 year and the other return periods. Currents reported in Table D.2 of extreme metocean parameters are valid for the Jacques Cartier Passage, which is located north of Anticosti Island, and for the region north of the Gaspé Peninsula where the Gaspé current flows. These two regions experience the highest values for the currents. Outside of these regions, current amplitude is weaker and more variable, being mainly wind-driven. On the other hand, as the shore is approached, the tidal currents increase as the bathymetry shallows. This increase in current amplitude is also observable with progress upstream. The region between Tadoussac and Quebec City experiences higher currents than stated in Table D.2. A Tidal Atlas[109, 120] is available for that region.

Table D.1 — Extreme air and water temperatures for Canadian offshore areas

Offshore area	Newfoundland Offshore		Gulf of St. Lawrence	Beaufort Sea	Nova Scotia Offshore (Sable Island Bank)
	Grand Banks	Deepwater			
Sea water temperatures °C					
Minimum extreme near surface	–1,7	–1,7	–1,8	–1,8	–1,6
Maximum near surface	15 to 19	15 to 19	15 to 20	5 to 10	15 to 20
Minimum near bottom [a]	–1,7	3	–1,8	–1,8	–1,3
Maximum near bottom	3 to 6	3	2 to 6	–1 to 5	18

Table D.1 *(continued)*

Air temperatures °C					
Minimum	−17 to −19	−17 to −19	-16	−40	−14 to −19
Maximum	22 to 25	22 to 25	24	15	30 to 35
[a] For Gulf of St. Lawrence: minimum temperature mid-depth (°C).					
Newfoundland offshore (Grand Banks)					
Metocean parameter	**Return period** *N* years				
	100	**50**	**10**	**5** [b]	**1**
Wind speed [a]					
10-min wind speed (m/s)	37 to 41	36 to 39	33 to 34	29 to 33	25 to 31
3-s gust wind speed (m/s)	50 to 55	48 to 52	42 to 45	38 to 42	34 to 39
Waves (see Table D.3)					
Current speed					
Surface (m/s)	1,3 to 1,7	1,2 to 1,6	1,1 to 1,3	1,0 to 1,2	0,9 to 1,0
Mid-depth (m/s)	0,9 to 1,1	0,8 to 1,1	0,7 to 1,0	0,6 to 1,0	0,5 to 0,9
Near-bottom (m/s)	0,9 to 1,0	0,8 to 1,0	0,7 to 0,8	0,6 to 0,8	0,5 to 0,7
Storm surge					
Surge above MSL (m)	0,70	–	0,61	0,46	0,50

Table D.2 — Extreme metocean parameters for Canadian offshore areas

Nova Scotia offshore (Sable Island Bank)					
Metocean parameter	**Return period** *N* years				
	100	**50**	**10**	**5** [b]	**1**
Wind speed [a]					
10-min (m/s)	41 to 45	40 to 43	35 to 38	30 to 34	25 to 30
3-s gust (m/s)	50 to 58	50 to 55	45 to 48	39 to 43	34 to 37
Waves (see Table D.3)					
Current speed					
Surface (m/s)	1,5 to 2,3	1,4 to 2,3	1,3 to 2,1	1,2 to 1,8	1,0 to 1,4
Mid-depth (m/s)	1,1 to 1,3	1,0 to 1,2	1,0 to 1,1	0,9 to 1,1	0,9 to 1,0
Near-bottom (m/s)	0,8 to 1,1	0,7 to 1,1	0,7 to 1,0	0,8 to 1,0	0,9 to 1,0
Storm surge					
Surge above MSL (m)	0,6 to 0,7	0,5 to 0,6	0,49	–	–
Canadian east coast deepwater					
Metocean parameter	**Return period** *N* years				
	100	**50** [c]	**10**	**5** [b]	**1**
Wind speed [a]					
10-min (m/s)	31,8	30,5	29,1	27,4	25,7
3-s gust (m/s)	42,8	41,1	39,3	37,1	34,8
Waves (see Table D.3)					

[a] Based on a reference height of 10 m above sea level.

[b] Based on average of 1-year and 10-year data. To be updated in future revisions of this annex.

[c] Based on average of 10-year and 100-year data. To be updated in future revisions of this annex.

Table D.2 *(continued)*

Current speed					
Surface (m/s)	1,3	1,23	1,15	1,08	1
Mid-depth (m/s)	1,09	1,03	0,97	0,92	0,86
Near-bottom (m/s)	0,96	0,90	0,83	0,77	0,7
Storm surge					
Surge above MSL (m)	–	–	–	–	–
Gulf of St. Lawrence (East of Rimouski to Cabot Strait)					
Metocean parameter	**Return period *N* years**				
	100	**50**	**10**	**5**	**1**
Wind speed [a]					
10-min (m/s)	–	–	–	–	–
3-s gust (m/s)	–	–	–	–	–
Waves (see Table D.3)					
Current speed					
Surface (m/s)	1,4 to 2,1	1,4 to 2,0	1,2 to 1,8	1,1 to 1,6	0,9 to 1,3
Mid-depth (m/s)	0,6 to 0,7	0,5 to 0,7	0,5 to 0,6	0,5 to 0,6	0,4 to 0,5
Near-bottom (m/s)	0,5 to 0,6	0,5 to 0,6	0,4 to 0,5	0,4 to 0,5	0,3 to 0,4
Storm surge					
Surge above MSL (m)	1,4 – 1,8	1,3 – 1,6	1,2 – 1,3	1,1	0,6
Beaufort Sea					
Metocean parameter	**Return period *N* years**				
	100	**50**	**10**	**5**	**1**
Wind speed [a]					
Hourly average (m/s)	31,7	29,2	26,9	23,9	16,7
1-min average (m/s)	41,7	38,9	35,8	32,2	29,7
Waves (see Table D.3)					
Storm surge					
Surge above MSL (m)	1,4 to 1,8	1,3 to 1,6	1,2 to 1,3	1,1	0,6

[a] Based on a reference height of 10 m above sea level.

[b] Based on average of 1-year and 10-year data. To be updated in future revisions of this annex.

[c] Based on average of 10-year and 100-year data. To be updated in future revisions of this annex.

Table D.3 — Extreme wave parameters for Canadian offshore areas

Scotian Shelf range (57 W to 66 W, shoreward of shelf edge)					
Return Period (years)					
	100	**50**	**10**	**5**	**1**
Maximum height (m)	20-26	19-24	17-22	16-20	12-16
Significant height (m)	11-14	10-13	9,5-12	9-10,5	6,5-9
Crest height (m)	12-16	10,5-14	10-13,5	9,5-12	7-10
Associated peak period (s)	14-16,5	14-16	13,5-15	12,5-14	11-12
Associated wind speed (m/s)	28-31	24-29	22-26	20-25	15-20
Scotian Shelf (Deep Panuke – 43,8 N, 60,8 W, depth 40 m)					
Return Period (years)					

Table D.3 *(continued)*

	100	50	10	5	1
Maximum height (m)	21,7	20,7	18,47	17,5	13,4
Significant height (m)	12,2	11,6	10,26	9,7	7,3
Crest height (m)	13,9	13,3	11,71	11,0	8,2
Associated peak period (s)	15,4	15,0	13,99	13,5	11,6
Associated wind speed (m/s)	30,2	29,2	25,66	24,0	17,6
Scotian Shelf (Chebucto – 43,7 N, 59,7 W, depth 83 m)					
Return Period (years)					
	100	**50**	**10**	**5**	**1**
Maximum height (m)	21,8	21,0	19,1	18,2	14,8
Significant height (m)	11,9	11,5	10,4	10,0	8,1
Crest height (m)	13,4	12,9	11,7	11,2	9,0
Associated peak period (s)	16,0	15,5	14,4	13,9	11,8
Associated wind speed (m/s)	30,6	29,7	26,0	24,4	17,7
Scotian Shelf (La Have Bank – 43,0 N, 64,0 W, depth 96 m)					
Return Period (years)					
	100	**50**	**10**	**5**	**1**
Maximum height (m)	23,3	22,2	19,7	18,6	14,2
Significant height (m)	13,0	12,4	10,9	10,3	7,7
Crest height (m)	14,4	13,7	12,1	11,4	8,6
Associated peak period (s)	15,7	15,2	14,1	13,6	11,5
Associated wind speed (m/s)	30,1	29,2	25,5	23,8	17,3
Grand Banks range (45 N to 49 N, 44 W to 50 W)					
Return Period (years)					
	100	**50**	**10**	**5**	**1**
Maximum height (m)	24-30	23-29	21-27	20-26	17-22
Significant height (m)	13,5-17	13-16	12-14,5	11-14	9,5-12
Crest height (m)	14-19	14-18	12,5-17	11,5-15,5 15,5	10,5-14
Associated peak period (s)	15-17	15-16,5	14,5-16	14-15,5	13-14,5
Associated wind speed (m/s)	30-33	28-32,5	26-30	25-28	19-25
Grand Banks (Terra Nova – 46,4 N, 48,4 W, depth 93 m)					
Return Period (years)					
	100	**50**	**10**	**5**	**1**
Maximum height (m)	26,1	25,2	23,0	22,0	18,1
Significant height (m)	14,4	13,8	12,6	12,1	10,0
Crest height (m)	16,1	15,5	14,1	13,5	11,1
Associated peak period (s)	15,8	15,5	14,8	14,5	13,1
Associated wind speed (m/s)	31,2	30,0	27,3	26,0	21,1
Grand Banks (S, Tempest – 47,1 N, 47,8 W, depth 180 m)					
Return Period (years)					
	100	**50**	**10**	**5**	**1**
Maximum height (m)	27,4	26,5	24,2	23,2	19,2

Table D.3 *(continued)*

Significant height (m)	15,1	14,6	13,3	12,7	10,5
Crest height (m)	16,8	16,3	14,9	14,2	11,1
Associated peak period (s)	16,1	15,8	15,2	14,8	13,5
Associated wind speed (m/s)	31,6	30,4	27,5	26,2	21,1
Grand Banks (Flemish Pass – 48,1 N, 46,1 W, depth 1 133 m)					
Return Period (years)					
	100	**50**	**10**	**5**	**1**
Maximum height (m)	28,5	27,6	25,5	24,6	20,8
Significant height (m)	15,7	15,2	14,0	13,5	11,3
Crest height (m)	17,5	17,0	15,7	15,1	12,8
Associated peak period (s)	16,6	16,3	15,6	15,3	14,0
Associated wind speed (m/s)	33,8	32,4	29,2	27,8	22,1
Grand Banks (Orphan Basin – 49,0 N, 48,0 W, depth 2 331 m)					
Return Period (years)					
	100	**50**	**10**	**5**	**1**
Maximum height (m)	27,0	26,2	24,1	23,2	19,6
Significant height (m)	14,6	14,2	13,1	12,6	10,7
Crest height (m)	16,7	16,1	14,9	14,3	12,0
Associated peak period (s)	15,6	15,4	14,9	14,6	13,6
Associated wind speed (m/s)	33,6	32,6	28,8	27,1	20,3
Gulf of St, Lawrence range (48 N to 49 N, 59 W to 62 W)					
Return Period (years)					
	100	**50**	**10**	**5**	**1**
Maximum height (m)	16-19,5	15-19	13-17	12,5-16	9,5-12,5
Significant height (m)	9-10,5	8-10	7,5-9	6,5-8,5	5,5-7
Crest height (m)	9,5-12,5	8,5-11,5	8-10,5	7,5-10	6-7,5
Associated peak period (s)	11-12,5	11-12	10-11,5	9,5-11,5	9-11
Associated wind speed (m/s)	26-28	25-27	23-25	20-24	16-21
Gulf of St, Lawrence (north central 48,0 N, 61,0 W, depth 214 m)					
Return Period (years)					
	100	**50**	**10**	**5**	**1**
Maximum height (m)	19,4	18,6	16,6	15,7	12,2
Significant height (m)	10,4	10,0	8,9	8,5	6,6
Crest height (m)	12,1	11,5	10,2	9,6	7,3
Associated peak period (s)	12,0	11,8	11,5	11,4	10,7
Associated wind speed (m/s)	26,9	26,1	24,3	23,5	20,3
Labrador Shelf range (52 N to 60 N, shoreward of shelf edge)					
Return Period (years)					
	100	**50**	**10**	**5**	**1**
Maximum height (m)	19-25	17-24	16-22	15-21	11-18
Significant height (m)	10-13,5	9,5-13	8,5-12	8-11,5	6-10
Crest height (m)	12-15,5	11-15	10-14	9-13	7-11
Associated peak period (s)	14-16,5	13,5-15,5	13-14,5	12,5-14	12-13

Table D.3 *(continued)*

Associated wind speed (m/s)	28-31	25-29	24-26	20-23	14-19
Davis Strait range (61 N to 70 N, west of Canada-Greenland boundary)					
Return Period (years)					
	100	**50**	**10**	**5**	**1**
Maximum height (m)	12-23	11-22	9-18	8-17	6-14
Significant height (m)	7-14	6-12,5	5-11	4,5-10	3,5-8
Crest height (m)	7,5-15	6,5-13,5	5,5-11,5	5-11	4-8,5
Associated peak period (s)	12-16	11-15,5	10-14	10-14	8-12,5
Associated wind speed (m/s)	23-27	20-25	19-23	18-21	11-14
Baffin Bay range (70 N to 75 N, west of Canada-Greenland boundary)					
Return Period (years)					
	100	**50**	**10**	**5**	**1**
Maximum height (m)	10-17	9-16	8-13	7-11	4-6
Significant height (m)	5,5-9,5	5-9	4,5-7,5	4-6,5	2,5-3,5
Crest height (m)	6-10,5	5,5-9,5	5-8	4,5-7	2,5-4
Associated peak period (s)	10,5-14	10-13	9,5-12	9-11,5	8-9,5
Associated wind speed (m/s)	19-23	18-21	15-18	13-17	8-11
Beaufort Sea range (70 N to 71 N, 132 W to 137 W)					
Return Period (years)					
	100	**50**	**10**	**5**	**1**
Maximum height (m)	9-16	8-15	;7-12	6-11	4,5-6
Significant height (m)	5-9	4,5-8	4-6,5	3-5,5	2-3
Crest height (m)	6,5-10	6-9,5	5-7,5	3,5-6,5	2,5-3,5
Associated peak period (s)	10,5-12	10-11,5	9,5-11	9-10	6,5-8
Associated wind speed (m/s)	23-24	21-23	18-19,5	15-18	11-12,5
Beaufort Sea (Kopanoar – 70,45 N, 135,0 W, depth 59 m)					
Return Period (years)					
	100	**50**	**10**	**5**	**1**
Maximum height (m)	13,23	12,6	10,2	9,3	5,6
Significant height (m)	7,2	6,7	5,5	5,0	2,9
Crest height (m)	8,1	7,6	6,2	5,6	3,4
Associated peak period (s)	11,0	10,7	9,9	9,5	7,6
Associated wind speed (m/s)	23,1	21,8	18,8	17,5	12,2

D.11 Sources of additional information

D.11.1 Information on meteorological parameters, e.g. prediction of severe weather, sea-state and icing conditions

Information Services Division

National Archives and Data Management Branch

Meteorological Service of Canada

Environment and Climate Change Canada

4905 Dufferin Street

Toronto, Ontario M3H 5T4

Canada

Telephone: (416) 739-4328

Fax: (416) 739-4446

Email: Climate.Services@ec.gc.ca

Climate Research Division

Science and Technology Branch

Environment and Climate Change Canada

4905 Dufferin Street

Toronto, Ontario M3H 5T4

Canada

Fax: (416) 739-5700

D.11.2 Oceanographic information

Department of Fisheries and Oceans Canada

Marine Environmental Data Service

12W082-200 Kent Street

Ottawa, Ontario K1A 0E6

Canada

Telephone: (613) 990-6065

Fax: (613) 993-4658

Email: services@meds-sdmm.dfo-mpo.gc.ca

http://www.meds-sdmm.dfo-mpo.gc.ca

Department of Fisheries and Oceans Canada

Bedford Institute of Oceanography

Ocean Sciences Division

P.O. Box 1006

Dartmouth, Nova Scotia B2Y 4A2

Canada

Telephone: (902) 426-8478

Fax: (902) 426-5153

https://www.mar.dfo-mpo.gc.ca/science/ocean/home.html

Department of Fisheries and Oceans

Institute of Ocean Sciences

Ocean Sciences and Productivity Division

P.O. Box 6000

9860 West Saanich Road

Sidney, British Columbia V8L 4B2

Canada

Telephone: (250) 363-6378

Fax: (250) 363-6690

Pêches et Océans Canada / Fisheries and Oceans Canada Institut Maurice-Lamontagne / Maurice Lamontagne Institute

850, route de la Mer, C.P. 1000

Mont-Joli (Qc),

CANADA G5H 3Z4

Tél.: (418) 775-0568

https://ogsl.ca/ocean/

Attn: Denis Lefaivre

Chercheur scientifique / Research Scientist

Océanographie opérationnelle / Operational Oceanography

Courriel - email: denis.lefaivre@dfo-mpo.gc.ca

In collaboration with Environment and Climate Change Canada, the Canadian Ice Service and the Canadian Hydrographic Service, 48-hour forecasts of surface currents, sea ice, surface water temperature and water levels are available in real time for the Gulf of St Lawrence at: https://ogsl.ca

D.11.3 Water depths and tides

Department of Fisheries and Oceans

Canadian Hydrographic Service

615 Booth Street

Ottawa, Ontario K1A 0E6

Canada

Telephone: (613) 995-5249

Fax: (613) 996-9053

https://www.charts.gc.ca/chs

D.11.4 Ice-related information

Environment and Climate Change Canada

Meteorological Service of Canada

Prediction Service Operations – Atlantic and Ice

Analysis and Forecast Operations

719 Heron Road, Sir Leonard Tilley Building, Annex E

Ottawa, Ontario K1A 0H3

Canada

Email: ec.cisclients-scgclients.ec@canada.ca

National Research Council Canada

Canadian Hydraulics Centre

Building M-32, Montreal Road

Ottawa, Ontario K1A 0R6

Canada

Telephone: (613) 993-9381

Fax: (613) 952-7679

D.11.5 Canadian east coast seabed conditions

Natural Resources Canada

Geological Survey of Canada (Atlantic)

P.O. Box 1006

Dartmouth, Nova Scotia B2Y 4A2

Canada

Telephone: (902) 426-2396

Fax: (902) 426-6186

Annex E
(informative)

Sakhalin/Sea of Okhotsk

E.1 Description of the region

Sakhalin Island is located at the eastern side of the Siberian mainland. It is surrounded by the Sea of Okhotsk on the northern and eastern sides and the Tartar Strait, which separates Sakhalin from the mainland (see Figure E.1). The population density on Sakhalin is small and mostly lower than 1,5 people per square kilometre. The only town with significant population is Yuzhno-Sakhalinsk, having about 200 000 inhabitants.

The Sea of Okhotsk is separated from the Pacific Ocean by the Kuril Islands and the Kamchatka Peninsula. The Sea of Okhotsk is connected to the Sea of Japan and the Tartar Strait by La Perouse Strait. By far the largest river in the area is the Amur, covering a catchment area of about 2 million square kilometres. The average discharge of the river Amur is 11 750 m^3/s (371 km^3/year). Almost 75 % of the annual discharge occurs during spring and summer (May to September), whereas only 25 % of the annual discharge occurs during autumn and winter.

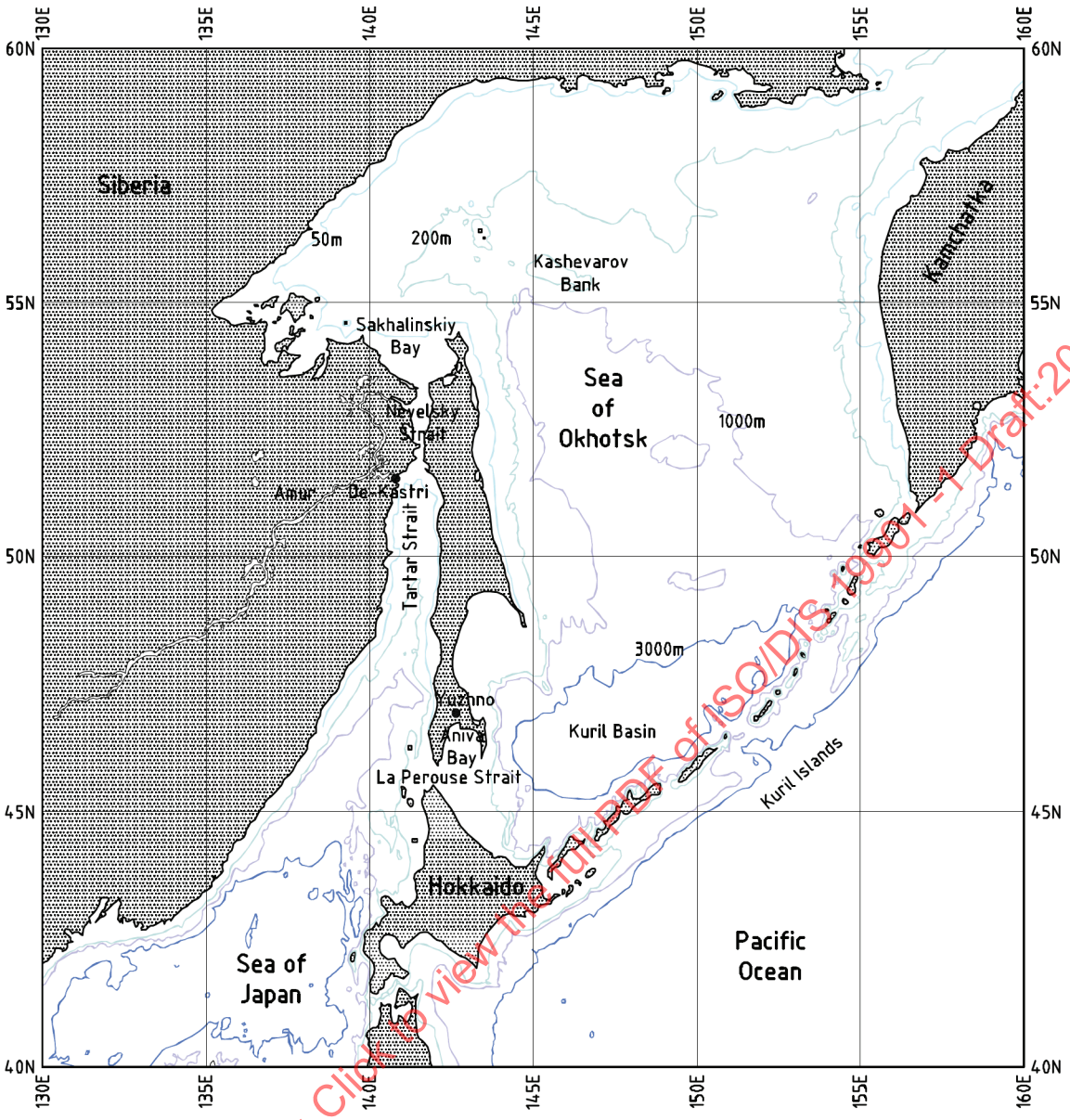

Figure E.1 — Map of Sakhalin showing locations of example metocean parameters

E.2 Data sources

Meteorological data for the Sakhalin area comes mainly from the Sakhalin Territorial Administration for Hydrometeorology and Environmental Monitoring (Sakhydromet) in Yuzhno-Sakhalinsk. Sakhydromet runs a comprehensive network of 35 observation stations, of which 21 are coastal stations. Observations of the most important meteorological parameters are made every 3 h. Depending on the station, continuous datasets over periods ranging from 10 years to more than 50 years are available.

Oceanographic data are available at Sakhydromet (mainly coastal observations of sea level, salinity and sea temperature) and at the Environmental Company of Sakhalin (ECS). Apart from the coastal observations, most of these data cover only small periods of time. Large amounts of current (profile) and water-level data were collected at several locations during periods of 6 months to 7 months in 1996-2003 along the Sakhalin northeast coast, in Aniva Bay (for one year) and near the De Kastri Terminal.

The most comprehensive hindcast database of winds, waves, (total) currents and water levels is the SIMOS-3 database, which was produced by Oceanweather as a Joint Industry Project. This database may provide

continuous hourly time series at hundreds of grid points all around Sakhalin Island over the period 1980 to 2005[130].

Sea-ice data collected in the area consists of airborne observations (over the period 1956-1990), satellite imagery, and local ice observations from coastal locations Based on these observations, ice maps were produced during several decades until the early 1990s. More recently, monthly or bi-weekly ice charts maps have been generated by the Arctic and Antarctic Research Institute (Russia) and the National Ice Centre (USA), mainly based on satellite imagery. Since the early 1930s, ice observations have been made at several coastal stations on Sakhalin Island. On the Sakhalin east coast, several marine radars were installed that are able to monitor the ice drift along the Sakhalin east coast.[131] More recently, large amounts of ice draft (and keel depth) data were collected by deploying ice profiling sonars at several locations along the Sakhalin northeast coast during periods of 6 to 7 months in 1996-2003. Finally, ice and ice/structure interaction observations have been made from the Molikpaq platform since its deployment in the Sea of Okhotsk in 1998.

E.3 Overview of regional climatology

Considering its longitude, latitude and marine location, the climate on Sakhalin is very severe, a result of its proximity to the Siberian continental land mass. The winter in Sakhalin is long and cold and the summer is short. In winter, strong winds from the continent may cause a drop in air temperature to –40 °C. In the southern part of the island winter temperatures are milder, but nevertheless there are frequent snowstorms, strong winds and generally heavy overcast cloud conditions.

Sea ice engulfs the coast from November to June in the north, from December to May along most of the east coast, and from January to March in Aniva Bay. The southwestern coastline of the island is always ice-free. Because of the presence of sea ice, the island is in fact an extension of the mainland during winter. Although the west coast climate is generally more severe than that of the east coast, ice extends further southward on the east coast of the island as a result of the cold southward–flowing East Sakhalin current. West of the island, the relatively warm Tsushima current flows northward on the western coast up to 51° N. Ice generally does not break up along the northern coast until the end of June.

The climate varies widely throughout Sakhalin, due to the mountain ranges that include peaks up to 1 400 m high, as well as the proximity of the sea. As a consequence, there is a large difference between the immediate coastal areas and the interior of the island. During winter, the sea provides additional warmth to the eastern coast, while during summer the sea significantly cools the northern and eastern portions of the island. This is attributed to the effect of the cold East Sakhalin current, as well as to the effect of the remaining drift ice. This effect contributes to the extreme fogginess along the eastern coastal areas in late spring and summer. Sunshine is rare in summer and the humid, cool weather is conducive to thick fog and drizzle.

E.4 Water depth, tides, storm surges and tsunamis

The Sea of Okhotsk consists of a moderately broad shelf to the north which gradually steepens to depths > 3 000 m to the south. Depths shallower than 200 m extend approximately 100 km off the coast of Kamchatka Peninsula and Sakhalin Island. Beyond the 200 m contour, the water depth increases to a broad area between 1 000 m and 2 000 m in the central part of the sea. Shallow banks are found in the northwestern basin, e.g. at the Kashevarov Bank.

The Sea of Japan is a deep basin with maximum depths of 3 700 m and has many of the circulation features found in deep ocean basins. The bottom topography slopes gently upward towards the northeast until reaching the Tartar Strait. Tartar Strait has a characteristic width of about 130 km. Water depths range from a maximum of 1 500 m in the south and a minimum water depth of about 4 m in the Nevelskoy Strait.

Tidal amplitudes vary widely over the area. Large tidal amplitudes have been observed along the shallow bays in the northwestern Sea of Okhotsk, in the Nevel'sky Strait, and near the northern edge of the Kuril Islands. Tides in the Sea of Okhotsk are dominated by diurnal constituents K1 and O1 whereas in most of the Tartar Strait, the semi-diurnal constituents M2 and S2 dominate[132].

Storm surges along the coastlines are mostly smaller than 1,5 m to 2,0 m. Only at specific locations, such as along the north side of Aniva Bay, may higher surges sometimes be observed during periods with strong

onshore winds. Tsunami waves may affect the area all around Sakhalin. Three sources may generally be distinguished:

a) trans-Pacific tsunamis caused by large earthquakes in the Pacific Ocean (typical period: 40-45 min),

b) tsunami sources in the Sea of Japan (typical period: 15 min), and

c) tsunamis caused along the Kuril Island chains (typical period: 12 min).

Extreme 100-year tsunami crest heights range from about 1,5 m along the Sakhalin east coast to about 2 m to 2,5 m in Aniva Bay.

E.5 Winds

The location of Sakhalin in the area between continental Asia and the Pacific Ocean is the major factor for its monsoonal climate.

During winter, a strong pressure gradient forms over Sakhalin, between the Siberian high-pressure system and the Aleutian low-pressure system, driven by the strong contrast in temperatures between the relatively warmer air over the Arctic Ocean and Bering and Okhotsk Seas and the much cooler air over the Siberian mainland. These strong pressure gradients produce consistently strong winds blowing from northerly directions (generally north and northwest) with prevailing speeds between 5 m/s and 10 m/s. The frequency and intensity of storms is highest during November and December. Extreme wind speeds during storms may reach 30 m/s to 35 m/s. Winter storms originate from the Chinese mainland or from waters near Japan, and they all tend to move northeastwards into the Bering Sea or Gulf of Alaska. Most of the storm tracks lie in the southern part of the island during winter.

The Siberian high-pressure system begins to break up in March, and the most rapid weather changes occur in April and May. Storms continue to move off the Asian mainland toward the western Aleutians. However the major storm tracks have, by this time of the year, moved northward and often cross Sakhalin Island. In spring, a high-pressure system starts to form over the Sea of Okhotsk, the high pressure being caused by the contrast between the cold frozen sea surface and the warming effect of the lands to the north.

With the onset of summer, the Siberian mainland becomes warmer than the surrounding seas, and a low-pressure system forms over the continent. Pressure gradients are weaker than in the winter, so the summer air circulation is less consistent over the region than during the winter. A large, semi-permanent, quasi-stationary high-pressure system dominates the entire North Pacific, including the Sea of Okhotsk. This pressure distribution generates predominantly light easterly or southeasterly winds (2 m/s to 5 m/s) that predominate across the island during the summer monsoon months. Extra-tropical storms, common during other months, decrease in number and intensity. The mean tracks run from the Chinese mainland northeastward to the Aleutians. Typhoons may affect the Sakhalin area during late summer. Such storms generally do not approach closely to the island, although the widespread clouds and precipitation may affect it. On occasion, typhoons leaving the East Asian Sea have caused cyclonic storms, associated with the polar front, to regenerate. In these cases, the storms stall and cause prolonged rainfall. Dying typhoons very occasionally enter the Sea of Okhotsk.

Autumn is a transitional season. The effects of the Pacific monsoon continue to enhance rainfall. Extratropical storms become more intense and frequent, causing the Aleutian low-pressure system to intensify and the North Pacific high-pressure system to weaken. Extra-tropical storms continue to form over the Asian continent and the waters around Japan. One of the principal storm tracks continues to cross Sakhalin Island. The other lies south of Japan. With the increase in storms, gales become more frequent.

E.6 Waves

The annual variation in wave climate is closely related to the atmospheric circulation over the Sea of Okhotsk. During the summer monsoon period (June to August), waves from the southeast or southerly sectors with heights between 0,5 m and 1,5 m occur mostly along the east coast. On the west coast, wave heights are often lower than 0,5 m during summer. In September, the wave height and direction become more variable in time because of the changing atmospheric processes, with prevailing waves of 1 m to 2 m along the east coast and

0,5 m to 1,5 m along the west coast. With the onset of the winter monsoons, the frequency of waves from the north and northeastern sectors grows in the Sea of Okhotsk. Prevailing wave heights are between 1,5 m and 2,5 m. In storms, wave heights are often between 5 m to 7 m high and they may even exceed 8 m during extremely severe storms. In the Tartar Strait, however, wave heights rarely exceed 4 m and are mainly from directions between southwest and northwest.

E.7 Currents

Both in the Sea of Okhotsk and Tartar Strait, a significant anti-clockwise residual current pattern is observed along its edges. In the centre of the Sea of Okhotsk, currents are usually small or negligible, whereas at the western boundary, along the Sakhalin east coast, there is a clear southward flow of water called the East Sakhalin Current.[133] Residual currents are highest at the northeastern tip of Sakhalin Island, where the eastward outflow from the Amur River and the anti-clockwise current in the Sea Of Okhotsk come together. Further south along the east coast, the residual current gradually decreases. Typical residual currents flow at between 0,2 m/s and 0,4 m/s. This cold southward flow occurs most of the year except for the months of May and June, when the flow sometimes reverses direction due to the prevailing south-southeasterly winds. Along the west coast of Sakhalin Island, a relatively warm northward flow occurs that may reach as far as 51° N.

Tidal currents are significant all around the island, except for the inner parts of Aniva Bay and some of the deeper parts of the Sea of Okhotsk and Tartar Strait where currents are mainly driven by the wind. Along the west coast of Sakhalin, semi-diurnal tidal constituents mainly control the current pattern. The highest tidal currents are found along the northeast coast of Sakhalin. This is due to the wide, shallow shelf in the northern part of the Sea of Okhotsk and the near-resonant trapping nature, because the natural frequency of the free oscillation is close to the diurnal tidal frequencies. This all results in a strong amplification of diurnal tidal currents, which are of the order of 1 m/s over the Kashevorov Bank[134] and even higher along the northeast coast of Sakhalin Island.

E.8 Sea ice

The ice cover that is found off Sakhalin Island is completely seasonal in nature, as the region is entirely ice-free during the summer and fall months. Only first-year ice is found in the area. It does not contain any multi-year ice floes, or glacial ice features such as icebergs. The waters off the eastern coastline of Sakhalin Island and in the northern half of the Tartar Strait are typically covered by sea ice for about half of the year.[135] The duration of the ice season gradually reduces southwards, to only 2 months in Aniva Bay. The southwestern coastline of Sakhalin Island is always ice-free, due to the northward flow of relatively warm water along the west coast.

Some indicative values for a number of ice parameters are given in Table E.1.

Table E.1 — Summary of ice conditions

Sea ice parameter	Indicative values of ice parameter					
	Sakhalin east coast (51° N to 55° N)		Aniva Bay (northern part)		Tartar Strait (50° N to 52° N)	
	Typical	Extreme	Typical	Extreme	Typical	Extreme
Start of ice season (date), ice concentration > 1/10	10 Dec	25 Nov	15 Jan	15-Dec	1 Nov	20 Oct
End of ice season (date), ice concentration < 1/10	1 June	15 June	1 Apr	20 Apr	15 Apr	10 May
Level ice thickness (m)	0,3 to 1,35	1,5	0,1 to 0,4	0,85	0,2 to 0,8	1,2
Rafted ice thickness (m)	1 to 2	3	0,2 to 0,8	1,25	0,5 to 0,8	1,5
Sail height (m)	1 to 2	5 to 6	0,5 to 1,0	3	0,5 to 1,0	2 to 4,5
Keel depth (m)	10 to 15	25	2,0 to 4,0	12	2 to 6	10
Ice movement (m/s)	0,5 to 1	1,5 to 2	0,1 to 0,2	0,7	0,3 to 0,5	1

Figures E.2 a) to g) show the probability lines of any ice in the Sea of Okhotsk in an average year.[136] Figures E.3 a) to g) show the probability lines of any ice in Tartar Strait in an average year [137].

At the start of the ice season mid-November, the first ice forms in the northerly and northwesterly reaches of the Sea of Okhotsk. Simultaneously, thin ice also forms locally in the shallow water parts along the Sakhalin northeast coast and in Sakhalinskiy Bay as air temperatures fall and the sea surface begins to cool.

During December, the ice formed in the northerly reaches of Sea of Okhotsk quickly spreads southwards under the influence of winds and currents, typically reaching locally formed ice cover off the northeast Sakhalin shelf in the early January period. In fact, most of the heavier ice that is found off the northeast coast of Sakhalin Island originates in the northwesterly part of the Sea of Okhotsk, which is often referred to as the “ice kitchen”. By mid January, the regional sea-ice has usually progressed towards the southern end of Sakhalin Island and the northern coast of Hokkaido, where ablation counterbalances its southward advance. Over the course of the winter, the ice cover continues to grow in general thickness and offshore extent, progressively becoming more heavily deformed with time, due to substantial relative motions within the pack. The winter pack-ice cover off Sakhalin Island typically reaches its maximum extent and severity sometime in March. Gradual loosening and deterioration of the ice begins to occur thereafter, as air temperature rises and spring approaches. Break-up usually commences in early to mid-May, with complete ice clearance normally seen by early June.

An important feature of the ice conditions that are found on the northeast Sakhalin shelf is the periodic presence of a band of open water or very thin ice, running parallel to the coast between the narrow land-fast ice zone and the heavier pack-ice areas towards the east. This feature, termed a flaw lead or polynya, is transient but may persist for periods of a few days to several weeks during winter. Flaw lead conditions occur in particular during the period early January to early March, when predominant winds and ice motions are from the northerly quadrants. From mid-March onwards, flaw lead conditions occur less frequently, because wind and ice drift directions become more mixed, and are often from south to north or from east to west.

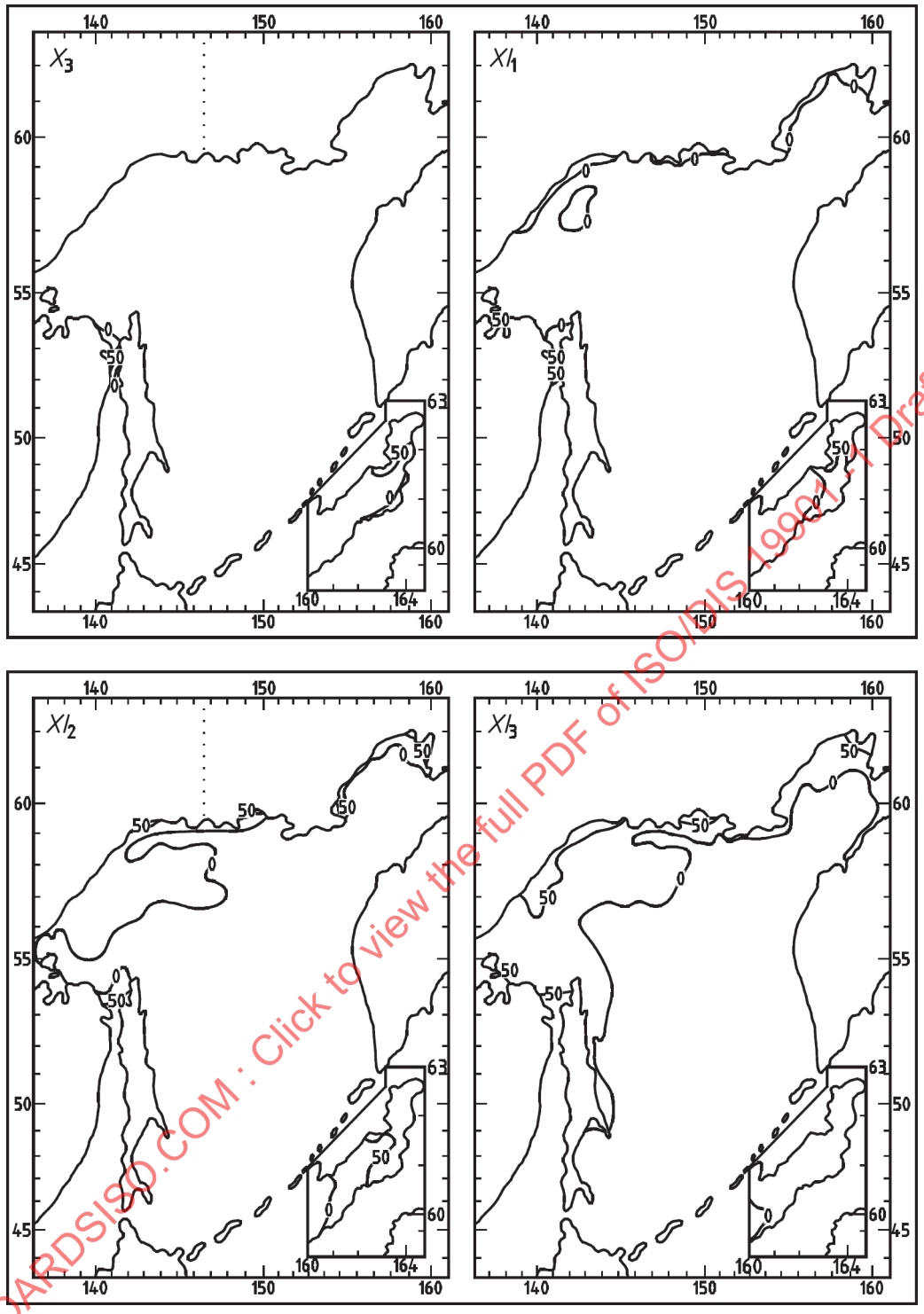

a) Probability lines of any ice in the Sea of Okhotsk — October (3rd period) to November (3rd period)

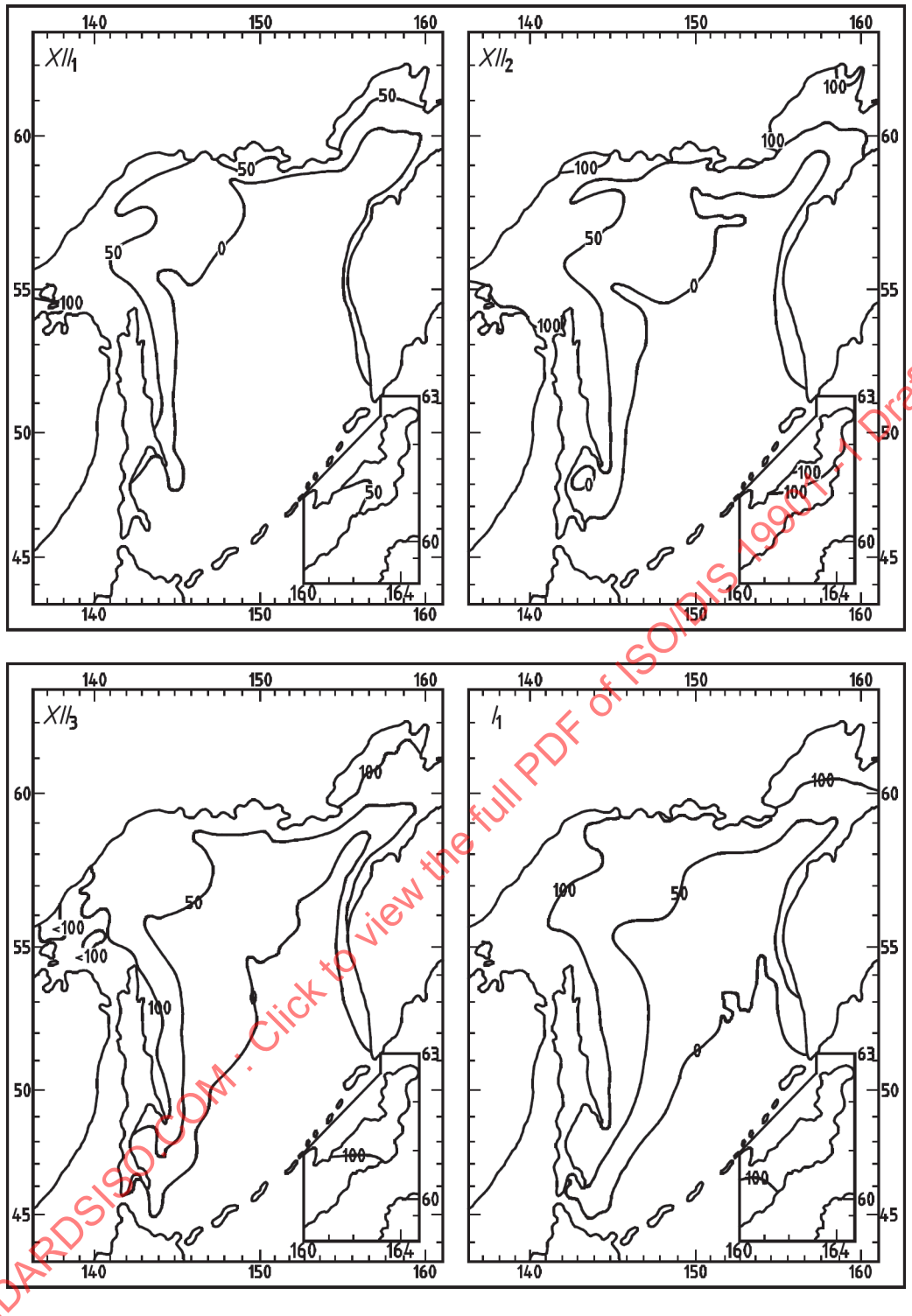

b) Probability lines of any ice in the Sea of Okhotsk — December (1st period) to January (1st period)

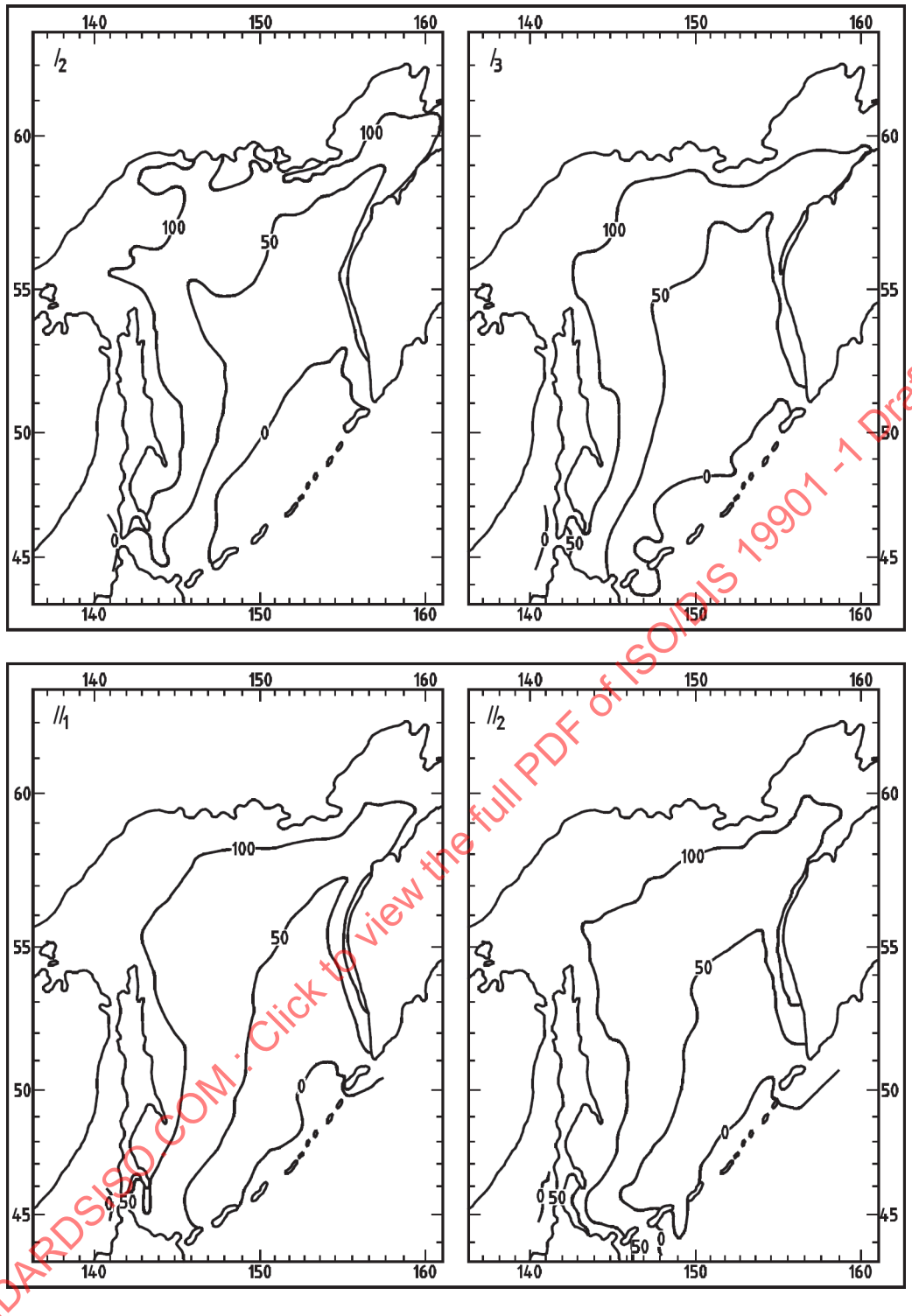

c) Probability lines of any ice in the Sea of Okhotsk — January (2nd period) to February (2nd period)

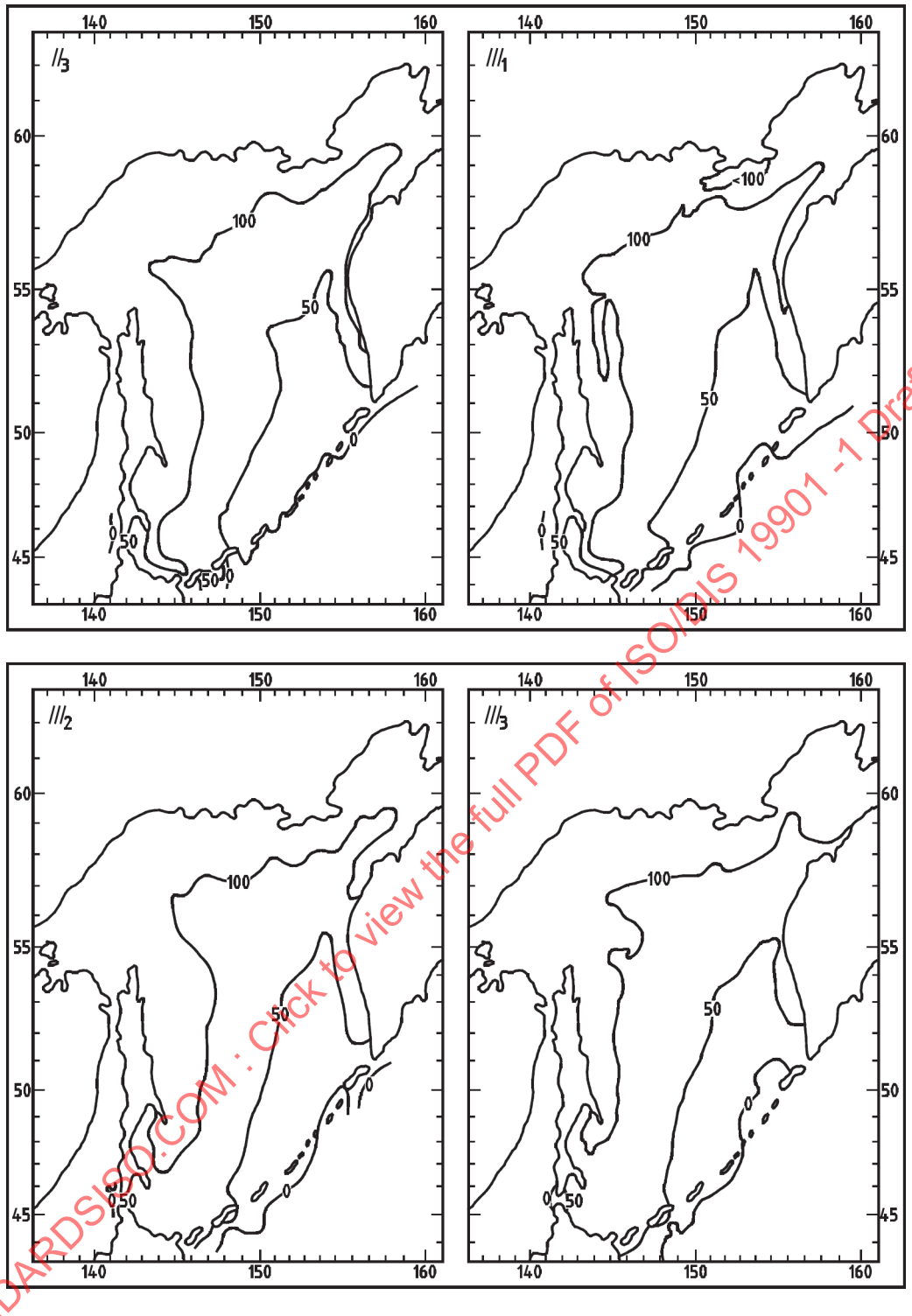

d) Probability lines of any ice in the Sea of Okhotsk — February (3rd period) to March (3rd period)

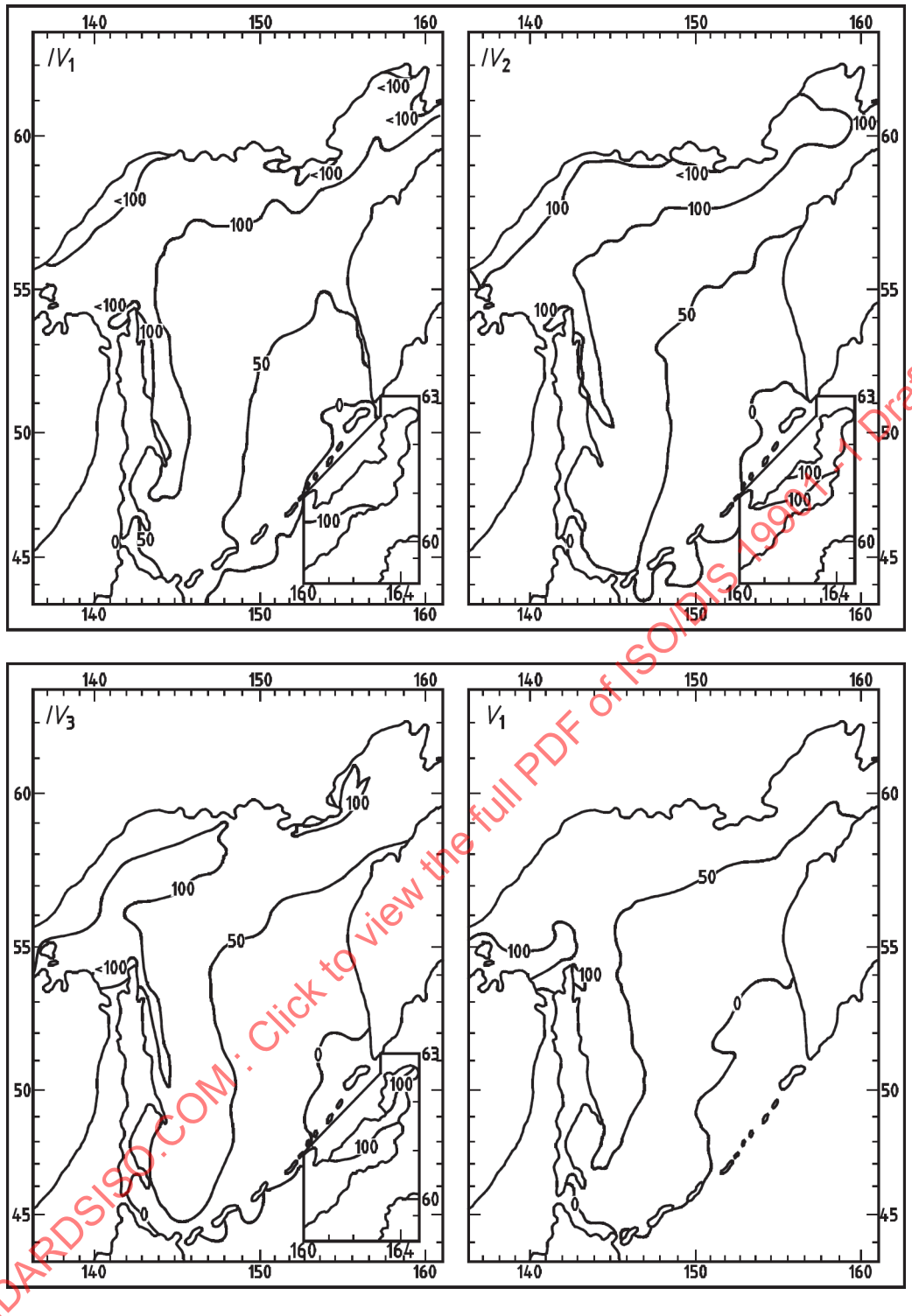

e) Probability lines of any ice in the Sea of Okhotsk — April (1st period) to May (1st period)

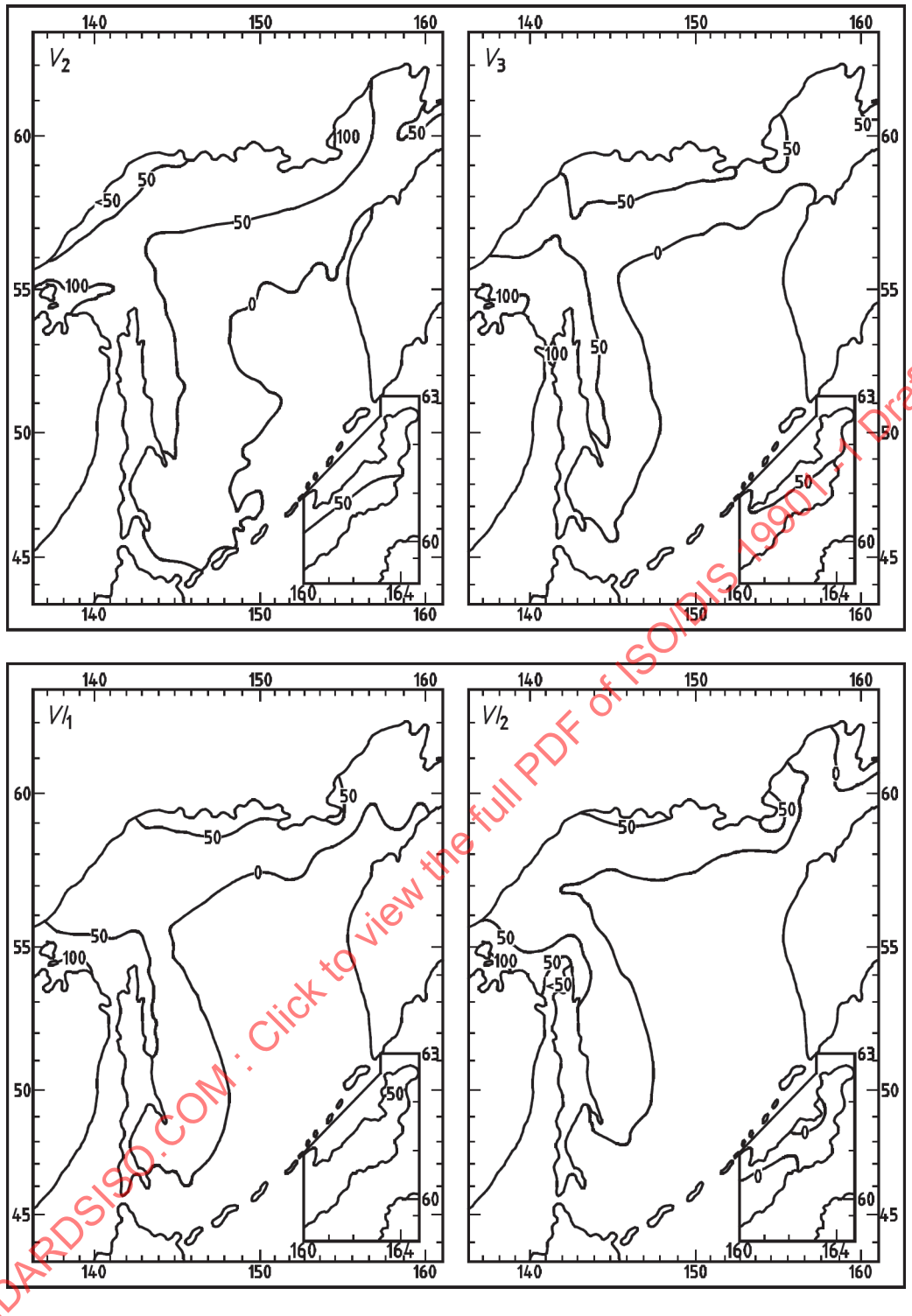

f) Probability lines of any ice in the Sea of Okhotsk — May (2nd period) to June (2nd period)

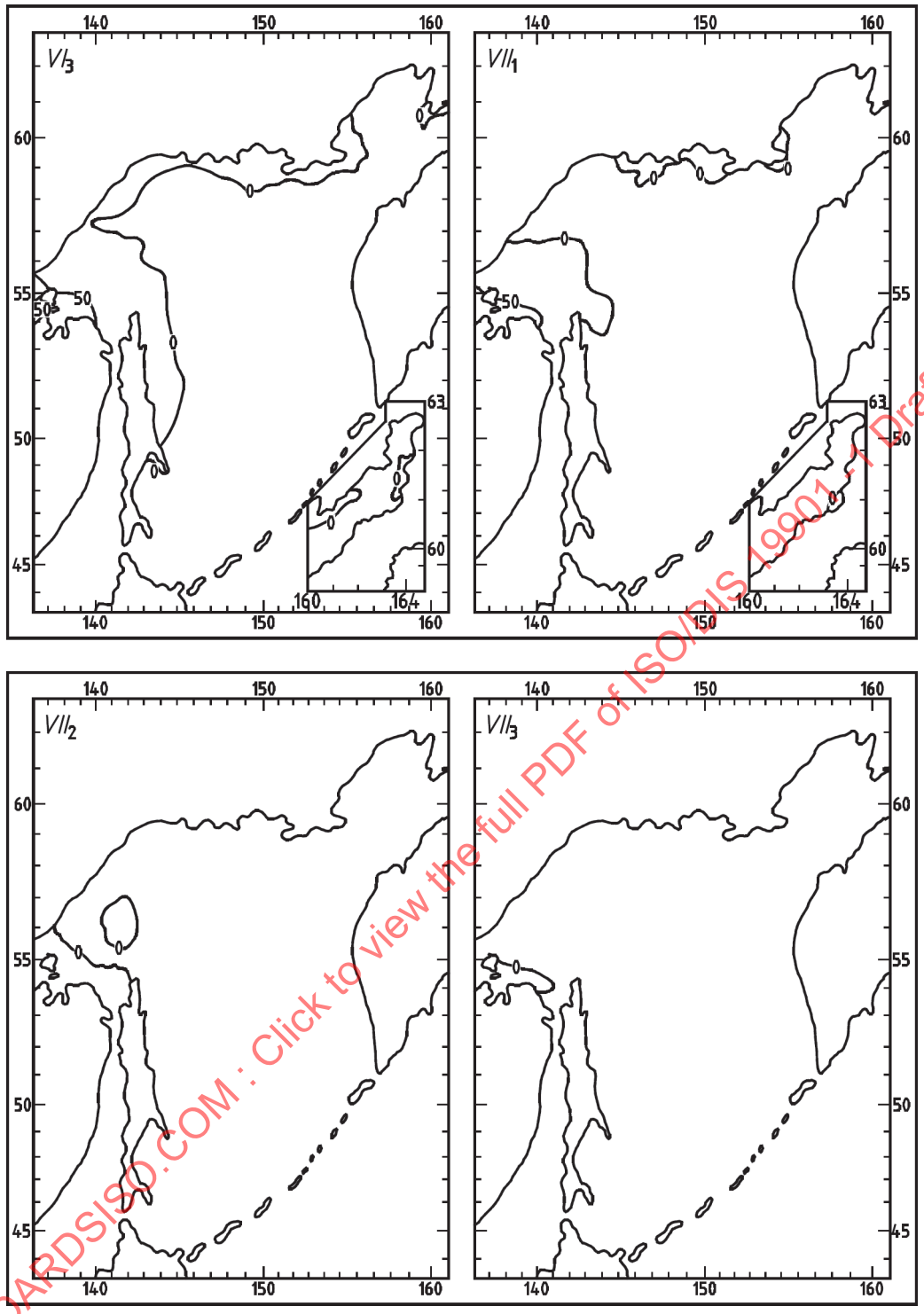

g) Probability lines of any ice in the Sea of Okhotsk — June (3rd period) to July (3rd period)

NOTE Index in the upper left corner indicates month (Roman numeral) and 10-day period in the month.

Figure E.2 — Probability of any ice in an average year[136] per given 10-day period

Figure E.3 a) to g) shows the probability lines of any ice in the Tartar Strait in an average year.[137] In contrast to the ice found in the Sea of Okhotsk, the ice in the Tartar Strait is much less deformed, due to slower current speeds and also the milder wave climate. Ice formation in the Tartar Strait starts end of November. During January and February, the ice extent and ice thickness steadily grow. In March, the area north of 49° N. is mostly covered with sea ice. Depending on prevailing wind direction, the heaviest ice is found along the

Sakhalin west coast or against the Siberian mainland. Depending upon the wind direction, leads are often formed along one of these coastlines, which may be used by vessels moving through the ice northwards or southwards. During early April melting starts, and in early May most of the Tartar Strait is free of ice, whereas there is usually still some ice around along the Sakhalin east coast around that time.

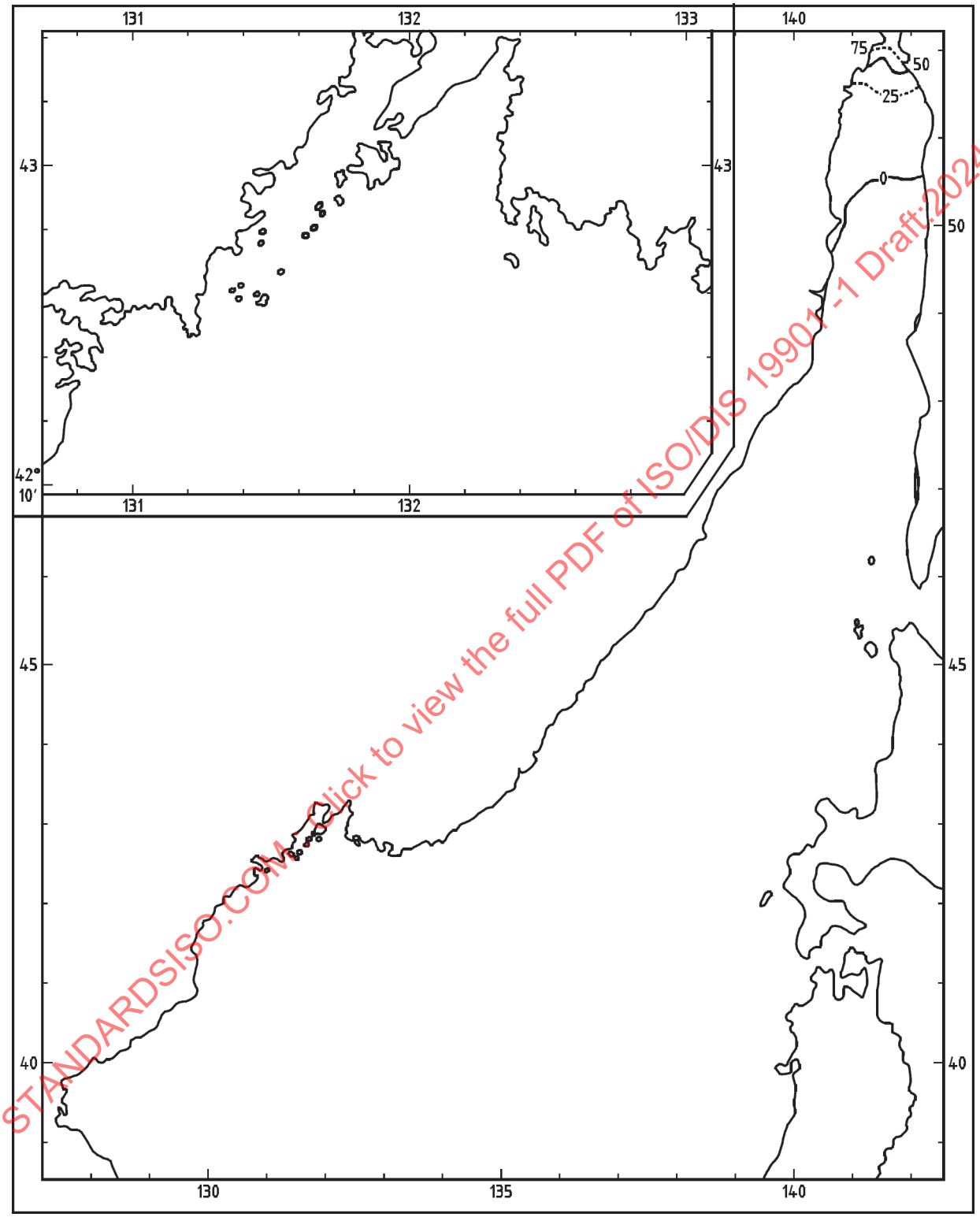

a) Probability of any ice in the Tartar Strait — Mid-November

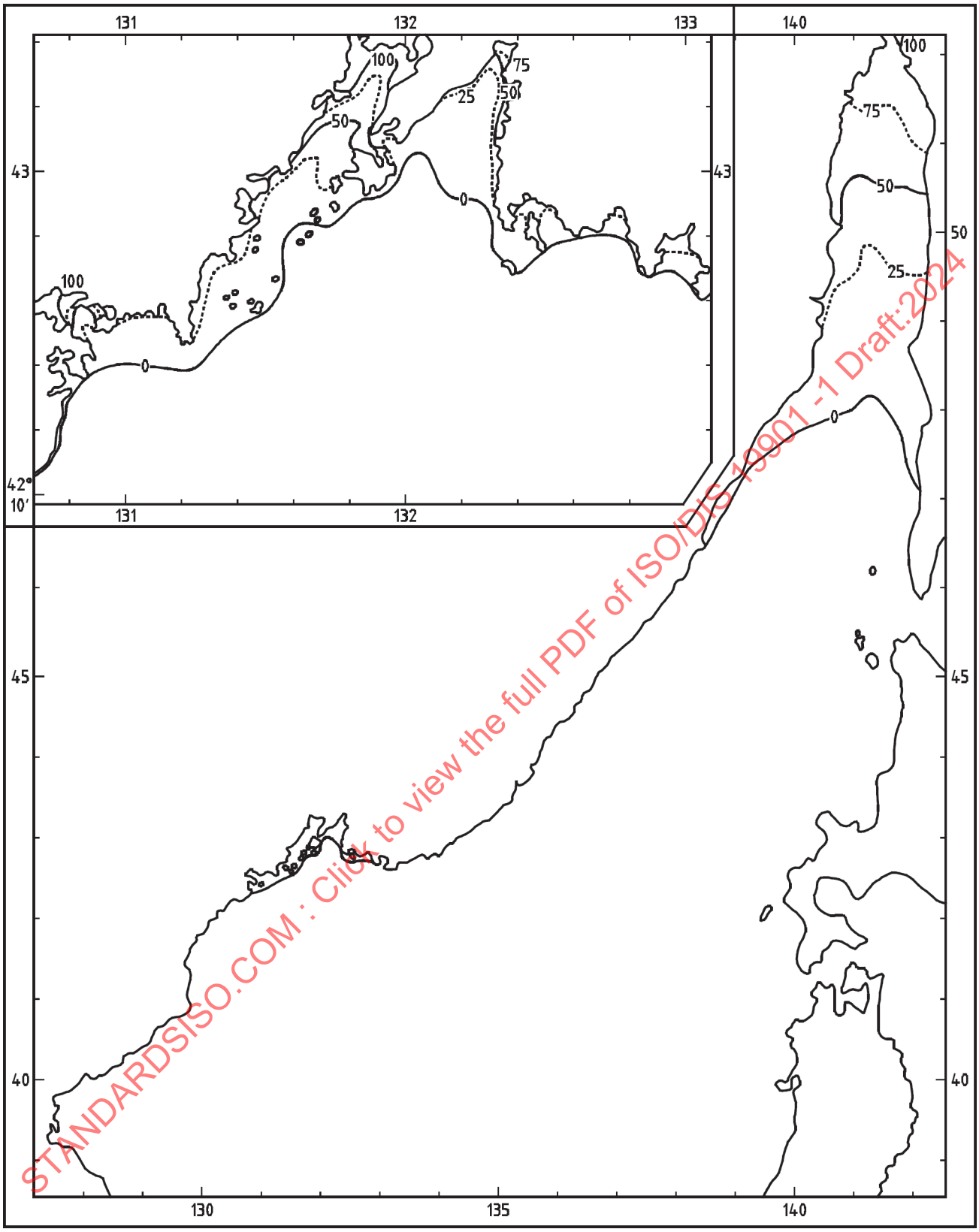

b) Probability of any ice in the Tartar Strait — Mid-December

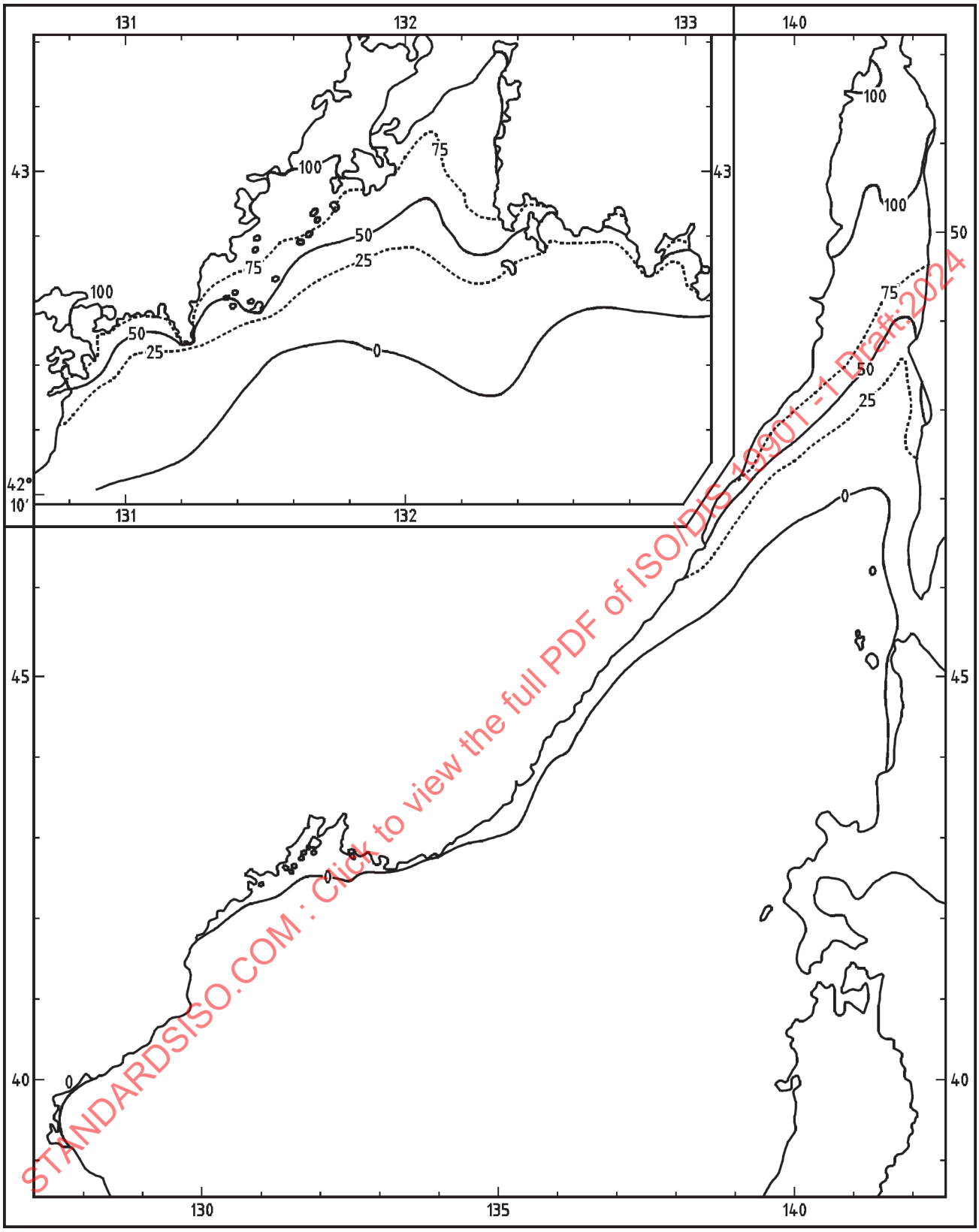

c) Probability of any ice in the Tartar Strait — Mid-January

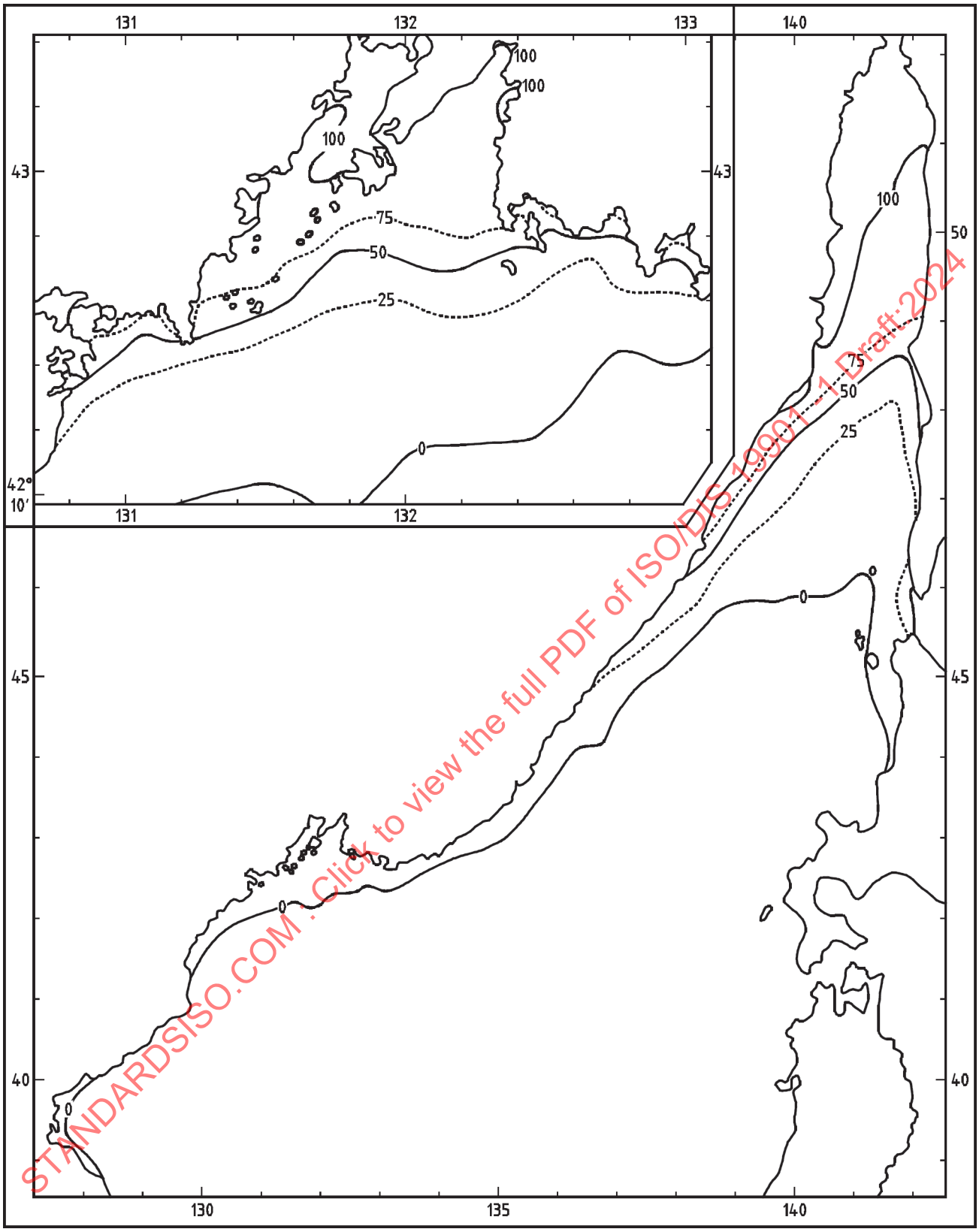

d) Probability of any ice in the Tartar Strait — Mid-February

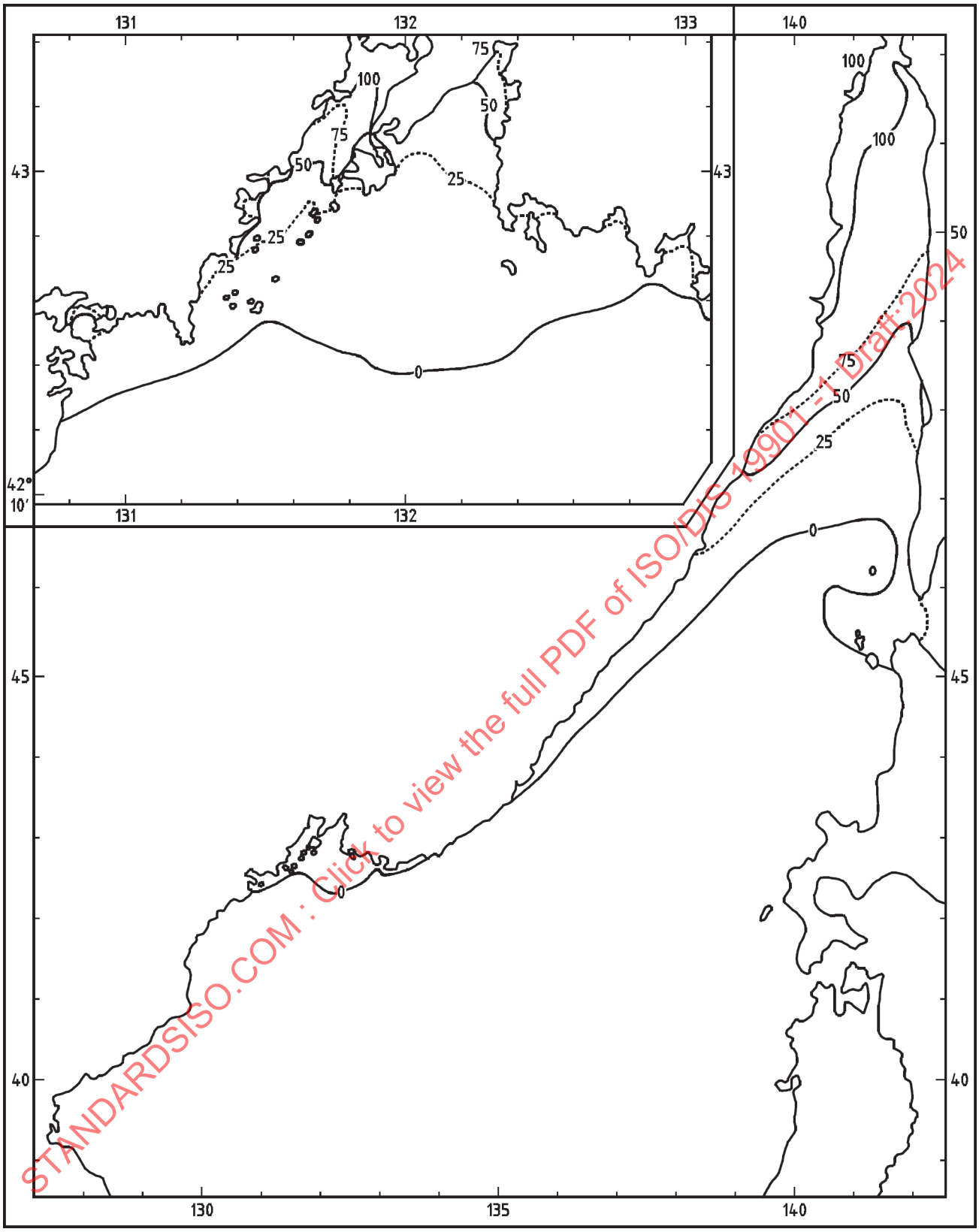

e) Probability of any ice in the Tartar Strait — Mid-March

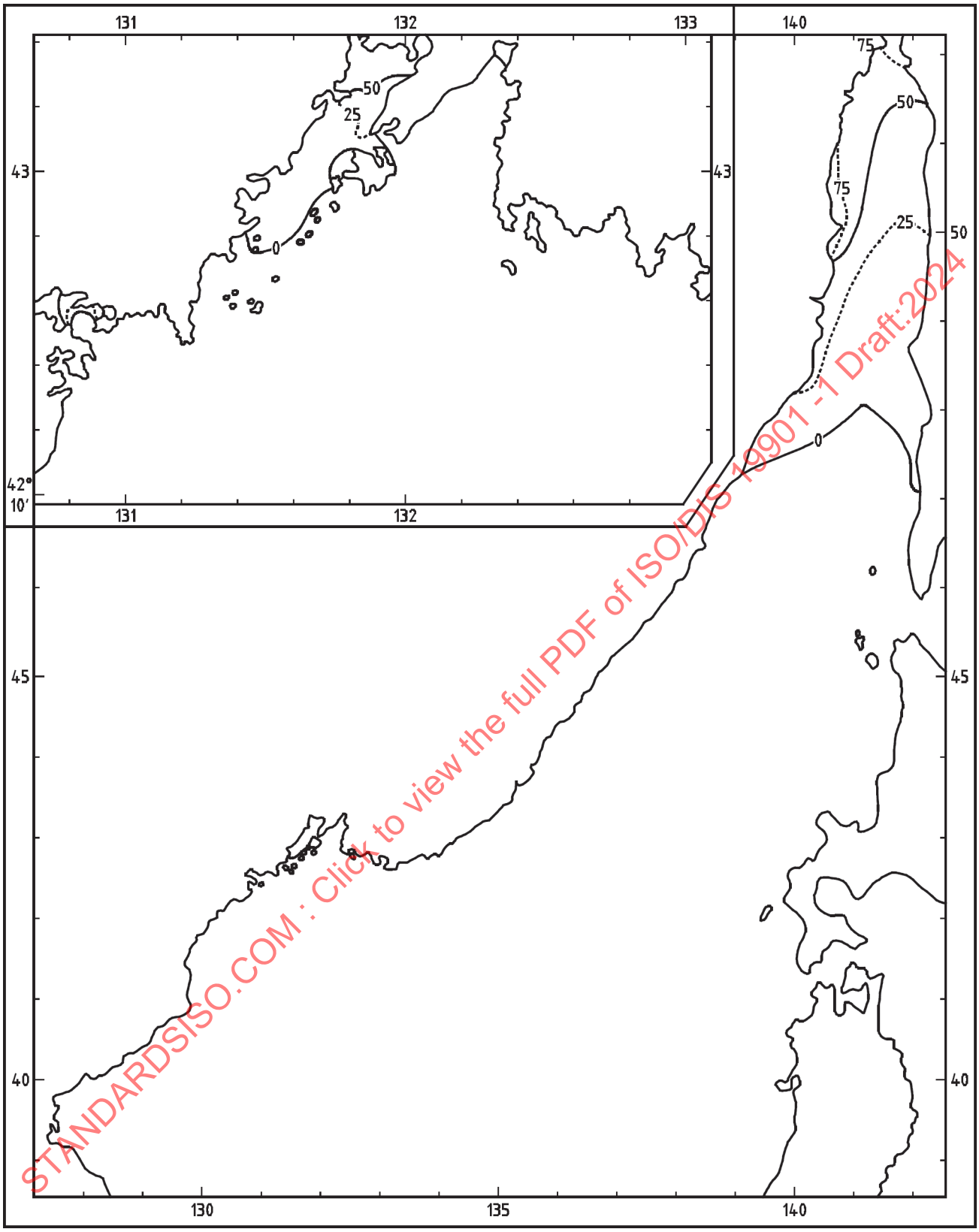

f) Probability of any ice in the Tartar Strait — Mid-April

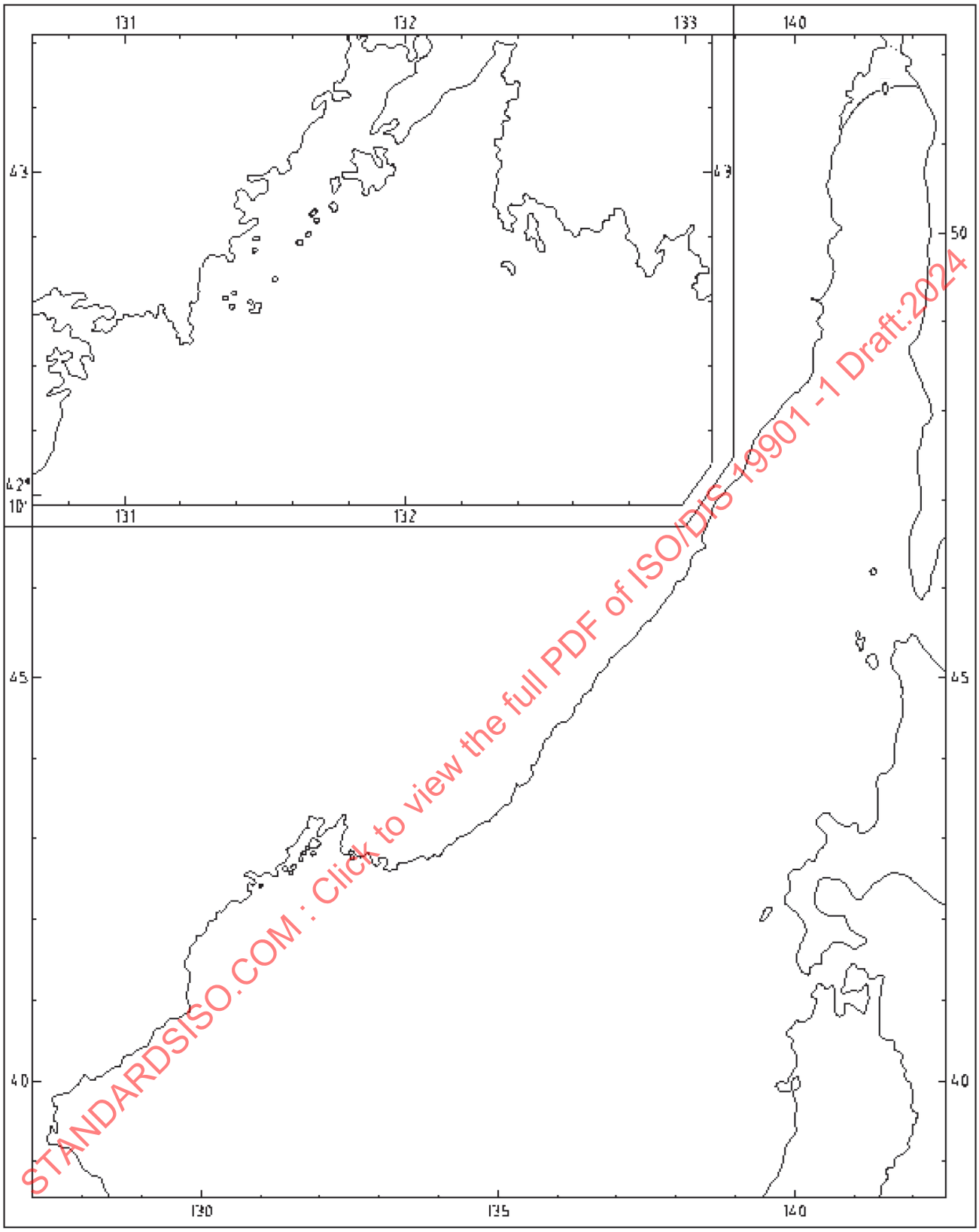

g) Probability of any ice in the Tartar Strait — Mid-May

Figure E.3 — Probability of any ice in the Tartar Strait in an average year [137]

E.9 Other environmental factors

E.9.1 Air temperature, precipitation, humidity and visibility

In winter, typical air temperatures range from −25 °C in the northwestern parts of the Sea of Okhotsk to −10 °C just south of Sakhalin Island. Absolute minima are considerably less than this, and may reach as low as −40 °C in the north and −30 °C in the south. In summer, typical air temperatures range from 10 °C in the north to almost 20 °C just south of Sakhalin Island. Absolute maxima range between 30 °C and 35 °C.

Low visibility and fog occur when the cooler sea meets relatively warm air. Fog occurs in particular along the Sakhalin east coast during summer, when the relatively warm and moist air is cooled by the cold seawater. Along the Sakhalin west coast, fog occurs less frequently due to the northward flow of relatively warm water.

Precipitation (which may be rain, sleet or snow) varies greatly across the island, largely due to its topography. The Pacific slopes of Sakhalin Island are particularly wet. Precipitation on the island is highest during the April to October warm season, with smaller amounts falling during the November to March cold season. Except for the northernmost tip of the island, the maximum precipitation falls in September for most locations. The mean annual precipitation ranges from < 600 mm/year in the northern parts of Sakhalin Island to > 1 100 mm/year locally in the south.

E.9.2 Sea temperature and salinity

In general, the sea surface temperature increases from north to south. Significant annual variations in sea temperature occur throughout the area, which attenuate with depth. Between May and November sea temperatures are positive, with the warmest water found near La Perouse Strait and near Hokkaido Island. During October and November, sea temperatures drop significantly to −1 °C to −1,8 °C, resulting in a large part of the Sea of Okhotsk and the Tartar Strait becoming covered with ice.

The salinities in the Sea of Okhotsk and Tartar Strait are largely determined by a balance between precipitation and evaporation, the effect of sea-ice formation and the discharge of fresh water, in particular by the Amur River. During summer and autumn, the salinity is generally less than during winter, when it increases due to sea-ice formation and a significant reduction of the continental freshwater discharge. During summer there is a marked salinity minimum around the northern tip of Sakhalin Island, associated with the freshwater discharge of the Amur.

E.9.3 Snow, atmospheric icing and sea-spray icing

On Sakhalin Island, snow cover generally persists for up to 200 days per year. Snow is expected in September in the north and by October along the entire coast. The snow season extends until May in the south and June in the north. About 70 to 90 days of snow occur yearly along Sakhalin Island shores. Blizzards occur frequently in winter, especially along coasts exposed to the north and west winds. Along the coasts, the snow melts in April or May, melting a few weeks later in the interior. Mean winter snowfall during a blizzard is typically between 10 cm and 15 cm. In the northern half of the island in the mountains, the maximum accumulated depth of snowfall may reach 100 cm but at most places it is usually not higher than 40 cm to 60 cm.

Ice accumulation on the hulls of floating vessels and on superstructures has the potential to become a serious hazard in the Sakhalin area. Atmospheric icing may occur when saturated air moves against a surface with temperatures below freezing (rime ice), during periods of fog which are accompanied by freezing conditions, and during freezing rain or drizzle (glaze ice). Sea-spray icing may occur if the air temperature is near the freezing point of seawater. Immediately near the sea surface, the main role is played by sea-spray icing. Its intensity decreases with height. From heights exceeding 40 m, atmospheric icing is predominant. Sea-spray icing may be considered negligible at elevations above 50 m to 60 m. In the Sakhalin area, sea-spray icing mainly occurs from October to December when the seawater is not yet frozen. In Aniva Bay it may occur throughout the entire winter period.

E.9.4 Waves in ice

Waves in ice regularly occur during winter along the Sakhalin east coast, in particular when the pack ice/open sea boundary is in the vicinity of the monitoring site. Waves may easily penetrate into the outer pack

ice with a thickness of 1,5 m to 2,5 m. Low-frequency waves have been observed in ice up to hundreds of kilometres from wave source regions[137].

E.10 Estimates of metocean parameters

E.10.1 Extreme metocean parameters

Indicative extreme values of metocean parameters are provided in Tables E.2 to E.8 for four areas around Sakhalin. The wind, wave and current values are independently derived marginal parameters; no account has been taken of conditional probability. As for all indicative values provided within the regional annexes of this part of ISO 19901, these data are provided to assist preliminary engineering concept selection; they are not suitable for design of offshore structures.

Table E.2 — Indicative values of metocean parameters — Sakhalin east coast (52,5° N to 55° N and water depths from 30 m to 100 m)

Metocean parameter	Return period *N* years				
	1	5	10	50	100
10-min mean wind speed (m/s)	24	27	29	31	32
Significant wave height (m)	8	9	9,5	10,7	11,5
Spectral peak period (s) [a]	12,9	13,7	14,1	14,9	15,5
Surface current speed (m/s) [b]	2,3	2,6	2,7	2,9	3,0
[a] Assume the peak spectral period may vary by ±10 % around these central estimates.					
[b] Assume the extreme current may vary by ±30 % around these central estimates.					

Table E.3 — Indicative values of metocean parameters — Sakhalin east coast (51° N to 52,5° N and water depths from 30 m to 100 m)

Metocean parameter	Return period *N* years				
	1	5	10	50	100
10-min mean wind speed (m/s)	25	28	30	34	36
Significant wave height (m)	8,5	9,5	10	10,7	11,5
Spectral peak period (s) [a]	13,3	14,1	14,4	14,9	15,5
Surface current speed (m/s) [b]	1,5	1,7	1,8	1,9	2,0
[a] Assume the peak spectral period may vary by ±10 % around these central estimates.					
[b] Assume the extreme current may vary by ±30 % around these central estimates.					

Table E.4 — Indicative values of metocean parameters — Aniva Bay (central, northern half)

Metocean parameter	Return period *N* years				
	1	5	10	50	100
10-min mean wind speed (m/s)	26	28	29	31	32
Significant wave height (m)	4,8	5,5	6	6,7	7,0
Spectral peak period (s) [a]	10	10,7	11,2	11,8	12,1
Surface current speed (m/s)	0,5	0,6	0,65	0,67	0,7
[a] Assume the peak spectral period may vary by ±10 % around these central estimates.					

Table E.5 — Indicative values of metocean parameters — Tartar Strait (51° N to 52° N and water depth of about 30 m)

Metocean parameter	Return period *N* years				
	1	5	10	50	100
10-min mean wind speed (m/s)	26	30	32	37	38
Significant wave height (m)	5,5	6	6,5	7	7,5
Spectral peak period (s) [a]	10,7	11,2	11,6	12,1	12,5
Surface current speed* (m/s)	0,3	0,4	0,6	0,7	0,8

[a] Assume the peak spectral period may vary by ±10 % around these central estimates.

Table E.6 — Monthly air temperature in Korsakov (46° 37′ N, 142° 47′ E) from 1966 to 2000

	Monthly air temperature °C												
	Jan	Feb	Mar	Apr	May	Jun	Jul	Aug	Sep	Oct	Nov	Dec	Year
Mean	−10,5	−9,9	−4,8	1,5	6,1	10,4	14,8	16,7	13,7	7,7	−0,1	−6,3	3,3
Highest	3,0	4,6	8,8	16,5	23,7	27,7	28,6	30,4	27,3	21,8	15,5	7,9	30,4
Lowest	−32,7	−29,1	−25,2	−17,5	−9,0	−2,2	1,7	4,6	−2,2	−8,0	−19,1	−26,2	−32,7

Table E.7 — Monthly air temperature in Odoptu (53° 22′ N, 143° 10′ E) from 1975 to 2000

	Monthly air temperature °C												
	Jan	Feb	Mar	Apr	May	Jun	Jul	Aug	Sep	Oct	Nov	Dec	Year
Mean	−18,5	−16,8	−12,0	−3,7	1,1	6,0	10,5	13,0	9,9	3,1	−7,3	−14,4	−2,4
Highest	−0,1	−0,8	8,0	11,8	25,6	31,3	32,1	32,4	25,0	17,8	9,0	1,0	32,4
Lowest	−38,6	−35,0	−33,2	−26,1	−11,0	−2,8	0,6	3,5	−0,4	−15,4	−25,2	−33,6	−38,6

Table E.8 — Sea temperature ranges — Indicative monthly-mean values

Area	Sea surface temperature °C	Sea floor temperature °C
Sakhalin east coast (49° N to 54° N)	−1,8 to +11	−1,8 to +2
Aniva Bay	−1,8 to +18	−1,8 to +14
Tartar Strait	−1,8 to +16	−1,8 to +10

E.10.2 Long-term distributions of metocean parameters

Long-term joint frequency distributions of the significant wave height H_s *versus* the spectral peak period are given in Tables E.9 to E.11 for three locations around Sakhalin Island based on the 25-year continuous hindcast data.[130] The presence of sea ice is indicated by $H_s < 0{,}01$.

Table E.9 — Percentage occurrence of total significant wave height *vs.* spectral peak period offshore Sakhalin NE coast (52,50° N, 143,66° E)

Significant wave height m	Spectral peak period s										
	0 to 1,99	2 to 3,99	4 to 5,99	6 to 7,99	8 to 9,99	10 to 11,99	12 to 13,99	14 to 15,99	16 to 17,99	> 18	TOTAL
< 0,01											33,38
0,01 to 0,99	0,51	3,74	13,74	9,36	3,19	0,49	0,08	0,00	0,00	0,00	31,11
1,00 to 1,99		0,13	9,01	7,96	5,59	1,67	0,40	0,05	0,00	0,00	24,80
2,00 to 2,99			1,07	3,04	1,97	1,04	0,27	0,06			7,44
3,00 to 3,99			0,00	0,50	0,94	0,59	0,15	0,02			2,20
4,00 to 4,99				0,03	0,27	0,31	0,09				0,71
5,00 to 5,99				0,00	0,03	0,15	0,07	0,00			0,25
6,00 to 6,99					0,00	0,04	0,04	0,00			0,08
7,00 to 7,99						0,00	0,01				0,01
8,00 to 8,99							0,01				0,01
TOTAL	0,51	3,86	23,82	20,89	11,98	4,30	1,10	0,14	0,00	0,00	100,0

Table E.10 — Percentage occurrence of total significant wave height *vs.* spectral peak period in Aniva Bay (46,45° N, 142,75° E)

Significant wave height m	Spectral peak period s										
	0 to 1,99	2 to 3,99	4 to 5,99	6 to 7,99	8 to 9,99	10 to 11,99	12 to 13,99	14 to 15,99	16 to 17,99	> 18	TOTAL
< 0,01											6,34
0,01 to 0,99	3,55	40,09	20,13	3,03	0,98	0,46	0,34	0,11	0,00	0,00	68,70
1,00 to 1,99		0,30	19,24	1,68	0,12	0,01	0,01	0,01			21,36
2,00 to 2,99			1,24	1,83	0,10	0,00	0,00				3,18
3,00 to 3,99			0,00	0,26	0,10	0,00	0,00				0,37
4,00 to 4,99				0,00	0,03	0,00					0,04
5,00 to 5,99					0,01	0,00					0,01
6,00 to 6,99					0,00						0,00
TOTAL	3,55	40,39	40,61	6,80	1,35	0,48	0,35	0,12	0,00	0,00	100,0

Table E.11 — Percentage occurrence of total significant wave height *vs.* spectral peak period in northern Tartar Strait (51,48° N, 141,44° E)

Significant wave height m	Spectral peak period s										
	0 to 1,99	**2 to 3,99**	**4 to 5,99**	**6 to 7,99**	**8 to 9,99**	**10 to 11,99**	**12 to 13,99**	**14 to 15,99**	**16 to 17,99**	**> 18**	**TOTAL**
< 0,01											21,81
0,01 to 0,99	3,64	25,96	18,59	3,14	0,50	0,05					51,89
1,00 to 1,99		0,19	17,82	2,48	0,17	0,02					20,68
2,00 to 2,99			1,69	2,86	0,13	0,00					4,68
3,00 to 3,99			0,00	0,43	0,38	0,00					0,80
4,00 to 4,99				0,01	0,10	0,00					0,12

Table E.11 *(continued)*

Significant wave height m	**Spectral peak period** s										
	0 to 1,99	**2 to 3,99**	**4 to 5,99**	**6 to 7,99**	**8 to 9,99**	**10 to 11,99**	**12 to 13,99**	**14 to 15,99**	**16 to 17,99**	**> 18**	**TOTAL**
5,00 to 5,99					0,00	0,01					0,01
6,00 to 6,99						0,00					0,00
TOTAL	3,64	26,15	38,10	8,92	1,28	0,09	0,00	0,00	0,00		100,0

Annex F
(informative)

Caspian Sea

F.1 Description of the region

This annex covers the Caspian Sea region. The Caspian Sea is situated east of the Black Sea, roughly within the coordinates 36° N to 47° N and 47° E to 54° E. It is a land-locked sea and extends approximately 1 200 km from north to south, with an average width of 325 km east to west, covering a total area of some 400 000 km^2[138]. As of 2018, the mean sea level (MSL) of the Caspian Sea was –about 27,9 m below Baltic Datum (equivalent to global mean sea level) and 0,1 m above Caspian Datum.

The Caspian Sea offers unique challenges to the oil and gas industry. The northern area is characterized by shallow water and is subject to winter icing and negative surges that may limit marine operations. The northern area also receives a large volume of freshwater discharge from rivers such as the Volga and Ural. The meteorology of the Caspian is complex, with the presence of nearby mountain ranges also causing significant area variations [138].

The Caspian may be considered to have four parts: northern, central, Apsheron and southern (Figure F.1). The north and central areas may be considered to be separated by a line from Chechen Island to Bautino, while the central and southern areas may be considered to be separated by the Apsheron Ridge, which stretches across the Caspian from Baku to Turkmenbashy. Most of the northern Caspian Sea is very shallow, with water depths of 9 m or less. In the northeast Caspian Sea, water depths are around 3 to 4 m The central Caspian Sea in the Derbent Depression has a depth of 788 m at its deepest point, while the southern Caspian has a maximum depth of 1 025 m in the South Caspian Depression. The Apsheron ridge, stretching from between Apsheron peninsula and the Cheleken peninsula, which separates the central and southern Caspian Seas, has water depths of less than 200 m.

The nations bordering the Caspian Sea region, and their corresponding lengths of coastline,[138] are:

— Azerbaijan: 850 km;

— Iran: 900 km;

— Kazakhstan: 2 320 km;

— Russia: 695 km; and

— Turkmenistan: 1 200 km.

In the middle Caspian Sea, the continental shelf is limited to depths of about 100 m. The shelf is narrow (about 40 km) along the western coast, but much wider (about 130 km) along the eastern coast. The continental slope extends between the shelf edge with depths of 500 m to 600 m[139].

In the southern Caspian Sea, the continental slope is very steep and extends to depths of 700 m to 800 m. The width of the continental shelf is broadly similar to that of the middle Caspian Sea, except on the southern coast where it is much narrower, with depths of 400 m only 5 km to 6 km from the coast[138].

Key

1	North	2	Central	3	Apsheron	4	South

Figure F.1 — Map of the Caspian Sea,[140] showing four designated regions: northern, central, Apsheron and southern Caspian

F.2 Data sources

The Caspian Environment Programme website, https://www.caspianenvironment.org/caspian.htm, gives a general overview of the Caspian Sea region. The book *The Caspian Sea*[138] describes the metocean conditions encountered in the Caspian Sea, and specifically refers to the ice conditions that may be expected in the northern Caspian Sea during the winter months.

Publicly available measured and modelled data are limited for the offshore areas of the Caspian Sea; most measured data are confined to land and coastal stations. With the growth in offshore oil industry activity from the late 1990s onwards, more extensive offshore metocean and ice data have now been collected. A number of national Institutions have carried out hindcast modelling of the Caspian Sea. In 2002, a dedicated oil industry Joint Industry Project (CASMOS: Caspian Sea Meteorological and Oceanographic Study [141]) hindcast the wind, wave, water-level and current conditions for the Caspian Sea. In 2006 to 2007, this work was updated to produce a 50-year continuous hindcast of metocean conditions on a grid of 10 km × 10 km at hourly intervals[142].

Following the Second World War, the Astrakhan Hydrometeorological Observatory routinely collected ice data. However in 1984/85 data collection ceased, and ice reports have not been available from this source since then (see Figure F.2). From 1992 onward, earth-observing satellites have collected data on ice coverage.

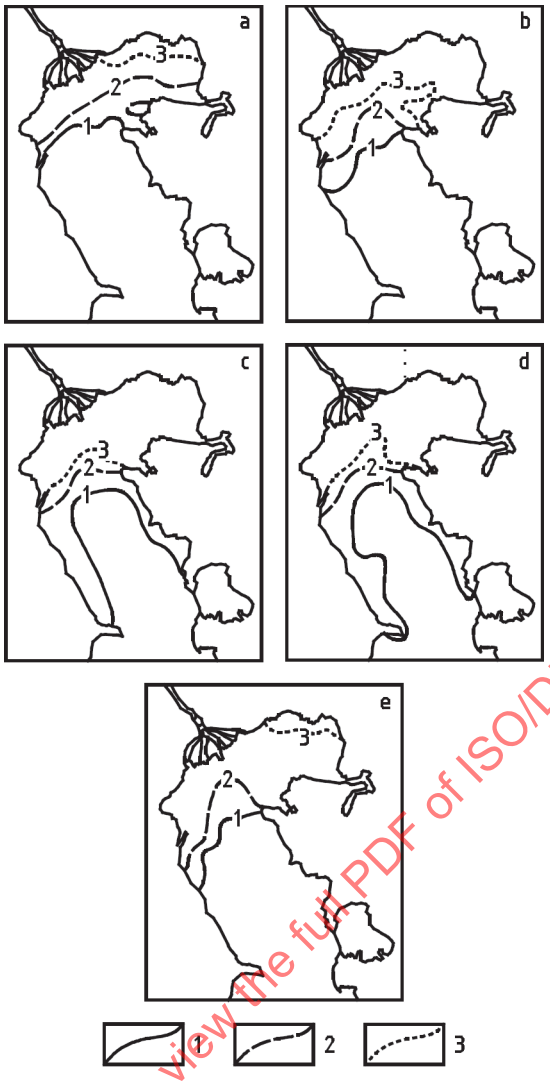

Key

a	November	b	December
c	January	d	February
e	March		
1	severe winter		
2	moderate winter		
3	mild winter		

Figure F.2 — Positions of the ice edge in the Caspian Sea by month and by winter severity[138]

F.3 Overview of regional climatology

The Caspian Sea is approximately 1 200 km from north to south, spanning more than one climatic zone, so the meteorology differs significantly across the region. In general terms, weather conditions in the Caspian Sea may be categorised, in oil industry terms, as ranging from mild to rough.

The Caspian Sea is influenced by a continental climate regime, which results in large ranges of temperature and widely varying seasonal wind regimes. In the south, summers are hot and dry, while the winters are warm. In the north, summers are similar to the south but the winters by contrast are cold with relatively low snowfall. During the winter, weather is dominated by the Siberian anti-cyclone that creates east to southeasterly winds of cold, clear air over the northern Caspian Sea. During the summer, the weather is

influenced by the Azores high-pressure zone, with the strongest and most persistent winds flowing from between west and north.

The region is subject to extra-tropical cyclones at the rate of about 10 strong events per year.[143] These approach from the west, southwest or south, although a significant number are also generated locally. Cyclones most often appear in January, March and October. In the south, in the region of the Apsheron peninsula, the number of days with wind speeds higher than 15 m/s is between 60 days and 80 days. In the northern Caspian Sea, the number is reduced to about half this value.

In the northern Caspian Sea, the strongest winds occur between November and April, with typical annual maxima of around 25 m/s, rising to near 30 m/s for a 25-year return period storm. The summer months are more benign, with wind speeds only rarely exceeding 15 m/s. The strongest winds in the northern Caspian tend to be from between southwest and west, although a more northwesterly component is apparent during the latter part of the year. The weather conditions may be locally quite variable due to topographic effects, notably due to the Caucasus mountains to the west and the localized topography to the north of Aktau. In the south, the topographic influence of the Apsheron peninsula and Caucasus is notable, with frequent winter storms that may last from 3 h to 120 h, with typical durations of 15 h to 18 h. These local storms are difficult to forecast accurately.

In the northern Caspian Sea, daily mean air temperatures vary significantly seasonally and from year to year, specifically during the winter period, when temperatures may fall to below –25 °C in some years, but only to around –10 °C in others. In the summer, air temperatures rise to between 30 °C and 35 °C with extremes around 40 °C.

In the southern Caspian Sea winter temperatures are warmer, at 3 °C to 12 °C, with infrequent snow and frosts. There are, however, occasional short-lived cold spells with temperatures as low as –19 °C. Temperatures rapidly increase in the spring and summer, reaching up to 30 °C offshore but as high as 36 °C in coastal regions to the west and 42 °C in the east.

F.4 Overview of regional hydrology

More than 130 rivers flow into the Caspian Sea, with a catchment of about $3{,}5 \times 10^6$ km^2. The Volga is the single largest river and accounts for nearly 80 % of the total river discharge into the Caspian Sea. Other significant rivers include the Kura (second largest), Ural, Terek and Sulak. These, with the Volga, account for 90 % of the total annual discharge into the Caspian Sea.

The greater part of the Volga River inflow enters the Caspian Sea through the western arms of the Volga Delta and becomes entrained in the flow down the western coast of the central Caspian Sea. Flow in the Volga reaches a maximum in May/June due to melt water, and slows to a minimum in July/August.

In the winter, the seawater temperature at the ice edge of the northern Caspian varies from 0 °C to 0,5 °C; in the central Caspian temperature ranges from 10 °C to 11 °C; and in the southern Caspian it is around 10 °C. In the summer months, the central and northern Caspian seawater temperatures are 24 °C to 25 °C; in the southern Caspian they are around 25 °C to 26 °C. Temperatures near the east coast are 1 °C to 2 °C lower than those near the west coast.

With the climatic differences between the northern and southern Caspian, the non-summer distribution of water temperatures is several degrees Centigrade between the major basins in the upper water column.[138] As summer approaches, temperatures become more uniform across the entire sea. Vertical thermal differences are small during most of the year; however, a strong thermocline develops in the upper 20 m to 40 m of the deeper portions of the central and southern Caspian in mid-summer and persists into early autumn.

The salinity of the Caspian Sea is roughly one third that of oceanic seas, being usually in the range 12,8 PSU to 12,9 PSU. Salinity may be as low as 2 PSU in regions subject to freshening by river inflow from the Volga and Ural Rivers, and may be as high as 14 PSU to 15 PSU in ‘evaporation patches’ in high summer.

F.5 Water depth, tides, long-term water levels and storm surges

F.5.1 Water depth

The Caspian Sea may be categorised into four distinct regions based on their physico-geographical characteristics:

a) the southern Caspian Sea, which is 1 025 m at its deepest point and is bounded to the north by the Apsheron ridge;

b) the Apsheron Ridge, which lies between Zhiloi Island and Cape Kuuli and has water depths ranging from a few metres to 200 m;

c) the central Caspian, commonly termed the Derbent Depression, which is 788 m at its deepest point;

d) the northern Caspian, which is typically less than 20 m deep, and is the shallow water region to the north of the Mangyshlak threshold.

In the southern Caspian Sea, the continental slope is very steep and extends to depths between 700 m and 800 m. The shelf is narrow (about 40 km) along the western coast, but much wider (about 130 km) along the eastern coast. The width of the shelf along the southern coast is much narrower; depths of 400 m occur only 5 km to 6 km from the coast.

Water depths in the Caspian Sea are generally referred to the Caspian Datum. This Datum is defined as 28 m below the Baltic Datum.

F.5.2 Long-term water levels

F.5.2.1 General

The water level in the Caspian Sea in 2018 was 27,9 m below the level of the world's oceans and 0,1 m above the Caspian Datum. However the level is subject to considerable variation over various timescales. Long-term water level fluctuations of up to 10 m have been recorded for the Caspian Sea.[140] Figure F.3 shows variations in MSL from 1840 to 2018. The main sources of these fluctuations are natural long-term changes in climate, the effects of global warming on the local climate, as well as anthropogenic effects such as changes in consumption of water from the Volga River and the effects of dikes on the Caspian surface area.

Recent work [144] has illustrated a strong correlation between the North Atlantic Oscillation (NAO) and the Caspian Sea level, probably as a result of depression activity associated with a strong NAO. At the present time, approximately 79 % of the inflow into the Caspian Sea is from rivers, with the Volga and Ural accounting for 94 % of this value.[143] About 20 % of the total inflow comes from rain, and the remaining 1 % comes from groundwater. Evaporation is the major source of outflow, accounting for some 97 %. The remaining 3 % of the outflow is through the Kara Bogaz Gol, which acts as an evaporation basin. In the late 1970s the USSR constructed a dam across the Gol, separating it from the Caspian Sea, in an attempt to stop the declining sea level in the Caspian. This dam was removed in June 1992, allowing water to once again flow from the Caspian to the Gol[140].

The Caspian Sea level reached its maximum in 1993. Since then the water level started to drop, in particular from 2008 onwards. The main reason for the drop is the increased evaporation of water caused by the overall higher air and water temperatures during the last decade, in combination with a slightly lower inflow of water from rivers and a reduction of the direct precipitation [145].

F.5.2.2 Seasonal water level

In addition to long-term trends, the level of the Caspian Sea is also subject to seasonal fluctuations. Levels are highest in July and lowest in December, with a mean annual level variation in the range 0,30 m to 0,40 m. This is shown in Figure F.4, which includes a 95 % confidence interval around the mean, based on the period 1978 to 1998. The seasonal peak has shifted from the month of July to June over the past century (see Figure 1.4 in reference [138]).

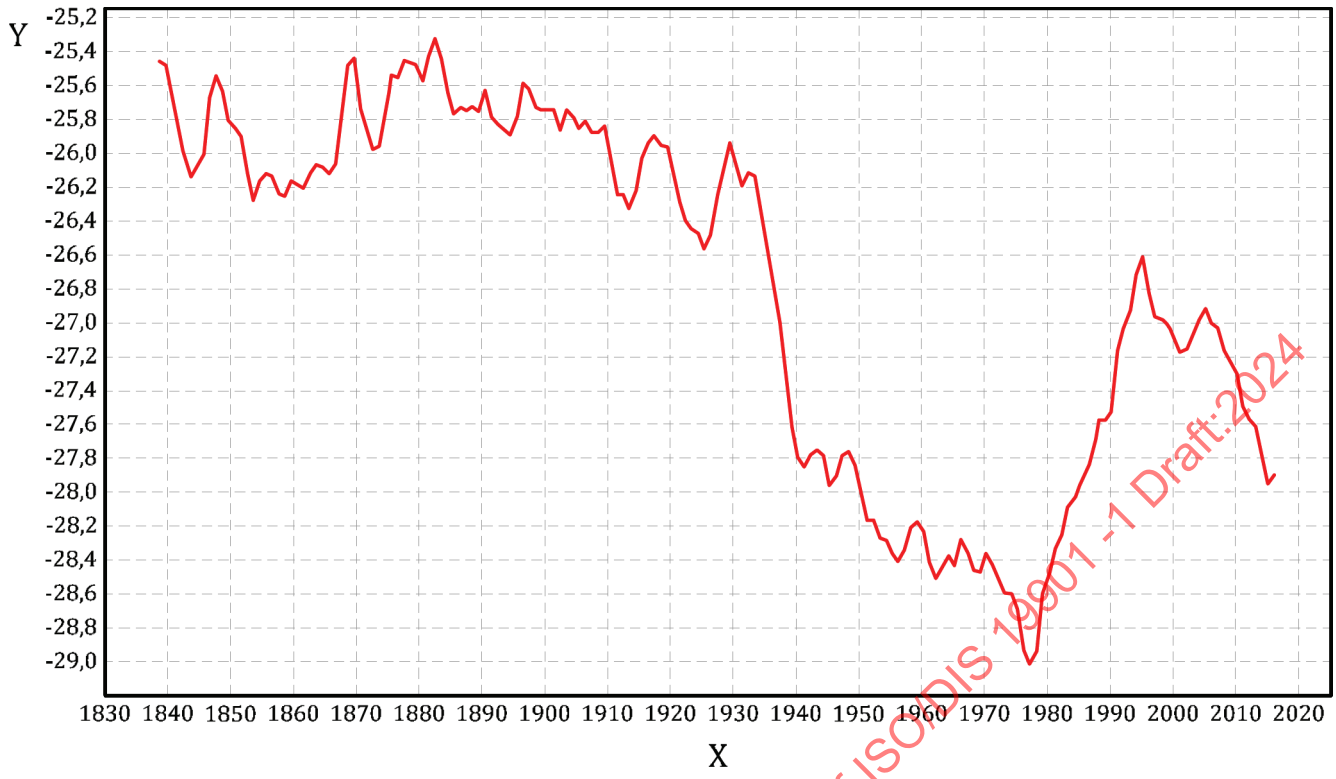

Key

X Year Y Annual mean Caspian sea level / m (Baltic datum

Figure F.3 — Long-term variation in Caspian Sea MSL

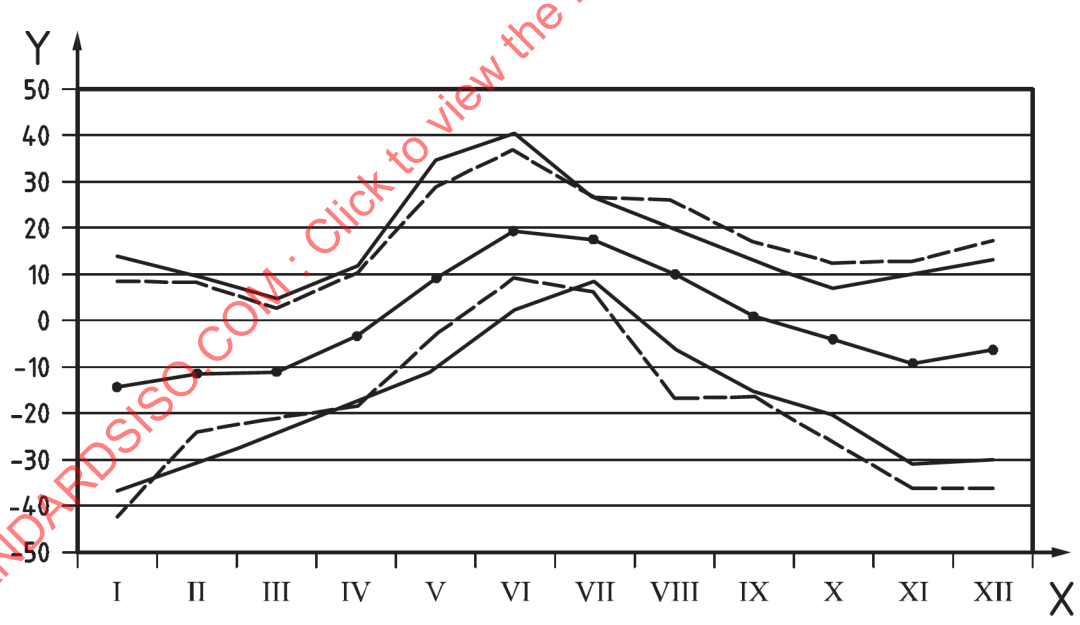

Key

X month Y water level deviation from annual mean (cm)

mean min/max 95 %

Figure F.4 — Seasonal fluctions in Caspian sea MSL

F.5.3 Tides, storm surges and seiches

The tidal range in the Caspian Sea is very small, on the order of only 0,1 m. However, significant water level fluctuations do occur as a result of wind forcing and seiching. Prolonged northerly winds may cause a drop in sea level that prevents the safe operation of vessels in shallow waters. A sudden reduction in the wind may cause the water to flow back rapidly and oscillate at a period consistent with a longitudinal seiche over the whole of the Caspian Sea, excluding the extremely shallow northern section. The dominant periods are 8,5 min to 8,7 min for a single seiche, and 4,4 h to 4,4 h for a double-node seiche. Detailed reports on the magnitude of the seiches are not available, although seiching has been observed in data in the vicinity of Bautino with an amplitude of less than 5 cm.

An example of negative and positive surges in the northern Caspian Sea is shown in Figure F.5. In the southern Caspian Sea, storm surges are generally small, varying from −0,1 m to +0,2 m.

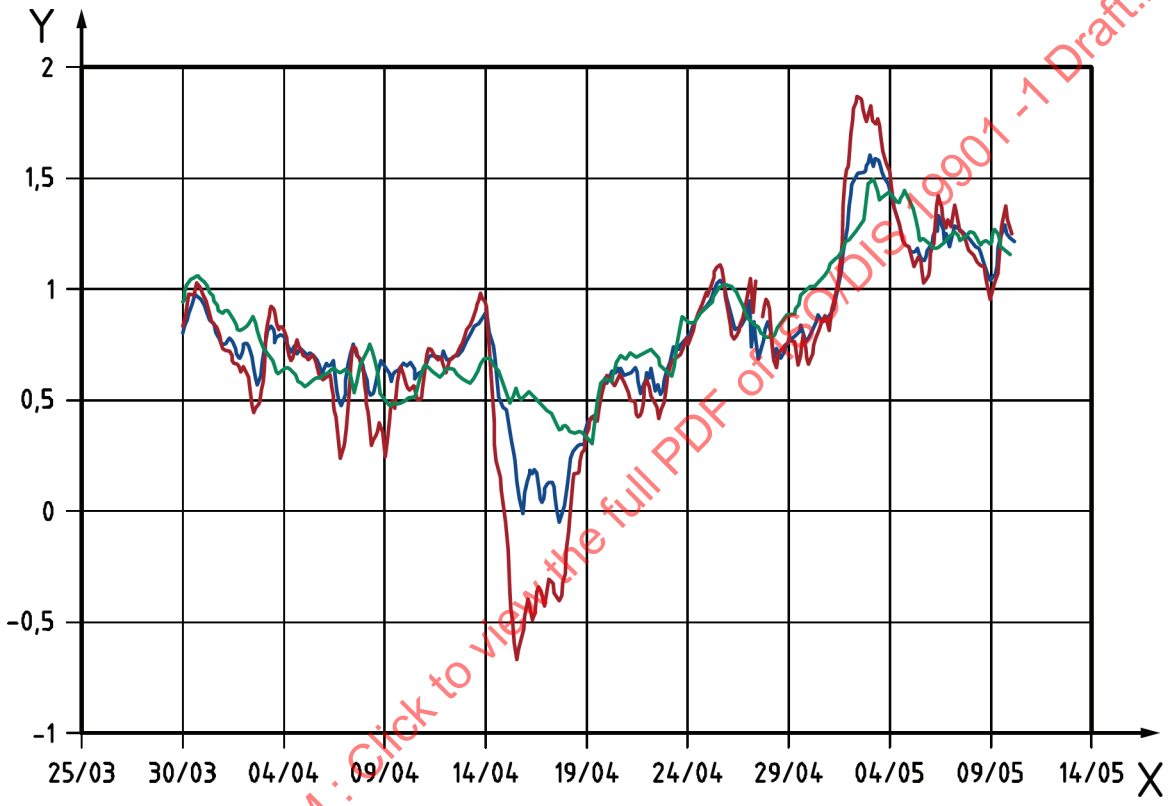

Key

X date (dd/mm) Y water level (m mean above Caspian datum)

kashagan kairan peshnoi

Figure F.5 — Storm surges in the northern Caspian Sea

F.6 Winds

In very general terms, the most frequent wind directions over the Caspian Sea are:

— summer – northerly; and

— winter – southeasterly.

The prevailing wind direction does vary in different regions. For example, in the western part of the central Caspian Sea, near the spurs of the Caucasian Mountains, the prevailing winds throughout the year are northwest and southeast, while ‘monsoon’ traits are clearly evident in the wind regime on the southern

Caspian's east coast. A similar regime is noted in the northern Caspian Sea, although dominant directions are closer to east and west.

Median wind speeds are in the range 5 m/s to 7 m/s, and a little higher (up to 9 m/s) in particularly windy regions such as the Apsheron Peninsula. Ten percent of wind speeds exceed 10 m/s to 12 m/s. Storms associated with wind speeds in excess of 25 m/s are usually from the northwest, north, northeast or southeast.

F.7 Waves

The most severe sea-states occur when strong winds blow over the longest fetches, namely during periods of sustained north/northwest or south/southeast winds.

The greatest storm activity develops over the open waters of the middle Caspian between Bautino and the Apsheron Peninsula (see Table F.1).

Table F.1 — Number of events per year with winds > 15 m/s

Location	Average number of events per year with wind speed > 15 m/s	Maximum number of events per year with wind speed > 15 m/s
Bautino	13	27
Apsheron Peninsula	20 to 30	45

F.8 Currents

The circulation of the Caspian Sea is unusual in that tides are very small, and currents are driven largely by regional weather systems.[139,147] The relationship between the forcing mechanisms and the actual observed currents is complex. The currents may be large, with speeds dependent on the location (water depth, position in the basin, shape of the seabed topography) and the wind system acting on the sea surface (magnitude, direction and degree of wind curl). Regional descriptions of the currents in the Caspian Sea describe several anticlockwise gyres, but these give only a broad indication of the flow. To understand the currents at a particular location, it is necessary to make site-specific measurements over a suitable period. Such measurements are strongly recommended for detailed engineering design.

Although currents are largely storm-driven, depending on the location and the wind direction, the peak currents may occur at the same time as the peak wind and waves or be delayed by several hours. For example, in the southern Caspian Sea the storm-generated currents from north or northwesterly winds peak approximately one day after the wind and waves, and come from the southwest. In this area, strong near-bed currents may occur during periods of benign wind and wave activity at the surface.

Generalized current flows in the Caspian Sea are shown in Figure F.6.

Figure F.6 — Generalized current flows in the Caspian Sea[148]

F.9 Other environmental factors

F.9.1 Marine growth

The density of fouling organisms in the Caspian Sea is expected to be from ~13 kg/m^2 to a maximum of 30 kg/m^2 to 40 kg/m^2 (barnacles being a major contributor). Fouling densities of 10 kg/m^2 to 12 kg/m^2 have occurred on ships, leading to 20 % to 30 % reduction in ship speed.

The hydroid Bougainvillia Megas may develop dense accretions inside intakes and pipelines open to the sea, hindering the flow of water. (Bougainvillia is a gelatinous organism that spreads itself in the form of a jellyfish or medusa)[138].

The extent of marine growth needs to be reviewed on an annual basis. If necessary, any growth will need to be removed by mechanical means.

F.9.2 Air temperature, precipitation, humidity, pressure, clouds and visibility

F.9.2.1 Air temperature

Air temperature varies greatly over the Caspian Sea due to the lengthy meridional dimension of its main axis. The average annual air temperature is 8 °C to 10 °C, 11 °C to 14 °C and 15 °C to 17 °C for the northern, central and southern regions respectively. A large variation in extreme temperatures also occurs. In the north the temperature may drop to −30 °C with the arrival of arctic air, whereas in the southern Caspian Sea the minimum temperature is −10 °C. The variation in air temperature is less in summer. High temperatures up to 42 °C to 44 °C are observed on the east coast.

Annual freezing degree days: Freezing degree days (FDDs) in the northern Caspian may vary significantly from year to year, with values as high as 1 500 in some years, and as low as 300. The number of FDDs has been related to ice thickness[149].

F.9.2.2 Precipitation — Rainfall

The amount of precipitation over the Caspian coastline is a function of the interaction of different air masses with the relief of the coastal areas and mountains. It may vary between 200 mm/year and 1 200 mm/year, depending upon the location. The distribution of precipitation above the sea area is relatively uneven but averages ~ 200 mm/year[150].

Rainfall in Atyrau (northern Caspian) has been measured since the end of the 19th century. Average annual rainfall at this site is ~160 mm, although this is highly variable with annual values falling as low as 50 mm and as high as 280 mm. Weekly rainfall is typically between 2 mm and 3 mm for most of the year, although double this amount may be expected between April and June. Heavy rainfall may occur at any time of the year, and weekly totals in excess of 15 mm have been recorded throughout the year. The highest weekly total was 95 mm, measured in July. See Figure F.7.

Snowfall is discussed in F.9.3.

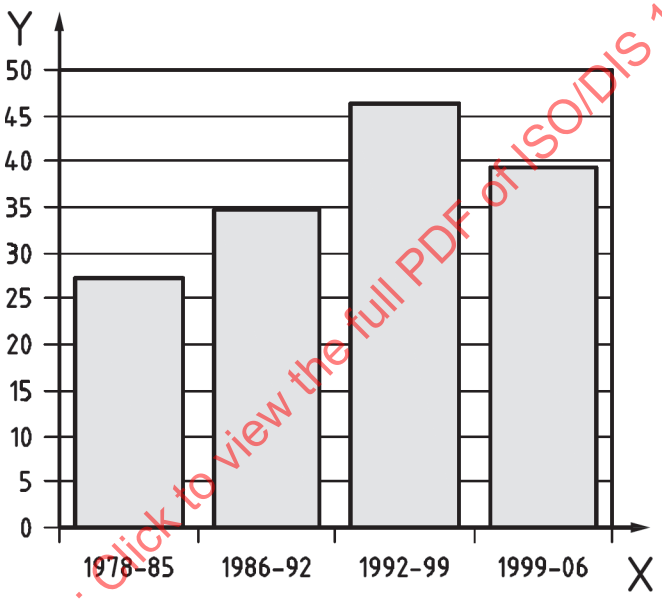

Key

X time in 7 year periods Y mean precipitation (mm)

Figure F.7 — Precipitation (mm) over winter season in Atyrau, northern Caspian Sea

F.9.2.3 Humidity

The humidity of the air above the Caspian Sea broadly increases from south to north, and from east to west.[150] It does not change significantly during the cold months, measuring on average 80 % to 87 % on the western coast and 75 % to 80 % on the eastern coast. Over the sea, it decreases from 90 % in the central parts of the Caspian Sea to 85 % in the southern Caspian. In the summer, at the coast humidity ranges on average between 55 % and 70 %, while over the sea it reaches an average of 80 %.

Along the northern shore, the mean daily humidity values vary from 90 % during December to February, to around 50 % during the summer (July and August). Fully saturated air may occur at anytime between October and March, with daily mean values of 100 % routinely recorded. During the summer months the air is drier, with daily maxima rarely exceeding 90 % between April and October. Minimum daily mean values rarely drop below 20 % in the summer and below 60 % in the winter. The humidity levels offshore tend to be

higher than those recorded at the coastal stations during the winter months, but offshore humidity tends to be greater between April and September.

F.9.2.4 Visibility — Fog and dust storms

For the majority of the Caspian Sea, fog is mostly observed during the spring. Its frequency decreases from the shore towards the open sea areas. In summer, fogs are mainly observed at daybreak and dissipate within 1 h to 3 h after sunrise, with heating of the atmosphere. In winter, advective fog at sea occurs at the outflow of warm air masses from the land. Its average duration is about 7 h to 8 h, and it may be observed at any time of the day. The greatest number of days with fog based on mean multiyear data (32 days to 38 days) is typical of the central Caspian Sea. More than half of fogs are observed during the cold period of the year.

In the northern Caspian Sea, fog is most common during both autumn and late winter; this is associated with the high humidity values during this period. The number of days with fog is highly variable from year to year, but poor visibility may persist for several days at a time.

The average number of days per month of dust storms at Fort Shevchenko is given in Table F.2.

Table F.2 — Average number of days per month with dust storms at Fort Shevchenko

Days per month with dust storms at Fort Shevchenko												
Jan	**Feb**	**Mar**	**Apr**	**May**	**Jun**	**Jul**	**Aug**	**Sep**	**Oct**	**Nov**	**Dec**	**Per year**
0,2	0,5	0,7	1	0,5	-	0,2	0,07	0,2	0,3	-	-	3,6

F.9.2.5 Daylight hours

Hours of daylight are a function of latitude. Over the Caspian Sea region, they range from 8 h to 9 h in December and from 15 h to 16 h in June.

F.9.2.6 Tornadoes/Waterspouts

Waterspouts and tornadic waterspouts are considered to be rare occurrences in the Caspian Sea, although there have been sightings in the northeast Caspian, at Baku, and between Fort Shevchenko and Aktau in recent years. Waterspouts form when there is moist unstable air, a warm water surface and a convergent boundary (i.e. a land- or sea-breeze front or other mesoscale wind feature). Tornadic waterspouts form in the same manner, but in addition the vertical wind shear causes rotation of the convective cloud (almost always a full-grown cumulonimbus). The strong winds associated with these features may cause considerable damage. The most recent documented sighting indicated that the tornadic waterspouts were Force 2 on the Fujita scale (wind speeds between 50 m/s and 70 m/s).

F.9.3 Sea ice and icebergs

Ice forms in the northern portions of the Caspian Sea in winter, but there is considerable variability in both the onset and the duration of the ice cover. During severe winters, ice formation may begin as early as October, but has been as late as the end of December or early January. The ice formation starts along the northern and eastern coastlines and works southward, typically reaching its maximum southward extension by January or February, as indicated in Figure F.2[138].

Thermal ice growth is modest compared to arctic regions, however the lack of snow cover and wind-induced ice movements during the freeze-up mean that the ice may layer easily, resulting in thicker ice. Level ice thicknesses may reach 70 cm in severe winters but are typically nearer to 50 cm during an average year. Locally, thicknesses may be considerably greater due to rafting or other factors. The low salinities also result in relatively strong ice.

The ice around the northern and eastern boundaries of the sea is typically land-fast; in the central region of the northeast Caspian Sea the stability of the ice is dependent on the severity of the winter, but pack ice will often be present for parts of the winter season. There are usually several significant movements in the course of a typical year, with recorded speeds of more than 0,5 m/s. The formation of ice piles (stamukha)

and ridges is common over much of the northern Caspian Sea; stamukha may reach heights of more than 10 m, but are typically less than 8 m. These features are grounded and result in indentation of the seabed and the formation of scours in the event that they move. The ice typically tends to start receding in March, commencing in the Ural Furrow in the centre of the basin. The entire region is generally ice-free by mid to end April. No multi-year ice is present in the Caspian Sea.

As there are no glaciers discharging into the Caspian, there are no icebergs.

Ice thickness and characteristics vary significantly across the area; data given in Table F.3 are for the central part of the northern Caspian. Ice formation further to the northeast tends to begin earlier and last longer; ice thickness also increases.

Table F.3 — Summary of ice conditions in the northern Caspian Sea

Sea Ice	Parameter	Average annual maximum value	Uncertainty in annual maximum values
Occurrence	first ice	mid-December	mid-November to early January
	last ice	end March	end February to early April
Level ice (first year)	landfast ice thickness (m)	0,5 – 0,6	+/– 0,2
	floe thickness (m)	0,3	variable due to rafting
Rafted ice	rafted ice thickness (m)	Rafted ice thickness may vary considerably in local areas; values of > 1 m are not uncommon	variable
Rubble fields	sail height (m)	2 to 5	+/– 3
	length (m)	≤ 1 000	variable
Ridges (first year)	sail height (m)	1 to 2	variable
	keel depth (m)	water depth limited	n/a
Stamukhas	water depth range (m)	0 to 8	
	sail height (m)	≤ 20	variable
Ice movement	speed in near-shore (m/s)	0,5	+/– 0,3
	speed in offshore (m/s)	0,5	+/– 0,3
Ice-induced scour	scour depth (m)	0,2 to 0,5	≤ 1,5

F.9.4 Snow, ice accretion and sea spray icing

As with sea ice, snowfall and ice accumulation on oil industry structures are design considerations only in the northern Caspian Sea.

Snowfall in the northern Caspian Sea is highly variable from year to year, with typical accumulated precipitation amounts between 25 mm and 50 mm per season (Atyrau), see Figure F.7. This is equivalent to between 25 cm and 40 cm of snowfall, given average ratio of 1:10; typical values for the ratio vary between 1:5 and 1:15 for fresh snow. Snow accretion is relatively rare offshore, but snowdrifts of more than 25 cm may develop during exceptional years. In exceptional years, precipitation over the winter season may exceed 100 mm.

Sea spray icing will occur on exposed structures during the winter period when air temperatures are low and wave action is significant. Light icing will also be encountered during foggy conditions when air temperatures are below freezing.

F.9.5 Tsunamis

Information on past tsunamis in the Caspian Sea is limited; only qualitative data are available. Table F.4 lists observations of past tsunami events.[151] In the Caspian Sea, earthquakes, mud volcanoes or submarine landslides may create tsunamis.

Table F.4 — Historical tsunamis and tsunami-like events observed in the Caspian Sea [151]

Date	Location	Description
743	Derbent	The area of the coast with fortifications was submerged in the sea.
918	Derbent	The part of the coast with fortifications was submerged in the sea.
957	Derbent	The fall of sea level caused horizontal displacement of the shoreline by 150 m from the equilibrium position.
1668	Terka	Part of the beach was submerged in the sea. The rise of water level was observed in the delta of the Terek River.
26.04.1868	Baku	Short-term rise and fall of sea level with amplitude about 0,45 m were observed.
09.03.1876	Oblivnoy Island	Unusual sea level oscillations occurred after strong underwater boom in conditions of dead calm. Event was observed from a ship.
27.06.1895	Krasnovodsk Bay	Flooding of north and west areas of Uzun-Ada as result of a large increase in water level in the bay. Large waves caused flooding of buildings and dock. A few wooden houses were taken away to the sea. Pipeline was destroyed.
31.12.1902	Baku	Unusual waves resulted in dangerous motion of ships in the port. Event was observed after destructive earthquake near Shimaha.
09.05.1933	Kuuli-Mayak	Sudden rise of sea level up to 1,35 m for 10 min. Fishing boats and equipment were taken away to sea.
12.04.1939	Livanov Shoal	The passing of a solitary wave of a large height was observed from two ships that were 15 miles from each other.
26.04.1960	Baku	Oscillations of sea level up to 1 m were observed for 2–3 h.
06.03.1986	Livanov Shoal	Unusual high-frequency sea level oscillations of 2 cm to 3 cm amplitude were observed over epicenter of earthquake during 1 min to 1,5 min. The event was fixed from a seiner and 45 fishing boats.

Seven offshore seismic areas have been identified as tsunamigenic (see Figure F.8). As tsunami sources are located on the continental shelf, tsunami waves are trapped along the coast. Thus tsunamis are anticipated to have a local character. Preliminary estimates of tsunami heights range from 0,5 m to 3 m.

As tsunami hazards are site-specific, it is recommended to carry out a site-specific assessment to estimate the risk. Such studies should be carried out in parallel with a seismic hazard assessment.

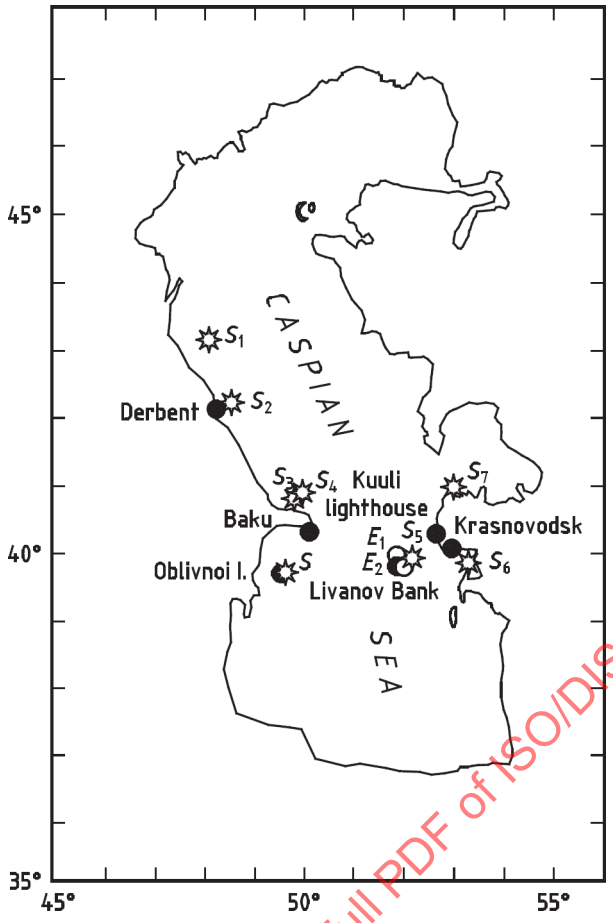

Key

Filled circles	Anomalous sea level observations
Asterisks	Zones of elevated seismic activity

Figure F.8 — Region of the Caspian Sea where historical tsunamis or anomalous sea levels were observed[151]

F.10 Estimates of metocean parameters

F.10.1 Extreme metocean parameters

Indicative extreme values of metocean parameters are provided in Tables F.5 to F.9 for four locations in the Caspian Sea. The wind, wave and current values are independently derived marginal parameters; no account has been taken of conditional probability. As for all indicative values provided within the regional annexes, these tables are provided to assist preliminary engineering concept selection; they are not suitable for design of offshore structures. In particular in the Northern part of the Caspian, there are large spatial differences in waves, surges and currents and so the values presented n Table F.5 are only indicative.

Table F.5 — Indicative values of metocean parameters for the north(eastern) Caspian Sea region

Metocean parameter	Return period *N* Years			
	1	**10**	**50**	**100**
Nominal water depth (m)	3,2	3,2	3,2	3,2
Wind speed at 10 m above MSL				
10-min mean (m/s)	22	27	30	32
3-s gust (m/s)	27	33	38	40
Waves				
Maximum height (m)	2,2	2,5	2,8	2,9
Significant height (m)	1,3	1,5	1,7	1,8
Direction (from)	W	W	W	W
Spectral peak period (s)	4,8	5,0	5,1	5,2
Surge				
Positive surge (m)	0,6	1,6	1,9	2,2
Negative surge (m)	1,2	2,0	2,6	2,8
Current speed				
Surface * (m/s)				
Mid-depth (m/s)	0,59	0,78	0,92	0,97
1 m above sea floor (m/s)				

Table F.6 — Indicative values of metocean parameters for the central Caspian Sea region

Metocean parameter	Return period *N* Years			
	1	**10**	**50**	**100**
Nominal water depth (m)	450	450	450	450
Wind speed at 10 m above MSL				
10-min mean (m/s)	25,8	32,0	37,1	39,4
3-s gust (m/s)	31,6	39,9	46,3	50,4
Waves				
Maximum height (m)	11,2	17,5	20,8	21,6
Significant height (m)	5,8	9,0	10,7	11,6
Direction (from)	NW/SE	NW/SE	NW/SE	NW/SE
Spectral peak period (s)	9,7	11,9	13,0	13,4
Surge				
Positive surge (m)	0,2	0,4*	0,55*	0,6
Negative surge (m)	0,3	0,4*	0,55*	0,6
Current speed				
Surface * (m/s)	0,95	1,2	1,30	1,40
Mid-depth (m/s)	0,60	0,8	0,80	0,95
1 m above sea floor (m/s)	0,60	0,8	0,80	0,95

Table F.7 — Indicative values of metocean parameters for the Apsheron Ridge area of the Caspian Sea

Metocean parameter	Return period *N* Years			
	1	**10**	**50**	**100**
Nominal water depth (m)	160	160	160	160
Wind speed at 10 m above MSL				
10-min mean (m/s)	28,8	34,6	38,9	41,1
3-s gust (m/s)	35,2	43,0	49,0	51,6
Waves				
Maximum height (m)	10,4	14,5	17,4	18,6
Significant height (m)	5,7	7,8	9,3	10,0
Direction (from)	N	N	N	N
Spectral peak period (s)	10,4	12,1	13,2	13,6
Surge				
Positive surge (m)	0,17	0,29	0,37	0,41
Negative surge (m)	0,08	0,22	0,31	0,35
Current speed				
Surface * (m/s)	0,40	0,70	0,91	1,00
Mid-depth (m/s)	0,40	0,70	0,91	0,90
1 m above sea floor (m/s)	0,50	0,50	0,80	1,00

Table F.8 — Indicative values of metocean parameters for the southern Caspian

Metocean parameter	Return period *N* years			
	1	**10**	**50**	**100**
Nominal water depth (m)	500	500	500	500
Wind speed at 10 m above MSL				
10-min mean (m/s)	29,0	34,7	39,1	41,2
3-s gust (m/s)	35,4	43,1	49,3	52,0
Waves				
Maximum height (m)	5,9	10,9	13,8	15,6
Significant height (m)	3,1	5,7	7,3	8,2
Direction (from)	NE	NE	NE	NE
Spectral peak period (s)	7,2	9,2	11,4	12,0
Surge				
Positive surge (m)	0,22	0,30	0,40	0,44
Negative surge (m)	0,10	0,23	0,34	0,39
Current speed				
Surface * (m/s)	0,20	0,36	0,53	0,60
Mid-depth (m/s)	0,20	0,36	0,53	0,60
1 m above sea floor (m/s)	0,16	0,30	0,43	0,49

Table F.9 — Indicative temperatures ranges for the Caspian Sea

Area	Air temperature °C	Sea surface temperature °C	Sea floor temperature °C
Northern Caspian	−30 to +40	−0,5 to +30	−0,5 to +30
Central Caspian	−6 to +40	1 to 28	5 to 5
Apsheron Ridge	−7 to +40	0 to 27	5,5 to 6,0
Southern Caspian	−7 to +40	0 to 27	4,5 to 6,0

F.10.2 Long-term distributions of wave parameters

Wave-scatter diagrams for two areas in the Caspian Sea are provided in Tables F.10 and F.11, comprising significant wave height and associated spectral peak wave period for combined wind sea and swell conditions based on data from a 50-year hindcast.

The shallow waters of the Mangyshlak threshold, defining the boundary between the central and northern Caspian Sea, largely prevent swell from the south entering the northern Caspian area. For the northern Caspian Sea, the wave climate is significantly influenced by water depth. In the deeper parts (where waves are larger) a JONSWAP spectrum with a gamma of between 1,2 and 3 has been recorded; but in the shallower areas where wave heights are restricted, higher values between 2,6 and 6 are more appropriate. For the rest of the Caspian Sea, a gamma value in the range 1,0 to 2,5 has been found.

The information in Tables F.10 and F.11 was generated from the CASMOS-2 hindcast model.[141,142,152] CASMOS-2 was validated against a limited number of *in situ* wave datasets. Sea-states should be assumed to represent a duration of 3 h. 28

Table F.10 — Percentage occurrence of total significant wave height *vs.* spectral peak period for a location in the northern Caspian Sea [142]

Significant wave height m	Peak period s							
	0 to 0,99	1 to 1,99	2 to 2,99	3 to 3,99	4 to 4,99	5 to 5,99	6 to 6,99	Total
0,00 to 0,49	20,1	17,2	19,8	20,1				77,2
0,50 to 0,99				22,3	0,1			22,4
1,00 to 1,49				0,05	0,3	0,05		0,4
> 1,50								
TOTAL	20,1	17,2	19,8	42,45	0,4	0,05	0,01	100,00

Table F.11 — Percentage occurrence of total significant wave height vs. spectral peak period for a location on the Apsheron Ridge area of the Caspian Sea

Significant wave height m	Peak period s													
	0 to 0,99	1 to 1,99	2 to 2,99	3 to 3,99	4 to 4,99	5 to 5,99	6 to 6,99	7 to 7,99	8 to 8,99	9 to 9,99	10 to 10,99	11 to 11,99	> 12	TOTAL
0,00 to 0,49	0,84	2,64	5,40	10,97	4,49	0,83	0,04	0,01	0,00	0,00	0,00	0,00	0,00	25,22
0,50 to 0,99				6,88	16,13	6,76	1,65	0,22	0,00	0,00	0,00	0,00	0,00	31,64
1,00 to 1,49				0,20	5,25	10,94	2,17	1,25	0,24	0,01	0,00	0,00	0,00	20,06
1,50 to 1,99				0,01	0,14	5,01	4,18	1,01	0,63	0,13	0,00	0,00	0,00	11,11
2,00 to 2,49					0,01	0,18	3,78	1,07	0,46	0,26	0,02	0,00	0,00	5,79
2,50 to 2,99						0,01	0,73	1,60	0,43	0,20	0,07	0,00	0,00	3,04
3,00 to 3,49							0,02	0,76	0,44	0,15	0,07	0,01	0,00	1,45
3,50 to 3,99								0,11	0,43	0,16	0,06	0,02	0,00	0,78
4,00 to 4,49									0,17	0,19	0,06	0,01	0,00	0,43
4,50 to 4,99									0,04	0,12	0,05	0,01	0,00	0,22

Table F.11 *(continued)*

Significant wave height m	**Peak period** s													
	0 to 0,99	1 to 1,99	2 to 2,99	3 to 3,99	4 to 4,99	5 to 5,99	6 to 6,99	7 to 7,99	8 to 8,99	9 to 9,99	10 to 10,99	11 to 11,99	> 12	TOTAL
5,00 to 5,49										0,05	0,05	0,01	0,00	0,11
5,50 to 5,99										0,02	0,03	0,01	0,00	0,06
6,00 to 6,49											0,02	0,01	0,00	0,03
6,50 to 6,99											0,01	0,01	0,00	0,02
7,00 to 7,49												0,01	0,00	0,01
7,50 to 7,99												0,01	0,00	0,01
TOTAL	0,84	2,64	5,40	18,06	26,02	23,74	12,57	6,02	2,84	1,31	0,44	0,11	0,01	100,00

Annex G
(informative)

South East Asian Sea

G.1 Description of region

The geographical extent of the region of the southern East Asian Sea is bounded by the land masses of Vietnam, Cambodia, Thailand and Malaysia to the north and west, the Borneo land mass to the south and the Philippines to the east, and is limited at 15° N to the north and the equator to the south, as shown in Figure G.1. The region includes the following areas, moving anticlockwise around the southern East Asian Sea:

— the waters offshore Vietnam,

— the Gulf of Thailand,

— the waters offshore Peninsular Malaysia,

— the waters offshore Natuna Island,

— the waters offshore Borneo,

— the waters offshore Philippines.

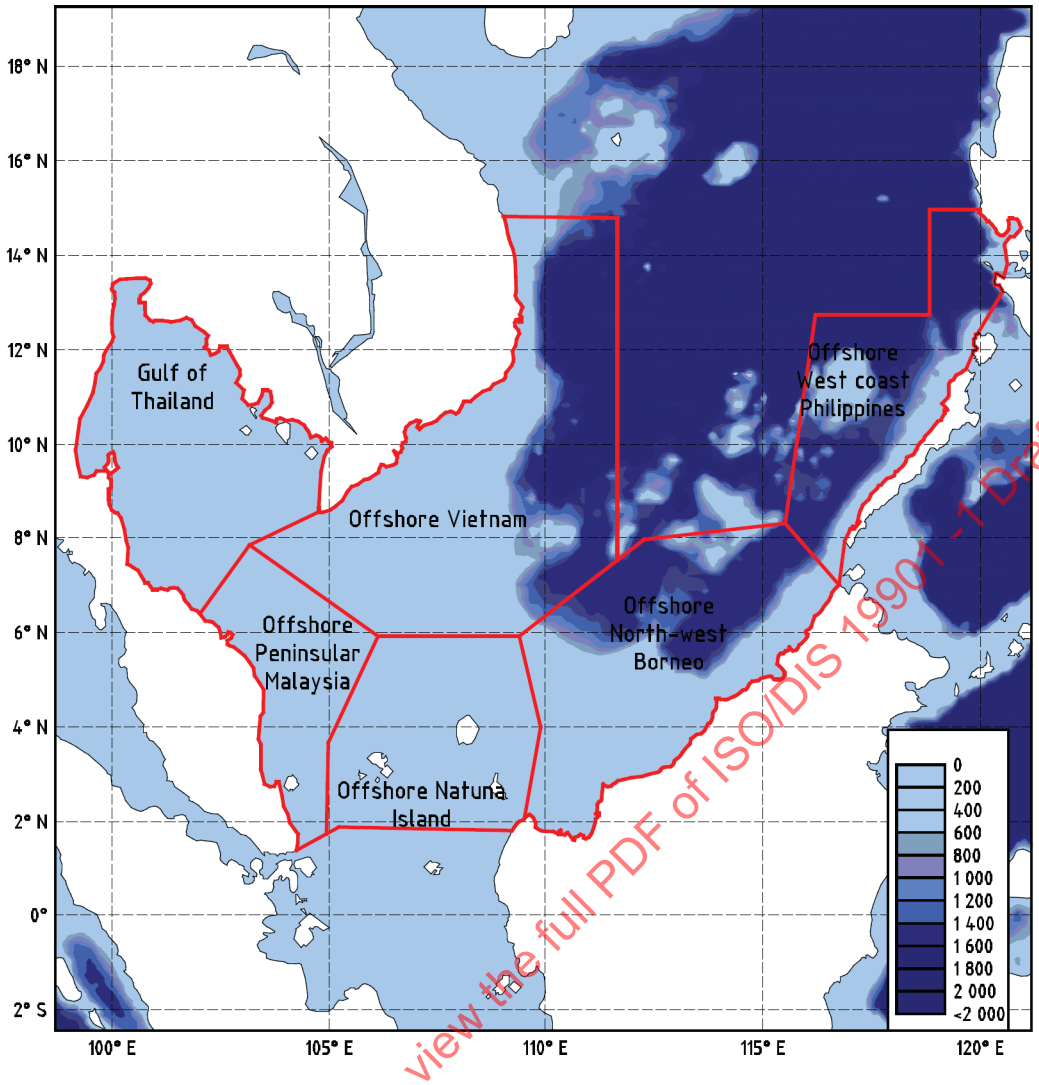

Figure G.1 — Geography of the southern East Asian Sea

G.2 Data sources

Measured data have been collected at many stations throughout the region, however much of the national data collected by government bodies are restricted to land stations or the coastal strip aimed at flood prevention and port operation. Data collected further offshore are often proprietary. Data may also be obtained from commercial organizations.

Satellite data are a major source of information for this region for wind and wave, as well as typhoon track data, a major consideration for many locations.

In addition to measured data, some joint industry-sponsored hindcast studies have been performed leading to extensive (but usually proprietary) datasets of winds, waves and, to a limited extent, currents. The main metocean hindcast dataset for the East Asian Sea is SEAFINE (SEAMOS South Fine Grid Study). The hindcast was developed by an IOGP Joint Industry Project (JIP).[153] The SEAFINE hindcast aimed at providing reliable wind, wave and current data on meteorological and oceanographic extreme and operational conditions in the region, and spans from July 1956 to June 2016. The continuous wave model covered the area from 9° S - 27° N and 99° E - 130° E, ran over the study area on a 28 km (0,25 degree) grid domain, while higher resolution 0,05 degree (~ 5,5 km) was applied to the courser model boundary spectra along its northern, eastern and southern boundaries. The input winds were derived from the National Center for Environmental Prediction (NCEP) hindcast and adjusted based on available wind measurements and QUIKSCAT scatterometer satellite data. Tropical Cyclones winds were modelled separately and blended into the continuous wind hindcast.

The hindcast winds and waves were extensively validated using available measurements. While overall the validation showed the winds and waves were resolved accurately, the winds in the southern SCS region were found to be overpredicted for extremes of the north-easterly monsoons; the SEAFINE hindcast also appeared to be struggling to resolve periods of very low winds (below 5 ms^{-1}).

3-D ocean circulation model HYCOM was run as part of SEAFINE JIP. The hindcast contains 1-hourly water level, current speed and direction with and without tide, salinity, and temperature information at up to 30 levels for the period from September 1992 to June 2012. Validations against the measurements showed that while surface currents were resolved reasonably well, through-the-water currents were often underpredicted. Tidal water levels were also on the lower side.

Even with SEAFINE hindcast, some criteria, such as current and squall criteria, will still need to be derived from measured datasets.

G.3 Overview of regional climatology

Compared to regions such as the Gulf of Mexico and the waters west of Shetland, the climate of the southern East Asian Sea is considered benign. The region is within the equatorial tropics and under the influence of the general wind systems of Southeast Asia produced by the wider regional atmospheric pressure distribution. There is typically a four-season pattern to the climate, with the following characteristics and approximate timings (both of which have considerable inter-annual variability):

a) northeast monsoon (November to March), characterized by predominantly northeastly winds, increased cloudiness and the heavy rainfall and thunderstorms often associated with the low pressure “trough” termed the “Inter-Tropical Convergence Zone” (ITCZ). Regular 'surges' in the monsoon winds increase wind speeds and raise wave heights. The risk of typhoons affecting the area continues through October to December only;

b) transition (April and May), when the winds are light (except during occasional squalls) and variable in direction, wave heights are low;

c) southwest monsoon (June to September), which is dominated by southwestly winds, which occasionally increase in speed due to typhoons approaching east of the Philippines, raising waves heights. Typically, the duration, wind speed and wave heights are lower than those experienced during the northeast monsoon except on the eastern boundary. Squall frequency and severity increases during this period; and

d) transition (October/November), showing changeable wind directions with an increase in wind speed and frequency of squalls.

The risk of typhoons affecting the southern East Asian Sea region is greatest October to December.

G.4 Water depths, tides and storm surges

Water depths in the areas are shown in Figure G.2. Much of the area within the East Asian Sea covering the Gulf of Thailand, waters offshore Peninsular Malaysia, waters offshore Natuna Island and the western part of the area denoted offshore Borneo, is contained within the continental shelf and is less than 200 m in depth. However, in water offshore Philippines, water offshore Vietnam and the eastern part of the area denoted waters offshore Borneo, water depths extend to 2 000 m. The southern East Asian Sea reaches a depth of approximately 5 000 m in the area near 120° E and 15° N.

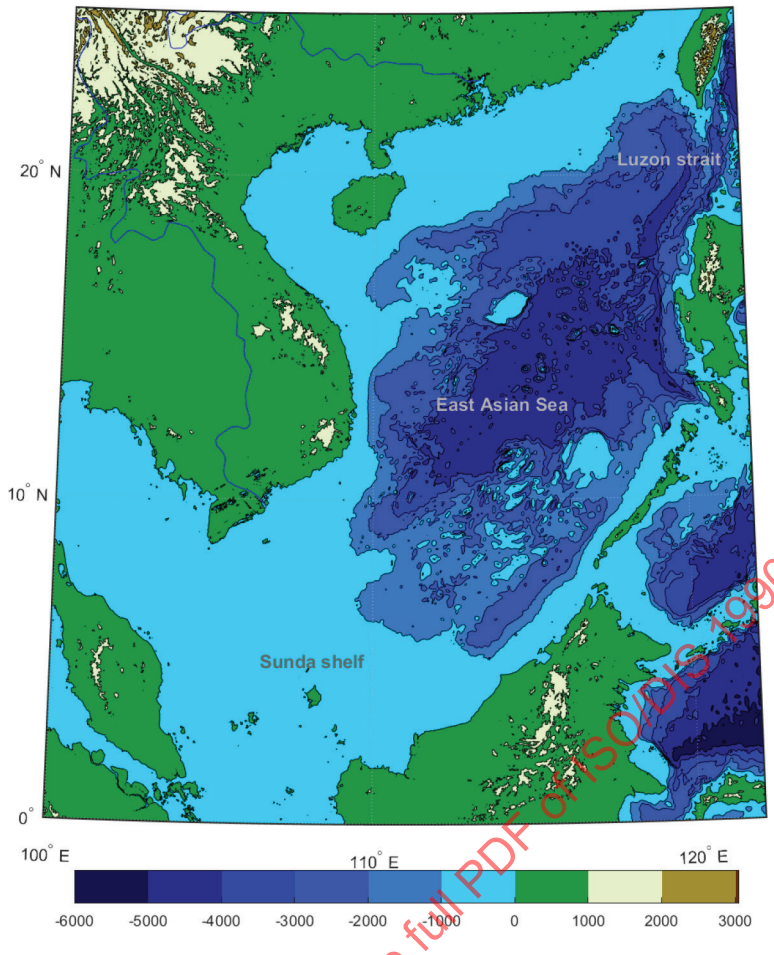

Figure G.2 — Bathymetry of the East Asian Sea

The tides in the bulk of the East Asian Sea are diurnal, with only one high tide and low tide per day and tidal ranges not exceeding 2 m. However there are exceptions, particularly around in the Gulf of Thailand and the waters offshore south Peninsular Malaysia towards the Strait of Karimata, where the tidal wave is reflected back, leading to semi-diurnal tides (two high and low tides per day). The largest tidal ranges are found in these areas; for example near the Sarawak River the tidal range is 3,6 m.

Storm surges may result from two mechanisms: monsoon surges and typhoons; the susceptibility of each area is dependent on its location relative to these forcing mechanisms. Vietnam and the Gulf of Thailand are particularly susceptible to storm surges associated with the passage of typhoons, while offshore Borneo and Peninsular Malaysia are more susceptible to storms surges associated with the northeast monsoon. Storm surges in conjunction with high tides are a common cause of flooding in these areas. Reference [154] reported that offshore Borneo experiences boreal winter storm surges associated with northeast monsoon that exceed 0,3 m (relative to Mean Sea Level), while in boreal summer (southwest monsoon), water levels offshore Borneo are often negative relative to Mean Sea Level, due to the influence of south-westerly winds.

G.5 Winds

There are four main sources of winds in the southern East Asian Sea:

— monsoon winds,

— squalls,

— winds associated with the passage of a typhoon, and

— land-sea breezes, which may be enhanced by local topography.

The significance of each is dependent on its relative location within the southern East Asian Sea.

Figures G.3 and G.4 show monthly spatial representations of 1-hour wind speed (1 % non-exceedance calculated from 59-year SEAFINE hindcast shown as contours), with monthly mean wind vectors in the background, in the East Asian Sea over the period of a year.

In a typical northeast monsoon (November to March), there is low pressure over northern Australia and high pressure over China, causing the monsoon winds to blow over the whole of the East Asian Sea, with typically the strongest winds over the northern part of the East Asian Sea. Occasionally, pressure will rise rapidly over southern China resulting in a 'surge' of increased wind and swell, during which the winds may reach gale force, even offshore Borneo. Between surges, the coastal land breeze may sometimes be fresh to strong in the late afternoon and early evening.

By April the overall surface pressure gradient in Southeast Asia is weak, causing the winds to become southwesterly in the southern East Asian Sea. The coastal sea breeze develops during this time. Squalls develop, often inland and drift out to sea overnight, but later in the period they form offshore overnight and then drift inshore in the morning.

In the southwest monsoon (June to September), the pressure is high over Australia and low over southwest China. The southeasterlies from Australia 're-curve' as they cross the Equator to become southwesterly, blowing towards China. The onset of the southwest monsoon is often abrupt and vigorous, starting about mid-June with sustained winds of 15 m/s to 20 m/s for two to three days and high seas offshore. Surges in the southwest monsoon, from a variety of causes, usually last about two days and often result in a series of 'stream squalls' moving from the southwest but also occasionally off the coast. The land breeze may become reasonably strong.

By October a weak area of low pressure develops over northwest Australia, and pressure over China starts to increase. At this time, northeasterly flow to the north of the ITCZ may trigger late surges in the southwesterly winds south of the ITCZ. The passage of typhoons across the Philippines into the East Asian Sea also increases at this time of the year. Although typhoons are rare south of 10° N, they enter the East Asian Sea more frequently in La Niña years. Typhoons may often produce heavy swell which, combined with rough seas from a simultaneous surge in the southwesterly monsoon, may produce severe cross-seas offshore. The winds usually increase during this time of the year and change direction. Squalls from the land also increase in frequency.

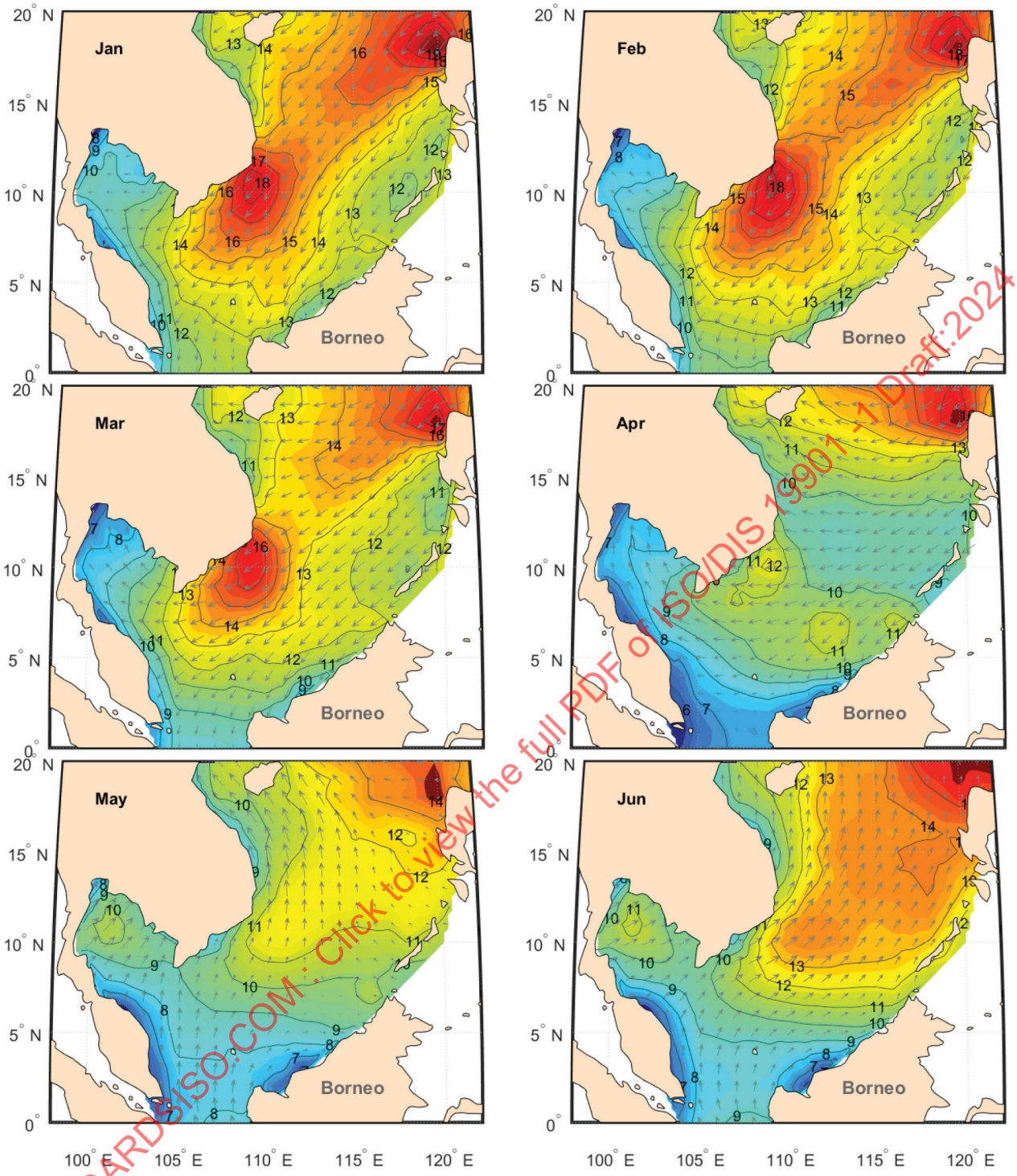

Figure G.3 — Spatial representation of 1 % exceedance of wind speed (1 hr, 10 m, in m/s) and mean monthly wind directions, from January to June

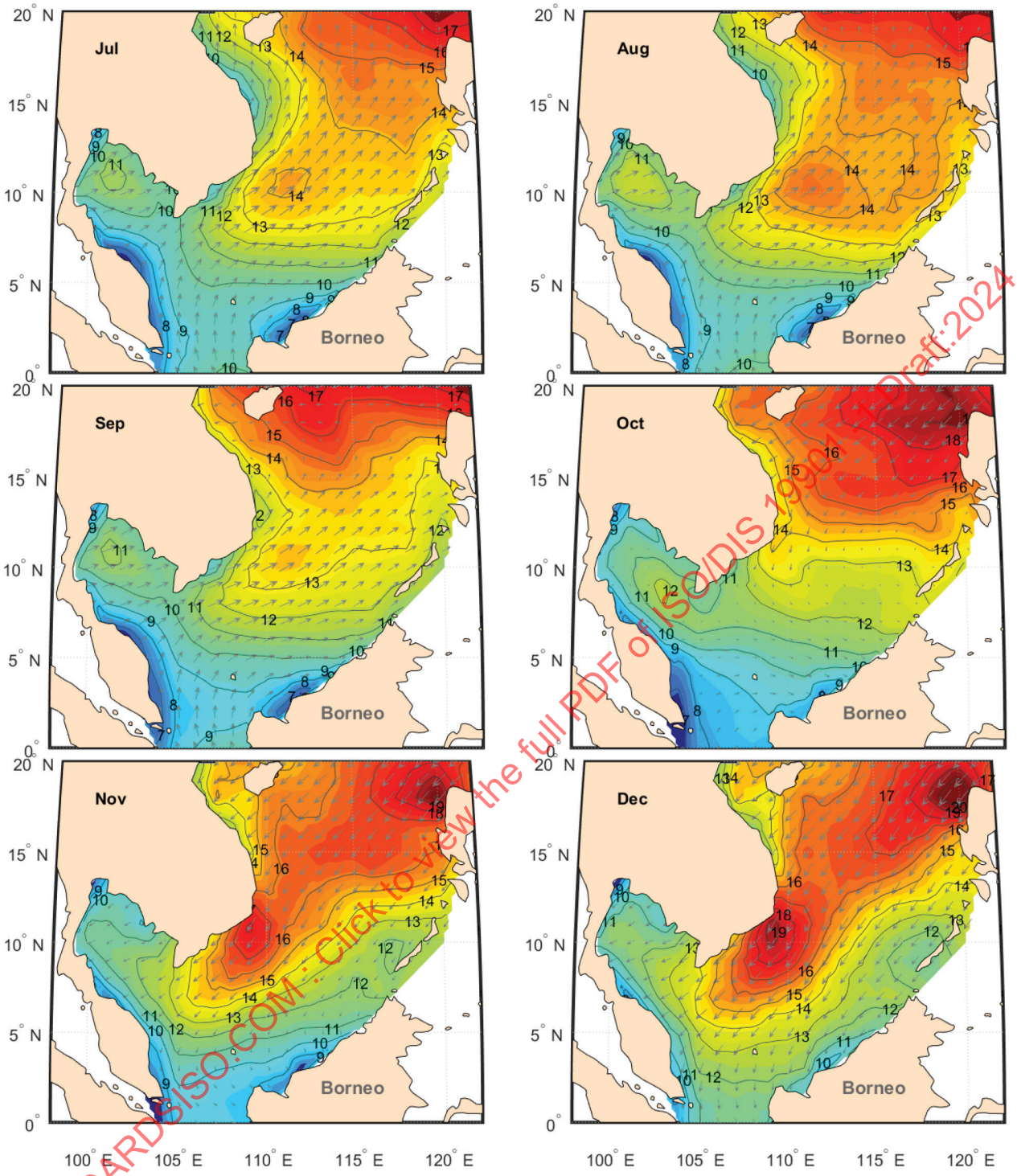

Figure G.4 — Spatial representation of 1 % exceedance of wind speed (1 hr, 10 m, in m/s) and mean monthly wind directions, from July to December

G.6 Waves

The East Asian Sea is effectively a semi-enclosed sea and hence, while strong winds may occur over the whole area, the wave characteristics vary according to the water depth and the fetch over which they have been generated. Where the fetch is restricted, the storm waves are shorter, steeper and lower. The two main mechanisms for the generation of storm waves are:

— waves associated with the monsoon surges;

— waves associated with the passage of a typhoon.

However, the fetch and water depth restriction typically means that conditions during southwest monsoon are most severe in the eastern part of the East Asian Sea and conditions during the northeast monsoon are most severe in the southern and western parts.

In a typical northeast monsoon (November to March), the strong north-northeast winds over the northern part of the East Asian Sea generate waves which propagate down the East Asian Sea, and high swells may reach waters offshore Borneo even if the local winds are fairly light. Oceanic swells are restricted in their ability to enter the East Asian Sea, and hence the longest swells in the southern East Asian Sea have a maximum period of 16 s to 18 s.

Figures G.5 and G.6 depict spatial representations of maximum significant wave heights in the East Asian Sea over the period of a year.

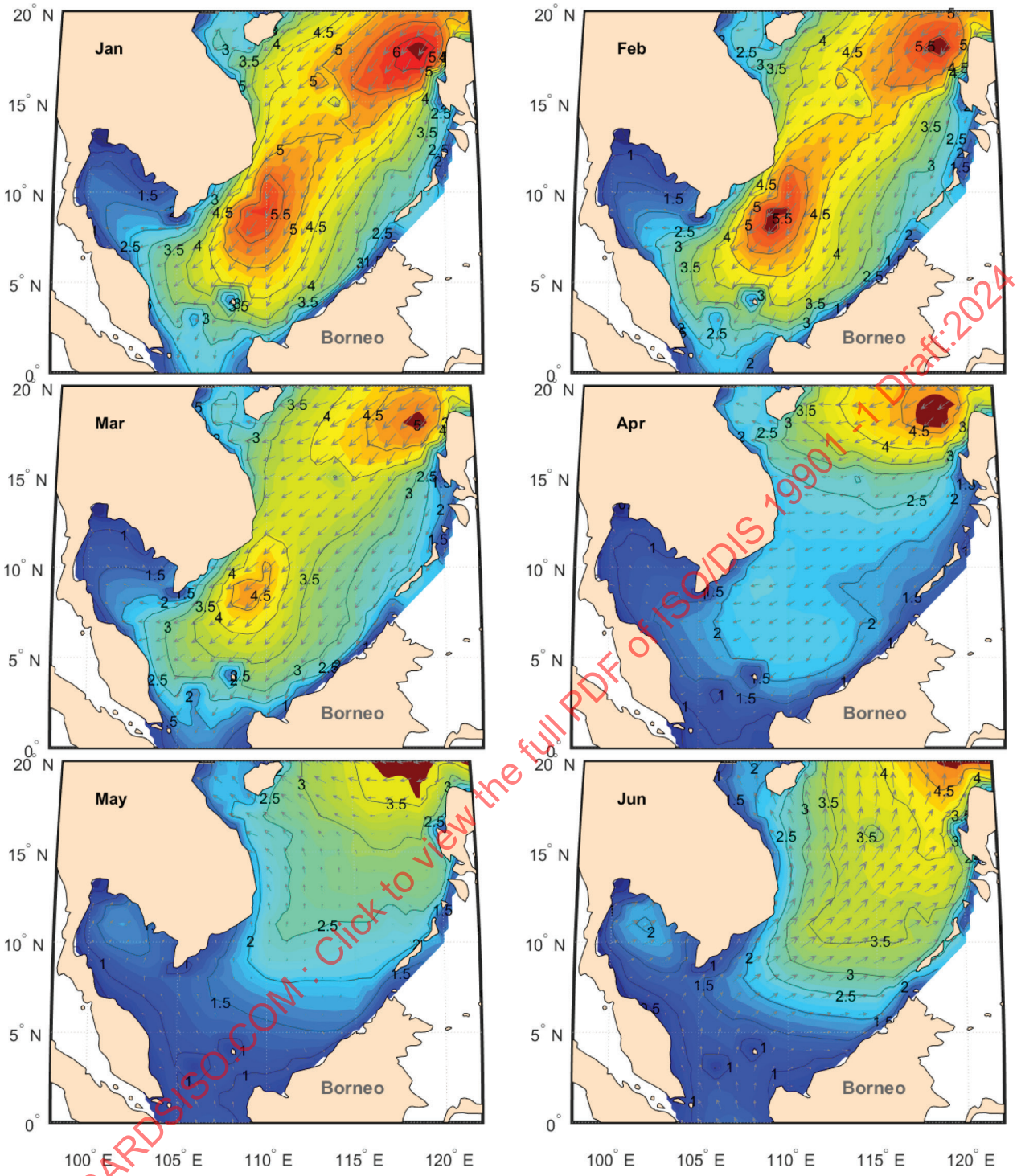

Figure G.5 — Spatial representation of 1 % exceedance of wind speed (1 hr, 10 m, in m/s) and mean monthly wind directions, from January to April

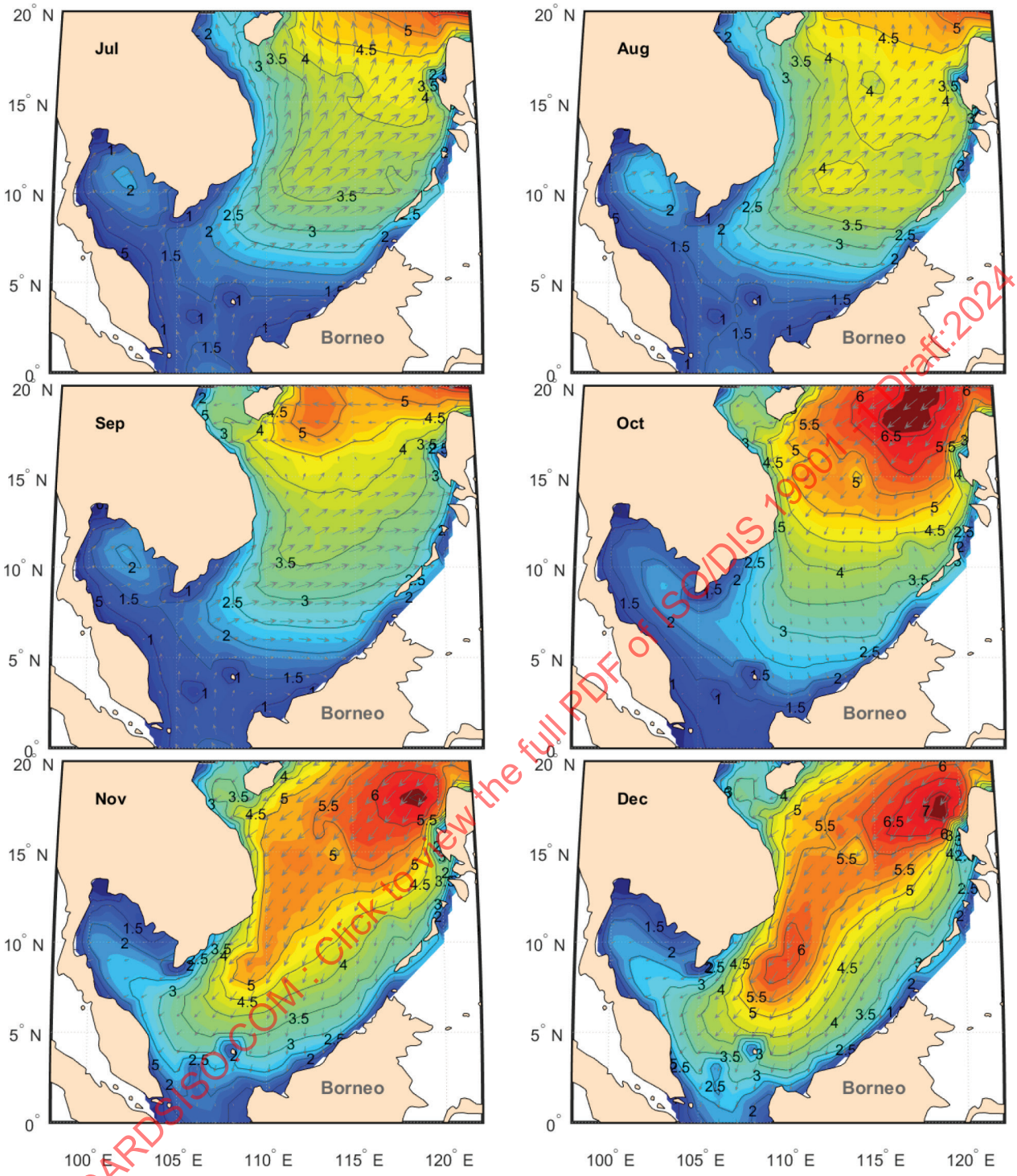

Figure G.6 — Spatial representation of 1 % exceedance of significant wave height (in m) and mean monthly wind directions, from July to December

G.7 Currents

G.7.1 General

Currents in the East Asian Sea are complex, vary substantially with location and are driven by a number of mechanisms, which include:

— tidal currents;

— surface-wind-driven currents;

— basin-response currents derived from tropical storms or strong monsoon surges;

— density-driven currents (particularly near the outflow of large rivers);

— internal waves.

G.7.2 Tidal currents

In many areas, particularly where the diurnal regime predominates, tidal currents are low in comparison to residual currents. However areas near the coast, around shoals and islands and in channels may experience stronger tidal currents.

In addition, several measurements have shown examples of high currents where fluctuations of the residual currents occur at the principal tidal period. This suggests that at some locations and with some forcing mechanisms, including typhoons, there may be coupling between tidal and residual currents.

G.7.3 Surface-wind-driven currents

The East Asian Sea is an enclosed sea forced by monsoonal winds. In the northeast monsoon, winds cause a flow to the south and southwest in most areas of the southern East Asian Sea. Offshore Vietnam and offshore Peninsular Malaysia, tide and wind-driven currents may combine to provide strong southwesterly and southerly currents respectively. Additionally, the reduced depth between Peninsular Malaysia and Borneo in the Strait of Karimata restricts the amount of water moving this way and causes the set-up of a circulation which results in an almost constant flow towards the northeast offshore Borneo. In the southwest monsoon, currents primarily move to the north or northwest in most locations.

G.7.4 Density-driven currents (particularly near the outflow of large rivers)

The presence of less-saline water masses due to the outflow of major rivers including the Mekong River, the Chao Phraya River flowing into the Gulf of Thailand, and the Kuching, Rajang and Baram rivers flowing into the South China Sea from Sarawak, causes some density-driven flow. However it should be noted that most Southeast Asian rivers hold considerable sediments, and the waters might be denser than expected from their salinity and temperature. Under some circumstances turbidity currents may be expected, especially during high flow periods.

G.7.5 Basin-response currents derived from tropical storms or strong monsoon surges

Strong currents have been observed offshore Vietnam and offshore Borneo along the edge of the continental shelf. At several locations, these strong currents coincided with a low-pressure system in the southern half of the East Asian Sea and tended to lag monsoon surges. Typically, the strong currents could also be observed in Vietnam several days preceding those in Borneo and appeared to progress as a Kelvin wave around the East Asian Sea, tracking the edge of the continental shelf and turning northeast along the Sabah coast.

G.7.6 Internal waves

Internal waves occur in the East Asian Sea in three regions:

a) between the Luzon Strait and Hainan,

b) along the Vietnamese coast, and

c) between Vietnam and Borneo.

They are observed most frequently during the summer (June and July) but have been observed in all months except November and December. It is thought that the waves are generated as follows:

— between the Luzon Strait and Hainan (outside the scope of this annex) waves are;

1) trans-basin waves generated by the shallow topography under the influences of the tide and the Kurshio current, and

2) internal waves generated near the continental shelf break by incident trans-basin waves or by tidal forcing.

— along the Vietnamese coast waves are;

1) trans-basin waves coming from the Luzon strait,

2) disorganized internal waves of unknown origin,

3) organized internal waves probably generated near the continental shelf break by incident tides.

— between Vietnam and Borneo, internal waves are influenced by;

1) the outflow of the Mekong river where internal waveforms are associated with the river plume, and

2) the broad continental shelf and appear to be tidally generated.

The areas covered by this annex where internal wave activity is known to occur (although this list may not be exclusive) include:

— offshore Vietnam,

— offshore Peninsular Malaysia,

— offshore Natuna Island.

G.8 Other environmental factors

G.8.1 Marine growth

Offshore in the southern East Asian Sea, the tropical marine environment means that marine growth of the order of 500 mm is common, with maximum marine growth occurring near the surface but below the surf zone. However site-specific studies are required to determine the variation with depth.

G.8.2 Snow and ice accretion

Snowfall and ice accumulation on structures are not design or operational considerations for the southern East Asian Sea.

G.8.3 Tsunamis

Tsunamis have been measured in the East Asian Sea, with seismic events along the tectonic plate boundaries as the most likely sources. The East Asian Sea is protected by low seismic activity landmasses to the north, west and south; consequently, it may only be affected by a tsunami that originates in or is able to enter the East Asian Sea. It is unlikely that seismic events along the Sumatra-Java plate boundary would seriously affect the East Asian Sea (the 2004 Indian Ocean tsunami had little measurable effect in the East Asian Sea) and there is only a low probability that any tsunami generated in the Pacific would have the correct directional and energy characteristics to enter the southern part of the East Asian Sea. The East Asian Sea is exposed to tsunami risk from the east due to the high level of seismic activities in the Taiwan and Philippines areas, associated with the Philippines plate boundary. The most active part of the Philippines plate boundary is around the island of Taiwan, which has experienced several earthquakes resulting in the generation of tsunamis, although recorded levels were only 0,2 m above sea level. There have been about 100 recorded tsunami events in and around the Philippines, although many of these have been small or confined to the east coast. There have been some significant events on the edge of the East Asian Sea and within the Sulu and Celebes Seas.

G.8.4 Air temperature, humidity, pressure and visibility and rainfall

High air temperatures are encountered throughout the region, with daily temperatures ranging between 22 °C and 36 °C. Maximum air temperatures generally occur between May and July, and minimum air temperatures may occur at any time of the year. Although minimum temperatures are often associated with night, they are also caused by squall (downdraft) events and may occur at any time of the day. January and February exhibit the smallest variation in daily temperature.

The relative humidity in this region is high and its value often exceeds 90 %, varying between 45 % and 100 %. Humidity varies both through the day and seasonally. Minimum humidity generally occurs between May and July, although maximum humidity may occur at any time of the year. Maximum humidity often occurs before dawn and in association with rainfall events.

Atmospheric pressure shows a significant diurnal (twice-daily) cycle caused by global atmospheric tides with a variation in the order of 0,5 kPa (5 mbar). Typically, the pressure varies between 100 kPa (1 000 mbar) and 102 kPa (1 020 mbar), excluding typhoon events when pressure may drop below this range depending on the severity of the typhoon and it track. There are some seasonal variations of pressure, with minimum pressure typically occurring in the April to May monsoon transition or associated with the passage of a typhoon (typically July to December), and maximum pressures typically occurring with northeast monsoon surges. The range of typical atmospheric pressures increases with latitude.

Visibility is not typically affected by fog in this region, although onshore locations may experience fog or mist most often at dawn. In an El Niño year with the associated dry conditions, haze from dust and smoke due to forest fires may affect visibility over larges areas of the East Asian Sea, particularly during the southwest monsoon since the typical sources of smoke particles are Sumatra, Peninsular Malaysia and Borneo. Smoke and the associated atmospheric condensation may have a significant detrimental effect on visibility. Heavy rain associated with squalls and thunderstorms may also significantly reduce local visibility for short periods.

G.8.5 Seawater temperature and salinity

Sea surface temperatures in the East Asian Sea south of 15° N range between 24 °C and 31 °C, and are typically warmer the nearer the equator. Surface water temperatures start to decrease with the onset of the northeast monsoon as the cold water pushes south, with a significant drop in temperature starting in November for offshore Vietnam but typically in December for the other locations, and the minimum monthly mean sea surface temperatures are usually experienced in January. In April the temperature increases, with the maximum typically occurring in May or June prior to the onset of the southwest monsoon.

The water column is generally stratified for water depths greater than 80 m, except during the northeast monsoon when the wave energy in the monsoon surges acts to break up the thermocline and cause mixing through the water column. For depths of 80 m to 140 m, maximum sea-bottom temperatures are often coincident with the first monsoon surge. Where the water is too shallow for a permanent thermocline, sea-bottom temperatures typically track the surface temperatures.

Sea surface salinities are generally between 32 PSU and 34 PSU. However, there is a significant reduction in salinity near the inflow of major rivers. The most significant of these is the Mekong River, the 12th-largest river in the world, by volume, discharging 475 km^3 of water annually. The inflow of this river also acts to significantly reduce water temperatures at times of high flow. Other significant rivers include the Chao Phraya River flowing into the Gulf of Thailand, and the Kuching, Rajang and Baram rivers flowing into the East Asian Sea from Sarawak.

G.9 Estimates of metocean parameters

G.9.1 Extreme metocean parameters

G.9.1.1 General

Indicative extreme values for wind, wave and current parameters are provide in Tables G.1 to G.13 for various return periods and for 13 locations across the waters of offshore Vietnam, the Gulf of Thailand, the

waters offshore Peninsular Malaysia, the waters offshore Natuna Island, the waters offshore Borneo and the waters offshore Philippines. The wind, wave and current values are independently derived marginal parameters, and no account has been taken of conditional probability. Table G.14 gives indicative values for other metocean parameters for offshore Borneo.

Extreme-value conditions in most areas of the East Asian Sea are dominated by typhoons, either because of the direct passage of typhoons or due to the swell generated by typhoons. In the areas further south, conditions may be dominated by the northeast monsoon.

The spatial and seasonal variability of metocean design criteria in the southern South China Sea is discussed in Reference [155]. Non-stationary extreme value analysis was performed using the Covariate Extreme Value Analysis,) for a 59-year long SEAFINE hindcast of winds (Figure G.7) and waves (Figure G.8), estimating metocean design criteria up to 10,000-year return period. Note that wind sensitive structures need to be checked against squall wind criteria, as these might exceed extreme winds derived from the historical hindcasts.

As with all values in the regional annexes of this part of ISO 19901, these figures are provided to assist with engineering concept selections and are not suitable for the design of offshore structures.

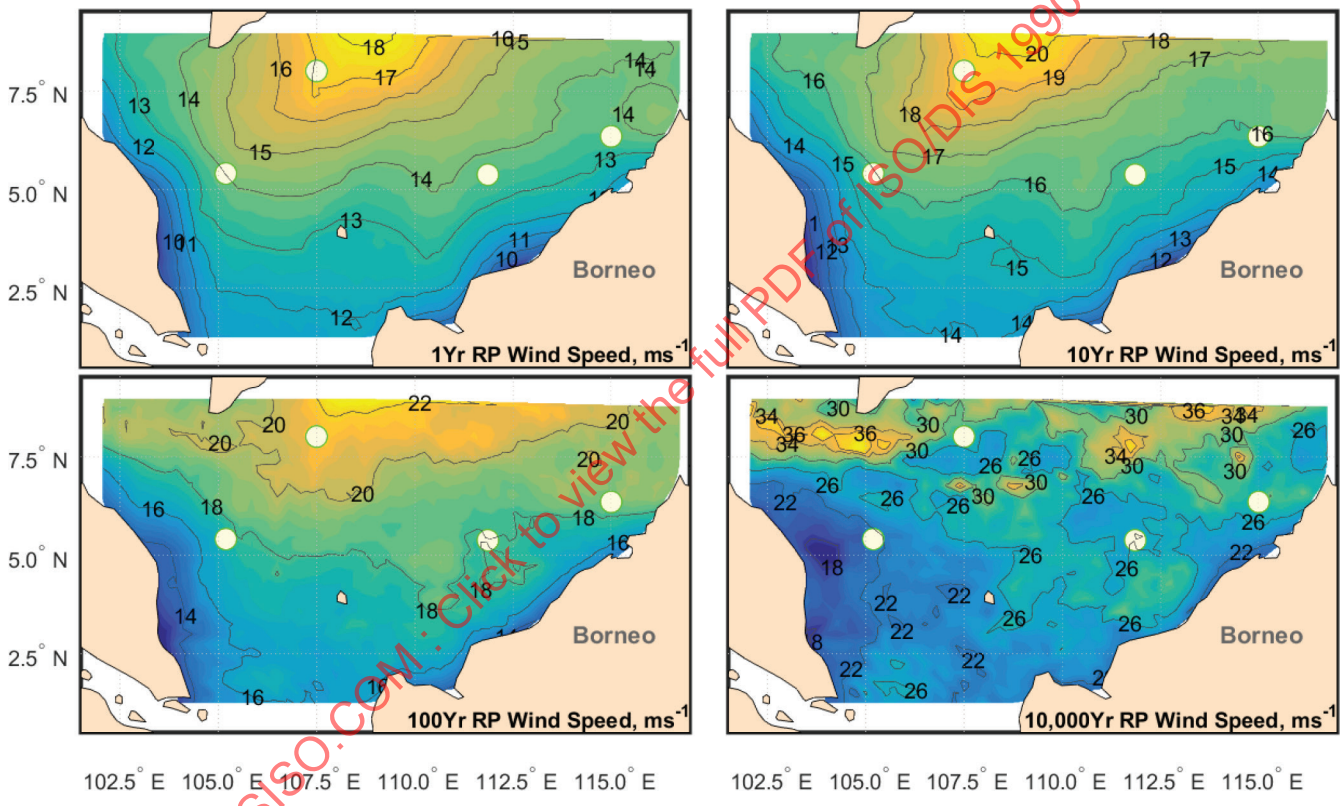

Figure G.7 — Contours of return period estimates of 1-hour wind speed (in m/s)

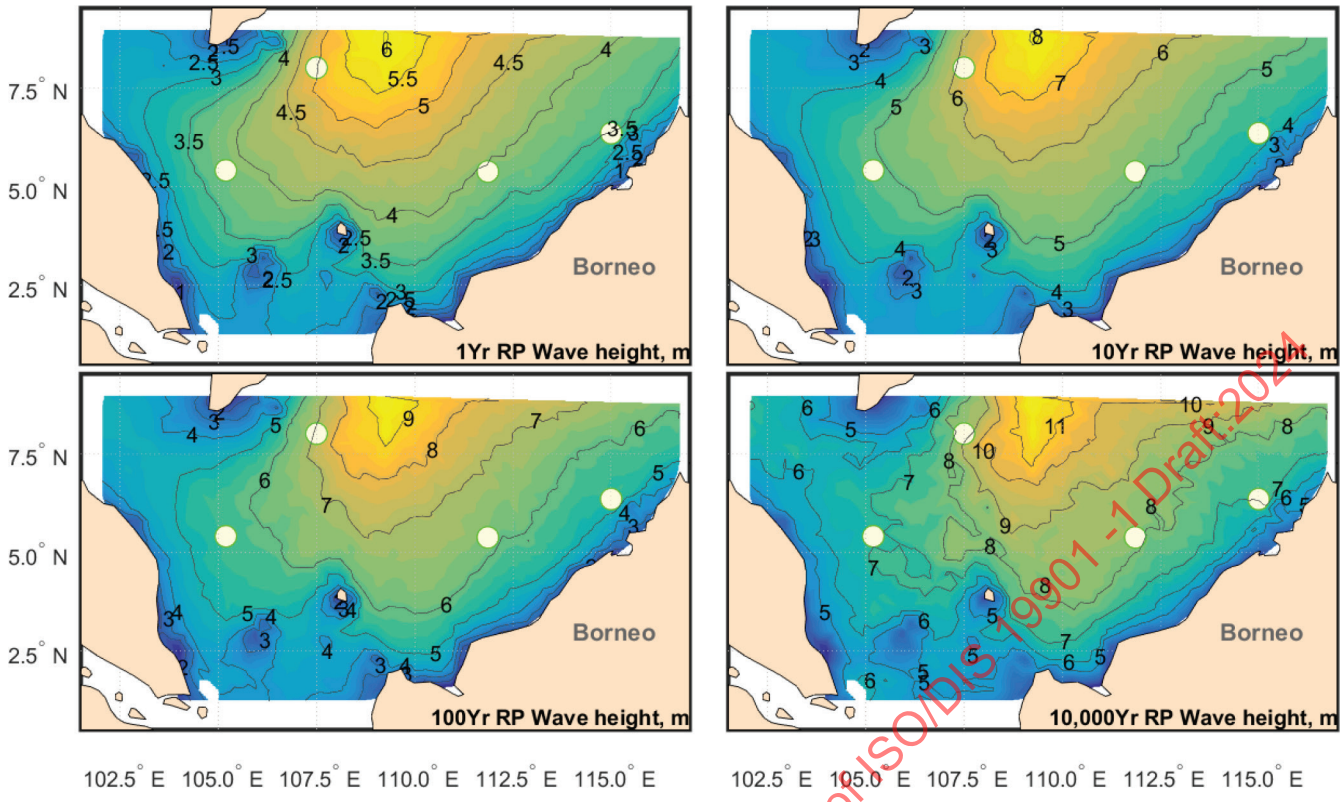

Figure G.8 — Contours of return period estimates of significant wave height (in m)

G.9.1.2 Waters offshore Vietnam

Offshore Vietnam, as the location farthest to the north which is covered in this annex, is subject to the frequent passage of typhoons; the typhoon track is significantly affected by the ENSO, with October, November and December the months most frequently affected. The area is also significantly influenced by the northeast monsoon.

Table G.1 — Offshore Vietnam — Shallow water

Metocean parameter	Return period *N* years				
	1	**5**	**10**	**50**	**100**
Nominal water depth	20 m (10° N, 108° E)				
Wind speed at 10 m above MSL					
1-h mean (m/s)	23,1	25,8	26,7	29,1	30,0
10-min mean (m/s)	26,8	29,9	31,0	33,8	34,8
1-min mean (m/s)	31,9	35,6	36,8	40,2	41,4
3-s gust (m/s)	38,6	43,1	44,6	48,6	50,1
Waves					
Significant height (m)	3,7	4,7	5,4	5,7	6,2
Maximum height (m)	7,1	9,0	10,2	10,7	11,8
Mean period (s)	6,7	7,6	8,1	8,3	8,7
Spectral peak period (s)	9,5	10,7	11,4	11,7	12,3
Wave direction (from)					
Extreme	NE	NE	NE	NE	NE

Table G.1 *(continued)*

Metocean parameter	Return period *N* years				
	1	**5**	**10**	**50**	**100**
Prevailing	NE	NE	NE	NE	NE
Current speed					
Surface (m/s)	1,14	1,22	1,31	1,41	1,50

Table G.2 — Offshore Vietnam — Deep water

Metocean parameter	Return period *N* years				
	1	**5**	**10**	**50**	**100**
Nominal water depth	1 800 m (12° N, 110° E)				
Wind speed at 10 m above MSL					
1-h mean (m/s)	38,5	43,0	44,5	48,5	50,0
10-min mean (m/s)	44,7	49,9	51,6	56,3	58,0
1-min mean (m/s)	53,1	59,3	61,4	66,9	69,0
3-s gust (m/s)	64,3	71,8	74,3	81,0	83,5
Waves					
Significant height (m)	7,3	8,3	8,7	9,6	10,0
Maximum height (m)	13,7	15,5	16,2	17,8	18,6
Mean period (s)	9,4	10,0	10,3	10,8	11,0
Spectral peak period (s)	13,3	14,2	14,5	15,2	15,6
Wave direction (from)					
Extreme	NE	NE	NE	NE	NE
Prevailing	NE	NE	NE	NE	NE
Current speed					
Surface (m/s)	1,75	1,86	2,00	2,16	2,30

G.9.1.3 Gulf of Thailand

The Gulf of Thailand is to some extent protected from both northeast and southwest monsoons; however typhoons do occasionally track into the Gulf of Thailand, causing extreme wave heights and wind speeds, and make extreme conditions in this area difficult to predict and requiring long datasets. The highest risk months for typhoon activity are October, November and December.

Table G.3 — Gulf of Thailand — North

Metocean parameter	Return period *N* years				
	1	**5**	**10**	**50**	**100**
Nominal water depth	75 m (10° N, 101° E)				
Wind speed at 10 m above MSL					
1-h mean (m/s)	35,4	39,6	40,9	44,6	46,0
10-min mean (m/s)	41,1	45,9	47,5	51,8	53,4
1-min mean (m/s)	48,9	54,6	56,5	61,6	63,5
3-s gust (m/s)	59,2	66,1	68,4	74,5	76,8
Waves					
Significant height (m)	7,3	8,3	8,7	9,6	10,0

Table G.3 *(continued)*

Metocean parameter	Return period *N* years				
	1	**5**	**10**	**50**	**100**
Maximum height (m)	13,7	15,5	16,2	17,8	18,6
Mean period (s)	9,4	10,0	10,3	10,8	11,0
Spectral peak period (s)	13,3	14,2	14,5	15,2	15,6
Wave direction (from)					
Extreme	E	E	E	E	E
Prevailing	WSW	WSW	WSW	WSW	WSW
Current speed (m/s)					
Surface					

Table G.4 — Gulf of Thailand — South

Metocean parameter	Return period *N* years				
	1	**5**	**10**	**50**	**100**
Nominal water depth	85 m (8° N, 103° E)				
Wind speed at 10 m above MSL					
1-h mean (m/s)	27,0	30,1	31,2	34,0	35,0
10-min mean (m/s)	31,3	34,9	36,1	39,4	40,6
1-min mean (m/s)	37,2	41,5	43,0	46,9	48,3
3-s gust (m/s)	45,0	50,3	52,0	56,7	58,5
Waves					
Significant height (m)	5,1	5,8	6,1	6,7	7,0
Maximum height (m)	9,7	11,0	11,5	12,6	13,2
Mean period (s)	7,9	8,4	8,6	9,0	9,2
Spectral peak period (s)	11,1	11,9	12,1	12,7	13,0
Wave direction (from)					
Extreme	NE	NE	NE	NE	NE
Prevailing	E	E	E	E	E
Current speed					
Surface (m/s)					

G.9.1.4 Offshore Peninsular Malaysia

Offshore Peninsular Malaysia is protected from the southwest monsoons but exposed to the northeast monsoons. The direct impact of typhoons is less likely due to the low latitude, but their influence should be considered.

Table G.5 — Offshore Peninsular Malaysia

Metocean parameter	Return period *N* years				
	1	**5**	**10**	**50**	**100**
Nominal water depth	70 m (6° N, 106° E)				
Wind speed at 10 m above MSL					
1-h mean (m/s)	22,3	24,9	25,8	28,1	29,0
10-min mean (m/s)	25,9	28,9	29,9	32,6	33,6
1-min mean (m/s)	30,8	34,4	35,6	38,8	40,0
3-s gust (m/s)	37,3	41,6	43,1	47,0	48,4
Waves					
Significant height (m)	5,8	6,6	7,0	7,7	8,0
Maximum height (m)	11,0	12,5	13,1	14,4	15,0
Mean period (s)	8,4	9,0	9,2	9,7	9,9
Spectral peak period (s)	11,9	12,7	13,0	13,6	13,9
Wave direction (from)					
Extreme	NE	NE	NE	NE	NE
Prevailing	NE	NE	NE	NE	NE
Current speed					
Surface (m/s)					

G.9.1.5 Offshore Natuna Island

Offshore Natuna Island is protected from the southwest monsoon but exposed to the northeast monsoon. The direct impact of typhoons is less likely due to the low latitude, but their influence should be considered.

Table G.6 — Offshore Natuna Island (South Natuna Sea)

Metocean parameter	Return period *N* years				
	1	**5**	**10**	**50**	**100**
Nominal water depth	60 m (3,5° N, 106° E)				
Wind speed at 10 m above MSL					
1-h mean (m/s)	20,0	22,4	23,1	25,2	26,0
10-min mean (m/s)	23,2	25,9	26,8	29,3	30,2
1-min mean (m/s)	27,6	30,9	31,9	34,8	35,9
3-s gust (m/s)	33,4	37,3	38,6	42,1	43,4
Waves					
Significant height (m)	5,1	5,8	6,1	6,7	7,0
Maximum height (m)	9,7	11,0	11,5	12,6	13,2
Mean period (s)	7,9	8,4	8,6	9,0	9,2
Spectral peak period (s)	11,1	11,9	12,1	12,7	13,0
Wave direction (from)					
Extreme	NE	NE	NE	NE	NE
Prevailing	NE	NE	NE	NE	NE
Current speed					
Surface (m/s)					

Table G.7 — Offshore Natuna Island (North Natuna Sea)

Metocean parameter	Return period *N* years				
	1	**5**	**10**	**50**	**100**
Nominal water depth	140 m (5° N, 110° E)				
Wind speed at 10 m above MSL					
1-h mean (m/s)	22,3	24,9	25,8	28,1	29,0
10-min mean (m/s)	25,9	28,9	29,9	32,6	33,6
1 min mean (m/s)	30,8	34,4	35,6	38,8	40,0
3-s gust (m/s)	37,3	41,6	43,1	47,0	48,4
Waves					
Significant height (m)	5,8	6,6	7,0	7,7	8,0
Maximum height (m)	11,0	12,5	13,1	14,4	15,0
Mean period (s)	8,4	9,0	9,2	9,7	9,9
Spectral peak period	11,9	12,7	13,0	13,6	13,9
Wave direction (from)					
Extreme	NNE	NNE	NNE	NNE	NNE
Prevailing	NE	NE	NE	NE	NE
Current speed					
Surface (m/s)	1,14	1,22	1,31	1,41	1,50

G.9.1.6 Waters offshore Borneo

The relative influence of the northeast and southwest monsoons varies across the waters offshore Borneo, with the northeast monsoon dominating in the western part, but reducing in the eastern areas due to sheltering provided by the Philippines. Conversely, the longer fetch length means that the southwest monsoon becomes more significant in the eastern part. The direct impact of typhoons is less likely due to the low latitude, but their influence should be considered and may still dominate design considerations.

Table G.8 — Offshore Borneo — Sarawak shallows

Metocean parameter	Return period *N* years				
	1	**5**	**10**	**50**	**100**
Nominal water depth	70 m				
Wind speed at 10 m above MSL					
1-h mean (m/s)	18,5	20,6	21,4	23,3	24,0
10-min mean (m/s)	21,4	23,9	24,8	27,0	27,8
1-min mean (m/s)	25,5	28,5	29,5	32,1	33,1
3-s gust (m/s)	30,9	34,5	35,7	38,9	40,1
Waves					
Significant height (m)	4,0	4,6	4,8	5,3	5,5
Maximum height (m)	7,7	8,7	9,1	10,0	10,4
Mean period (s)	7,0	7,5	7,6	8,0	8,2
Spectral peak period (s)	9,9	10,5	10,8	11,3	11,5
Wave direction (from)					
Extreme	N	N	N	N	N

Table G.8 *(continued)*

Metocean parameter	Return period *N* years				
	1	**5**	**10**	**50**	**100**
Prevailing	NNE	NNE	NNE	NNE	NNE
Current speed					
Surface (m/s)	1,06	1,13	1,22	1,32	1,40

Table G.9 — Offshore Borneo — Sarawak shelf edge

Metocean parameter	Return period *N* years				
	1	**5**	**10**	**50**	**100**
Nominal water depth	140 m				
Wind speed at 10 m above MSL					
1-h mean (m/s)	21,6	24,1	24,9	27,2	28,0
10-min mean (m/s)	25,0	27,9	28,9	31,5	32,5
1-min mean (m/s)	29,8	33,2	34,4	37,5	38,6
3-s gust (m/s)	36,0	40,2	41,6	45,4	46,8
Waves					
Significant height (m)	5,5	6,3	6,6	7,3	7,6
Maximum height (m)	10,5	11,9	12,5	13,7	14,2
Mean period (s)	8,2	8,8	9,0	9,4	9,6
Spectral peak period (s)	11,6	12,4	12,6	13,3	13,6
Wave direction (from)					
Extreme	NW	NW	NW	NW	NW
Prevailing	NNE	NNE	NNE	NNE	NNE
Current speed					
Surface (m/s)	1,56	1,66	1,78	1,93	2,05

Table G.10 — Offshore Borneo – Sabah shallows

Metocean parameter	Return period *N* years				
	1	**5**	**10**	**50**	**100**
Nominal water depth	50 m				
Wind speed at 10 m above MSL					
1-h mean (m/s)	20,0	22,4	23,1	25,2	26,0
10-min mean (m/s)	23,2	25,9	26,8	29,3	30,2
1-min mean (m/s)	27,6	30,9	31,9	34,8	35,9
3-s gust (m/s)	33,4	37,3	38,6	42,1	43,4
Waves					
Significant height (m)	3,7	4,2	4,4	4,8	5,0
Maximum height (m)	6,6	7,5	7,9	8,6	9,0
Mean period (s)	6,5	6,9	7,1	7,4	7,6
Spectral peak period (s)	10,1	10,7	11,0	11,5	11,8
Wave direction (from)					
Extreme	W	W	W	W	W

Table G.10 *(continued)*

Metocean parameter	Return period *N* years				
	1	**5**	**10**	**50**	**100**
Prevailing	NNE/W	NNE/W	NNE/W	NNE/W	NNE/W
Current speed					
Surface (m/s)	0,99	1,05	1,13	1,22	1,30

Table G.11 — Offshore Borneo — Sabah shelf edge

Metocean parameter	Return period *N* years				
	1	**5**	**10**	**50**	**100**
Nominal water depth	120 m				
Wind speed at 10 m above MSL					
1-h mean (m/s)	20,8	23,2	24,0	26,2	27,0
10-min mean (m/s)	24,1	26,9	27,9	30,4	31,3
1-min mean (m/s)	28,7	32,0	33,2	36,1	37,3
3-s gust (m/s)	34,7	38,8	40,1	43,7	45,1
Waves					
Significant height (m)	4,9	5,6	5,8	6,4	6,7
Maximum height (m)	9,3	10,6	11,1	12,2	12,7
Mean period (s)	7,3	7,8	8,0	8,4	8,5
Spectral peak period (s)	10,3	11,0	11,2	11,8	12,0
Wave direction (from)					
Extreme	WNW	WNW	WNW	WNW	WNW
Prevailing	NNE/W	NNE/W	NNE/W	NNE/W	NNE/W
Current speed					
Surface (m/s)	2,13	2,27	2,44	2,63	2,80

Table G.12 — Offshore Borneo — Sabah deepwater

Metocean parameter	Return period *N* years				
	1	**5**	**10**	**50**	**100**
Nominal water depth	1 500 m				
Wind speed at 10 m above MSL					
1-h mean (m/s)	20,8	23,2	24,0	26,2	27,0
10-min mean (m/s)	24,1	26,9	27,9	30,4	31,3
1-min mean (m/s)	28,7	32,0	33,2	36,1	37,3
3-s gust (m/s)	34,7	38,8	40,1	43,7	45,1
Waves					
Significant height (m)	5,1	5,8	6,1	6,7	7,0
Maximum height (m)	9,7	11,0	11,5	12,7	13,2
Mean period (s)	7,7	8,2	8,4	8,8	9,0
Spectral peak period (s)	10,8	11,5	11,8	12,4	12,7
Wave direction (from)					
Extreme	NW	NW	NW	NW	NW

Table G.12 *(continued)*

Metocean parameter	Return period N years				
	1	**5**	**10**	**50**	**100**
Prevailing	NNE/WSW	NNE/WSW	NNE/WSW	NNE/WSW	NNE/WSW
Current speed					
Surface (m/s)	1,40	1,56	1,64	1,80	1,86

G.9.1.7 Offshore Philippines

Offshore Philippines (Palawan Island), being in the north of the area covered in this annex, is subject to the frequent passage of typhoons, both those that cross into the East Asian Sea and those that remain east of the Philippines. Although the typhoon track is significantly affected by the ENSO, typhoons may typically influence the area from May to December.

Table G.13 — Offshore Philippines — Palawan area

Metocean parameter	Return period N years				
	1	**5**	**10**	**50**	**100**
Nominal water depth	1 000 m				
Wind speed at 10 m above MSL					
1-h mean (m/s)	38,5	43,0	44,5	48,5	50,0
10-min mean (m/s)	44,7	49,9	51,6	56,3	58,0
1-min mean (m/s)	53,1	59,3	61,4	66,9	69,0
3-s gust (m/s)	64,3	71,8	74,3	81,0	83,5
Waves					
Significant height (m)	11,7	13,3	13,9	15,4	16,0
Maximum height (m)	21,6	24,4	25,5	28,1	29,2
Mean period (s)	11,9	12,7	13,0	13,7	14,0
Spectral peak period (s)	16,8	17,9	18,3	19,3	19,7
Wave direction (from)					
Extreme	NNW	NNW	NNW	NNW	NNW
Prevailing	NNE/WSW	NNE/WSW	NNE/WSW	NNE/WSW	NNE/WSW
Current speed (m/s)					
Surface	1,22	1,30	1,39	1,50	1,60

Table G.14 — Indicative extreme values for other metocean parameters

	Temperature		
	°C		
	Min	**Mean**	**Max**
Air Temperature	20	27,9	34,5
Air Humidity (%)	45	75	100
Sea surface (MSL)	24,2	28,4	30,7
20 m below MSL	24,2	28,4	30,7
60 m below MSL	22,2	25,9	29,4

Table G.14 *(continued)*

	Temperature		
	°C		
	Min	**Mean**	**Max**
100 m below MSL	20,5	23,8	28,7
140 m below MSL	15,2	18,4	24,9
200 m below MSL	13,1	15,2	19,6
400 m below MSL	8,6	10,1	12,0
600 m below MSL	6,3	7,5	8,8
800 m below MSL	4,8	5,7	6,5
1 000 m below MSL	3,9	4,7	5,4

G.9.2 Squall Design Criteria

In the near-equatorial regions where tropical cyclones are infrequent, squalls may control design of wind sensitive structures. Squalls measured offshore Borneo were analysed in SEAFINE JIP, Reference [153], with indicative squall design criteria shown below. Vertical squall wind profile derived from measurements offshore West Africa are proposed, Reference [156].

As with all values in the regional annexes of this part of ISO 19901, these figures are provided to assist with engineering concept selections and are not suitable for the design of offshore structures.

Table G.15 — Indicative extreme squall criteria for offshore Borneo (1 min, 10 m, in ms^{-1})

Return Period	1-yr	5-yr	10-yr	20-yr	50-yr	100-yr
Offshore Sarawak and Brunei	22	25	26	27	28	29
Offshore Borneo -Sabah	23	26	27	28	30	31

Annex H
(informative)

Mediterranean Sea

H.1 Description of region

H.1.1 General

The Mediterranean Sea is a mid-latitude, semi-enclosed, marginal sea characterized by high salinities, temperatures and densities. It is located on the western side of a large continental area, and is surrounded by Europe to the north, Africa to the south and Asia to the east, as shown in Figure H.1 (taken from Reference [157]). It is connected to the Atlantic Ocean through the narrow Strait of Gibraltar and to the Black Sea through the Dardanelles and Bosphorous straits. It is composed by two basins, known as the Western Mediterranean Basin and the Eastern Mediterranean Basin, that are connected by the Strait of Sicily, that has a maximum depth of about 500 m.

The geographical scope of this annex includes the Western Mediterranean Basin and the Eastern Mediterranean Basin whereas the marginal basins Marmara Sea and the Black Sea will be included in future update.

H.1.2 West Mediterranean Basin

The Western Mediterranean contains the Alborán Sea, the Catalan Sea (named also Balearic), the Algerian-Provençal Sea and the Tyrrhenian Sea. The Alborán Sea is in the westernmost Mediterranean Sea and forms a narrow (100 km) approach to the Strait of Gibraltar. It is connected to the North Atlantic through the Strait of Gibraltar which is 15 km wide and 300 m deep. It has an area of 54 000 km^2 and a maximum depth of nearly 1 500 m in the western basin and about 2 000 m at its eastern limit.

The Catalan Sea lies in the north-western Mediterranean Sea between the Iberian coast and the Balearic Island. Most of the area is less than 2 000 m deep and is closed to outside access below 1 000 m except north of Menorca. The larger sub-basin of the West Mediterranean Sea is the Algerian-Provençal sea. Leaving the Alborán Sea to the west, it extends with a triangular shape from the Gulf of Valencia to the Ligurian Sea. Its maximum depth is 2 900 m, near the western coasts of Sardinia. It is characterized in its most western part, by the large deep-sea cone of the Ebro river, where the continental shelf reaches a width of 60 km. Along the northern coasts, up to Genoa, the continental shelf is practically absent, it is not wider than 3-9 km. Here the sea bottom descends rapidly to depths over 2 000 m and is characterized by several submarine canyons that cut across it. The Tyrrhenian Sea is an almost triangular shaped depression, between Sardinia and peninsular Italy. It communicates with the other basins through 4 passages: a 300-400 m deep channel puts it in communication with the Ligurian Sea; a wide, 2 000 m deep channel between Sicily and Sardinia connects it to the Algerian basin; the Boniface Strait (that is 50 m deep) connects it to the Provence basin; and finally, the Strait of Messina is the connection (100 m deep) with the Ionian Sea. The maximum depth of the sea is 3785 metres. The Tyrrhenian Sea is situated near where the African and Eurasian Plates meet; therefore mountain chains and active volcanoes such as Mount Marsili are found in its depths.

H.1.3 East Mediterranean Basin

Four sub-sea basins may be identified in the East Mediterranean Basin: the Ionian, the Levantine, the Adriatic and the Aegean Seas. The Ionian Sea lies between Italy and Greece to the north, and Libya and Tunisia to the south, and it is an elongated embayment in the Mediterranean Sea with a maximum depth of about 5 000 m south of Greece. The Ionian Sea is characterized by the subduction of the Afrimay plate under the Calabrian Arc, making it one of the most geologically active areas in the Mediterranean Basin. The Levantine Sea is bordered by Turkey in the north, Syria, Lebanon, Israel and the Gaza Strip in the east, Egypt in the south, and the Aegean Sea in the northwest. The western border to the open Mediterranean (there also called Libyan Sea) is defined as a line from the cape Ras al-Helal in Libya to the island of Gavdos, south of Crete. The largest

island in the Levantine Sea is Cyprus. The greatest depth of 4 384 m is found in the Pliny Trench, about 80 km south of Crete. The Levantine Sea stretches over an area of 320 000 km^2. The Nile Delta Cone and the East Mediterranean coast define its southwestern and eastern margins.

The Levantine Sea has depths of about 2 500–3 000 m in the centre of the basin and a maximum depth of 4 500 m in a depression located southeast of Rhodes Island. The Adriatic Sea is an elongated basin, with its major axis in the northwest–southeast direction, located in the central Mediterranean, between the Italian peninsula and the Balkans. Its northern section is very shallow and gently sloping, with an average bottom depth of about 35 m. The middle Adriatic is 140 m deep on average, with the two Pomo Depressions reaching 260 m. The southern section is characterized by a wide depression more than 1 200 m deep.

The water exchange with the Mediterranean Sea takes place through the Otranto Channel, whose sill is 800 m deep. The eastern coast is generally high and rocky, whereas the western coast is low and mostly sandy. Many rivers discharge into the basin, with significant influence on the circulation, particularly relevant being the Po River in the northern basin, and the ensemble of the Albanian rivers in the southern basin. The Aegean Sea joins the Levantine through several passages located between Greece, Turkey, Crete and Rhodes. Analogously to the Ionian Sea, the Aegean Sea finds its origin and morphological characteristics in the subduction of the Afrimay plate, in this case underneath Greece. This too is an area of intense volcanic and seismic phenomena (the caldera on the Island of Santorini is a well known feature). It is characterized by the presence of over 200 islands and is subdivided into various minor basins, such as the Crete sub-basin, surrounded by a trench that is 2 500 m deep.

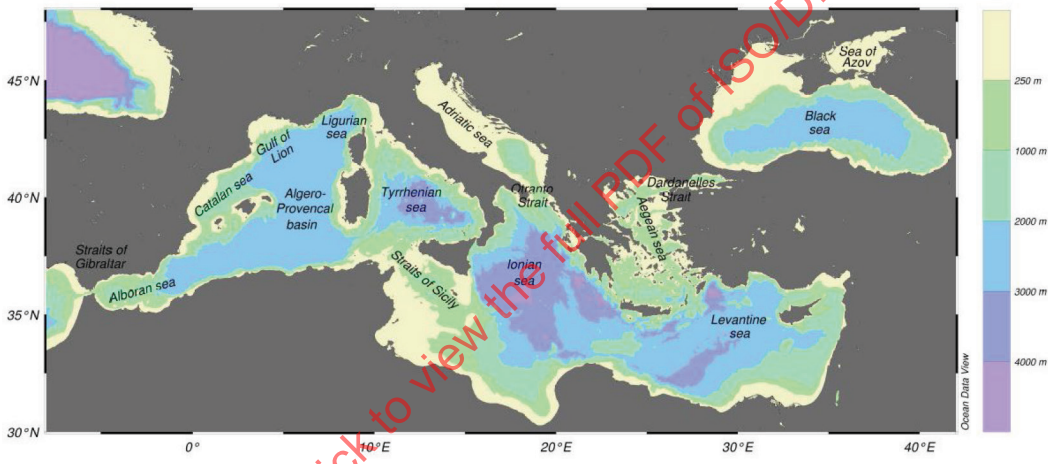

Figure H.1 — Major seas, connecting straits and bottom topography of Mediterranean Sea (taken from Ref. [157]).

H.2 Data sources

Data regarding metocean conditions in the region are available from a variety of sources.

With regards wind, waves and current conditions, data have been taken from Oil and Gas projects executed in the various regions of the Mediterranean Sea. They are based on hindcast dataset, as an example:

— the 44 years long hindcast dataset obtained by the EU-funded research project HIPOCAS (http://www.mar.ist.utl.pt/hipocas/index.asp),

— the Oceanweather Mediterranean Wind Wave model GROW-Fine (https://www.oceanweather.com/metocean/mediterranean/index.html),

— the Mediterranean hindcast models developed by DHI and HyMOLab (http://www.emodnet.eu/mediterranean_wind_wave_model_0) and

— the Mediterranean Reanalysis dataset obtained using the models NEMO-OPA (https://marine.copernicus.eu/).

Moreover, extensive measurement campaigns have been performed and collected data used to validate data models or to extrapolate missing information.

Other variables have been taken from literature (see references in dedicated paragraphs) and from the Admiralty Pilots of the area (see References [158], [159], [160], [161] and [162]).

H.3 Overview of regional climatology

The Mediterranean Sea is characterized, for the most part, by the climate named "Mediterranean". It is characterized by mild wet winters and warm to hot, dry summers. The major controlling influences on the climate of Mediterranean region is exercised by the Azores anticyclone, the sub-tropical high-pressure belt centred over the Atlantic. In winter its possible north expansion is responsible for disturbed weather in the region in combination with the Atlantic depression, at the opposite, in summer the Azores anticyclone expands toward the Mediterranean Sea resulting in stable weather condition. However, in recent year, due to climate change, the summer conditions are frequently dominated by Afrimay anticyclone. From October to March, the atmospheric pressure is lower over the Mediterranean Sea than the surrounding land masses and the Atlantic depressions move into the Mediterranean Sea from northwest bringing disturbed weather, most of these depressions have associated cold frontal systems giving rise to severe squalls and thunderstorms, that in the North Africa coast could induce sand-storms. Sometimes these depressions give origin to strong low-pressure systems over the Balearic Island, the Gulf of Genova and the Ionian Sea that slowly moves toward east and southeast (Figure H.2, Ref. [158]). In winter the Siberian Anticyclone occasionally extends towards west up to the Balkans or the Central Europe inducing strong north and northeast winds (Bora). In spring the low-pressure systems gradually become less frequent and less intense up to the summer when the atmospheric disturbances become relatively rare.

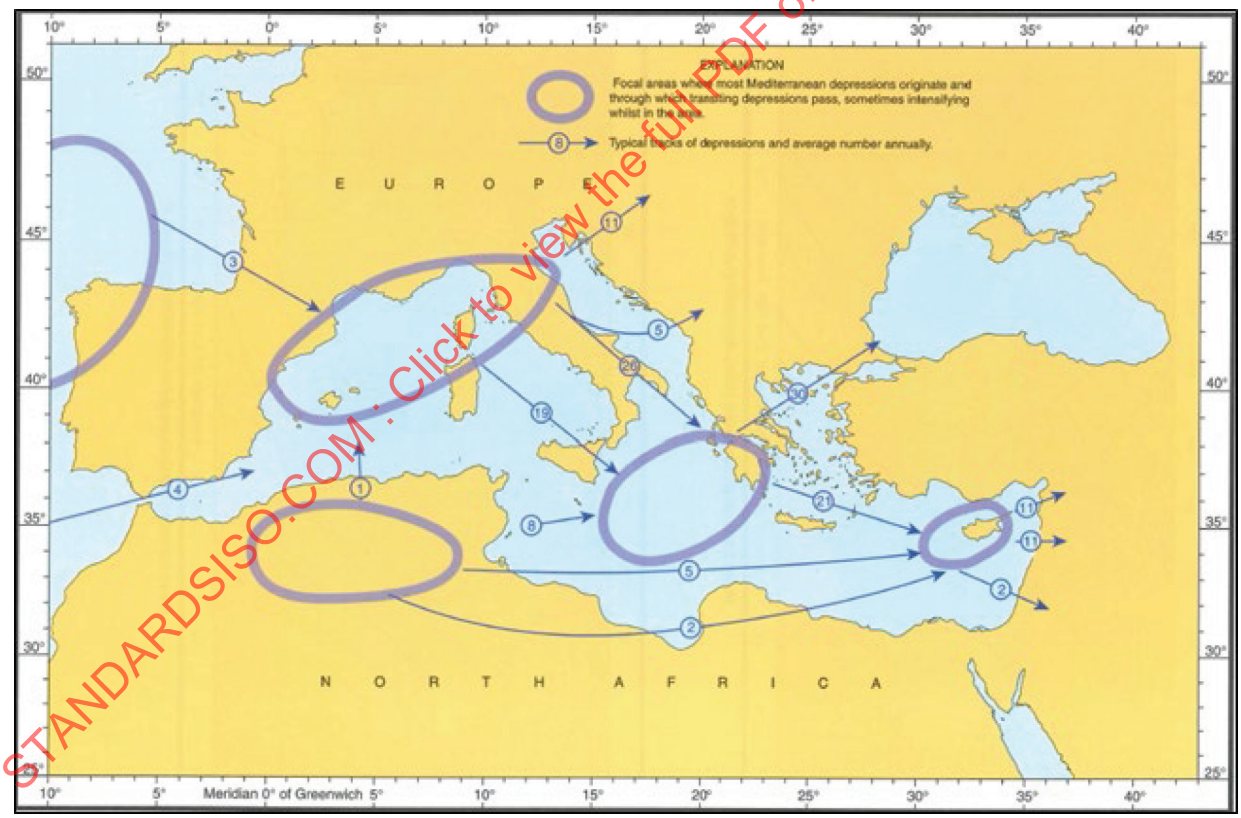

Figure H.2 — Typical disturbances tracks over the Mediterranean Sea – Taken from Ref. [158]

At the end of the summer the interaction between the first Atlantic depressions and the warm sea water could occasionally originate the so called Medicanes or Tropical Like Cyclones (TLC) (Figure H.3).

Although the TLC are small and weaker compared with the tropical cyclones, they show many features characterizing hurricanes such as a warm core and a clear sky eye at the centre of the storm surrounded

by intense thunderstorms. A majority of Medicanes form over two separate regions. The first, more conducive for development than the other, encompasses an area of the Western Mediterranean bordered by the Balearic Islands, southern France and the shorelines of the islands of Corsica and Sardinia. The second identified region of development, in the Ionian Sea between Sicily and Greece and stretching south to Libya, is less favourable for cyclogenesis. An additional two regions, in the Aegean and Adriatic seas, produce fewer Medicanes, while activity is minimal in the Levantine region. However, the occurrence of the TLC may be considered as a rare event with a low probability of occurrence, about 1 event per year.

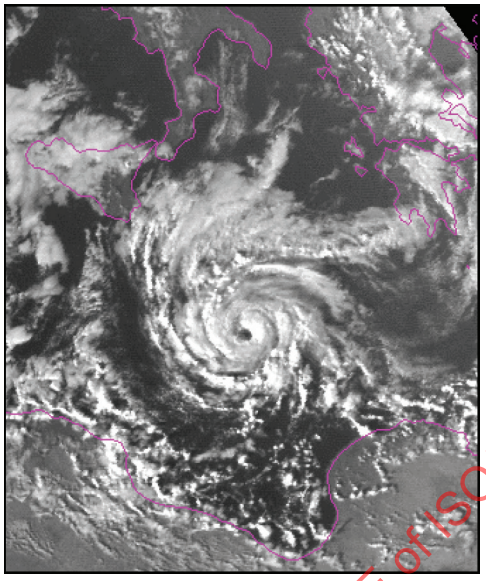

Figure H.3 — The Tropical Like Cyclone Celeno occurred in autumn 1995. Satellite Imagery.

H.4 Water depth, tides and storm surges

The Mediterranean Sea is characterized by rough bottom topography with a narrow continental shelf (<200 m) and a steep continental slope (Figure H.1 taken from Ref. [157]). The western and the eastern basins communicate through the Strait of Sicily and present peculiar topographic depressions characterized by great depths. The most important depressions are the Algero-Provençal basins (maximum depth of about 2 900 m), the Tyrrhenian Sea (about 3 900 m), the Ionian abyssal plain (About 4 200 m), and the Hellenic trench that runs from the Ionian into the Levantine basins (about 5 000 m); finally, in the Levantine basis, the deepest areas are the Rhodes depression (about 4 200 m) in the north and the Herodotus abyssal plain (about 3 000 m) in the south.

Tides in the Mediterranean Sea have amplitudes of the order of few centimetres, except for the Adriatic Sea, the Aegean Sea and the Gulf of Gabès where tides have important ranges and are amplified by resonance phenomena. Consequently, the Mediterranean basin's sea level extremes are mainly related to storm surges rather than to the combination of tides and surge. Storm surges may have significant differences between the various Mediterranean regions, due to the topography of each area and the storm characteristics.

H.5 Winds

The Mediterranean Sea is surrounded by a complex system of mountain chains, with peaks ranging between 1 500 m and 4 800 m. This complex orography has the effect of distorting large synoptic structures and produces local winds of sustained speed which, over some areas of the region, burst almost all over the year (Figure H.4 taken from Ref. [157]).

In the Alborán Sea, the West-Southwest Vendaval occurs mainly from October to November and from February to March, when it may be very strong, whereas the easterly Levante blows in all seasons, but in winter it may be strong and long lasting (up to 10 days). The north-northwest cold and dry Mistral blows in

the Gulf of Lion, occasionally up to the Afrimay coasts. When it enters the Tyrrhenian Sea, the Mistral takes the name of Maestrale, assuming a more marked southward direction.

The central part of the Mediterranean is swept, especially in winter, by the westerly-south-westerly Libeccio and by the wet and warm Sirocco, which, especially in autumn, blow from south to east, producing the well-known storm surges in the Adriatic Sea, flooding the Venice Lagoon. The Bora is a north-easterly strong and cold wind affecting the entire Adriatic Sea, classified as an orographic or downslope wind.

The Levantine Basin, during the summer is affected by persistent and moderate winds blowing from north to northwest and called Etesian (or Meltemi) winds. The Etesian winds are originated by the seasonal strengthening and extension toward east of the Azores Anticyclone and low pressure over the Syria.

The other important wind affecting the Eastern Mediterranean Sea is the Scirocco; it is called Ghibli in Libya and Khamsin between Cyrenaica and Lebanon. The Ghibli is the pre-frontal wind generated by intense Atlantic disturbances approaching to the Mediterranean Sea, it is generally characterized by the advection of very hot and dry air from the Sahara Desert and that may be accompanied by sandstorms in the North Africa coast. After the passage of these disturbances the wind rapidly veers to north-west and decreases in intensity.

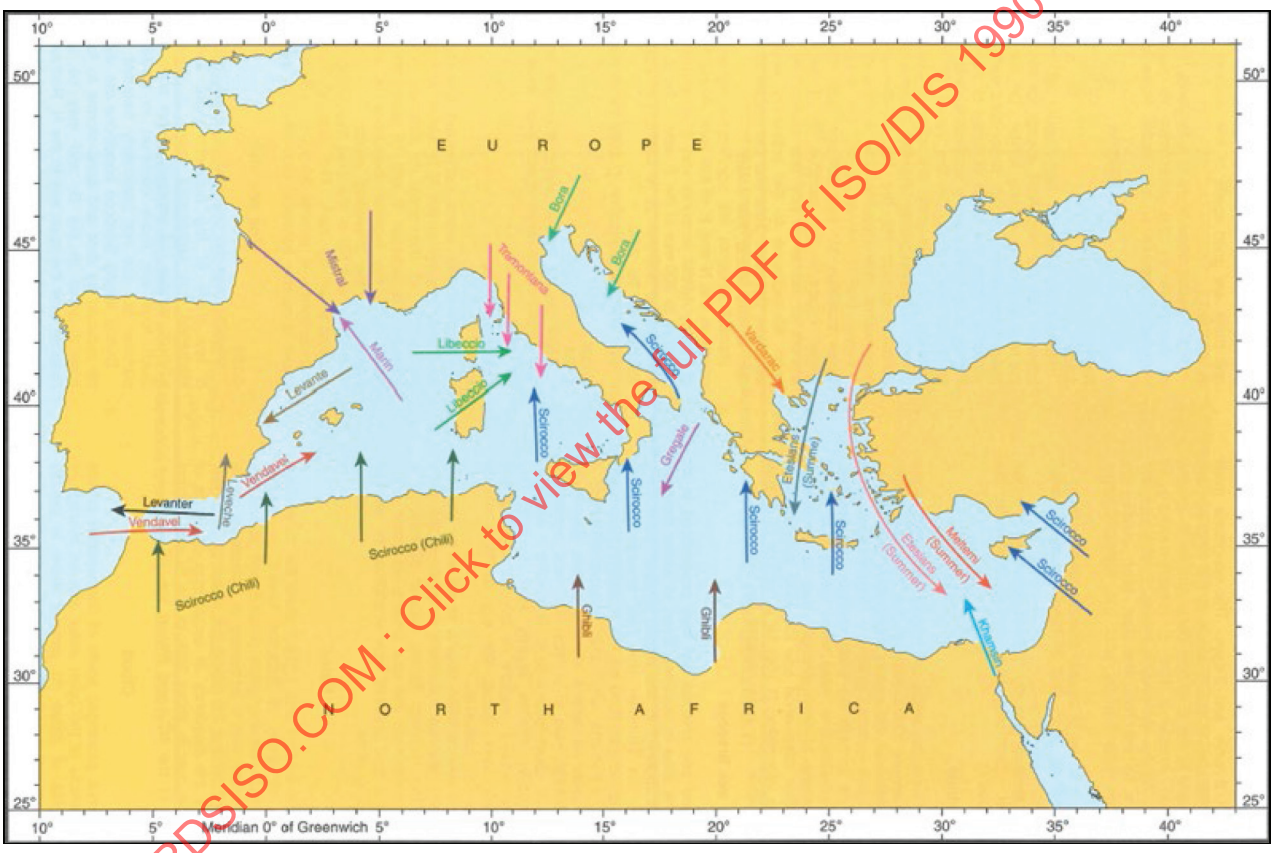

Figure H.4 — Typical wind over the Mediterranean Sea – picture – taken from Ref. [157]

H.6 Waves

Wave fields dynamics are conditioned by wind regimes shown in Figure H.4. The highest waves are located where high wind speed and long fetch are simultaneously present. The largest significant wave heights are in the western Mediterranean and in the Ionian Sea (1-year return period extreme respectively $H_s \geq 7$ m and $H_s \geq 4$ m). Two separate maxima of significant wave heights are in the Eastern Mediterranean Sea, one in the Aegean and another in the Levantine basin (respectively 1-year return period extreme $H_s \geq 3$ m and $H_s \geq 4$ m). The Scirocco produces waves maxima in the Northern Ionian Sea and in the Southern Adriatic (1-year return period extreme $H_s \geq$ about 5,5 m). The maximum due to the Bora wind is present in the Northern Adriatic

Sea (1-year return period extreme Hs≥5 m) and that due to the Vendavales wind in the Alborán Sea (1-year return period extreme Hs≥7 m).

In order to highlight seasonality and differences between two basins and give an indication of the mean climate, Figure H.5 and Figure H.6 show, respectively, the winter and summer spatial distribution of mean value of Hs. These figures are taken from Ref. [163] i.e. the wind and Wave Atlas of the Mediterranean Sea that is based on the information derived from the archive of the European Centre for Medium-Range Weather Forecasts, UK, then calibrated on the base of the data available from the ERS1-2 and Topex satellites.

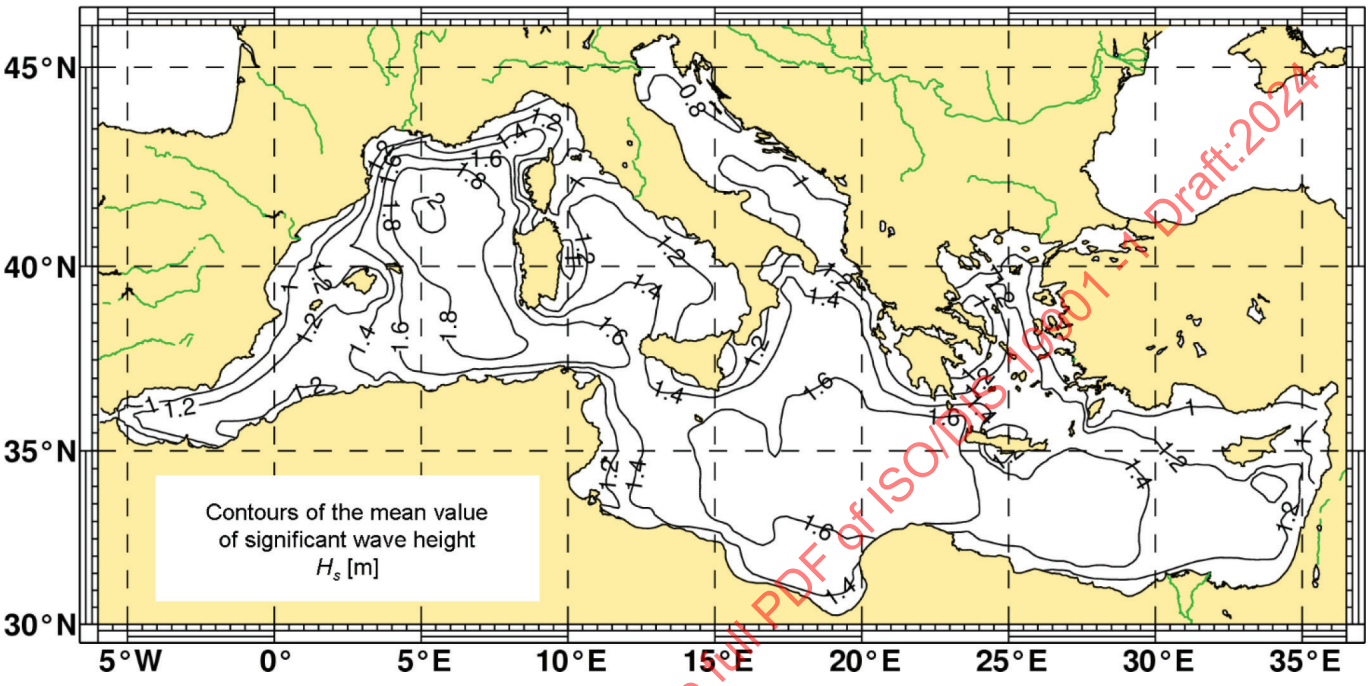

Figure H.5 — Spatial distribution of mean value of Hs - Winter (Taken from Ref. [163])

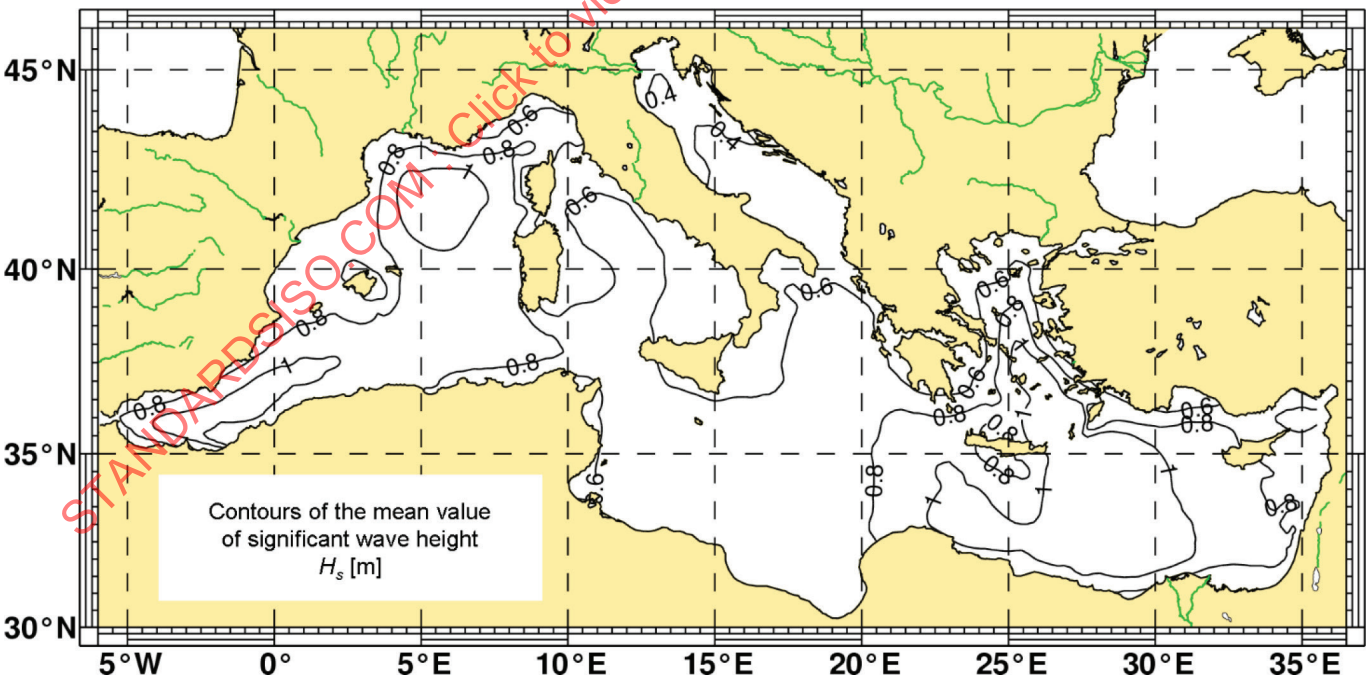

Figure H.6 — Spatial distribution of mean value of Hs - Summer (Taken from Ref. [163])

H.7 Currents

The whole Mediterranean is a concentration basin (evaporation exceeds precipitation and runoff). The water deficit is supplied by the inflow of the Atlantic Water (AW), that flows from the Strait of Gibraltar eastward along the North Afrimay coast and then bifurcates, partly entering the eastern basin through the Sicily Channel and partly proceeding to the northwest along the Tyrrhenian Coast and recirculating westward as the Northern Current (Figure H.7 taken from Ref. [170]).

The net result of the air-sea interactions in the entire Mediterranean is an outflow of salty water through the Strait of Gibraltar; the main water mass that constitute this salty and relatively warm outflow is the Levantine Intermediate Water (LIW). The LIW, formed in the Eastern Levantine sub-basin, sinks to a depth between 200 and 500 m and spreads out across the entire Mediterranean basin at this intermediate depth. The LIW proceeds essentially westward along several pathways and eventually outflows in the Atlantic Sea (Figure H.8 taken from Ref. [170]).

Deep convection occurs in the Gulf of Lions in the Western Mediterranean and in the Adriatic Sea. In the Gulf of Lions, the formation of deep water is mainly triggered by the atmosphere with strong local winds, which lead to a high latent heat loss for the sea and by a topographic control. The Adriatic Sea, due to its location (the northernmost part of the Mediterranean Sea), to mountain orography, and to the relatively large amount of the freshwater river run-off, represents a dilution basin. In addition, due to strong winter heat losses, it is a region where deep water formation processes take place. The path of the MDW (Mediterranean Deep Water) is depicted in Figure H.9 (taken from Ref. [170]). The general circulation is characterized by several eddies at the mesoscale.

Information about constancies and main directions of the surface circulation are done in Figure H.10 and Figure H.11, respectively for winter and summer season.

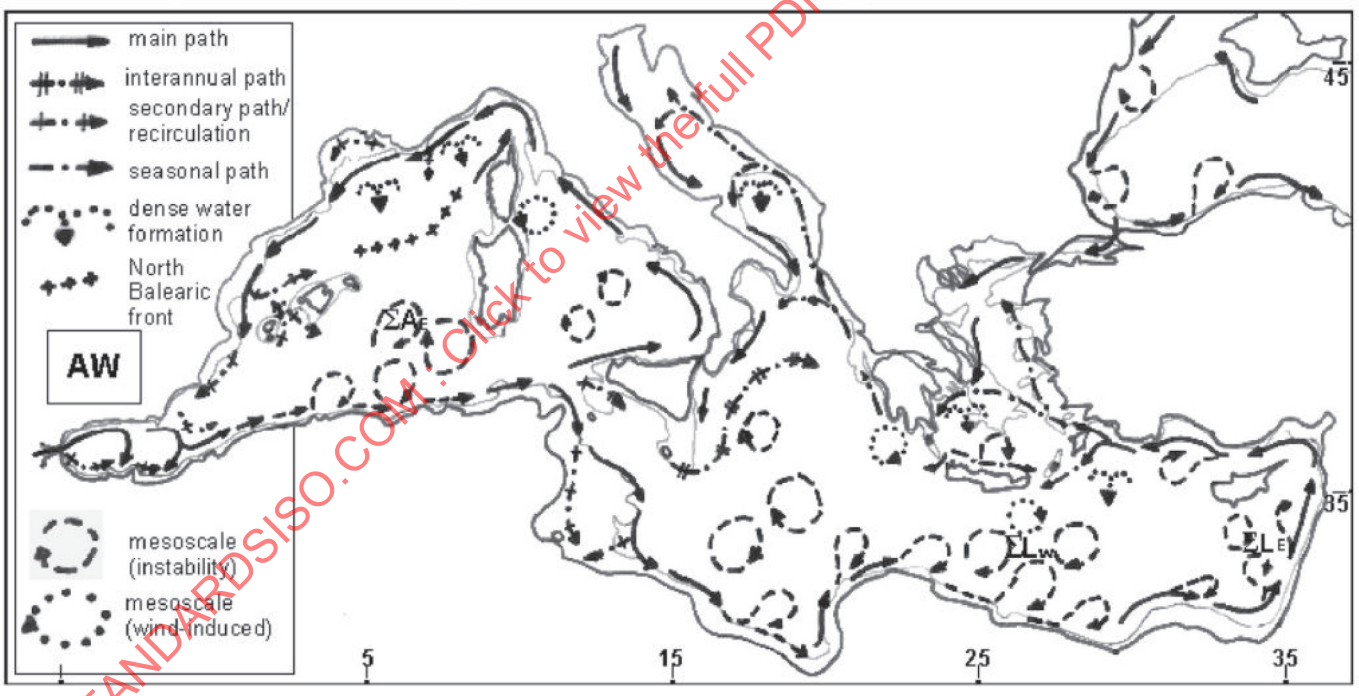

Figure H.7 — Surface Atlantic Water (AW) circulation (Taken from Ref.[170].)

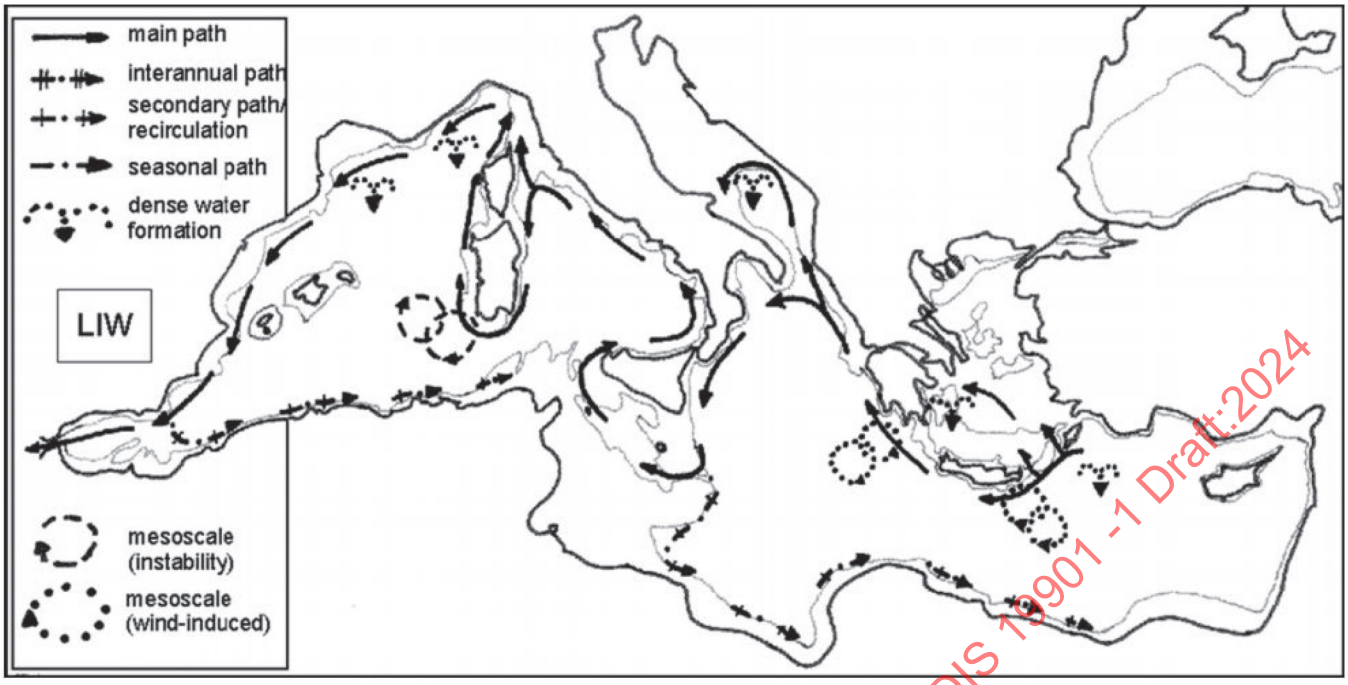

Figure H.8 — Levantine Intermediate Water (LIW) circulation at 500 m depth (Taken from Ref. [170])

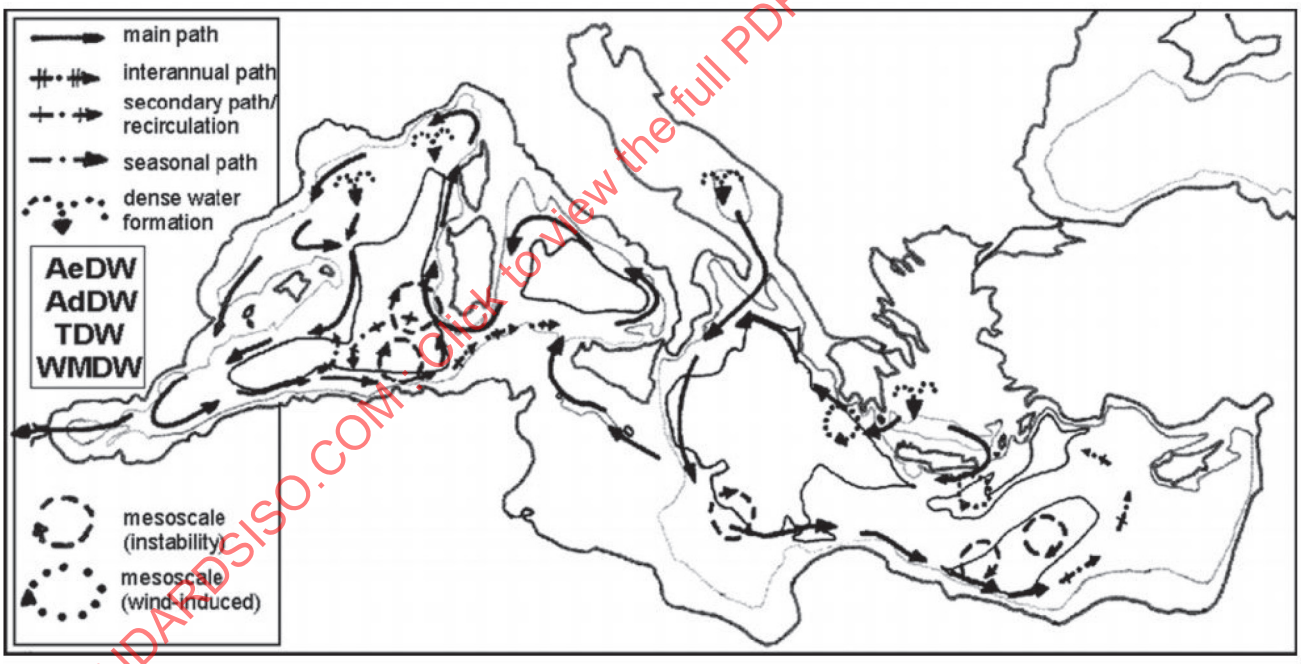

Figure H.9 — Deep Water circulation. AeDW, AdDW, TDW and WMDW denote the Aegean, Adriatic, Tyrrhenian and Western Mediterranean Deep Waters, respectively (Taken from Ref. [170])

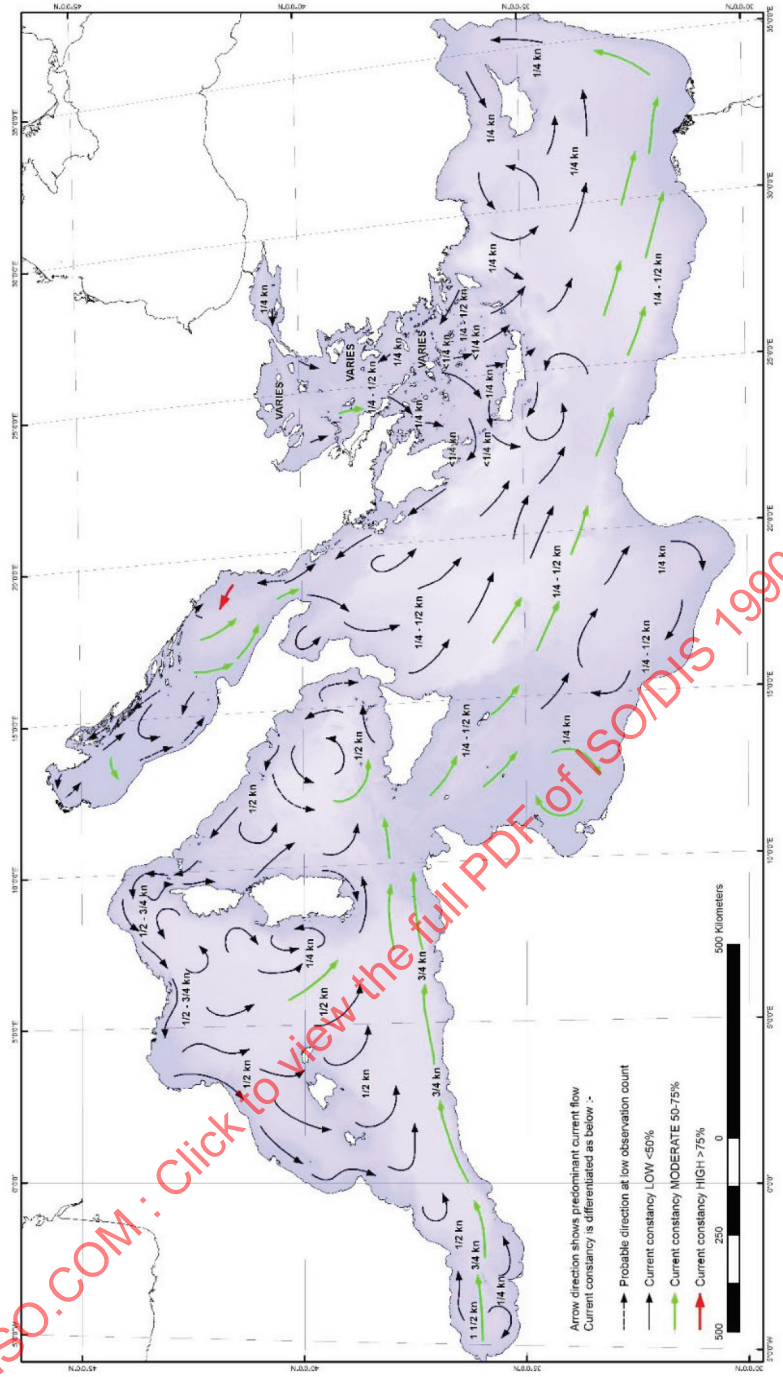

Figure H.10 — Surface Circulation – Winter (Composition of five images taken from the PILOT of the Mediterranean region[158][159][160][161][162])

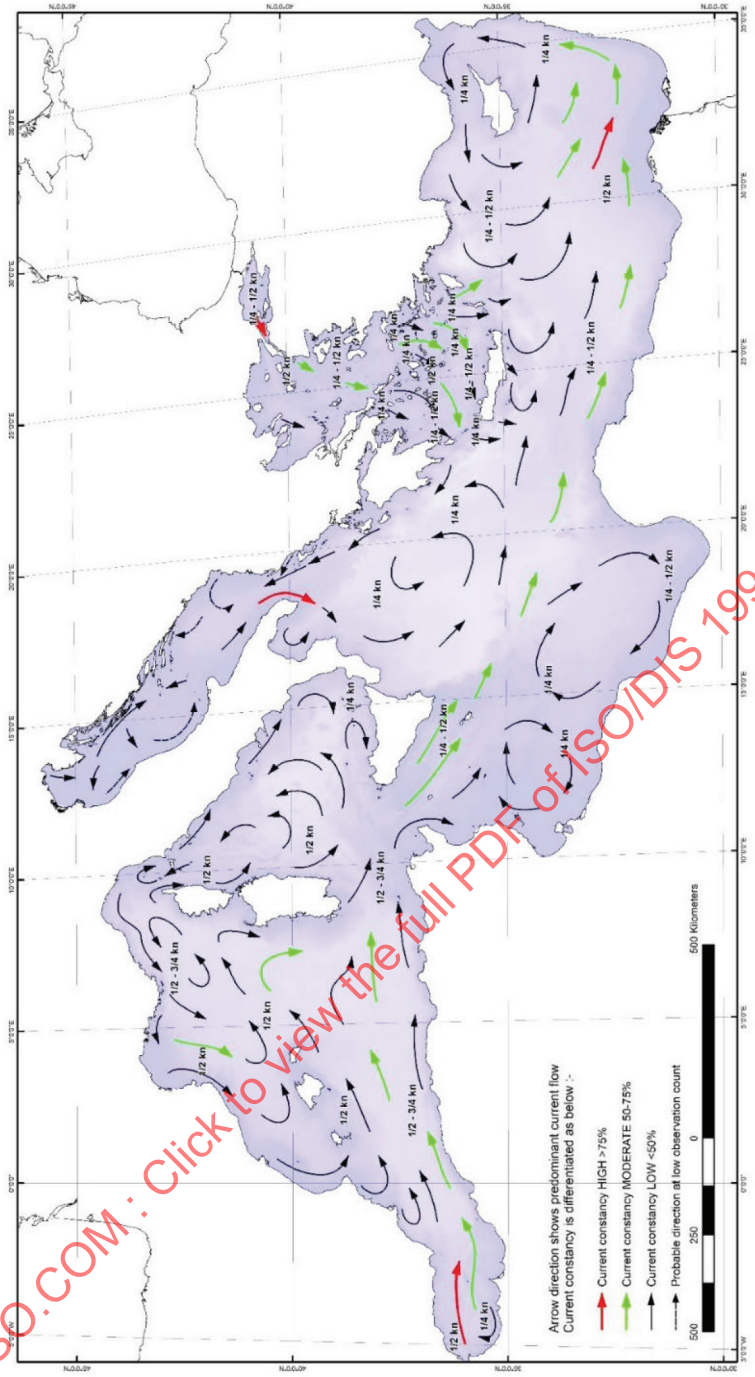

Figure H.11 — Surface Circulation – Summer (Composition of five images taken from the PILOT of the Mediterranean region[158][159][160][161][162])

H.8 Other environmental factors

H.8.1 Marine growth

Sporadic data available from Oil and Gas projects and academic studies give up to about 10 cm in the first 20 m of water depth and up to about 7 cm from 20 m to 70 m water depth. Density typically ranges from 1 300 Kg/m^3 to 1 650 kg/m^3. An exception is in the North Adriatic in front of the Po Delta. In fact, in this area, due to the abundance of nutrients, the marine growth reaches 20-30 cm of thickness in 12 months with density of 1 560 kg/m^3; the biomass values at Ravenna are the highest recorded from offshore structures in

the Mediterranean Sea (Platforms Antares and PCWA, respectively at water depth 12 m and 14 m). (See Ref. [164-166]).

H.8.2 Tsunamis

The tsunami is a series of travelling ocean waves of extremely long length generated primarily by earthquakes occurring below or near the ocean floor. Underwater volcanic eruptions and landslides may also generate tsunamis. In the deep ocean, the tsunami waves propagate across the deep ocean with a speed exceeding 800 kilometres per hour and a wave height of only a few tens of centimetres. Tsunami waves are distinguished from ordinary ocean waves by their great length between wave crests, often exceeding 100 km or more in the deep ocean, and by the time between these crests, ranging from 10 minutes to an hour. As they reach the shallow waters of the coast, the waves slow down and the water may pile up into a wall of destruction tens of meters or more in height.

The main tsunamigenic zones of the Mediterranean Sea are shown in Figure H.12 and the maximum wave heights in the coast are documented in literature (Table H.1 taken from Ref. [168]). A total of 290 tsunami events are documented to have occurred in the European and Mediterranean seas since 6150 B.C. to present days in the INGV website:

https://www.arcgis.com/apps/StorytellingTextLegend/index.html?appid=8329c2ad9b7f43c18562bdddc6c1ad26 (Ref. [167]).

As tsunami hazards are site-specific, it is recommended to carry out a site-specific assessment to estimate the risk. Such studies should be carried out in parallel with a seismic hazard assessment.

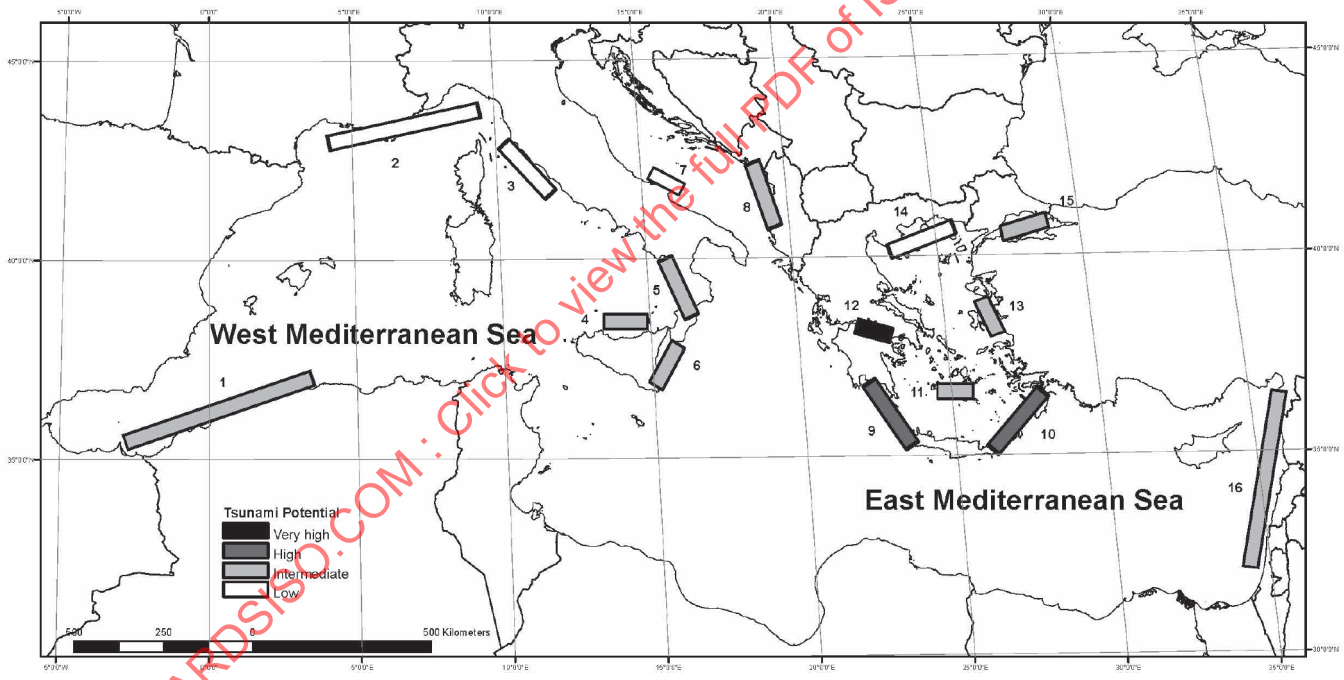

Figure H.12 — The main tsunamigenic zones of the Mediterranean Sea. Tsunami potential classified in a relative scale according to the frequency of occurrence and intensity of tsunamis

Table H.1 — List of Tsunamis for which maximum wave height (runup) in the coast is documented up to 2002

West Mediterranean Sea - List of Tsunamis		
Year	**Region**	**h(cm)**
1773	Tangiers	900
1783	Messina Straits	900
1887	Liguria – Cote d' Azur	150

Table H.1 *(continued)*

1905	Tyrrhenian Calabria	600
1908	Messina Straits	1 300
1916	Stromboli Island	1 000
1930	Stromboli Island	250
1979	Liguria – Cote d' Azur	300
2002	Stromboli Island	900
East Mediterranean Sea - List of Tsunamis		
Year	**Region**	**h(cm)**
1650	Thera Island, South Aegean Sea	2 000
1748	West Corinth Gulf, Central Greece	1 000
1794	Central Corinth Gulf	300
1817	West Corinth Gulf, Central Greece	500
1861	West Corinth Gulf, Central Greece	210
1866	Kythira Island, South-West Aegean Sea	800
1893	North Aegean Sea	100
1899	South Ionian Sea	100
1914	Lefkada Island, Ionian Sea	300
1932	Strymonikos Gulf, North Aegean Sea	200
1948	Karpathos Island, South-East Aegean Sea	400
1948	Lefkada Island, Ionian Sea	100
1949	Chios Island, East Aegean Sea	200
1956	Cyclades, South Aegean Sea	1 500
1963	West Corinth Gulf, Central Greece	500
1965	West Corinth Gulf, Central Greece	300
1981	East Corinth Gulf, Central Greece	30
1983	Kefalonia Island, Ionian Sea	50
1991	Leros Island, East Aegean Sea	50
1995	West Corinth Gulf, Central Greece	100
1996	West Corinth Gulf, Central Greece	200
2 000	Heraklion, North Crete Island	50
2002	Rhodes Island, East Aegean Sea	200

H.8.3 Internal solitary waves (solitons)

Information about internal wave in the Mediterranean Sea are available in the literature. In particular, a full description of the phenomenology and characteristic for each area in the world are reported in the "An Atlas of Internal Solitary-like Waves and their Properties" (Ref.[169]).

The Straits of Gibraltar and Messina are areas where strong internal solitary waves are generated by the interaction of tidal currents with shallow underwater ridges located within the straits. In the Strait of Gibraltar, during most tidal cycles, eastward propagating internal waves are generated through the interaction of the flow with the Camarinal Sill (see Figure H.13). The waves are released about the time of high water and propagate eastward along the strait as an internal bore. Table H.2 presents a summary of eastward propagating internal wave characteristics. The values have been reported in the literature and derived from both in-situ and remote sensing data sources.

Table H.2 — Summary of eastward propagating internal wave characteristics

Table	Characteristic
Amplitude Factor	-50 to -80 (m)
Long Wave Speed	1 to 2 (m/s)
Maximum Wavelength	1 to 4 (Km)
Wave Period	5 to 19 (min)
Surface Width	1 to 1,5 (Km)
Packet Length	3 to 20 (km)
Along Crest Length	15 to 150 (km)
Packet Separation	25 to 30 (km)

Despite the small tidal displacements encountered in the Mediterranean Sea, large gradients of tidal displacements are present along the Strait of Messina, because the semidiurnal tides in the Tyrrhenian and Ionian Seas are approximately in phase opposition. These gradients, acting on the water body constrained by the strait topography, force intense tidal currents, which may be as large as 3 m/s in the sill region.

Satellite images have been analysed showing that 1) solitons are more frequent in summer; 2) the northward propagating waves have an average propagation speed of 1,00 m/s and the southward propagating waves have an average propagation speed of 0,91 m/s; 3) the southward propagating internal bores are released from the sill between 1 and 5 hours after maximum northward tidal flow at Punta Pezzo, northward propagating internal bores between 2 and 6 hours after maximum southward tidal flow at Punta Pezzo, that is, between 8 and 12 hours after maximum northward tidal flow at Punta Pezzo; and 4) the spatial separation ranges from 500 m to 1 900 m for southward propagating wave trains, and from 350 m to 1 000 m for northward propagating wave trains.

Internal wave occurrences have been also observed in the Gulf of Lyons, the Adriatic Sea, around the island of Pantelleria in the Strait of Sicily, and among the Cretan Arc Straits. Additionally, satellite imagery shows internal waves signatures in the Malta Channel and along the east coast of Spain.

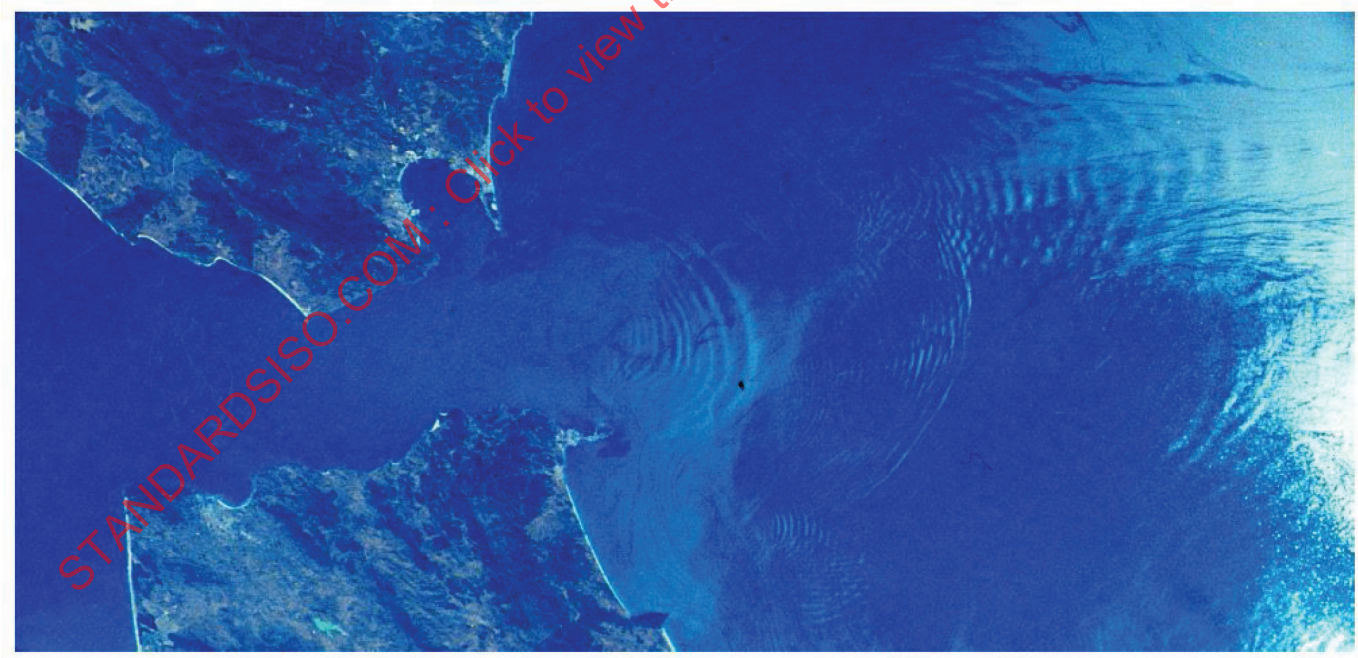

Figure H.13 — Astronaut photograph (STS41G-34-81) of Gibraltar region acquired on 11 October 1984 at 1222 UTC. The image shows three packets of solitons to the east of Gibraltar. Older packets are visible along Spanish and Morocmay coasts. [Image courtesy of Earth Sciences and Image Analysis Laboratory, NASA Johnson Space Centre (http://eol.jsc.nasa.gov)]

H.8.4 Air temperature, precipitation, humidity and visibility

H.8.4.1 Air temperature

Across the basin, air temperatures decrease to the north, with some mitigation by the Mediterranean Sea occurring along coastlines in the winter. Air temperatures are higher in summer and lower in winter. In general, the coldest month is February and the warmest one is August.

In the western part of the Mediterranean Sea, at the open sea, the mean minimum temperature is between 9 °C and 11 °C in February and in the north and 25 °C to 27 °C in August and in the south. The lowest temperatures tend to be associated with winds between northwest and northeast whilst south winds usually bring higher temperatures. Frost occurs in coastal areas in the northeast of the West Mediterranean Basin (France) in winter but is rare in the southeast.

The Adriatic Sea is characterized by mean air temperature in January of around 7 °C to 8 °C in the North Adriatic, about 11 °C in the central parts. In August, normally the warmest month, air temperature rises to around 23 °C to 24 °C and 24 °C to 25 °C, respectively. Frost may occur in the North Adriatic during the winter months when extreme temperatures may be lower than 10 °C. The frequency and severity of frosts steadily decreases towards the south of the area.

The eastern part of the Mediterranean Sea is characterized by mean temperature over the open sea in January ranging from 13 °C to 16 °C in winter and from 25 °C to 27 °C in summer. Frost is rare in the south but does occur on a few occasions in winter in Cyprus, Lebanon, Syria and the coastal areas of Turkey.

H.8.4.2 Precipitation – Rainfall, Thunderstorms and Snow

Rainfall is very seasonal with relatively dry summers and wet autumns and winters although there is considerable variation across the whole Mediterranean region (from about 200 mm/year in Almeria and south of Tunisia to 1 600 mm/year on the east coast of the Adriatic Sea). Much of the rainfall in the region occurs as heavy downpours of short duration. The driest month is usually July and the wettest period between October and December. The orientation of coasts has a large effect on rainfall due to prevailing winds. In both Iberia and Greece, for example, western coasts have double the amount of precipitation found on eastern coasts.

In the western basin of the Mediterranean Sea, snow rarely falls at sea level. Snow is rarely reported along the coasts of West Greece and South Italy but on the east coast of South Adriatic snow occurs on around 1 to 2 days each winter, and farther north near Trieste about 6 days each winter. With regards Levantine Sea and Aegean Sea, snow usually falls in winter in coastal areas above about 1 200 m but rarely at sea level, even in the northernmost part of the basins.

Thunderstorms occur in the whole West Mediterranean basin and sometimes occur with hail. They are most frequent in late summer and autumn. In the western basin of the Mediterranean Sea, the area most susceptible to thunderstorms are between Genoa and Naples, which have the frequency of between 36 and 41 thunderstorms for year. In the Adriatic Sea, thunderstorms are more frequent in north and central areas in summer (6-10 per month in the north). Along the coast of Greece thunderstorms are most frequent in autumn and winter with a frequency of 6 and 8 per month in November and December. In the East Mediterranean Basin, thunderstorms are most frequent in the north of Levantine Sea in winter and rare across the whole of the area in summer. The annual frequency is between 2 and 10 along the North African coast. In the north and northeast of the area thunderstorms may be accompanied by hail. The annual frequency of thunderstorms is around 30 to 35 with nearly all of those occurring between October and early May.

H.8.4.3 Humidity

In the Mediterranean basin, there is no significant variation of humidity across the region, but wind direction is often an important factor. Low humidity tends to be associated with north wind and, in contrast, south winds such as Scirocco become both warm and humid and may result in unpleasant and oppressive conditions with mist on south-facing coasts of the region where most warm air flows over a relatively cool sea, particularly in late winter. Maximum humidity normally occurs around dawn and the minimum in the early afternoon.

H.8.4.4 Visibility

In the West Mediterranean basin, the frequency of fog is less than 2 % of occasions over the open sea and around 2 % to 3 % between July and September in the extreme west of the area towards the Strait of Gibraltar. Reduced visibility occurs with South Scirocco winds and may affect a large area. Sandstorms off the North African coast, which may reduce the visibility to under 1 km, are usually short lived and localized. The Scirocco usually becomes moist as it extends north over the Tyrrhenian Sea and tends to form mist and cloud on windward coasts. Around Malta, Sicily and South Italy, Scirocco winds may result in poor visibility for a few days and are most likely to occur when the sea temperature is at its lowest in late winter.

The Adriatic Sea in characterized by highest frequency of fog in the north between November and April. Visibility of less than 8 km is recorded on around 4 % to 6 % of occasions in the south except for the month of May when the frequency is slightly higher. Over the North Adriatic the frequency is around 12 % of occasions.

In the Levantine sea the visibility is usually good in open sea but with a few days of fog between April and August. During strong Scirocco conditions the visibility may be reduced by dust and sandstorms to fog limits in coastal areas in the south and may be significantly over the open sea in the north. Mirages are a frequent occurrence in summer in coastal areas in the south and near Cyprus on calm summer mornings.

H.9 Sea water temperature and salinity

The western basin presents lower temperature values than the eastern basin. This is related to the modification of the Atlantic Water that changes its characteristics during the circulation into the entire basin. Another important feature consists in the different values occurring during the various months. There is a mean shift of about 7 °C between March to June in both regions. The zone with the lowest temperature values is the Adriatic Sea.

Regarding the salinity distributions, there is a homogeneous increase of salinity from the Strait of Gibraltar, where it is about 36,6 psu, to the eastern basin, where the values exceed 39 psu, in particular in the Levantine basin. These high values are strictly connected to the air surface interaction, the strong evaporation that exceeds precipitation, and the river runoff. In fact, the zones with the lowest salinity values are placed on river estuaries, as the North Adriatic. Furthermore, in the western basin the highest values of salinity occur during winter and spring; whereas the eastern basin has the higher values in summer and autumn, except for the Adriatic Sea that presents the highest values in winter.

H.10 Estimates of met ocean parameters

H.10.1 Extreme metocean parameter

Indicative extreme values for wind, wave and current parameters are provided in the following Tables for various return periods and for locations in the Mediterranean Sea. The wind, wave and current values are independently derived marginal parameters, and no account has been taken of conditional probability. As with all values in the regional annexes of this part of ISO 19901, these metocean data are provided to assist with engineering concept selections and are not suitable for the design of offshore structures.

Table H.3 — Indicative values of Metocean parameters – Offshore Alborán Sea

Metocean parameter	Return period N years			
	1	10	50	100
Nominal water depth	1 000 m			
Wind Speed at 10 m above MSL				
1-h mean (m/s)	18,4	21,8	24,0	25,0
10-min mean (m/s)	19,9	23,6	26,2	27,2
1-min mean (m/s)	21,7	26,1	28,9	30,2
3-s gust (m/s)	24,2	29,2	32,5	34,0

Table H.3 *(continued)*

Metocean parameter	Return period N years			
	1	10	50	100
Waves				
Significant height (m)	7,1	9,4	11,1	11,8
Maximum heigth (m)	13,4	17,6	20,6	22,0
Extreme Wave Direction (from)	NE/W	NE/W	NE/W	NE/W
Spectral peak period (s)	10,7	11,6	12,2	12,4
Current Speed				
Bottom (m/s)	0,20	0,20	0,20	0,20

Table H.4 — Indicative values of Metocean parameters – Offshore Balearic Sea

Metocean parameter	Return period N years			
	1	10	50	100
Nominal water depth	60 m			
Wind Speed at 10 m above MSL				
1-h mean (m/s)	15,3	18,7	21,2	22,1
10-min mean (m/s)	16,6	20,4	23,2	24,3
1-min mean (m/s)	21,7	26,7	30,4	31,8
3-s gust (m/s)	23,9	29,4	33,4	35,0
Waves				
Significant height (m)	2,9	5,1	6,9	7,7
Maximum heigth (m)	5,3	9,1	12,4	13,9
Extreme Wave Direction (from)	NE	NE	NE	NE
Spectral peak period (s)	13,0	14,0	15,0	15,0
Current Speed				
Bottom (m/s)	0,20	0,20	0,20	0,20

Table H.5 — Indicative values of Metocean parameters – Offshore South of Tyrrhenian Sea

Metocean parameter	Return period N years			
	1	10	50	100
Nominal water depth	700			
Wind Speed at 10 m above MSL				
1-h mean (m/s)	15,7	19,5	20,9	24,2
10-min mean (m/s)	17,0	21,3	22,9	26,7
1-min mean (m/s)	18,9	23,6	25,4	29,6
3-s gust (m/s)	21,3	26,6	28,6	33,3
Waves				
Significant height (m)	5,5	7,1	8,1	9,8
Maximum heigth (m)	10,5	13,4	14,4	17,0
Extreme Wave Direction (from)	NW	NW	NW	NW
Spectral peak period (s)	10,1	11,0	11,5	12,1
Current Speed				
Bottom (m/s)	0,25	0,30	0,35	0,38

Table H.6 — Indicative values of Metocean parameters – Offshore North of Tyrrhenian Sea

Metocean parameter	Return period N years			
	1	10	50	100
Nominal water depth	100 m			
Wind Speed at 10 m above MSL				
1-h mean (m/s)	19,5	22,6	23,3	25,7
10-min mean (m/s)	20,6	23,6	26,7	27,2
1-min mean (m/s)	24,2	28,3	31,5	31,9
3-s gust (m/s)	29,3	33,9	35,5	38,6
Waves				
Significant height (m)	4,7	6,7	6,9	7,2
Maximum heigth (m)	8,8	12,6	12,9	13,5
Extreme Wave Direction (from)	N/NE	N/NE	N/NE	N/NE
Spectral peak period (s)	9,2	11,0	11,3	11,5
Current Speed				
Bottom (m/s)	0,20	0,25	0,27	0,28

Table H.7 — Indicative values of Metocean parameters - Offshore South of Sicily Coast

Metocean parameter	Return period N years			
	1	10	50	100
Nominal water depth	50 m			
Wind Speed at 10 m above MSL				
1-h mean (m/s)	18,2	21,7	24,2	25,3
10-min mean (m/s)	19,7	23,6	26,4	27,6
1-min mean (m/s)	21,5	25,9	29,2	30,6
3-s gust (m/s)	23,9	29,0	32,8	34,5
Waves				
Significant height (m)	4,1	5,2	5,9	6,2
Maximum heigth (m)	7,5	9,3	10,5	11,0
Extreme Wave Direction (from)	SW/S	SW/S	SW/S	SW/S
Spectral peak period (s)	9,6	10,3	10,7	10,9
Current Speed				
Bottom (m/s)	0,40	0,54	0,64	0,69

Table H.8 — Indicative values of Metocean parameters – Offshore North Adriatic Sea

Metocean parameter	Return period N years			
	1	10	50	100
Nominal water depth	35 m			
Wind Speed at 10 m above MSL				
1-h mean (m/s)	15,8	18,5	20,3	21,1
10-min mean (m/s)	17,6	20,2	22,4	22,9
1-min mean (m/s)	20,2	23,8	27,0	27,3
3-s gust (m/s)	25,5	29,9	31,7	33,4
Waves				
Significant height (m)	3,0	4,8	6,0	6,6
Maximum heigth (m)	5,6	8,9	11,2	12,3

Table H.8 *(continued)*

Metocean parameter	Return period N years			
	1	10	50	100
Extreme Wave Direction (from)	SE	SE	SE	SE
Spectral peak period (s)	8,6	9,9	10,8	11,8
Current Speed				
Bottom (m/s)	0,41	0,46	0,50	0,51

Table H.9 — Indicative values of Metocean parameters - Central Offshore Central Adriatic - Italy Side

Metocean parameter	Return period N years			
	1	10	50	100
Nominal water depth	70 m			
Wind Speed at 10 m above MSL				
1-h mean (m/s)	22,3	25,7	28,3	29,9
10-min mean (m/s)	24,2	28,1	31,1	32,9
1-min mean (m/s)	26,7	32,8	34,6	36,8
3-s gust (m/s)	29,9	37,1	39,2	41,8
Waves				
Significant height (m)	4,2	5,6	6,6	7,0
Maximum heigth (m)	7,7	10,2	11,9	12,6
Extreme Wave Direction (from)	E/SE	E/SE	E/SE	E/SE
Spectral peak period (s)	8,3	9,2	9,7	9,9
Current Speed				
Bottom (m/s)	0,38	0,47	0,54	0,57

Table H.10 — Indicative values of Metocean parameters – Adriatic Sea – Otranto Strait

Metocean parameter	Return period N years			
	1	10	50	100
Nominal water depth	400 m			
Wind Speed at 10 m above MSL				
1-h mean (m/s)	23,0	26,0	28,1	29,0
10-min mean (m/s)	25,0	28,4	30,9	31,9
1-min mean (m/s)	27,6	31,5	34,4	35,6
3-s gust (m/s)	31,0	35,6	39,0	40,4
Waves				
Significant height (m)	5,8	7,3	8,0	8,9
Maximum heigth (m)	10,8	13,7	15,0	16,6
Extreme Wave Direction (from)	S	S	S	S
Spectral peak period (s)	10,3	11,3	11,7	12,3
Current Speed				
Bottom (m/s)	0,39	0,47	0,53	0,55

Table H.11 — Indicative values of Metocean parameters – Offshore Ionian Sea between Italy and Greece

Metocean parameter	Return period N years			
	1	10	50	100
Nominal water depth	1 000 m			
Wind Speed at 10 m above MSL				
1-h mean (m/s)	19,8	22,5	24,2	24,9
10-min mean (m/s)	21,4	24,5	26,4	27,2
1-min mean (m/s)	24,7	28,0	30,1	31,0
3-s gust (m/s)	29,9	34,0	36,6	37,6
Waves				
Significant height (m)	6,3	7,6	8,6	8,9
Maximum heigth (m)	11,9	14,5	16,2	17,0
Extreme Wave Direction (from)	S	S	S	S
Spectral peak period (s)	11,4	13,9	16,0	16,9
Current Speed				
Bottom (m/s)	0,30	0,40	0,50	0,50

Table H.12 — Indicative values of Metocean parameters - Levantine Sea – Offshore Egypt

Metocean parameter	Return period N years			
	1	10	50	100
Nominal water depth	150 m			
Wind Speed at 10 m above MSL				
1-h mean (m/s)	18,0	22,2	24,4	25,8
10-min mean (m/s)	19,4	24,1	26,6	28,2
1-min mean (m/s)	21,2	26,6	29,4	31,3
3-s gust (m/s)	23,6	29,8	33,1	35,3
Waves				
Significant height (m)	4,4	6,1	7,0	7,4
Maximum heigth (m)	8,3	11,4	13,2	13,9
Extreme Wave Direction (from)	NW	NW	NW	NW
Spectral peak period (s)	10,6	11,7	12,2	12,4
Current Speed				
Bottom (m/s)	0,50	0,57	0,62	0,64

Table H.13 — Indicative values of Metocean parameters – Levantine Sea – Offshore South Cyprus

Metocean parameter	Return period N years			
	1	10	50	100
Nominal water depth	1 500 m			
Wind Speed at 10 m above MSL				
1-h mean (m/s)	20,1	23,1	25,0	25,8
10-min mean (m/s)	21,8	25,1	27,3	28,2
1-min mean (m/s)	23,9	27,7	30,2	31,3
3-s gust (m/s)	26,6	31,1	34,1	35,3
Waves				
Significant height (m)	5,5	7,3	8,2	9,4
Maximum heigth (m)	10,4	13,8	15,3	17,6

Table H.13 *(continued)*

Metocean parameter	Return period N years			
	1	10	50	100
Extreme Wave Direction (from)	SW	SW	SW	SW
Spectral peak period (s)	11,4	13,2	14,0	15,1
Current Speed				
Bottom (m/s)	0,07	0,12	0,15	0,16

Table H.14 — Indicative values of Metocean parameters – Offshore Aegean Sea

Metocean parameter	Return period N years			
	1	10	50	100
Nominal water depth	40 m			
Wind Speed at 10 m above MSL				
1-h mean (m/s)	19,6	22,5	24,2	24,9
10-min mean (m/s)	21,2	24,4	26,4	27,2
1-min mean (m/s)	23,2	27,0	29,2	30,1
3-s gust (m/s)	25,9	30,2	32,9	34,0
Waves				
Significant height (m)	3,4	4,2	4,6	4,8
Maximum heigth (m)	6,6	7,8	8,6	8,9
Extreme Wave Direction (from)	S	S	S	S
Spectral peak period (s)	7,2	8,0	8,4	8,7
Current Speed				
Bottom (m/s)	0,41	0,57	0,68	0,73

H.10.2 Long-term distribution of metocean parameters

Long-term joint frequency distributions of the significant wave height Hs versus the spectral peak period are given in Tables H.15, H.16, H.17 and H.18 for four locations (offshore Balearic Sea, Ionian Sea, Adriatic Sea and Levantine Sea. Distributions are based on hindcast data). In particular the distribution at offshore Balearic Sea is based on 44 years long hindcast dataset obtained by the EU-funded research project HIPOCAS (http://www.mar.ist.utl.pt/hipocas/index.asp), the distribution of the central part of the Adriatic Sea come from a hindcast model covering the period 2000-2010 and set and run for an Oil and Gas project by DHI, the distribution for the Ionian Sea in comes from 16 years hindcast data derived by ECMWF global model, the distribution at Levantine Sea come from 35 years (1979 - 2013) hindcasted time series of the extracted from the hindcast study of entire Mediterranean Sea carried out by DHI.

Table H.15 — Percentage occurrence of total significant wave height vs. spectral peak period Offshore Balearic Sea

Significant Wave Heigth m	Peak Period s									
	< 2	2 to 4	4 to 6	6 to 8	8 to 10	10 to 12	12 to 14	14 to 16	> 16	TOTAL
0,0 to 0,5	0,031	23,538	10,798	2,218	0,027	0,001	0,000	0,000	0,000	36,614
0,5 to 1,0	0,000	12,656	18,105	8,369	1,921	0,048	0,000	0,000	0,000	41,099
1,0 to 1,5	0,000	0,108	7,310	3,878	1,839	0,419	0,002	0,000	0,000	13,556
1,5 to 2,0	0,000	0,001	1,600	2,584	0,634	0,308	0,004	0,000	0,000	5,131
2,0 to 2,5	0,000	0,000	0,146	1,393	0,363	0,113	0,002	0,000	0,000	2,017
2,5 to 3,0	0,000	0,000	0,005	0,573	0,259	0,052	0,003	0,000	0,000	0,893
3,0 to 3,5	0,000	0,000	0,000	0,116	0,217	0,047	0,001	0,000	0,000	0,381

Table H.15 *(continued)*

Significant Wave Heigth m	Peak Period s									
	< 2	2 to 4	4 to 6	6 to 8	8 to 10	10 to 12	12 to 14	14 to 16	> 16	TOTAL
3,5 to 4,0	0,000	0,000	0,000	0,015	0,103	0,025	0,001	0,000	0,000	0,143
4,0 to 4,5	0,000	0,000	0,000	0,002	0,042	0,028	0,002	0,000	0,000	0,073
4,5 to 5,0	0,000	0,000	0,000	0,000	0,013	0,021	0,002	0,000	0,000	0,036
5,0 to 5,5	0,000	0,000	0,000	0,000	0,004	0,011	0,003	0,000	0,000	0,018
5,5 to 6,0	0,000	0,000	0,000	0,000	0,001	0,009	0,001	0,000	0,000	0,011
> 6,0	0,000	0,000	0,000	0,000	0,000	0,009	0,013	0,006	0,000	0,029
Total	0,031	36,303	37,965	19,148	5,422	1,091	0,033	0,006	0,000	100,000

Table H.16 — Percentage occurrence of total significant wave height vs. spectral peak period Offshore Central Adriatic Sea

Significant Wave Heigth m	Peak Period s											
	0 to 1	1 to 2	2 to 3	3 to 4	4 to 5	5 to 6	6 to 7	7 to 8	8 to 9	9 to 10	> 10	TOTAL
0,00 to 0,25	0,000	0,425	5,814	3,548	1,575	0,755	0,171	0,036	0,010	0,005	0,002	12,343
0,25 to 0,50	0,000	0,061	7,342	13,443	5,761	2,530	1,271	0,226	0,019	0,003	0,002	30,658
0,50 to 0,75	0,000	0,000	0,664	8,482	8,043	2,663	1,300	0,584	0,069	0,005	0,001	21,811
0,75 to 1,00	0,000	0,000	0,004	1,678	5,741	3,096	1,158	0,676	0,138	0,013	0,003	12,507
1,00 to 1,50	0,000	0,000	0,000	0,127	3,208	5,265	2,030	1,122	0,384	0,061	0,005	12,202
1,50 to 2,00	0,000	0,000	0,000	0,000	0,094	2,301	2,021	0,777	0,281	0,061	0,005	5,540
2,00 to 2,50	0,000	0,000	0,000	0,000	0,000	0,144	1,755	0,483	0,221	0,043	0,009	2,655
2,50 to 3,00	0,000	0,000	0,000	0,000	0,000	0,001	0,513	0,618	0,144	0,037	0,004	1,317
3,00 to 3,50	0,000	0,000	0,000	0,000	0,000	0,000	0,019	0,452	0,090	0,028	0,003	0,592
3,50 to 4,00	0,000	0,000	0,000	0,000	0,000	0,000	0,000	0,137	0,066	0,025	0,001	0,229
4,00 to 4,50	0,000	0,000	0,000	0,000	0,000	0,000	0,000	0,013	0,053	0,011	0,004	0,081
4,50 to 5,00	0,000	0,000	0,000	0,000	0,000	0,000	0,000	0,000	0,025	0,014	0,007	0,046
5,00 to 5,50	0,000	0,000	0,000	0,000	0,000	0,000	0,000	0,000	0,010	0,003	0,003	0,016
5,0 to 6,00	0,000	0,000	0,000	0,000	0,000	0,000	0,000	0,000	0,001	0,001	0,001	0,003
Total	0,000	0,486	13,824	27,278	24,422	16,755	10,238	5,124	1,511	0,310	0,050	100,000

Table H.17 — Percentage occurrence of total significant wave height vs. spectral peak period Offshore Ionian Sea

Significant Wave Heigth m	Peak Period s											
	< 2	2 to 3	3 to 4	4 to 5	5 to 6	6 to 7	7 to 8	8 to 9	9 to 10	10 to 11	> 11	TOTAL
0,0 to 0,5	0,080	5,850	19,620	7,300	1,600	0,250	0,050	0,030	0,010	0,000	0,000	34,800
0,5 to 1,0	0,000	0,280	12,990	13,080	5,220	1,620	0,270	0,030	0,010	0,010	0,000	33,510
1,0 to 1,5	0,000	0,000	0,410	8,350	4,800	2,060	0,500	0,080	0,000	0,000	0,000	16,190
1,5 to 2,0	0,000	0,000	0,000	1,080	4,580	1,660	0,550	0,080	0,020	0,010	0,000	7,980
2,0 to 2,5	0,000	0,000	0,000	0,010	1,500	1,570	0,440	0,070	0,030	0,000	0,000	3,630
2,5 to 3,0	0,000	0,000	0,000	0,000	0,230	1,120	0,420	0,080	0,030	0,010	0,000	1,880
3,0 to 3,5	0,000	0,000	0,000	0,000	0,030	0,410	0,450	0,100	0,000	0,000	0,000	0,990

Table H.17 *(continued)*

Significant Wave Heigth m	Peak Period s											
	< 2	2 to 3	3 to 4	4 to 5	5 to 6	6 to 7	7 to 8	8 to 9	9 to 10	10 to 11	> 11	TOTAL
3,5 to 4,0	0,000	0,000	0,000	0,000	0,000	0,150	0,310	0,040	0,030	0,000	0,000	0,530
4,0 to 4,5	0,000	0,000	0,000	0,000	0,000	0,050	0,170	0,070	0,000	0,000	0,000	0,290
4,5 to 5,0	0,000	0,000	0,000	0,000	0,000	0,000	0,040	0,060	0,000	0,010	0,000	0,110
5,0 to 5,5	0,000	0,000	0,000	0,000	0,000	0,000	0,010	0,040	0,000	0,000	0,000	0,050
5,5 to 6,0	0,000	0,000	0,000	0,000	0,000	0,000	0,010	0,010	0,020	0,010	0,000	0,040
6,0 to 6,5	0,000	0,000	0,000	0,000	0,000	0,000	0,000	0,010	0,000	0,000	0,000	0,010
6,5 to 7,0	0,000	0,000	0,000	0,000	0,000	0,000	0,000	0,010	0,000	0,000	0,000	0,010
> 7,0	0,000	0,000	0,000	0,000	0,000	0,000	0,000	0,000	0,000	0,000	0,000	0,000
Total	0,080	6,130	33,030	29,820	17,960	8,880	3,220	0,690	0,150	0,040	0,000	100,000

Table H.18 — Percentage occurrence of total significant wave height vs. spectral peak period Offshore Levantine Sea - Egypt

Signifi-cant Wave Heigth m	Peak Period s															
	< 2	2 to 3	3 to 4	4 to 5	5 to 6	6 to 7	7 to 8	8 to 9	9 to 10	10 to 11	11 to 12	12 to 13	13 to 14	14 to 15	15 to 16	TOTAL
0,0 to 0,5	0,004	0,512	2,478	4,539	2,514	0,463	0,301	0,156	0,110	0,066	0,043	0,013	0,002	0,002	0,000	11,202
0,5 to 1,0	0,000	0,096	3,535	9,324	15,177	15,987	6,219	1,557	0,466	0,206	0,062	0,030	0,009	0,003	0,000	52,670
1,0 to 1,5	0,000	0,000	0,054	1,765	3,257	4,806	8,551	2,276	1,149	0,470	0,106	0,029	0,007	0,002	0,000	22,471
1,5 to 2,0	0,000	0,000	0,000	0,076	0,558	1,096	2,295	2,287	0,645	0,376	0,160	0,029	0,004	0,001	0,000	7,527
2,0 to 2,5	0,000	0,000	0,000	0,000	0,089	0,220	0,709	1,141	0,599	0,185	0,090	0,018	0,001	0,000	0,000	3,051
2,5 to 3,0	0,000	0,000	0,000	0,000	0,015	0,032	0,194	0,478	0,497	0,175	0,050	0,015	0,000	0,000	0,000	1,456
3,0 to 3,5	0,000	0,000	0,000	0,000	0,000	0,007	0,024	0,203	0,317	0,185	0,053	0,008	0,000	0,000	0,000	0,797
3,5 to 4,0	0,000	0,000	0,000	0,000	0,000	0,000	0,001	0,039	0,181	0,139	0,046	0,008	0,000	0,000	0,000	0,414
4,0 to 4,5	0,000	0,000	0,000	0,000	0,000	0,000	0,000	0,005	0,064	0,107	0,038	0,015	0,001	0,000	0,000	0,231
4,5 to 5,0	0,000	0,000	0,000	0,000	0,000	0,000	0,000	0,001	0,015	0,057	0,028	0,007	0,000	0,000	0,000	0,107
5,0 to 5,5	0,000	0,000	0,000	0,000	0,000	0,000	0,000	0,000	0,002	0,024	0,021	0,004	0,000	0,000	0,000	0,051
5,5 to 6,0	0,000	0,000	0,000	0,000	0,000	0,000	0,000	0,000	0,000	0,006	0,007	0,003	0,001	0,000	0,000	0,016
6,0 to 6,5	0,000	0,000	0,000	0,000	0,000	0,000	0,000	0,000	0,000	0,000	0,002	0,002	0,000	0,000	0,000	0,005
>6,5	0,000	0,000	0,000	0,000	0,000	0,000	0,000	0,000	0,000	0,000	0,002	0,002	0,000	0,000	0,000	0,004
Total	0,004	0,608	6,068	15,704	21,609	22,611	18,292	8,143	4,043	1,998	0,706	0,182	0,025	0,007	0,000	100,000

Annex I
(informative)

Brazil

I.1 Description of region

Offshore Brazil has many sedimentary basins with distinct meteorological and oceanographic characteristics. This annex addresses some regions of Oil and Gas interest with a brief description of their general metocean conditions. The first section presents general features of the Brazilian Equatorial Margin, which is divided in two sub-regions for better description. The next section presents the main characteristics of the Sergipe Basin, located offshore the Brazilian East coast. The last section presents metocean characteristics for Campos and Santos Basins at the Southeastern Brazilian continental margin. These three regions are identified on a map of the general pattern of the ocean surface circulation in South Atlantic (Figure I.1), as described in[171].

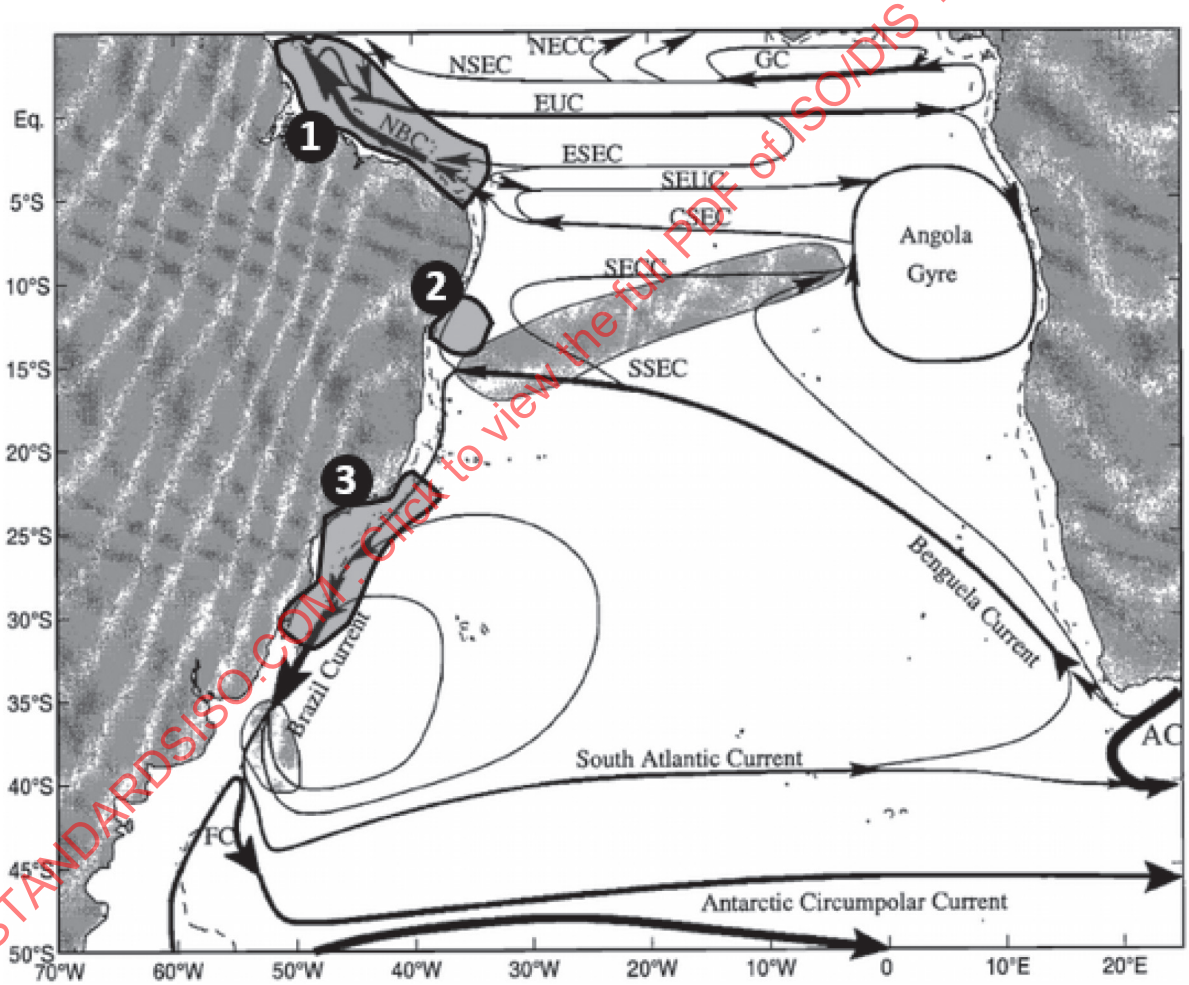

Figure I.1 — Dominant surface ocean currents in South Atlantic with the numbered shadow areas indicating the Brazilian Equatorial Margin (1), Sergipe Basin (2) and the contiguous region of Campos and Santos Basins (3). Figure source: [Ref.171]

A general description of metocean conditions in the tropical east coast of South America is the absence of hurricanes and the occurrence of extreme storms related to extratropical and subtropical cyclonic systems.

Wind and wave conditions in the region are generally benign, with mean wind speeds (the 10 min averaged 10 m height Ws10) lower than 12 m/s, and wave significant heights (Hs) lower than 3 m at most of the time. In winter, the passage of cold fronts may bring violent squalls with gust of more than 15 m/s.

Surface currents can reach 1,5 m/s across the whole region, except in the strong North Brazil Current jet at the west Equatorial Margin where currents may reach up to 2,5 m/s. The presence of multiple fast flowing eddies and meanders occurs in most regions.

I.2 Offshore North Brazil (Equatorial Margin)

I.2.1 Description of the region

The geographical scope of this section is the Brazilian sector on the Northern Atlantic coast of South America, named Brazilian Equatorial Margin (BEM). It extends for about 2 000 km between longitudes 36° W-52° W (Fig I.2). Offshore areas of Venezuela, Trinidad, Guyana, Suriname and French Guyana are not in the scope of this annex.

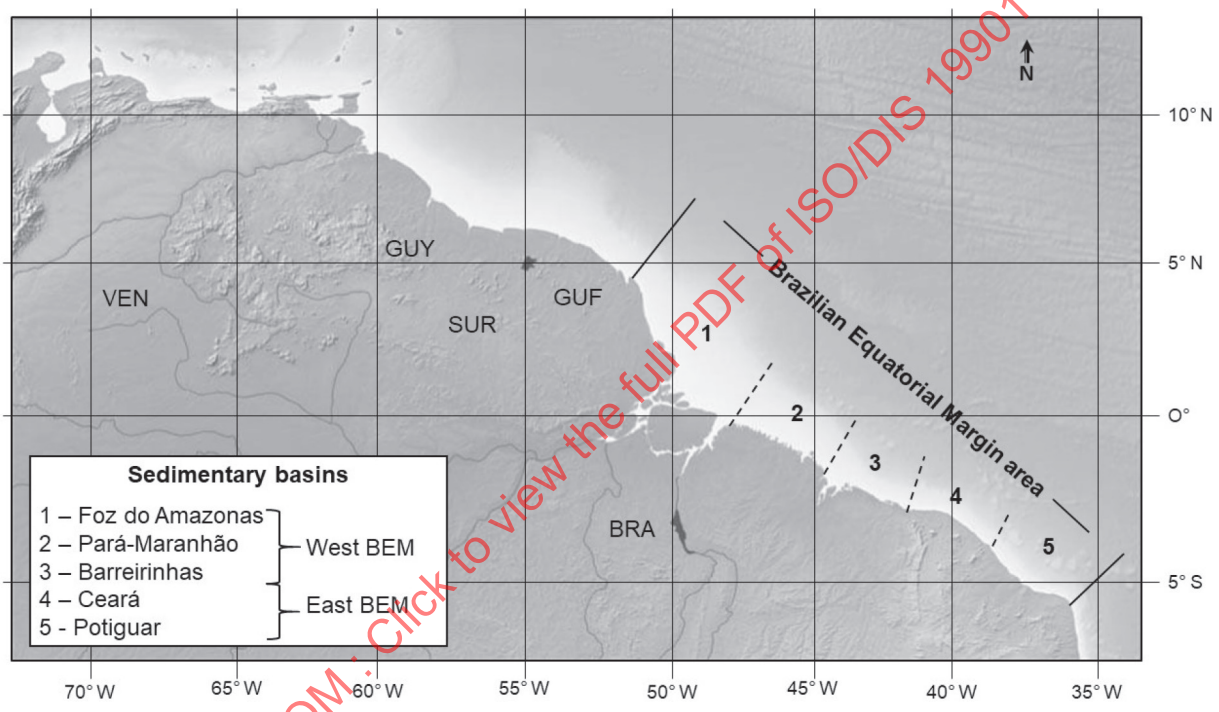

Figure I.2 — Map of the northernmost Atlantic coast of South America, showing the Brazilian Equatorial Margin area and its five sedimentary basins.

The development of BEM started in Early Cretaceous during the Gondwna breakup, as a series of continental rift basins,[172] resulting in five sedimentary basins limited by fracture zones. In order to better represent general meteorological and oceanographic characteristics for these basins, the entire area was divided in two sub-regions: Western BEM (covering Foz do Amazonas, Pará-Maranhão and Barreirinhas sedimentary basins) and Eastern BEM (covering Ceará and Potiguar basins).

The major atmospheric feature in the Equatorial region is the Intertropical Convergence Zone (ITCZ), which is a persistent global belt of convergence of trade winds corresponding to intense convective activity. It has a zonal orientation following the maximum sea-surface temperature, with a well-defined seasonal meridional migration[173].

Oceanographic characteristics of this region are mainly forced by the exchange of water between the Northern and Southern Hemispheres as part of the Atlantic Meridional Overturning Circulation (AMOC). The northward heat transport near the surface is compensated by a southward flow of colder water below 1 000 metres. These fluxes become the upper cell of the AMOC. This asymmetry of the net heat flux across

the Equator is responsible for a slightly warmer Northern Hemisphere and for the mean position of the ITCZ being just north of the Equator[174].

I.2.2 Winds

The prevailing meteorological feature in the western equatorial Atlantic is the ITCZ, the zonal band of strong convection and heavy precipitation generated by convergence of the trade winds. This low atmospheric pressure band migrates seasonally from 9° N in the end of boreal summer to 2° N in the end of boreal winter, and is strongly controlled by the sea surface temperature (SST) with warmer waters favoring deep tropospheric convection and determining the surface wind patterns. Due to this zonal asymmetry, the time-averaged winds at the Equator (i.e. over BEM) are northward and the net wind is annually modulated, typically more intense in August and weaker in March (Fig. I.3) [175-177].

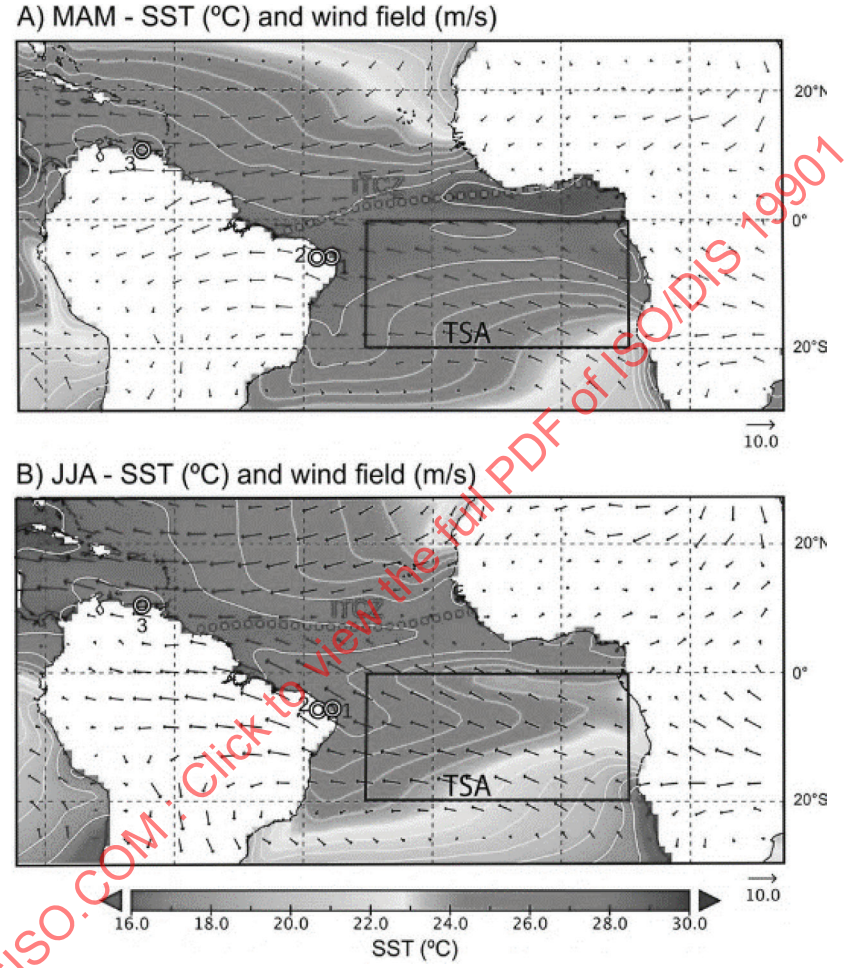

Figure I.3 – Mean sea surface temperature (SST) and 850 hPa wind field (sticks in m/s) over tropical Atlantic Basin for (A) March, April and May and (B) June, July and August, averaged over 1982-2016. ITCZ position is based in maximum precipitation. TSA stands for Tropical South Atlantic. Figure source: Ref.[177]

Interannual global phenomena, such as El Niño-Southern Oscillation (ENSO) conditions, also affect the atmospheric circulation on the Equatorial Atlantic by regulating the convergence of surface winds from both hemispheres[178,179].

I.2.3 Waves

Typical wave climatology in the BEM is mostly linked to the persistent easterlies trade winds, resulting in short period waves from NE-SE. This local wave climate follows the seasonal wind intensity variability due to the ITCZ excursion, with more energetic sea-states regularly reaching BEM coast when local easterlies

winds are stronger during the boreal summer.[180] Seasonal signal on the local wind sea becomes more evident in the eastern part of BEM (Fig. I.4).

However, well-developed bimodal spectra eventually occur in the region, with presence of lower frequency waves originated by subtropical cyclones at higher latitudes of the North Atlantic Ocean as a result of the extensive wind fetch, particularly in boreal winter (Fig. I.4). Arrival of wave groups from the North direction at the equatorial region has been associated with the interannual variability of the NAO (North Atlantic Oscillation) index.[181,182] Seasonal extreme events (i.e. hurricanes and tropical storms) in the tropical North Atlantic occasionally generate high period waves from N-NE. This temporal variability may modify wave climate distribution in the BEM.

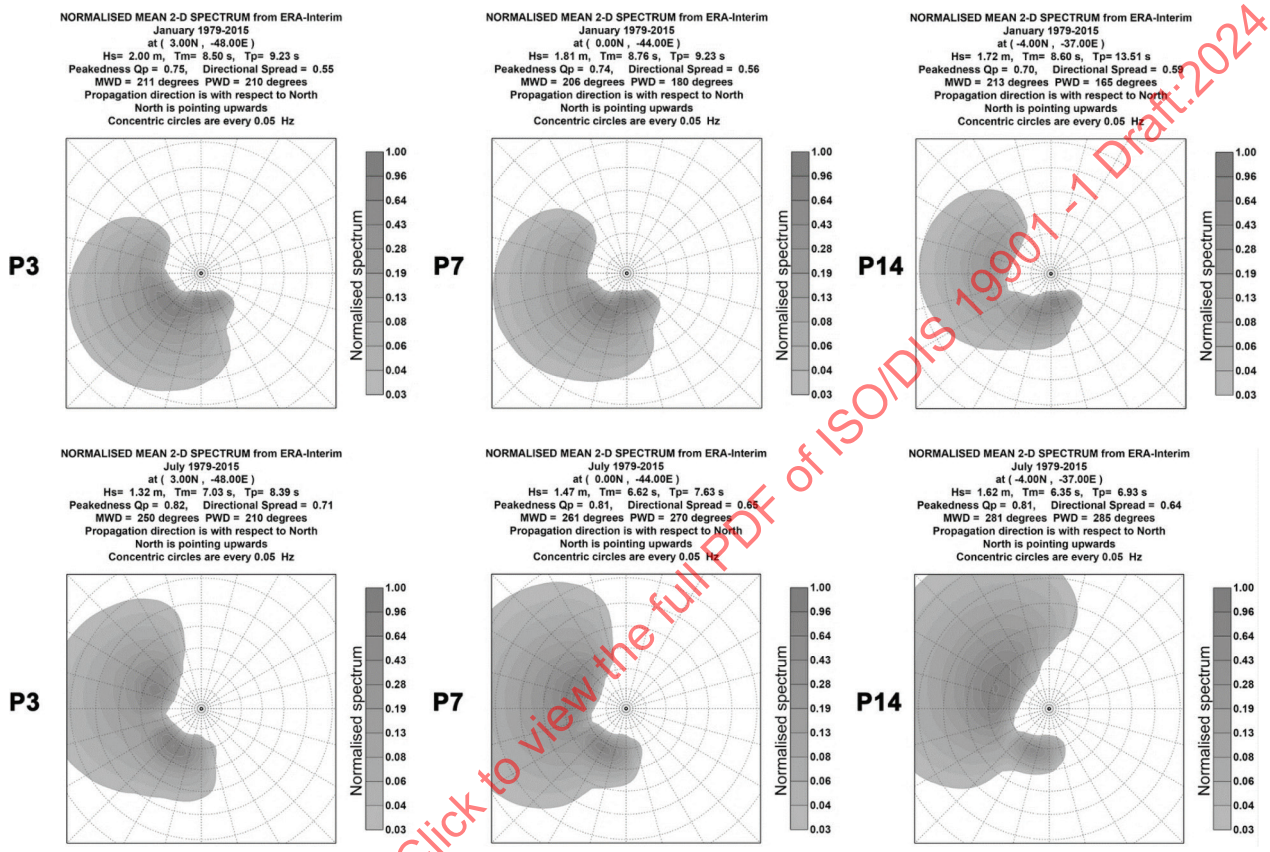

Figure I.4 — Monthly mean 2D wave spectrum of 35 years reanalysis database from the ERA-Interim project in BEM for January (upper panels) and July (lower panels). Wave direction points in the direction to which waves propagate. Datapoints are located at the Foz do Amazonas (P3), Barreirinhas (P7) and Potiguar (P14) basins. North points upward and concentric circles are every 0,05 Hz. Figure source[180]:

I.2.4 Ocean currents

Ocean currents in the BEM are embedded in the upper cell of the AMOC. The dominant circulation feature is the North Brazil Current (NBC) which is a western boundary current. NBC carries warm water into the Northern Hemisphere and has its origin in the complex system of westward Equatorial currents across the Atlantic. After turning west around Cape São Roque at 5° S / 35° W, the subsurface North Brazil Undercurrent (NBUC) is overlaid by waters carried by the surface-intensified South Equatorial Current (SEC) from the eastern part of the ocean basin. This undercurrent follows the shelf slope with maximum intensities up to 1 m/s around 150-200 m depth and emerges near 40º W to become NBC. Velocities intensify up to 2 m/s towards the west path with a weak seasonal signal related to the ICTZ meridional positioning. The NBC separates from the South Amerimay coastline at 6°-8° N and curves back on itself (retroflects) to feed both the North Equatorial Countercurrent (NECC) and Equatorial Undercurrent (EUC). It sheds 4-6 warm-core anticyclonic (clockwise) eddies annually which translate northwestwards for 3-4 months towards the Caribbean (Fig I.5). These NBC vortices may exceed 450 km in overall diameter and 2 000 m on vertical extent.

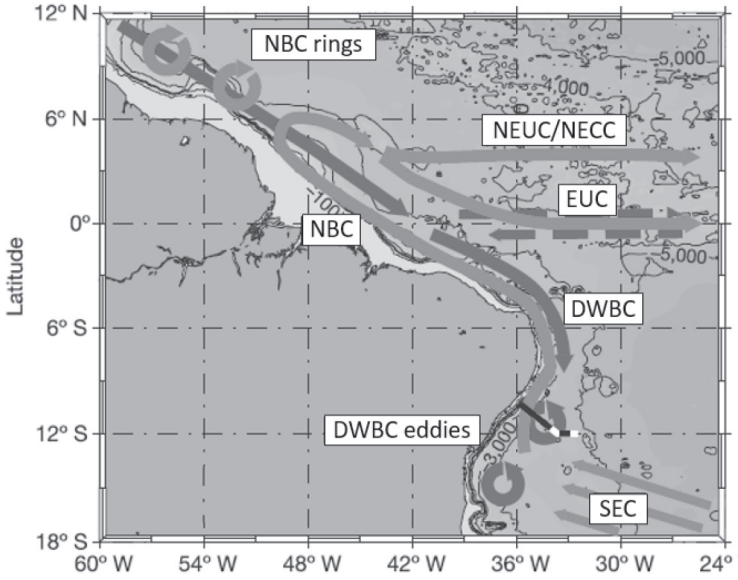

Figure I.5 — Schematic representation of circulation in Western Tropical Atlantic, with mean currents and eddy generation areas of warm water in lighter gray and cold water in darker grey. Current branches indicated are the South Equatorial Current (SEC), the North Brazil Current (NBC), the Equatorial Undercurrent (EUC), the North Equatorial Undercurrent (NEUC) merged with the North Equatorial Counter Current (NECC) and the Deep Water Boundary Current (DWBC). Figure source: Ref. [183]

The vertical water masses distribution in the BEM has the Tropical Surface Water (TSW), South Atlantic Central Water (SACW) and Antarctic Intermediate Water (AAIW) moving northward in the upper 1 200 m (Fig. I.6). This flow is compensated by the deeper North Atlantic Deep Water (NADW), moving southward between 1 200 and 4 000 m, forming the upper cell of the AMOC.

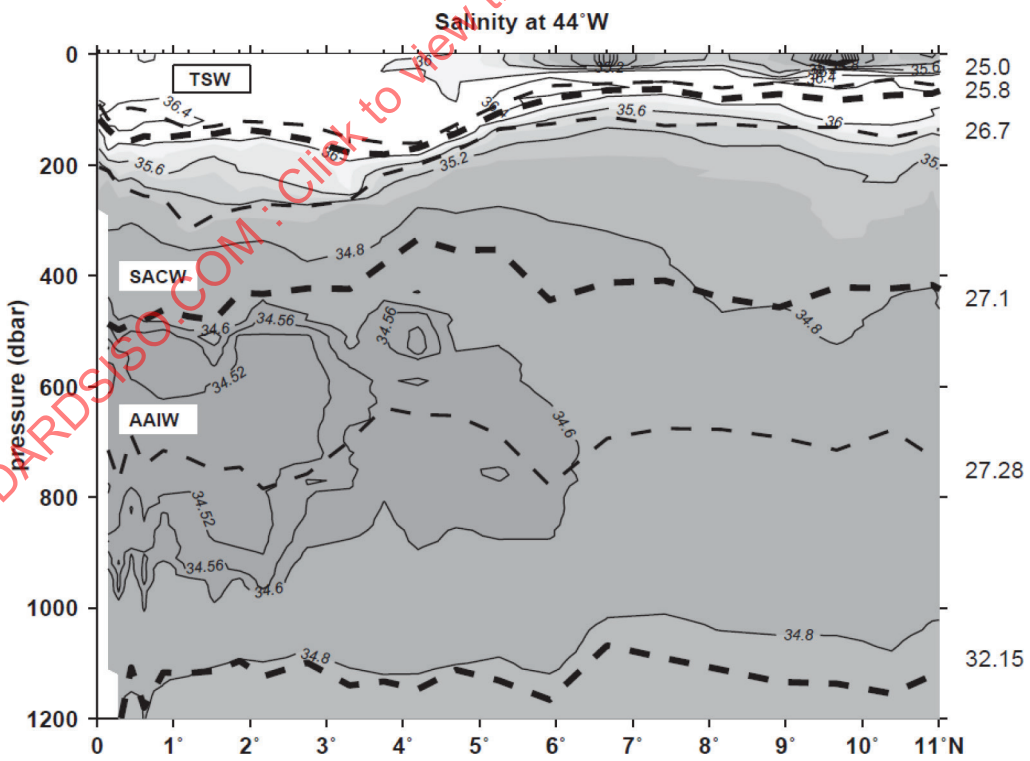

Figure I.6 — Salinity contour snapshot in the upper 1 200 m along 44° N showing water mass boundaries of Tropical Surface Water (TSW), South Atlantic Central Water (SACW) and Antarctic Intermediate Water (AAIW). Figure source: Ref. [184]

At the edge of the BEM at 5-8°N the NBC bends away from the coastline and retroflects to feed the North Equatorial Countercurrent. This NBC retroflection is most intense in the boreal autumn. Eventually the flow dynamics provides enough vorticity to shed anticyclonic eddies (the NBC rings) which may exceed 400 km in diameter. These rings have a complex vertical structure extending up to 900 m depth and may translate for 3-4 months to reach the Caribbean Sea, 1 500 km northwestward the generation area.

A detailed description of circulation and water masses in the BEM region may be found in references [183 to 188], and a comprehensive understanding of the NBC rings and retroflection formation processes is provided by several scientific papers [references 189 to 198].

I.2.5 Tides and Tidal Currents

Tides on the ports of Brazilian Equatorial Margin are predominantly semi-diurnal. It is recommended the use of tidal tables and charts provided by the Brazilian Navy (Centro de Hidrografia da Marinha – CHM). Tidal tables of Brazilian ports may be accessed through the site https://www.marinha.mil.br/chm/tabuas-de-mare.

I.2.6 Tables with Estimates of Metocean Parameters for the Equatorial Region

Indicative values of wind, wave and current parameters for some return periods are provided in Tables I.1 and I.2 for offshore Brazilian Equatorial Margin areas. The first table contains values for Foz do Amazonas, Pará-Maranhão and Barreirinhas Basins (West BEM), and the last one shows values for Ceará and Potiguar Basins (East BEM).

However, this information should not replace the detailed, site-specific parameters which should be obtained for design or assessment of particular structure that is to be constructed for or operated at the particular site.

Table I.1 — Indicative values of metocean parameters – West Brazilian Equatorial Margin

Metocean parameter	Return period N Years			
	1	10	50	100
Nominal water depth	deeper than 1 000 m			
10-min mean wind speed (m/s)[a]	12,4	14,3	16,7	17,7
Significant wave height (m)	3,5	4,4	5,1	5,4
Spectral peak period (s)	13,8	14,1	14,8	15,1
Surface current speed (m/s)	2,28	2,69	2,92	3,01
[a] Based on a reference height of 10 m above sea level.				

Table I.2 — Indicative values of metocean parameters – East Brazilian Equatorial Margin

Metocean parameter	Return period N Years			
	1	10	50	100
Nominal water depth	deeper than 100 m			
10-min mean wind speed (m/s)[a]	17,3	20,3	22,5	23,4
Significant wave height (m)	3,4	3,8	4,0	4,2
Spectral peak period (s)	14,7	16,4	17,5	18,0
Surface current speed (m/s)	0,74	1,12	1,36	1,45
[a] Based on a reference height of 10 m above sea level.				

I.3 Offshore East Brazil (Sergipe Basin)

The geographical scope of this section is the offshore Sergipe Basin, located off the coast of East Brazil. It stretches for about 100 km along the coast centered in 11° S and 37° W. It has a 15-40 km wide continental

shelf with a steep slope where the water depth changes from 100 m to 2 000 m in less than 20 km horizontally (Fig I.7).

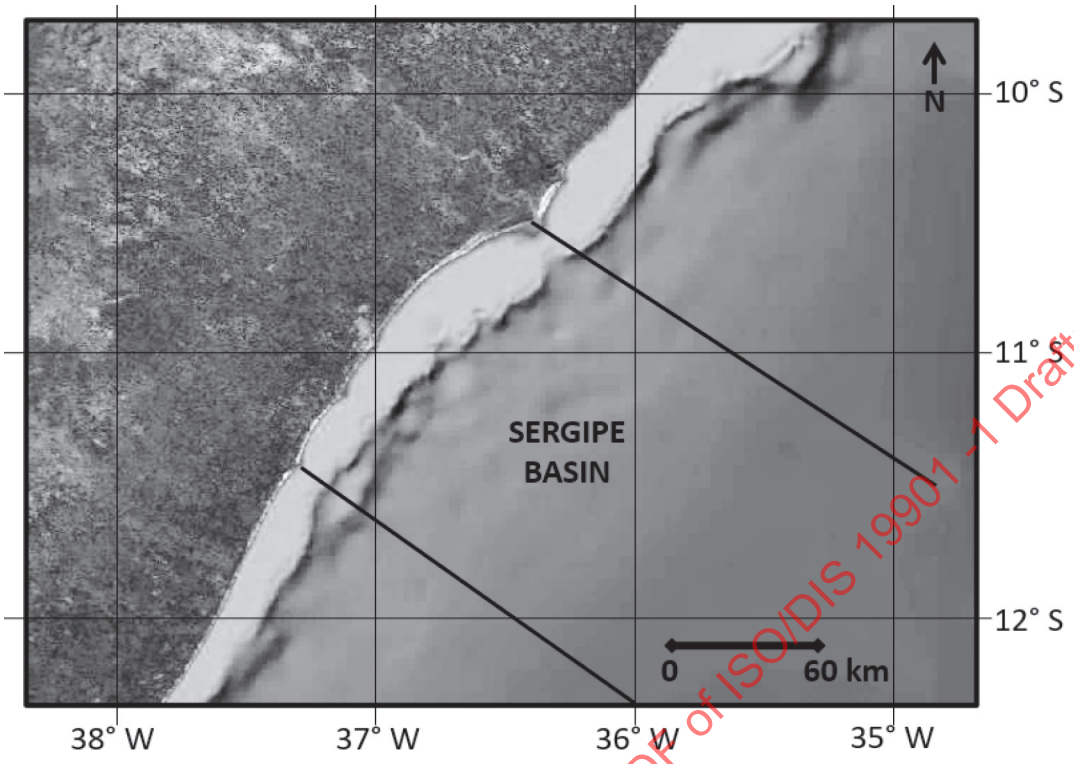

Figure I.7 — Map of the Northeastern coast of South America showing Sergipe Basin.

I.3.1 Description of the region

Sergipe Basin is delimited by regional basement highs. Structural orientation follows various dipping faults caused by a sequence of tectonic events related to the oblique opening of the South Atlantic Ocean in Late Jurassic. This geometric configuration allowed accumulation of post-rift sedimentation with turbidite sandstones deposit from Upper Cretaceous as a major exploration play[199,200].

I.3.2 Winds

Wind climatology of the Sergipe Basin is characterized by the zonal transition from the subtropical semi-stationary system South Atlantic Subtropical Anticyclone (SASA) to the equatorial ICTZ (Fig. H.8). This seasonal pattern has a long-term component related to the interannual anomaly of the sea surface temperature.[201] Averaged monthly wind speed varies between 5 and 7 m/s, with higher values in austral winter following the northwestward migration of the SASA. Local extreme winds may reach values higher than 15 m/s from South-Southeast during occasional passage of a cold front system.

Atmospheric conditions at Sergipe Basin are also influenced by a number of global large-scale phenomena. The interaction of ENSO and MJO (Madden-Julian Oscillation) may bring interannual variability either enhancing or weakening the observed anomalies in meteorological parameters as responses of the SASA annual migration cycle[202,203].

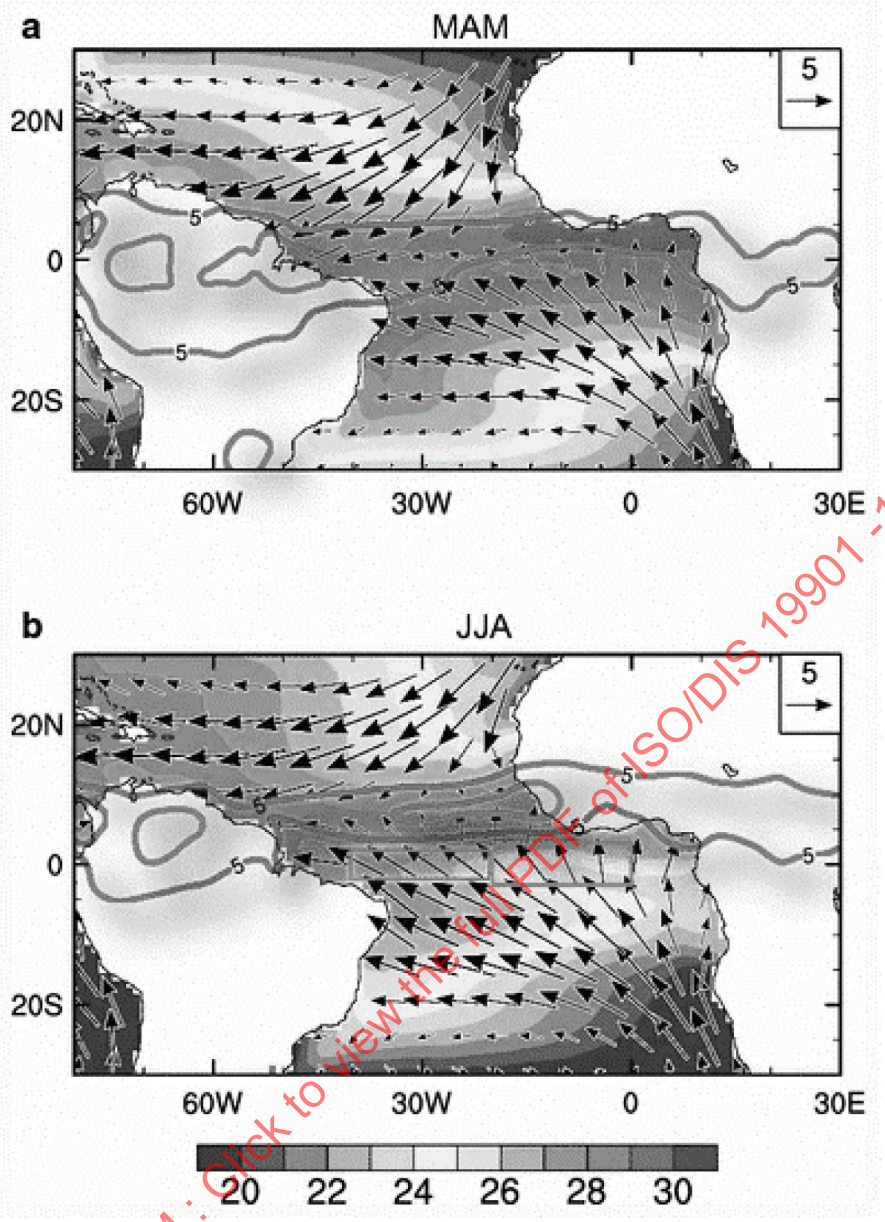

Figure I.8 — Seasonal migration of the SASA and the ITCZ in the tropical Atlantic, from ERA Interim surface winds (vectors, reference 5 m/s), optimum interpolation sea surface temperature (shadow bar below, in C°) and precipitation from GPCP (Global *Precipitation* Climatology Project, 5 and 10 mm/day contour over the Equator). Figure source: Ref: [201]

I.3.3 Waves

Variations in the position and intensity of the SASA semi-stationary system largely influence the offshore wave field in Sergipe Basin. Higher significant wave heights Hs occur in austral winter and spring following the northwestward migration of the wave generation zone on the northern sector of the anticyclonic SASA system and the presence of extensive fetches and slightly stronger East winds at this time of the year (Fig. I.9).

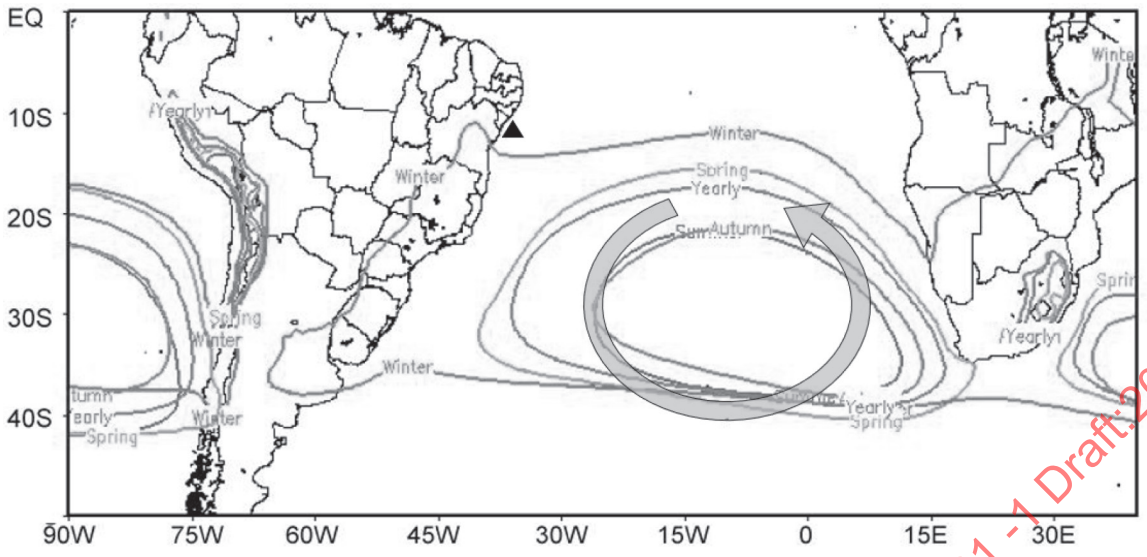

Figure I.9 — Seasonal migration and yearly mean position of the 1 018 hPa isobar from ERA Interim for the 1979-2005 period, showing the South Atlantic Subtropical Anticyclone migration to NW during austral spring and winter. Black triangle indicates the Sergipe Basin region and the circular arrow represents the anticlockwise wind circulation due to SASA. Figure source: Ref: [204]

Wave groups associated with the northeastward progression of frontal systems caused by extratropical cyclones in the southern Atlantic may occasionally reach Sergipe Basin. Although sporadic throughout the year, these remotely generated waves become more frequent from April to September during austral autumn and winter, with direction from S-SE and higher Tp than the predominant East direction wave field.

I.3.4 Ocean Currents

Global large-scale circulation of the South Atlantic Ocean modulates the ocean current system in the upper 1 000-m water column offshore Sergipe Basin. The South Equatorial Current (SEC) is the northern branch of the subtropical gyre carrying surface waters zonally from Africa across the South Atlantic Ocean. It bifurcates at the Brazilian shelf into the southward Brazil Current (BC) and the northward North Brazil Undercurrent (NBUC) around latitude 15° S near the surface, shifting poleward with increasing depth (Figs. I.10 and I.11). NBUC is the main oceanographic feature in Sergipe Basin closely following the continental slope. It is approximately 100 km wide and reaches 1 200 m down in the water column. Top intensities of 1,0-1,5 m/s are commonly observed in the flow jet 200-300 m below surface.

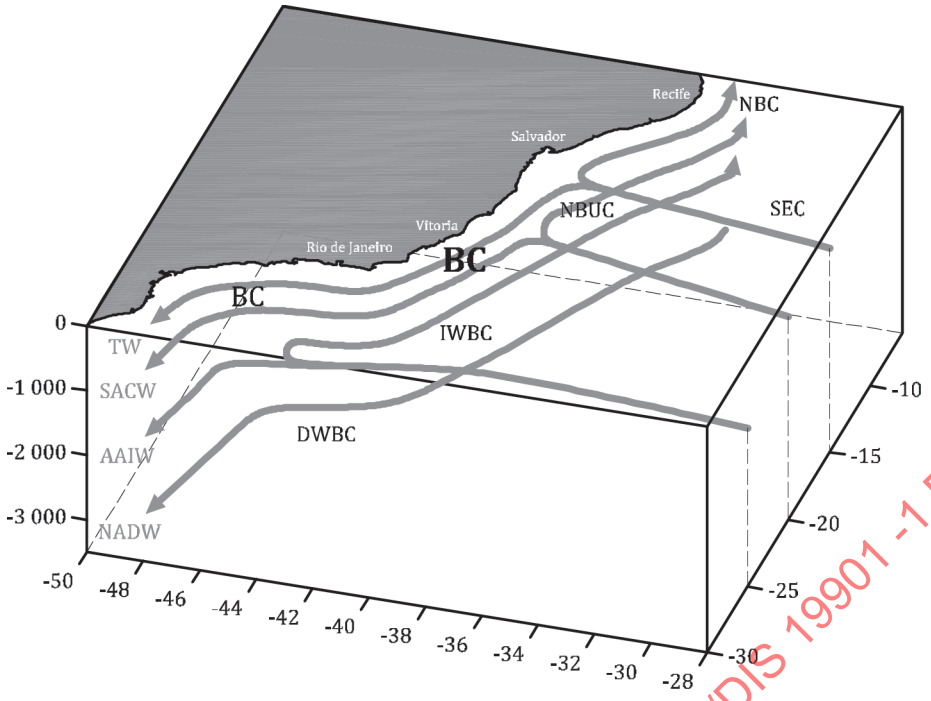

Figure I.10 — 3-D depiction of the TW (Tropical Water), SACW (South Atlantic Central Water), AAIW (Antarctic Intermediate Water) and NADW (North Atlantic Deep Water) water masses being transported by the complex Western Boundary Currents structure off the eastern coast of Brazil. Current names are South Equatorial Current (SEC), North Brazil Undercurrent (NBUC), North Brazil Current (NBC), Brazil Current (BC), Intermediate Western Boundary Current (IWBC) and Deep Western Boundary Current (DWBC). Figure source: Ref.[205]

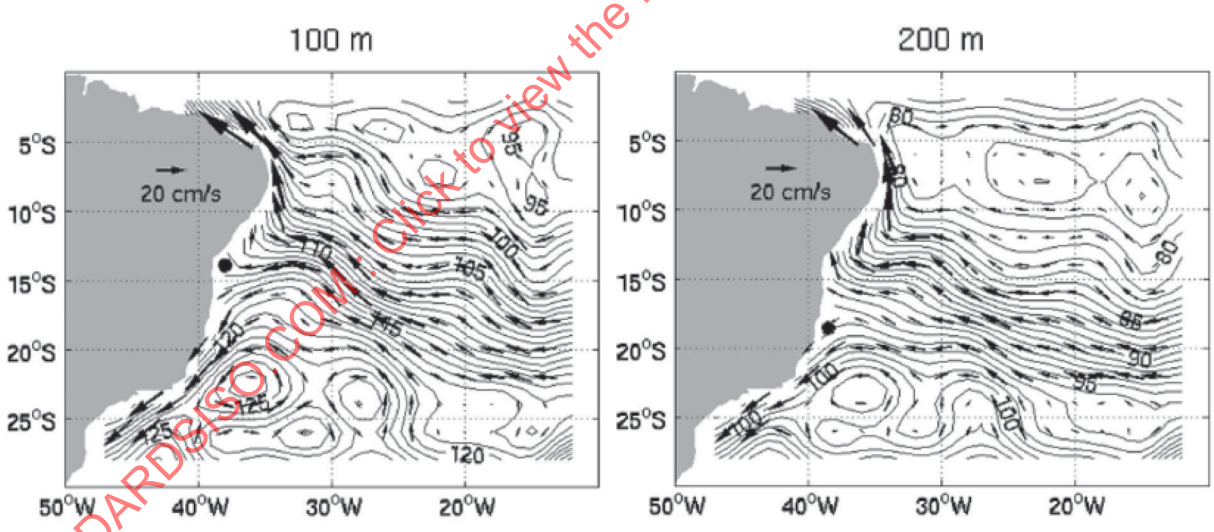

Figure I.11 — Annual mean geostrophic circulation of Southwest Atlantic depicting the westward South Equatorial Current, the northward North Brazil Undercurrent and southward Brazil Current based on hydrographic measurements. Black dots indicate the location of the SEC bifurcation at 100 and 200 m below surface. Contours show dynamic height in 0,1 $m^2 s^{-2}$ interval from hydrographic dataset. Figure source: Ref: [206]

The latitude of the SEC bifurcation varies annually with a larger excursion in the upper layers compared to the deeper levels. Its northernmost (southernmost) latitude in austral winter (austral spring/summer) follows the N-S motion of the ITCZ-SASA coupled system[205] and is ultimately associated to ENSO and MJO interannual atmospheric forcing. This seasonal variability has been connected to the local wind forcing for the upper thermocline and it modulates the NBUC flow. Strong surface currents in the Sergipe Basin are

more likely during austral winter, and lower intensities in the end of the year, though interannual and intra seasonal variabilities signals may also be observed. The NBUC transports 20-25 Sv northward, composed of Tropical Surface Water (TSW), South Atlantic Central Water (SACW) and Antarctic Intermediate Water (AAIW). A southward flow of the North Atlantic Deep Water (NADW) is present below AAIW levels, with a maximum speed of 0,3-0,5 m/s at 1 800-2 000 m below the surface[207].

I.3.5 Tides and Tidal Currents

Sergipe coast presents a semi-diurnal mesotidal regime. It is recommended the use of tidal tables and charts provided by the Brazilian Navy (Centro de Hidrografia da Marinha – CHM) that may be accessed through https://www.marinha.mil.br/chm/tabuas-de-mare.

I.3.6 Tables with Estimates of Metocean Parameters for Sergipe Basin, NE Brazil

Indicative values of wind, wave and current parameters for some return periods are provided in Table I.3 for Sergipe Basin, offshore Northeast Brazil. However, this information should not replace the detailed, site-specific parameters which should be obtained for design or assessment of particular structures that are to be constructed for or operated at a particular site.

Table I.3 — Indicative values of Metocean parameters – Sergipe Basin

Metocean parameter	Return period N Years			
	1	10	50	100
Nominal water depth	deeper than 50 m			
10-min mean wind speed (m/s)[a]	17,1	21,9	25,3	26,8
Significant wave height (m)	3,8	4,9	5,6	5,9
Spectral peak period (s)	12,0	12,3	13,0	13,0
Surface current speed (m/s)	1,00	1,33	1,36	1,42

[a] Based on a reference height of 10 m above sea level.

I.4 Offshore Southeast Brazil (Santos and Campos Basins)

I.4.1 Description of the region

The Campos and Santos Basins are contiguous offshore sedimentary basins located near the western border of the South Atlantic Ocean. Campos Basin is about 350 km long and extends from latitude 20° S to latitude 23° S. Santos Basin is about 800 km long and extends from 23° S to 28° S. Both basins jointly cover approximately 300,000 km^2 of total area (Fig. I.12).

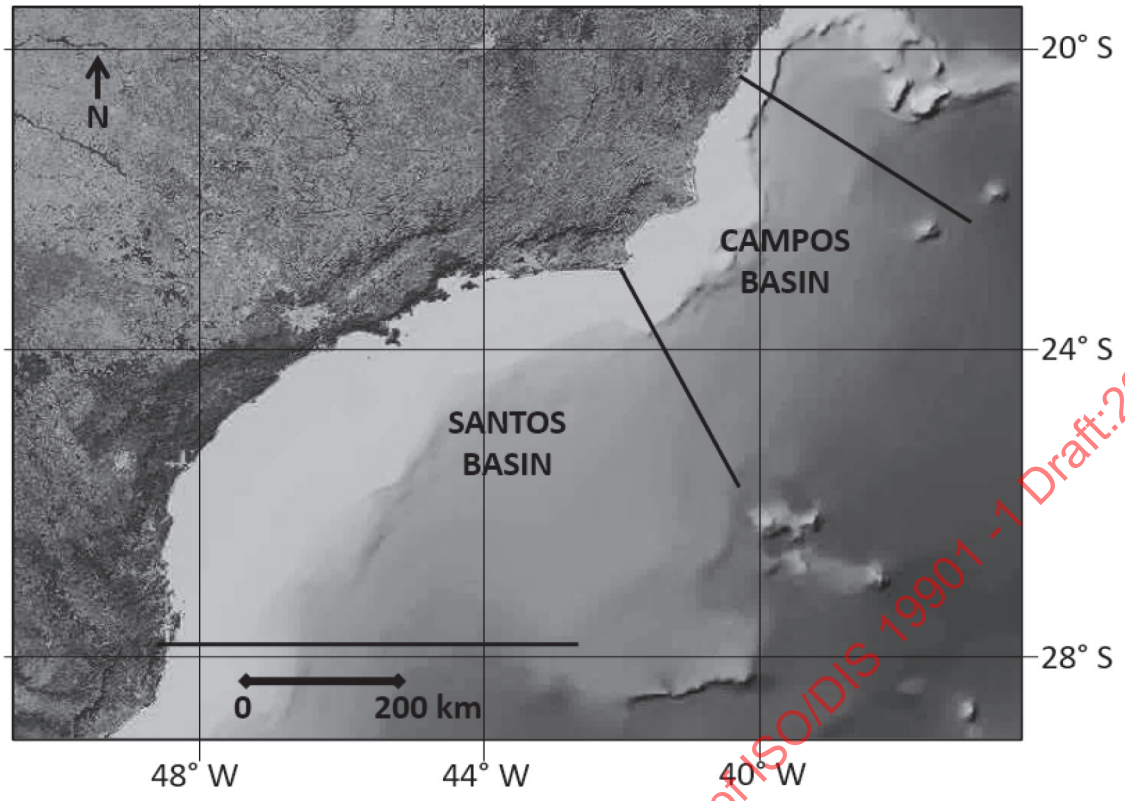

Figure I.12 — Map of the Eastern coast of South America showing Campos and Santos Basins.

The formation and development of both basins are related to the intense pre-Aptian (circa 180 mya) magmatic activity associated with Atlantic Ocean opening. Sequence of lacustrine and marine sediments in the later rifting phase set conditions for large areas of pre-salt deposits. A more stable tectonic period allowed deposition of Cenozoic sediments on the top of the ancient salt deposits mainly in Campos Basin due to the larger drainage area[208,209].

Atmospheric circulation of the tropical South Atlantic is mainly characterized by the semi-stationary system South Atlantic Subtropical Anticyclone (SASA). Over this large region of high pressure, transient weather systems such as cold fronts, cyclones and mesoscale systems occur and modify the dominant weather patterns. Variations of atmospheric pressure, temperature, and wind are related to the interaction of these systems.

The main oceanographic feature in this region is the western boundary current system associated with the South Atlantic sub-tropical gyre. Thus, the Santos and Campos basins are subjected to intense mesoscale activity associated with the Brazil Current (BC) on the surface, the Antarctic Intermediate Current (AAIC) on the middle water column, and the Deep Western Boundary Current (DWBC) in the lower levels along the continental slope. Further offshore, the oceanic circulation is driven by eddies associated with instabilities and contribution of the general circulation of the South Atlantic Ocean.

I.4.2 Winds

Winds on the South-East Brazilian offshore sedimentary basins are strongly influenced by the South Atlantic Subtropical Anti-Cyclone (SASA). The central position of this anti-cyclone moves form 32°S/5°W in late austral summer to 27°S/8°W in the austral winter. In addition to this annual shift on the position of the SASA, El Niño-Southern Oscillation variability are also correlated to meridional anomalies in the SASA position. The dominant Northeast and East winds over Santos and Campos basins are usually caused by the western border of the SASA and usually indicate good weather conditions. Due to the annual changes in the configuration of the high pressure South Atlantic gyre, mean wind intensities are slightly higher during spring and summer months (Oct-Mar) and lower in mid-autumn (May). Occasional transient extratropical and subtropical cyclones may cause changes in the dominant winds (Fig. I.13). These transient systems

strongly control the passage of cold fronts and are responsible for bad weather conditions associated with Southwest and South winds [203,210-212].

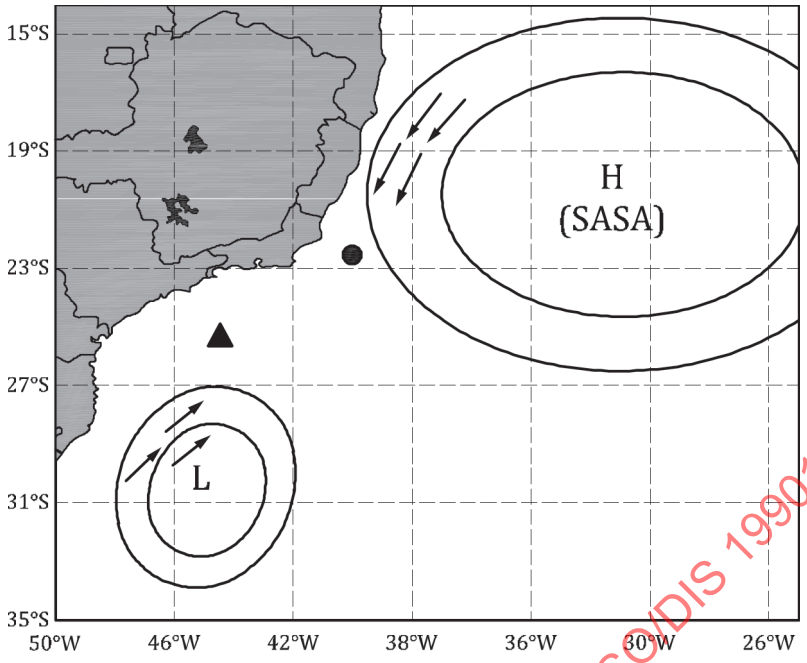

Figure I.13 — Representation of the dominant NE winds generated by the high pressure South Atlantic Subtropical Anticyclonic (SASA) and the occasional SW winds generated by transient low-pressure cyclonic systems. Black circle indicates Campos Basin and black triangle indicates Santos Basins. Figure source: Ref. [210]

I.4.3 Waves

Wave climatology in both Campos and Santos Basins is mainly influenced by the winds associated with the semi-permanent anticyclonic system SASA, with dominant East and Northeast winds generating characteristic sea wind waves with periods lower than 10 s and fetch-limited heights. Bimodal seas may occur in situations of higher period swells arriving from the Southeast-Southwest quadrants originating from distant cyclonic systems in higher latitudes further South.[213,214] The seasonal variation of the directional distribution of significant wave height Hs and spectral peak periods is presented in Fig. I.14.

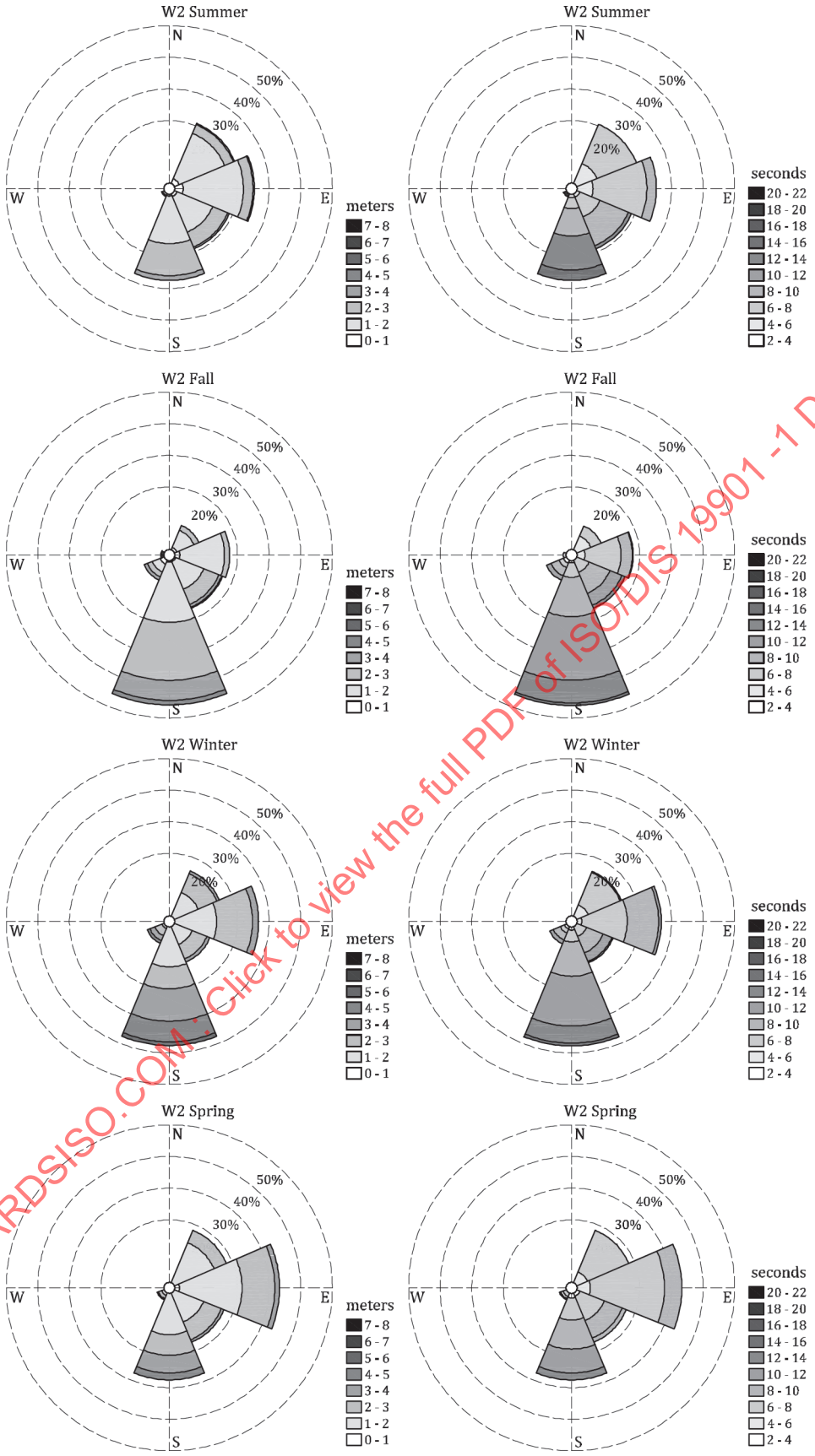

Figure I.14 — Directional histograms of seasonal wave height (left) and period (right) for Santos Basin from NWW3 hindcast reanalysis. Bars point in the direction from which waves approach. Figure Source: Ref. [182]

I.4.4 Ocean Currents

Ocean circulation in the Campos and Santos Basins regions is governed by the western branch of the South Atlantic Gyre. This flow is characterized by a strong vertical shear and is usually split in the Brazil Current (BC), the Intermediate Western Boundary Current (IWBC), and the Deep Western Boundary Current (DWBC), with the occurrence of persistent meanders and eddies in both Campos and Santos Basins. The BC is a shallow, warm and salty southward flow adjacent the Brazilian shelf break between 20° S and 28° S. It is ~100 km wide, approximately 500 m deep, and has a higher maximum surface speed in Campos (up to 1,5 m/s) than in the northern Santos Basin. Underneath the BC, IWBC flows northeastward and has a vertical extent of approximately 1,300 m, a width of ~60 km, and intensities up to 0,5 m/s. The DWBC transports North Atlantic Deep Water (NADW) southward following the lower continental slope at 2,500-3,000 m isobath and over the São Paulo Plateau in Santos Basin (Fig. I.10). The strength of this bidirectional western boundary flow depends on the bifurcation of the South Equatorial Current over the Brazilian coast [215-218].

The BC develops intense meso-scale activity while flowing adjacent to the South Americnay shelf break. Frontal meanders and occasional eddies are normal features in both basins. Campos Basin eddies have water-mass composition made up of both cooler upwelling waters and the warmer southward flowing Brazil Current water. The occurrence of coastal seasonal wind-driven upwelling in the region is more pronounced on the inner shelf near Cabo Frio at the limit of Campos and Santos Basin. Occasional eddy induced upwelling intensifies prevailing costal upwelling and increasing the horizontal density gradient between colder coastal waters and warmer BC tropical waters [219,220].

A comprehensive description of the circulation and water masses in Campos and Santos basins is provided by several scientific papers [221 to 231].

I.4.5 Tides and Tidal Currents

The tidal regime on the coast of Campos and Santos Basin is characterized by a semi-diurnal period microtide. It is recommended the use of tidal tables and charts provided by the Brazilian Navy (Centro de Hidrografia da Marinha – CHM). Tidal tables of Brazilian ports may be accessed through the site https://www.marinha.mil.br/chm/tabuas-de-mare.

I.4.6 Tables with Estimates of Metocean Parameter for the SE Brazil

Indicative values of wind, wave and current parameters for some return periods are provided in Tables I.4 and I.5 respectively for Campos and Santos Basin, offshore Southeast Brazil. However, this information should not replace the detailed, site-specific parameters which should be obtained for the design or assessment of particular structures that are to be constructed for or operated at a particular site.

Table I.4 — Indicative values of Metocean parameters – Campos Basin

Metocean parameter	Return period N Years			
	1	10	50	100
Nominal water depth	deeper than 200 m			
10-min mean wind speed (m/s)[a]	18,6	24,5	29,5	31,9
Significant wave height (m)	6,4	7,8	8,8	9,2
Spectral peak period (s)	13,8	14,8	15,0	15,5
Surface current speed (m/s)	1,47	1,76	1,97	2,06

[a] Based on a reference height of 10 m above sea level.

Table I.5 — Indicative values of Metocean parameters – Santos Basin

Metocean parameter	Return period N Years			
	1	10	50	100
Nominal water depth	deeper than 100 m			
10-min mean wind speed (m/s)[a]	20,4	27,9	32,1	34,5
Significant wave height (m)	6,9	9,2	10,6	11,2
Spectral peak period (s)	13,0	14,5	16,0	16,6
Surface current speed (m/s)	1,39	1,57	1,68	1,72

[a] Based on a reference height of 10 m above sea level.

Annex J
(informative)

US Gulf of Mexico

J.1 Description of Region

The geographical extent of the region is the waters of the Gulf of Mexico that fall within the United States exclusive economic zone, which is generally the portion of the Gulf of Mexico north of 26 °N, as shown in Figure J.1, and which includes the lease blocks shown in Figure J.2 and Figure J.3.

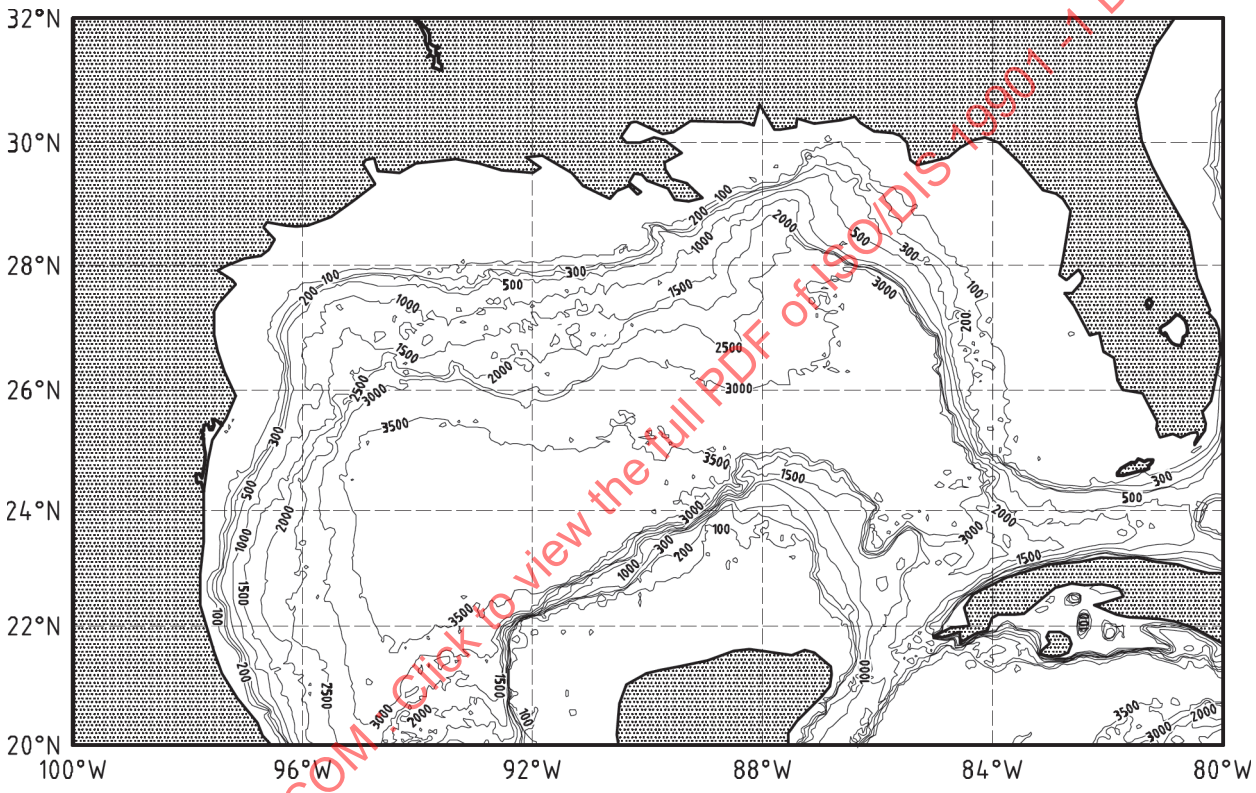

Figure J.1 — Gulf of Mexico (Bathymetry in m)

The Gulf of Mexico has a total area of 1,587,000 km2. The US Gulf coast is 2 625 km long and comprises the coasts of the following US states (from west to east with coastline lengths):

Texas	591 km;
Louisiana	639 km;
Mississippi	71 km;
Alabama	85 km;
Florida	1 239 km (Gulf coastline only).

Offshore Florida, Alabama, and Mississippi, the width of the continental shelf varies between 25 km and 125 km wide, with water depths at the shelf break of between 60 m and 100 m. Further west, off the Mississippi River delta, the continental shelf width is less than 20 km and increases to 200 km offshore

central and western Louisiana and Texas. Waters along the shelf are generally less than 100 m deep. Water depths off the shelf can exceed 3 000 m.

Freshwater runoff from approximately two-thirds of the continental United States empties into the northern Gulf, with most of the inflow coming via the Mississippi River.

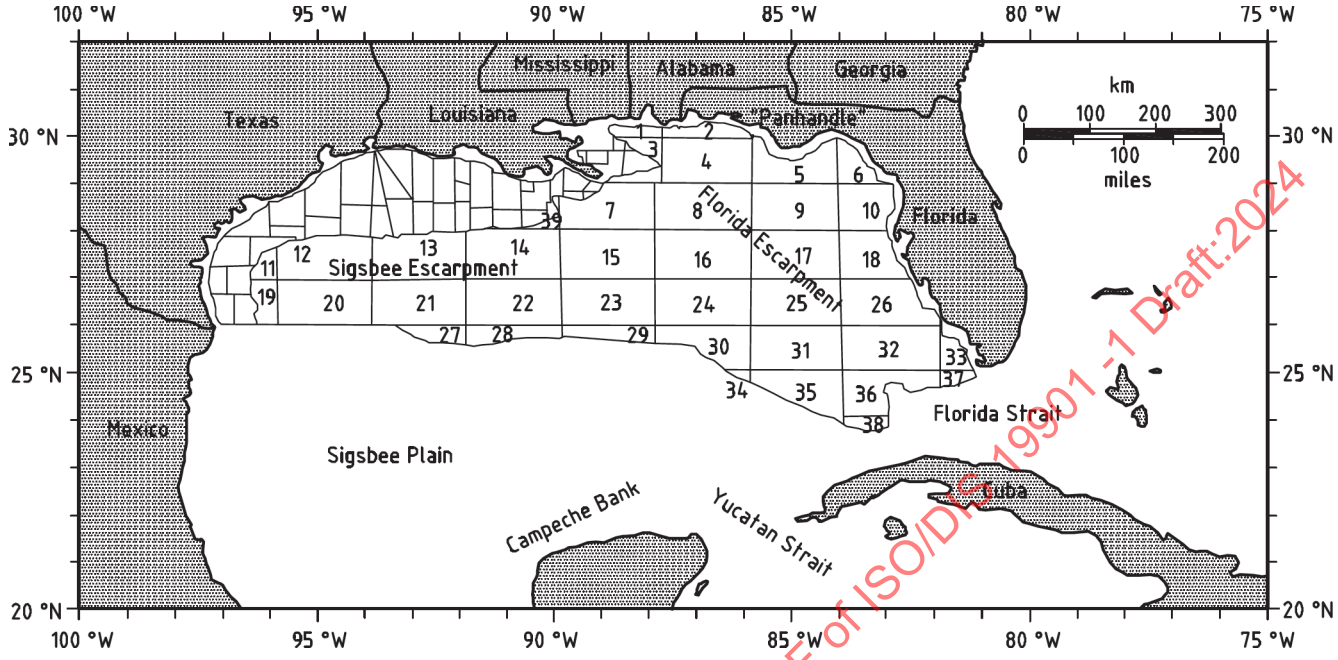

Key

1	Mobile	14	Green Canyon	27	Sigsbee Escarpment
2	Pensacola	15	Atwater Valley	28	Amery Terrace
3	Viosca Knoll	16	Lloyd Ridge	29	Lund South
4	Destin Dome	17	The Elbow	30	Florida Plain
5	Apalachicola	18	Saint Petersburg	31	Howell Hook
6	Gainesville	19	Port Isabel	32	Pulley Ridge
7	Mississippi Canyon	20	Alaminos Canyon	33	Miami
8	De Soto Canyon	21	Keathley Canyon	34	Campeche Escarpment
9	Florida Middle Ground	22	Walker Ridge	35	Rankin
10	Tarpon Springs	23	Lund	36	Dry Tortugas
11	Corpus Christi	24	Henderson	37	Key West
12	East Breaks	25	Vernon Basin	38	Tortugas Valley
13	Garden Banks	26	Charlotte Harbor	39	Ewing Bank

Figure J.2 — US Outer Continental Shelf and Deep Water Lease Areas

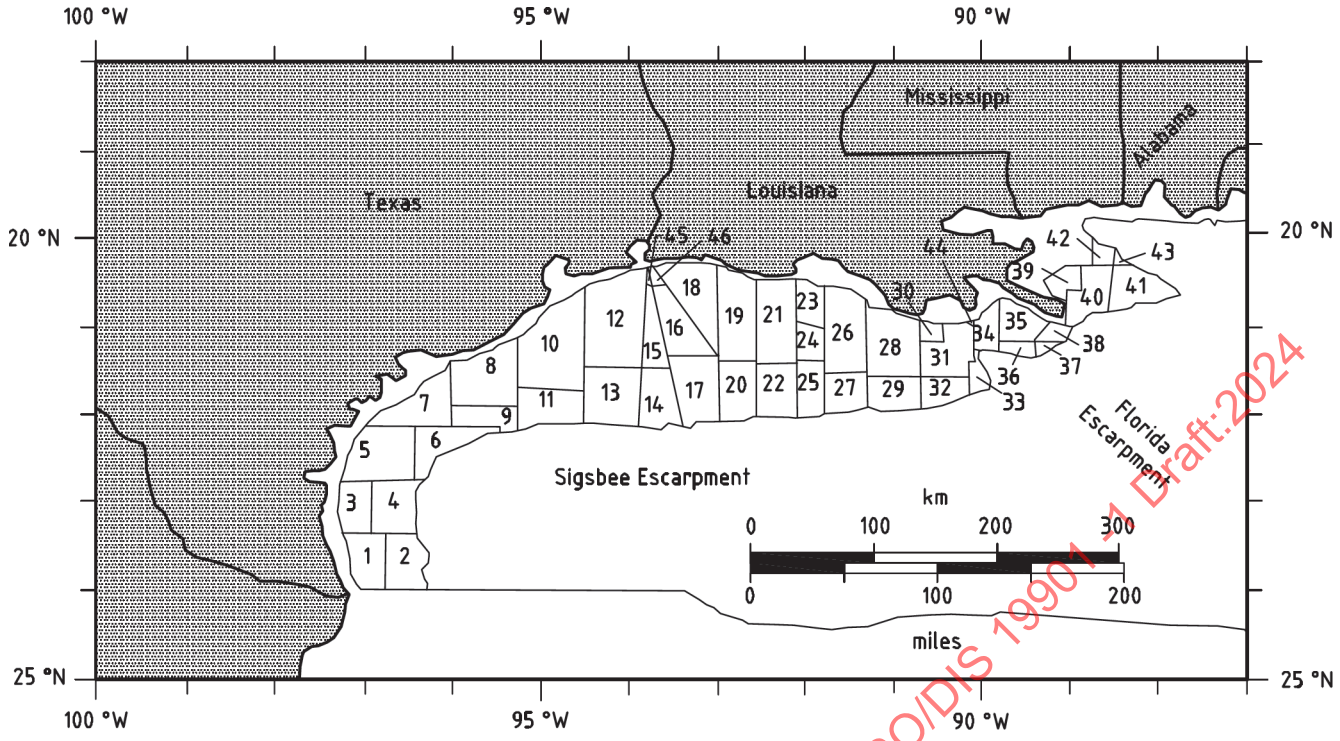

Key

1	South Padre Island	17	West Cameron South	33	Grand Isle
2	South Padre Island East	18	West Cameron	34	Grand Isle
3	North Padre Island	19	East Cameron	35	West Delta
4	North Padre Island East	20	East Cameron South	36	West Delta South
5	Mustang Island	21	Vermilion	37	South Pass South & East
6	Mustang Island East	22	Vermilion South	38	South Pass
7	Matagorda Island	23	South Marsh Island North	39	Breton Sound
8	Brazos	24	South Marsh Island	40	Main Pass
9	Brazos South	25	South Marsh Island South	41	Main Pass South & East
10	Galveston	26	Eugene Island	42	Chandeleur
11	Galveston South	27	Eugene Island South	43	Chandeleur East
12	High Island	28	Ship Shoal	44	Bay Marchand
13	High Island South	29	Ship Shoal South	45	Sabine Pass (TX)
14	High Island East South	30	South Pelto	46	Sabine Pass (LA)
15	High Island East	31	South Timbalier		
16	West Cameron West	32	South Timbalier South		

Figure J.3 — US Inner Continental Shelf Lease Areas

J.2 Data Sources

The northern offshore area of the Gulf of Mexico is one of the most studied regions in terms of its meteorology and physical oceanography. Wind, wave, and meteorological measurements have been made at many stations throughout the area over the past 30 years, both on and off the continental shelf. Much of these data have been recorded under sponsorship of the US government and are available from the National Data Buoy Center.[238] Extensive data on the statistics and climatology of tropical cyclones affecting the Gulf of Mexico may be obtained from the archives of the National Hurricane Center[239]; however, there is evidence that cyclone data from the early (pre-1950) period are biased low.[240,241] Various industry-sponsored measurement programs have also been conducted, and data are generally available for purchase or trade.

In addition to measured wind and wave data, several important industry-sponsored numerical hindcast studies of both extreme and operational winds and waves (including storm surges and storm currents) have been performed, most notably the Gulf of Mexico Storm Hindcast of Oceanographic Extremes (GUMSHOE[242]) and Winter Extremes (WINX[243]) studies from the early 1990s, and more recently the proprietary Gulf of Mexico Oceanographic Study (GOMOS[244]). The US Army Corps of Engineers (USACE) MORPHOS numerical studies provide an additional source of information for storm surges and shallow water wave conditions.[245] Select wind, wave, current, and surge hindcasts of individual major hurricanes have also been sponsored by the US Minerals Management Service (MMS); its successor organization, the Bureau of Ocean Energy Management, Regulation, and Enforcement (BOEMRE); and finally the Bureau of Safety and Environmental Enforcement (BSEE) and the Bureau of Ocean Energy Management (BOEM), which replaced BOEMRE in 2011[246].

A number of current and water quality measurements (temperature, salinity, chemical composition) have also been made in the region over the years, both in shallow and deep water. Many of these studies have been sponsored by the MMS[247 to 249]. In 1982, MMS began a series of data collection programs starting in the eastern Gulf[250] and culminating in 1985 with the LATEX study of the central northern Gulf. The LATEX study results have been archived with the National Oceanographic Data Center (NODC).[248] MMS contracted with Texas A&M University to reanalyse and synthesize all available data (including some industry data) on the Gulf; the results of this comprehensive study were published in 2001.[251] BOEM has supported studies of deep water Gulf currents as part of its Gulf of Mexico Region's Environmental Studies Program[252]. Measurements made along the Sigsbee Escarpment as part of this program provide data on topographic Rossby waves (TRWs).

The industry has also taken an active role in collecting measurements.[253] The Eddy joint industry project (EJIP), an industry collaborative effort, has sponsored measurements in the deeper waters of the region over the period from 1983 through 2004. The Climatology and Simulation of Eddies (CASE) joint industry project, another industry effort, used the EJIP data to develop numerical models for use in estimating design currents in deep water associated with the Loop Current and warm eddies, the most notable being the Gulf Eddy Model (GEM)[254] and a corresponding historical hindcast database of eddies and Loop Current intrusions. CASE and EJIP merged in 2005 to become CASE-EJIP, and since that time have sponsored numerical models for eddy forecasting, investigations of cold core eddies, updates to the GEM hindcast database (through 2013 as of the date of this document), hurricane and Loop Current/eddy interaction (both wave fields and currents), development of a new synthetic eddy model and studies of storm wave crests. The ongoing EddyWatch[255] program in the Gulf of Mexico is also a source of historical eddy observations. Eddy tracking with satellite data and drifting buoys is now routine in the Gulf, and forecast services are available from several vendors.

The industry DeepStar[256] program also supports research into the Gulf of Mexico environment; recent projects have included an evaluation of Loop Current forecast models, an examination of the connection between the frequency of intense hurricanes and the presence of the Loop Current, and a numerical study of TRWs.

J.3 Overview of Regional Climatology

The climate in the Gulf of Mexico ranges from tropical to temperate. Summer wind and wave conditions are generally benign, with warm temperatures and high relative humidity. Some coastal areas are periodically affected by fog. In winter there are occasional freezes in the coastal areas. Sea ice and snow are not encountered in the Gulf.

There are occasional thunderstorms, squalls, waterspouts, and on rare occasion, tornadoes in the coastal areas. Overall the storm climate in the Gulf is dominated by tropical cyclones in the summer season and extratropical cyclones and cold air intrusions in the winter season.

Locally, tropical cyclones are referred to as a tropical depression if the maximum 10 m 1 min sustained wind is less than 17,5 m/s, a tropical storm if the wind is between 17,5 and 32,9 m/s, and a hurricane if the wind is greater than or equal to 32,9 m/s.

The North Atlantic Basin Hurricane Season, which includes the Gulf of Mexico, officially runs from June 1 through November 30; however, tropical cyclones have occurred in every calendar month. The months typically seeing the highest frequency of tropical cyclone activity are August, September, and October. On average, three tropical storms or hurricanes can be expected to form in or enter the Gulf each year, although

the number is highly variable. These storms can originate in the Gulf, the Caribbean Sea, or in the North Atlantic Ocean, with the largest most intense storms generally being those that form outside the Gulf and propagate into it (see Figure J.4 for typical storm tracks). Cyclones that bring tropical storm force winds to the operating areas of the Gulf of Mexico within 24 h of storm genesis are generally referred to as “sudden storms.” Tropical cyclone activity is believed related to cycles in the North Atlantic Oscillation (NAO) and “El Niño” events, and hence there may exist decadal variations in severity patterns. There is much debate about the effect of global climate change on tropical cyclone activity.[257,258] Changes in storm occurrence rates, central pressure, and track positions are possible and could affect the long-term distribution of extreme wind, wave, and current conditions. There is also strong evidence that within the Gulf of Mexico the presence of the Loop Current and eddies from it (described below) are responsible for regional variations of the rate of encounter of large intense hurricanes[259-262].

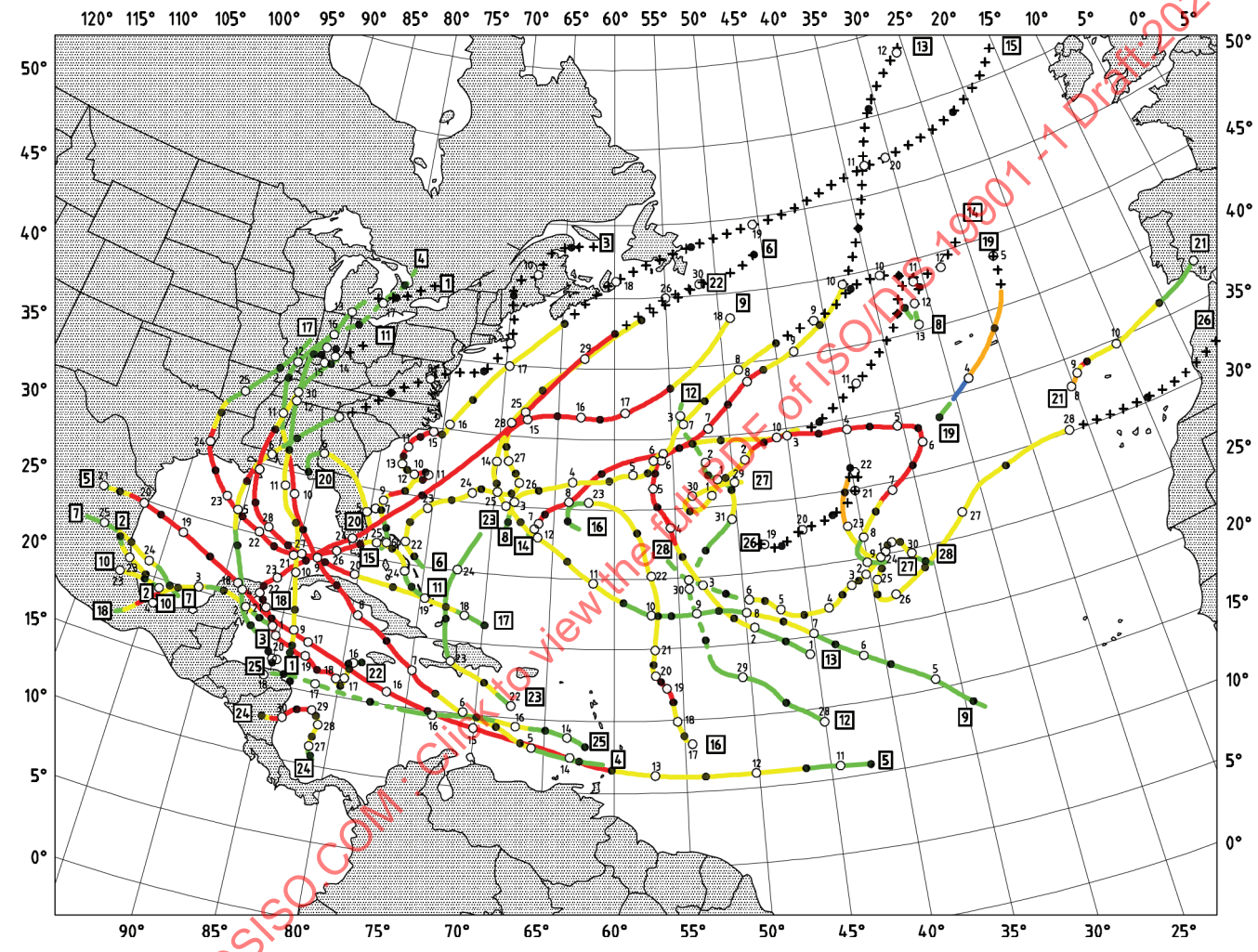

Key

- Hurricane (H)
- Tropical storm (T)
- Tropical depression
- Extratropical
- Wave/Low
- Subtropical depression
- Subtropical storm (ST)
- Position at 0000 UTC
- Position/date at 1200 UTC
- Tropical cyclone number

Figure J.4 — Tracks of Tropical Cyclones, 2005

The most severe extratropical cyclones and cold air intrusions generally occur in the months of October through March, hence the local term “winter storms.” Fronts associated with extratropical cyclones generally move over the Gulf from the north, or sweep across the Gulf from west to east. The cyclone centres are generally located well to the north of the Gulf, but on occasion enter it or actually form within it. Depending on the geometry of passage, an extratropical storm may generate strong winds from the southeast, and will hence be referred to as a “Southeaster.” Cold air intrusions can also result in severe storm conditions in the Gulf. These events, typically referred to as “Northers,” consist of intrusions of cold arctic air out over the Gulf behind cold fronts [263]; the cold air overlying the relatively warmer Gulf waters results in an unstable atmosphere and consequently strong winds and rain.

An important oceanographic feature of the deep water Gulf is the Loop Current (see Figure J.5). The Loop Current is a warm-water current that enters the Gulf through the Yucatan Strait, flows generally northward in the eastern Gulf, then turns southward along the west Florida coast, and exits through the Florida Strait as the Florida Current. It is detectable to around 800 m below the surface. A characteristic of the Loop Current is its periodic northward intrusion into the eastern Gulf; these intrusions occur every 4 to 16 months. The northward penetration of the Loop usually reaches about 28–29° N and is followed by the shedding of a large eddy (a Loop Current Eddy, also known as a Warm Core Eddy) with a diameter ranging from 150 to 450 km with clockwise rotation. After an eddy is shed, the Loop Current retracts to the south, usually below 26° N, and starts the cycle again.

After separating, a Loop Current Eddy can attach and detach several times. Eventually, the eddy moves to the west or southwest at an average translation speed of about 3 km/day. The energy of the eddy slowly decays to about half its original strength by the time it gets to the western Gulf. There, the Loop Current Eddy usually slowly breaks down into a series of smaller cyclonic and anti-cyclonic eddies. The dissipation process can take more than a year.

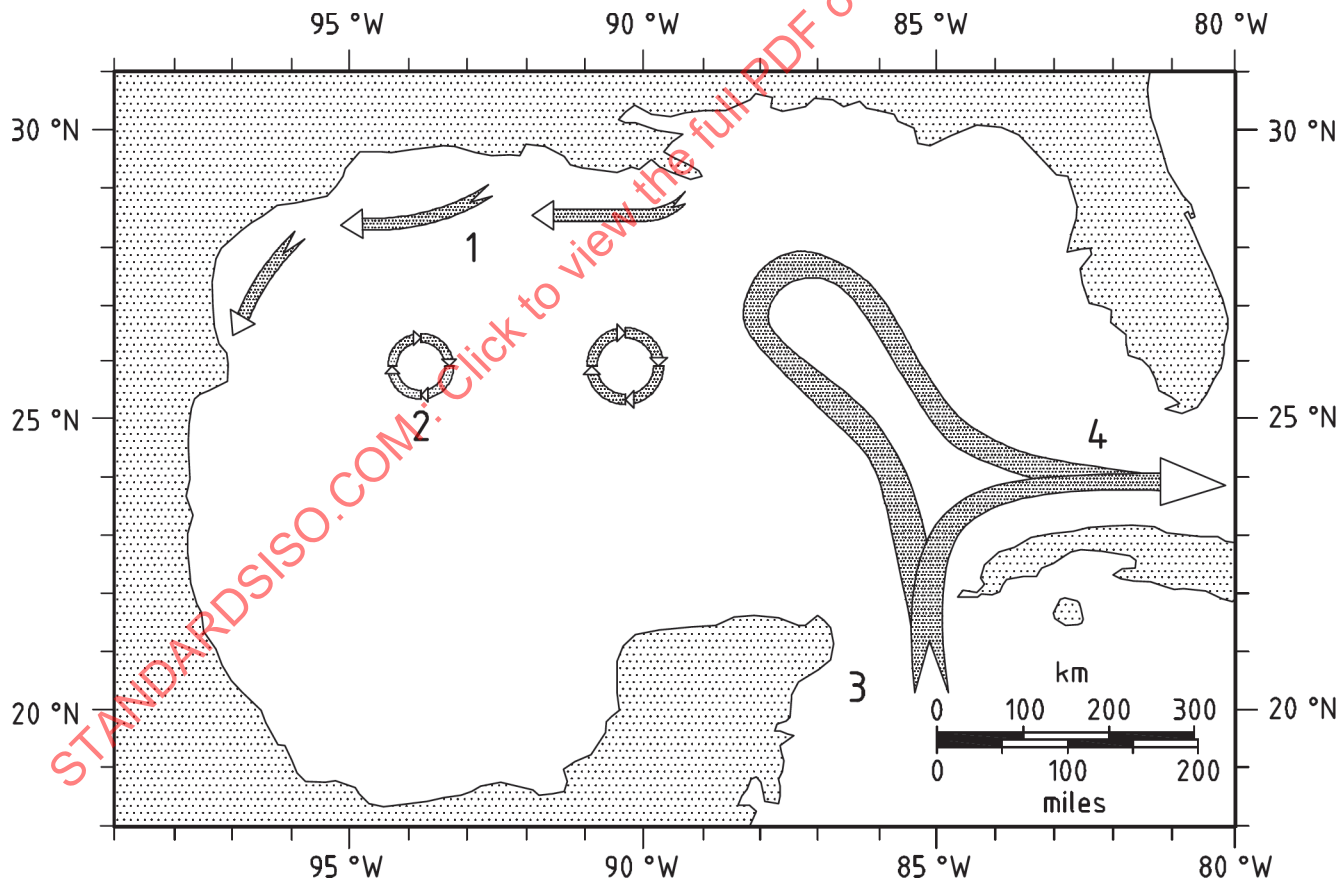

Key

1 Shelf current
2 Loop Current Eddy
3 Yucatan current
4 Florida current

Figure J.5 — Circulation in the Gulf of Mexico

J.4 Water Depth, Tides, and Storm Surge

Tides in much of the US Gulf of Mexico can be characterized as diurnal, although some areas of the Florida coast show semi-diurnal behaviour, whereas others along the Texas coast are mixed semi-diurnal. Tide range is generally less than 1,0 m in near shore areas, and decreases rapidly offshore to about 0,3 m in deep water.

With the modest tide ranges within the Gulf, mean lower low water (MLLW) and mean higher high water (MHHW) are often taken as the low and high water references for Gulf of Mexico metocean criteria. MLLW is the average of the lower low water height of each tidal day. Likewise, MHHW is the average of the higher high water height of each tidal day.

The highest storm surge in the Gulf results primarily from the passage of hurricanes and can exceed 8 m along the low-lying coastal areas as in Hurricane Katrina (2005).[264] Surge decreases offshore, but can still reach levels of 1 m in deep water.[265] Winter storms will not generally create high surge conditions along the northern Gulf coast; however, some events like the “Storm of the Century” (1993) have caused surges in excess of 3 m along the Florida coast[266].

J.5 Winds

The mean background wind flow in the northern portion of the Gulf of Mexico is governed by the mid-latitude westerlies, whereas in the southern portion, south of 26 °N, it is dominated by the easterly trade winds. The general circulation is controlled by the North Atlantic subtropical high (known as the Bermuda High when it is in the western portion of the Atlantic). Anti-cyclonic flow around the southern edge of the Bermuda High produces the Trade Winds.

Winds from hurricanes will dominate extreme design conditions. In addition to generating 1 h 10 m winds in excess of 30 m/s, the passage of a hurricane is associated with high seas, heavy rain, and strong currents in the upper layer of the ocean. The most intense hurricanes will generate 1 min 10 m winds in excess of 69 m/s. The direction of the wind at a particular site depends on the direction of hurricane travel, and its position relative to the site. Tropical storms and hurricanes are relatively localized events, even when considering large storms (see Figure J.6); the most severe winds are generally within 100 km of the storm track, and conditions are more severe on the right side of the storm track. The passage of a hurricane typically affects a site for 24 h or less. Hurricane severity is often reported with reference to the Saffir-Simpson wind speed scale; it is emphasized that this scale is solely a measure of sustained wind speeds, and may be an extremely poor indicator of how severe other environment conditions such as waves and surge may be. An example of this is Hurricane Ike (2008), which while being a Category 2 storm, generated wave heights and surge levels commonly associated with more intense storms by virtue of its large size and slow speed.

Extratropical cyclones and cold air intrusions will dominate conditions outside the summer months, generating 1 h 10 m winds in excess of 15 m/s. Gusty winds and rain associated with their passage will affect large areas of the Gulf and can last for several days. Severe occurrences of these winter storms can produce 1 h 10 m winds exceeding gale force (24,5 m/s).

For the Gulf of Mexico, wind profiles and time-averaging relations appropriate for winter storms conditions are defined in A.7.3.2, for hurricanes (tropical cyclones) are defined in A.7.3.3, and for squalls are defined in A.7.3.4. Wind spectra appropriate for winter storm conditions are defined in A.7.4.2 and for hurricanes are defined in A.7.4.3. Squalls are highly transient events and are normally analysed in the time domain.

Thunderstorms, squalls, waterspouts, and on rare occasion tornadoes will also be encountered in the Gulf of Mexico. The 10-year 1 min 10 m peak wind associated with squalls is nearly 30 m/s. Waterspouts may produce localized 3 s 10 m gusts in excess of 30 m/s. Tornadoes are generally not considered as a design condition in the Gulf of Mexico due to their infrequence and small area of effect (northern edge of the Gulf, and small spatial scale).